ADA042365

DEVELOPMENT OF ADDITIONAL

HAZARD ASSESSMENT MODELS

FINAL REPORT

MARCH 1977

Document is available to the U.S. Public through the
National Technical Information Service,
Springfield, Virginia 22161

PREPARED FOR

U.S. DEPARTMENT OF TRANSPORTATION

UNITED STATES COAST GUARD
OFFICE OF RESEARCH AND DEVELOPMENT
WASHINGTON, D.C. 20590

NOTICE

This document is disseminated under the sponsorship of the U. S. Department
of Transportation in the interest of information exchange. The United States
Government assumes no liability for the contents or use thereof.

The United States Government does not endorse products or manufacturers.
Trade or manufacturers' names appear herein solely because they are considered
essential to the object of this report.

1. Report No.	2. Government Accession No.	3. Recipient's Catalog No.
CG-D-36-77		

4. Title and Subtitle		5. Report Date
Development of Additional Hazard Assessment Models		March 1977
		6. Performing Organization Code

7. Author's	8. Performing Organization Report No.
Phani P.K. Raj, Peter M. O'Farrel	-74685-3

9. Performing Organization Name and Address	10. Work Unit No. (TRAIS)
Arthur D. Little, Inc. Acorn Park Cambridge, Mass. 02140	
	11. Contract or Grant No.
	DOT-CG-24,655A-Mod 16
	13. Type of Report and Period Covered

12. Sponsoring Agency Name and Address	13. Type of Report and Period Covered
Department of Transportation United States Coast Guard Washington, D.C. 20590	Technical Report
	14. Sponsoring Agency Code
	G-DSA-1

15. Supplementary Notes

The U. S. Coast Guard Office of Research and Development's technical representative for the work performed herein was Dr. M. C. Parnarouskis.

16. Abstract

Five additional assessment models have been developed to delineate the hazards caused by chemicals with specific properties when they are accidentally released in different environmental conditions. These models describe the sinking, spreading and dissolution of heavy liquids in a river, dissolution of heavier than water low boiling point liquids released underwater, spreading on water of continuously released oil (including experimental results) and cryogenic liquids, and the release of chemicals that react with water. The heating by fire and consequent rupture of a propylene barge tanks is also investigated.

17. Key Words	18. Distribution Statement
Dissolution, Spreading, Boiling, Heating, Rupture, Reaction.	Document is available to the public through the National Technical Information Service, Springfield, Virginia 22161.

19. Security Classif. (of this report)	20. Security Classif. (of this page)	21. No. of Pages	22. Price
Unclassified	Unclassified	306	

Form DOT F 1700.7 (8-72)   Reproduction of completed page authorized

ACKNOWLEDGEMENTS

TABLE OF CONTENTS

TABLE OF CONTENTS (continued)

TABLE OF CONTENTS (continued)

SUMMARY

A number of analytical models were generated by Arthur D. Little, Inc. for the U.S. Coast Guard during the development of the Chemical Hazard Response Information System (CHRIS) to delineate the behavior of the chemicals when spilled on water and to calculate the hazard presented by the spills. Models were made of phenomena such as liquid spread and fire, dispersion of vapor, radiation from fires, and dissolution and dispersion in water of a variety of chemicals. The primary purpose of the development of such analytical models was to provide the United States Coast Guard with a predictive tool and capability to estimate the extent of hazard zones and based on the results of such calculations to take appropriate response action in the case of a real chemical spill situation.

Most of the models developed by Arthur D. Little, Inc. under Phase I of the model development task of the CHRIS program were presented to the United States Coast Guard in a report in 1973 (CHRIS Manual 3, Analytical Models in Support of the Hazard Assessment Handbook - DOT-CG-24,665A, July 1973) and the physical system formulations and the mathematical analysis were published as an NTIS report dated January 1974 (NTIS #AD776617).

The rationale behind the development of the physical models described in the above reports was to group the chemicals according to certain of their physical and chemical characteristics. A hazard assessment tree was formulated, the branches of which represented various physical mechanisms that different chemicals undergo, such as surface boiling, evaporation, sinking and dissolution, etc. Each branch ended in a hazard situation such as vapor dispersion or fire (thermal radiation hazard) or water pollution. In developing the analytical models described in the above two reports, the best available information from the literature, together with well established procedures of physical modeling, were used.

In Phase I of modeling, not all the possible physical phenomena that the chemical could undergo when spilled on the water surface were considered. For example, the sinking and spreading on the riverbed and subsequent dissolution of a slowly dissolving chemical had been left out even though there were several chemicals belonging to this category. Other models where the mode of release was important in the estimation of the hazard had not been thoroughly analyzed. An example in this category is the continuous release, spread with fire of a cryogenic, flammable, liquefied gas.

This report presents the results of the Phase II effort under the CHRIS project. This effort consisted of modeling various physical phenomena that occur following chemical spills on water and those hazards presented by the marine transportation of a variety of chemicals. Six primary models presented in this report encompass a wide spectrum of physical phenomena, ranging from the sinking to and spreading on the river bed of heavier than water chemicals to the specific explosion hazards presented by exposure to fire of a pressurized propylene barge. In general, the models are applicable only to liquid chemicals. Described below are the models, their objectives, achievements, limitations, and their usefulness to the USCG in the task of hazard assessment. More detailed descriptions of these models are presented in the following chapters of this report.

The model describing the sinking and spreading on the riverbed of heavy insoluble liquids is described in Chapter I. The dissolution and dispersion of chemicals with finite but low solubility is considered in Chapter II. The dissolution of cold soluble chemicals when released underwater is discussed in Chapter III. Chapter IV deals with the results from a series of laboratory experiments in which oil was spilled on water at a continuous rate. Theoretical analysis of the spread problem without and with mass loss of the continuosly spilled liquid is also given in Chapter IV. In Chapter V, the heating and rupture of

2

a pressurized propylene tank (on a barge) exposed to fire is modeled. Chapter VI is an extension of Chapter V and contains the calculations for estimating the cooling (by a water spray) needed to prevent the propylene tank from rupturing when exposed to fire. Modeling of the reaction between water and three specific reactive chemicals is given in Chapter VII.

Chapter I: Sinking to and Spreading on the River Bed of an Insoluble, Heavier Than Water, Liquid Chemical

The model considered in Chapter I on the sinking and spreading of heavy insoluble liquids on river beds is in two parts. The first part deals with the sinking of the liquid in the form of globules to the river bed. Methods have been developed to estimate the size of the globules, their trajectory (the distance from the spill point to the impact point on the river bed), and the time required for sinking. Established theories of liquid drop breakup have been utilized. The second part of the chapter presents the model of the spreading of the liquid on the river bottom. This model is based on a two-stage spread, the first being controlled by the gravity-inertial forces and the second stage by the hydrodynamics of the flow in the river. This model results in a description of the shape of the pool and the duration of spread.

The usefulness, achievements, and limitations of the model discussed in Chapter I are given below.

Usefulness to USCG

- The model presented forms an important part of and an essential input for calculating the dissolution rates of slowly dissolving, sunken liquids. Hence, it is an extremely useful model in that the hazard from heavy, dissolving chemicals can now be made.

Achievements

- We have developed the mathematical tools to predict the location of impact of the heavy liquids on the river bed for a given surface spill location. In addition the

3

spreading time on the ground and the final area of spread
have been modeled. Such a model was not previously available
in the literature.

Limitations

Because of the several assumptions made in the derivations, there
are certain limitations imposed on the model. These are as follows:

- Knowledge of bed roughness is needed since predictions are
  quite sensitive to this number.

- The spreading model assumes instantaneous release on the
  river bed. However, example shows that sinking time is
  large compared to spreading time. The instantaneous
  release assumption leads to an under estimation of the
  time of spread, but has very little effect on the dis-
  solution calculations. As such the effect of this
  assumption on hazard assessment is minimal.

- The model is valid only for a turbulent river. No
  account is taken of the possible grade in the river bed,
  vortices or undulatory in the water body. Estuary regions
  have not been explicitly considered, but the results may
  be applicable to estuary regions during the ebb and flood
  flows, when considered seapartely.

Chapter II: Dissolution and Dispersion of Chemicals of Finite Solubility

This chapter presents the models for the dissolution and dispersion
in water of chemicals that are soluble in low concentrations. For
heavier than water chemicals, the spread model developed in Chapter I
is used together with well-established mass transfer correlations to
obtain the dissolution rates. A significant result derived in this
chapter is that the shape of the pool has small effect on the dissolution
rate. Also, another derivation has been given which modifies the standard
mass transfer correlations (for flow over a flat plate) taking into
account the fully developed character of the velocity distribution in
the river.

4

For lighter than water chemicals, the dissolution rate is estimated by using eddy diffusivity surface renewal theories. The validity of predictions of these theories has been well established in the literature by aeration experiments in rivers.

For both heavier than water and lighter than water chemicals, the important result of interest is the dissolution rate. Once this rate is established for a given chemical, it can then be used in dispersion models to obtain the concentration of the chemical in the river. For the heavy chemicals, a line source model is developed, and for the lighter than water chemicals, a traveling, expanding volume source model is developed.

The usefulness, achievements, and limitations of the models discussed in Chapter II are given below.

Usefulness to USCG

● A mathematical tool has been provided to predict the pollutant concentration, its timewise variation and the duration for which the pollution lasts at any station within a river, for the slow dissolution of a chemical. Based on the predictions, USCG can take appropriate action, such as alerting the cities downstream, or salvaging the chemical by dredging the river bottom, etc.

Achievements

These models:

● Predict the dissolution rate of slowly soluble chemicals, settled at the river bottom.

● Show the insensitivity of the total dissolution rate to the shape of the "liquid" pool on the river bed.

● Describe dissolution in a turbulent stream in which the hydrodynamic boundary layer is completely developed and the mass transfer boundary layer still developing.

- Predict the rate of dissolution of a floating liquid on water, using well established surface renewal theories and experimental data on aeration of rivers.

- Describe dispersion in rivers with stationary area source and sources moving with the stream.

Limitations

- The models give a simplistic view of the river as a channel in which fully developed water flow occurs.

- They do not take into account fluid flow peculiarities due to large rocks, vortices, etc. on the river bed, disturbances due to bridges, piers, etc.

- The models are applicable only for a unidirectional flow and not for estuaries.

- There is a lack of experimental data for backup.

Chapter III: Dissolution of Cold and Soluble Chemicals Under Water

The release of cold and soluble chemicals under water and the calculation of their dissolution rates in water have been considered in Chapter III. The models developed are for liquids whose boiling temperatures are considerably lower than the ambient water temperature and whose liquid densities are higher than that of water. Therefore, when these liquids released under water, they boil. Two kinds of dissolution of the liquids are considered. The first model deals with the dissolution of vapor formed. The effect of variation in the hydrostatic pressure on the dissolution rate during the ascent of vapor bubble is also considered. The second model deals with the nondissolving but boiling phenomenon.

The specific examples considered indicate that the distances over which a liquid drop-vapor combination rises before all the liquid is evaporated are relatively short and that even for shallow depths of release (of greater than 10 feet), appreciable amounts of vapors dissolve in water.

The usefulness, achievements, and limitations of the models
discussed in Chapter III are given below.

Usefulness to USCG

- A mathematical tool has been developed to predict the
  rate of boiling and dissolution of a liquid chemical
  (whose boiling temperature is lower than that of the
  ambient) when released at different depths. Depending
  on the chemical and the type of pollution that can be
  tolerated, deliberate leaks at controlled rate and depth
  may be undertaken by USCG from, say, a disabled barge.
  In such cases, the pollution hazard can be calculated
  using the models presented.

Achievements

- Two kinds of dissolutions have been analyzed:
  - Gas bubbles dissolving when released underwater; and
  - Liquid boiling without dissolving, when released
    underwater.

- Predictions of time to rise to the surface as well as
  the amount of dissolution/boiling during the upward
  sojourn of bubbles or liquid drops have been made.

- Predictions of water pollution and air pollution
  have been given.

- Discussions of the peculiarities in boiling of liquid
  drops in another liquid have been given.

- A specific example to predict the dissolution rate
  on n-Butane has been worked out.

Limitations

- Existing heat and mass transfer (or relations) were
  used without regard to the rapidity of the reaction.

7

- The effect of pressure variations on boiling temperature
  was not considered.

- It was an assumption that even though the liquid is
  heavier than water, the combined vapor-liquid system
  is lighter than water and therefore rises.

- There is a lack of experimental data to extend the methods
  of analyses indicated to other chemicals.

Chapter IV: Spreading on the Water Surface of a Continuously Released
             Lighter Than Water Immiscible Liquid

Chapter IV deals with the general problem of the spread of a
lighter than water liquid on the water surface when released con-
tinuously. The chapter is in four parts. The first part describes
the details of an experimental study of the spread of oils on water
(when released at a constant flow rate). The experiment consisted of
releasing oil at a steady rate on the surface of water taken in a
trough and photographing, on movie film, the development of the slick
in time. Three types of oils, namely, detergent motor oil, non-
detergent motor oil, and castor oil, were used in the study. The
significant result from the study was that the radius of the spread
front increased in direct proportion with the square root of time after
spill.

The second part of Chapter IV presents a theoretical analysis of
the problem. The model developed uses the ideas of hydraulic jump in
liquids and Pohlhaussen's technique to evaluate the spread radius as
a function of time. Only the global mass conservation equation coupled
with the small amplitude wave velocity equation were used in this analysis.
The results indicate that in a brief initial period, the radius of spread
increases directly as time and later it varies as the square root of
time, agreeing completely with the experimental evidence. In the
third part, the analysis is extended to take into account the mass loss
by evaporation in the case of spread on water of a uniformly released

8

cryogenic liquid. The result indicates that the time to spread to the final maximum area, consistent with the release rate, can be significant. Finally, in the last part of Chapter IV, an analysis and methodology are given for calculating the thermal radiation intensity and dosage from a fire on an expanding pool of flammable liquid which is being released uniformly. The calculation includes the results obtained in the earlier two parts.

The usefulness, achievements, and limitations of the models discussed in Chapter IV are given below.

Experimental Investigation of Continuously Released Oil Spread on Water

Usefulness to USCG

- Experiments add teeth to any theory, and as such, the results of oil spread experiments are very useful. In addition, because of the dimensional analysis, the results could be extrapolated to large spill sizes. It is essential for the USCG to have this information to prevent the off-shore oil spills from polluting the beaches.

Achievements

- The radius of continuously released oil on water has been observed to grow as the square root of the time.

- Oil properties other than the density do not seem to have and effect.

- A dimensional analysis method has been developed to correlate a considerable amount of data from experiments in which parameters vary over orders of magnitude.

- A contribution has been made to pollution literature where data and analysis do not exist to characterize continuously released oil spread.

Analytical Modeling of Release, Spread, and Fire Hazard Due to a Continuous Release of Cold Liquefied Gases

Usefulness to USCG

- Depending upon the type of liquid that is being spilled (oil, LNG, etc.) and the duration over which spill has occurred, remedial action can be taken, because calculations of the size of the spill at the given time can be made from the above models. For example, the length of boom necessary to contain an oil spill may be calculated easily. In the case of expanding pool fire, the distance to the radiation hazard can easily be obtained.

- Because of the prediction by the thermal hazard distance by the model, corrective action may be taken well in advance before receiving, say, an LNG ship into a port.

Achievements

- An experimental program to determine the rate of spread of oil released continuously has been completed.

- An analysis of the above problem has been made which includes:

  - Modeling the spread of a non-evaporating liquid (such as oil) on water when released continuously;

  - Modeling the spread when mass loss is also present, as in the case of cold liquefied gas boiling, is achieved and;

  - Thermal radiation from expanding burning pool.

- The mathematical models developed involved very difficult concepts rendered simple by making suitable physically valid assumptions.

- Predictions of the model for non-evaporative spreading agree with experimental evidence extremely well.

- Predictions of spread time and hazard distance for LNG spills on water give values which are close to what one would "expect" by experience.

10

Limitations

- A complete set of the extremely complicated non-linear
  differential equations could not be solved.

- There is a lack of experimental backup for the case of
  spread with mass loss.

Chapter V: Heating, Rupture, and Release of a Pressurized Cargo in a Fire

The specific problem of the heating of a tank on a barge exposed
to fire is considered in Chapter V. The object of the analysis is
to calculate from models the time to rupture of a tank exposed to
fire. The methodology used in the analysis is very general and
could be applied to the study of any tank configuration, heat source,
or chemical in the tank. For the sake of illustrating the methodology,
a pressurized propylene tank on a barge exposed to two different kinds
of fire scenarios is considered.

In the first fire scenario, the fire is external to the barge,
in which case the entire top of the tank is exposed to the fire. In
the second case, a "hold fire" is considered. The method of analysis
in each case involves writing down appropriate thermodynamic and
energy equations for different "thermodynamic systems" within the tank
and also accounts for the heating of the tank walls.

The results from the analysis indicate that the vents provided are
adequate to handle all of the vapor that would be generated by exposing
the tank surface above the rain shield to a flame radiation of 30,000
Btu/hr ft^2. The tank failure occurs due to the overheating of the wall
in contact with vapor and its consequent strength reduction. The
estimate of the time of rupture varies between 16 and 20 minutes.

The usefulness, achievements, and limitations of the models
discussed in Chapter V are given below.

ii

Usefulness to USCG

- The time at which the tank is likely to rupture can
  be quickly obtained.

Achievements

- A complete and rigorous model has been developed for
  pressure rise in the tank, taking into account the
  variability of propylene property with temperature
  and pressure.

- Timewise description of pressure and steel wall
  temperature has been given.

- Prediction of time of rupture has been made.

- Two possible fire situations have been considered.

- The computer program developed can be utilized for
  any other liquid or tank size.

Limitations

- Several physically valid assumptions which have not,
  however, been fully justified by experiments, have
  been made.

- In some cases, overly conservative assumptions have
  been made.

- Model predictions have not been checked against available
  data from a large-scale test conducted by DOT with propane
  railroad tank cars.

Chapter VI: On the Cooling by Water Deluging of a Propylene Barge Tank Exposed to Fire

The analysis presented in Chapter VI can be summarized as an
extension of the analysis in Chapter V. The significant question that
arises when a barge containing a pressurized liquid is exposed to a
fire is "whether it is worthwhile and safe to cool the tank exposed
to fire by spraying it with water from a fire boat." The analysis

presented in this chapter attempts to partially answer this question. However, because of the several unknowns in an actual situation and the need to assume certain idealistic conditions in a mathematical analysis, the results presented should be viewed with caution.

The analysis presented calculates both the amount of water needed to significantly cool the hot tank wall and the time for cool down. It is seen that the time for cool down is short. Also, the amount of water needed to cool the entire surface of a typical propylene barge tank is well below the rated delivery rates from conventional fire boats. However, there exists a possibility that all of the sprayed water is not uniformly distributed over the tank surface - a crucial assumption made in the theory.

The usefulness, achievements, and limitations of the analysis presented in Chapter VI are given below.

Usefulness to USCG

The analysis presented indicates that the water throw capacity of the existing fire boats is sufficient to cool the propylene barge tank surface so that the tank pressure does not rise due to exposure to fire. However, considerable judgement has to be used before a fire boat can be sent to the vicinity of an already fire exposed tank, because of the possibility of explosion of the tank.

Achievements

- A simplified analysis of an exceedingly complicated physical phenomena has been accomplished.

- The analysis gives overall estimates of the water requirement to cool the tank surface, the wall temperature history and the time to cool of a propylene tank exposed to fire.

Limitations

- Because the effect of the thermal stresses that may develop during the tank wall cooling has been neglected in the analysis, it is not possible to make a strong recommendation

13

as to whether spraying the hot tank wall with water is
desirable. There may occur situations where water spraying
and the resulting non-uniform thermal stress would cause
an early rupture of the tank. One is not even sure that
consideration of the stresses (thermal) would lead to
better predictions, because there is always the uncertainty
over the uniformity of tank wall coverage by the water
spray. As such the results of this model should be used
only as an aid to the hazard analysis and decisions have to
be taken on the basis of experience and scientific judgement.

Chapter VII: Reactive Chemical Models

A few important chemicals which are transported in bulk on
waterways react with water if spilled. To evaluate the hazards resulting
from such spills, one must consider the products of reaction in addition
to the original spilled chemical. Each situation is, in fact, a
specific case. Some chemicals react very rapidly, and it is then a
good assumption to neglect any downstream hazards except those due to
the products. In most cases, however, the chemicals react at finite
rates and, in a hazard analysis, the reaction kinetics and heat and
mass transfer limitations must be examined to determine the rates of
decomposition. Since a general model cannot be developed, the problems
involved in modeling reactive chemical spills are illustrated by example
cases. Three chemicals were chosen for three completely different
ways in which they react with water. These are considered in Chapter
VII.

Chlorosulfonic acid typifies a chemical that reacts almost instan-
taneously. Phosgene and nitrogen dioxide were selected as reaction
rates are slower and, in many instances, are limited by mass transfer
limitations. In all three cases, the physcial properties of the chemicals
are discussed and the reaction kinetics and mechanism outlined. With
this framework, the consequences of spills are considered and the rates
of product generation calculated.

It must be emphasized that the predicted rates of decomposition are based on theory; no experimental data exist to confirm the estimates.

It is felt that the models developed increase the variety and the range of chemicals that now are being considered in the hazard evaluations in CHRIS. As indicated earlier, most of the models are based on theoretical formulation of the real life physical problems encountered in chemical spills; however, the best available information from the literature and well established modeling procedures were used. However, the only way that one can be sure of the accuracy of any theoretical prediction is to test the theory against certain controlled experiments. We therefore recommend that several experimental programs be undertaken within the scope of chemical spill models.

The usefulness, achievements, and limitations of the models developed in Chapter VII are presented below.

Usefulness to USCG.

The models developed indicate the variety of ways in which individual reactive chemicals can react with water. These analyses show that each chemical belonging to the "reactive chemical" group has to be considered separately.

The examples given in this chapter identify the types of hazards and the extent of hazards to be expected from reactive chemical. The modeling has served a useful purpose in indicating the variety and the extremely complicated nature of modeling reactive chemicals.

Achievements

- Three chemicals having considerably different reactive characters have been chosen and their reactions with water analyzed.

- Reaction rates have been calculated and dissolution rates of products of reaction analyzed.

Limitations

- Only 3 chemicals have been considered out of a great number of possible candidates.

- In the case of the reaction of chlorosulfonic acid with water, no reaction rate calculations have been made, because of the rapidity of reaction.

- The dynamics of spills do not form a part of the analysis.

The present report describes several models that have been developed to bridge the gap that existed in hazard evaluation methodology. However, the modeling is far from complete. Such phenomena as polymerization and degradation of chemicals have not been considered. Also, the behavior of solid chemicals and semi-liquid chemicals have not been touched upon at all. Finally, it is to be noted that all of the models presented in this report are theoretical models, only a few of which have direct experimental backing. This does not, however, mean that the physical systems are not properly modeled. The only question is one of adequacy, because nature in its infinite variety of behaviors has on occasion acted in completely different ways than assumed by a theoretician. The only way to be sure of both modeling and its applicability (when extrapolated) to large real-size spills is to first conduct several scaled experiments on all, or at least some of the theoretically modeled phenomena.

BACKGROUND

A number of analytical models were generated during the development of the Chemical Hazard Response Information System (CHRIS) to delineate the behavior of the chemicals when spilled on water and to calculate the hazard presented by the spills. Phenomena such as liquid spread and fire, dispersion of vapor radiation from fires, and dissolution and dispersion in water of a variety of chemicals were modeled. The primary purpose of the development of such analytical models was to provide the United States Coast Guard with a predictive tool and capability to estimate the extent of hazard zones and based on the results of such calculations to take appropriate response action in the case of a real chemical spill situation.

Most of the models developed under Phase I of the model development task under the CHRIS program have been presented to the United States Coast Guard in a report in 1973, and the physical system formulations and the mathematical analysis have been published as an NTIS report dated January 1974. The rationale behind the development of the physical models described in the above reports was to group the chemicals according to certain of their physical and chemical characteristics. A hazard assessment tree was formulated, the different branches of which represented different physical mechanisms that different chemicals undergo, such as surface boiling, evaporation, sin-ing and dissolution, etc. Each branch ended in a hazard situation such as vapor dispersion or fire (thermal radiation hazard) or water pollution. In developing the analytical models presented in the above two reports, the best available information from the literature, together with well established procedures of physical modeling, were used.

In Phase I of modeling, not all the possible physical phenomena that the chemical could undergo when spilled on the water surface were considered. For example, the sinking and spreading on the riverbed and subsequent dissolution of a slowly dissolving chemical had been left out even though there were several chemicals belonging to this category. Other models where the mode of release was important in the estimation of the hazard had not been thoroughly analyzed. An example in this category is the continuous release, spread with fire of a cryogenic, flammable, liquefied gas.

17

In the present report, several models have been developed to bridge
the gap that existed in hazard evaluation methodology. However, the modeling
is far from complete. Such phenomena as polymerization and degradation of
chemicals have not been considered. Also, the behavior of solid chemicals and
semi-liquid chemicals have not been touched upon at all. Finally, it is to
be noted that all of the models presented in this report are theoretical
models, only a few of which have direct experimental backing. This does
not, however, mean that the physical systems are not properly modeled.
The only question is one of adequacy, because nature in its infinite
variety of behaviors has on occasion acted in completely different ways
than assumed by a theoretician. The only way to be sure of both modeling
and its applicability (when extrapolated) to large real-size spills is
to first conduct several scaled experiments on all, or at least some,
of the theoretically modeled phenomena.

CHAPTER I

SINKING TO AND SPREADING ON THE RIVER BED OF AN INSOLUBLE, HEAVIER THAN WATER LIQUID CHEMICAL

OBJECTIVES

The objectives of the analyses presented in this chapter are to calculate the following for the spill on the water surface of a slowly dissolving liquid chemical:

- The distance from the spill location on the water surface at which the liquid reaches the river bed.

- The spread time, shape, and maximum area of spread of the liquid pool on the river bed.

INTRODUCTION

The ever-increasing maritime traffic on the navigable rivers within the United States poses threats of collision accidents between ships, ship and barge, barge and barge, and so on. A variety of chemicals are carried in barges. Some of these chemicals are either insoluble in water or have very low solubility.

Many towns and cities along the river banks use the river water to supply the drinking water needs of the communities. Therefore, a chemical spill in a river may produce a public health hazard. In addition the aquatic life in the river itself may also be affected. If the chemical that is spilled is totally insoluble in water and does not react with other dissolved chemicals, then there does not exist any threat from the spilled chemical. However, some chemicals dissolve slowly, resulting in a long duration hazard. Slow dissolution implies low chemical concentrations in water which, however, does not necessarily mean a smaller hazard zone. Some of the chemicals are hazardous to human health and to aquatic life even in very low concentrations. Therefore, there exists a need to understand and be able to predict the dissolution rates of slowly dissolving chemicals in streams.

19

When the chemical is a liquid and heavier than water, it is very
likely that the liquid will break up into globules after it is spilled
on water. These globules will be carried downstream by the stream
current and at the same time tend to settle down. The location of
the point of contact of the liquid globules and the river bed depends
on the size of the globules, the stream velocity, and the stream
turbulence. This problem of the liquid breakup and settling is
analyzed in Section 1. The major assumption made in this analysis
is that there is no dissolution of the chemical during the settling
process. This is in keeping with the very low solubility of the
liquid chemical.

When the liquid globules reach the river bed, they may again
coalesce and form a liquid pool on the bed surface. This pool will
spread by the action of both gravity (the liquid being heavier than
water) and stream current. In Section 2, this spreading problem is
analyzed. The final area of spread and the shape of the pool are
important parameters necessary for the calculation of the pollution
hazard. The dissolution and dispersion models are treated in
Chapter II of this report. It is expected that the results from
this chapter will be inputs to and complement the analyses presented
in Chapter II.

THEORETICAL DEVELOPMENT

Section 1: Rate of Settling in a Stream of a Suddenly Released, Heavier than Water, Liquid Chemical

When a blob of heavier than water liquid is spilled on water,
it breaks up into smaller globules of liquid during the process of
sinking. A wide spectrum of liquid drop sizes are expected to be
formed during the breakup process. However, from the considerations
of the equilibrium between dynamic forces caused by the motion and
the surface tension forces, it can be shown that drop sizes above
a certain mean* radius cannot exist. Such an analysis has already

---

* The word "mean" refers to the average value of an odd-shaped blob and
does not refer to the ensemble average size of the different sized
liquid globules.

been performed, and the details are given in a report to the USCG.[1]
For the calculations presented below, we use this maximum radius as
the characteristic radius of the blobs. This radius is given by

$$R = 1.87 \sqrt{\frac{\sigma}{g(\rho_{liq} - \rho_w)}} \qquad (1)$$

where

    R   = radius of the largest stable liquid drop

The terminal velocity of the largest drop is given by

$$U = 2.07 \left[\frac{g\sigma}{\rho_w} \left(\frac{\rho_{liq}}{\rho_w} - 1 \right) \right]^{1/4} \qquad (2)$$

Equation 2 indicates that the terminal velocity is dependent on the
properties of liquid and water. Implicity the size of the drop has
been included in equation 2. Also equation 2 is correct only if
the drag coefficient is a constant which is indeed the case when
the Reynolds number for drop motion is in the "highly turbulent"
region ($Re_d > 10^3$). However, when one considers the fact that all
these drops are falling down in the stream under the action of gravity
and are continuously accelerated until the terminal velocity is
reached, it is clear that the drag coefficient varies (decreases)
continuously. In the case of small drops, this rate of settling
may be impeded by the stream turbulence, i.e., the fluctuating
components of vertical velocity in the stream. This latter phenomena
may result in the suspension of the small diameter liquid drops in
the stream. Only the larger size drops reach the river bottom.

The critical size of drops that will be held in suspension depends on the intensity of turbulence, the density of the liquid and the terminal velocity of the drops. Yalin[6] has treated the problem of sediment suspension in river water and this analysis is partially applicable to the present situation. However, Yalin's analysis is for a steady state condition which does not exist in the problem under consideration (wherein a given mass of heavy liquid is spilled into a water way). It can be argued that all liquid drops have to settle to the river bottom ultimately irrespective of their size. Their settling time is greatly influenced by the size and turbulence. For a first approximation it is suggested that the following criterion be used to estimate the fraction of spilled mass that may be in suspension for a "long time".

$$U_{critical}(R) < \sqrt{\overline{u'^2}} \qquad (3)$$

where

U(R) is the terminal velocity for a liquid drop of radius R and

$\sqrt{\overline{u'^2}}$ is the root mean square fluctuating stream velocity in the depthwise direction.

It is to be kept in mind that the criterion indicated in Equation (3) is purely speculative and needs experimental verification. The size of the particles that will be in suspension for a long time will depend in general on the statistics of turbulence, the distribution of intensity in the depthwise direction, the density of the particle and its geometric shape (indicated by the value of the terminal velocity). The simple criterion given in Equation (3) is based on the argument that particles having terminal velocities lower than the turbulent velocity scale (r.m.s. fluctuations) are easily liable to be tossed around.

22

It can be shown that for a nondeformable sphere of diameter d falling slowly in water (at $Re_d \lesssim 100$) the terminal velocity is given by[2]

$$[U(R)]_{laminar} = \frac{2}{9} \frac{R^2}{\nu_w} g \, (\rho/\rho_w - 1) \tag{4}$$

Assuming that $\sqrt{\overline{u'^2}} \simeq 0.1$ m/s for a typical river and using $\rho_\ell/\rho_w \simeq 1.2$, we can show using equations 3 and 4 that drops of diameter less than 1 mm will be in suspension. Those with diameters larger than this will settle.

Since the frequency distribution of the diameters is not known apriori, a conservative approach is to assume that all of the liquid spilled reaches the bottom.

Hence, with settling velocity given by equation 2, we have the settling time

$$t_{settling} = \frac{\text{depth of stream}}{\text{velocity of settling}} = \frac{d}{U} \tag{5}$$

The horizontal location at which the liquid hits the river bed is given by

$$X = u_s t = \frac{u_s}{U} d \tag{6}$$

Section 2: Spread of a Heavy Liquid on the River Bed

A heavy liquid chemical released into a river settles to the bottom of the river. Subsequently, the liquid spreads on the river due to the action of its own weight and the shear force induced by the flow of water. The spreading of the liquid continues until the thickness of the liquid film is smaller than the roughness protrusions of the river bed. At this stage, the liquid fills up all the "valleys" in the rough bed and stops spreading.

During the shear force induced spreading, the liquid spreads preferentially in the downstream direction. .Should the river bed slope upwards (i.e., the depth of the river decrease), it is possible that the liquid also will be dragged up. The model presented below has not considered this problem explicitly; in fact, the model assumes the river bed surface to be essentially horizontal.

23

The spreading is modeled in two phases. In the first phase (in which the liquid is assumed to be released instantaneously at the river bottom), the liquid spread is due only to the effective gravitational acceleration. The force resisting the spread is the inertia of the system. In the second phase of spread, the tangential drag induced by the river flow becomes important. This is also modeled. The objective of the analysis presented in this section is to obtain the shape and duration of spread and the maximum area of spread. The following assumptions are made:

Assumptions

- The liquid is assumed to be released instantaneously at a single point on the bottom of the river.

- During the spreading of the liquid, no mass loss by dissolution occurs.

- Liquid pool spreads until its thickness is equal to the mean roughness of the bed.

Since the mass of liquid in the spreading pool is a constant, the final spread area can be easily established if the final (mean) thickness to which the liquid spreads is known. Since the final thickness of the pool is assumed to be equal to the mean bed roughness, it is necessary to know the river bed roughness data. However, this may not be readily available.

The river frictional characteristic represented by the Manning friction factor is related to the bed roughness. A tabulation is given by Merrit[3] for evaluating the Manning friction factor (n) for various channels with different bed roughnesses. Streeter[4] has obtained, using the logarithmic velocity law for turbulent flow, a relationship between Manning friction factor (n) and mean bed roughness (e). This relationship with the dimensional terms expressed in S.I. units is*

$$\frac{R_h^{1/6}}{n} = 20.72 + 3.84 \ln\left(\frac{R_h}{e}\right) \tag{7}$$

---

*In FPS units with e and R_h in feet and g in ft/sec^2, the same relationship becomes

$$\frac{1.49}{\sqrt{8g}} \frac{R_h^{1/6}}{n} = 1.14 + 2 \log_{10} \frac{4R_h}{e} \tag{7a}$$

24

Also, in the above equation the effect of R_h is small and therefore the equation can be considered as a relation between e and n. Table I-1 shows the relationship between e and n for various values of e and R_h. As can be seen from the table, equation 7a is a very poor way of estimating the value of e for a given value of n and R_h because of its extreme sensitivity. However, since no other method exists to estimate the value of the bed roughness, equation 7 has to be used <u>when no roughness data are given</u>.

Figure I-1 is a plot of the equation 7 and calculated data from Table I-1. The figure indicates that a dimensional correlation between e and n can be given by

$$e = 10^{[3.8173 - \frac{8.571 \times 10^{-2}}{n}]} \tag{8}$$

where e is in inches and n is dimensionless. This correlation is valid only within the ranges $10 \text{ ft} \leq R_h \leq 100 \text{ ft}$ and $e < 4$ inches.

Spreading

The spreading of an instantaneously released (on the river bed) liquid is modeled in two stages. These two stages of spread are illustrated in Figures I-2a and I-2b respectively.

1. In the first stage, the spread velocity due to gravity spreading is assumed to be much greater than the stream velocity. In this case, the stream velocity has little effect on the spreading rate during this phase. Hence, the spread is essentially radial.

2. The second phase of spreading begins when the radial velocity of spread of the pool is equal to the "local" stream velocity (at the height equal to the mean film thickness of the pool). In this phase, the downstream end of the liquid pool is "pulled" by the stream at its local velocity, whereas the upstream end of the pool is stationary. The cross stream spread is assumed to take place at a gravity spread velocity corresponding to the film thickness at the instant under consideration.

Table I-1

(Table Obtained from Equation 7a)

e in inches	R_h in feet	e/R_h (dimensionless)	n (dimensionless)
0.5		4.17×10^{-3}	0.0192
1.0		8.33×10^{-3}	0.0210
1.5	10	1.25×10^{-2}	0.0222
2.0		1.67×10^{-2}	0.0231
0.5		8.33×10^{-4}	0.0210
1.0		1.67×10^{-3}	0.0226
1.5	50	2.50×10^{-3}	0.0236
2.0		3.33×10^{-3}	0.0244
0.5		4.17×10^{-4}	0.0220
1.0		8.33×10^{-4}	0.0235
1.5	100	1.25×10^{-3}	0.0245
2.0		1.67×10^{-3}	0.0253
3.5	100	2.92×10^{-3}	0.0270

The above can be represented by

$$\log e \ (inches) = c_1 - c_2/n$$

R_h ft	c_1	c_2
10	3.251	6.813×10^{-2}
50	3.950	$8.9 \ \ \times 10^{-2}$
100	4.251	$10.0 \ \ \times 10^{-2}$
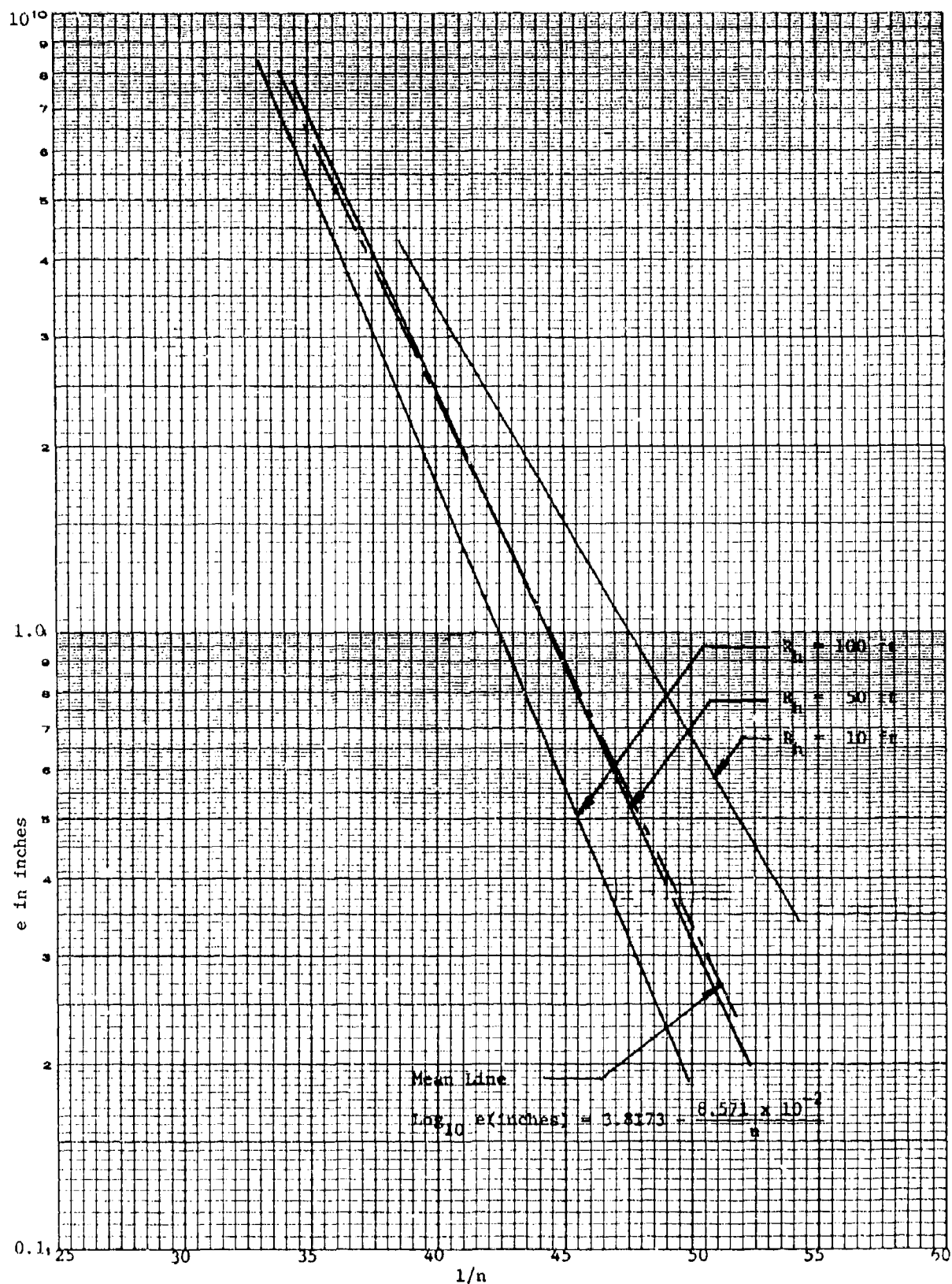
FIGURE I-1
Relationship Between River Bed Roughness Dimension (e) and Manning Friction Factor (n)

27
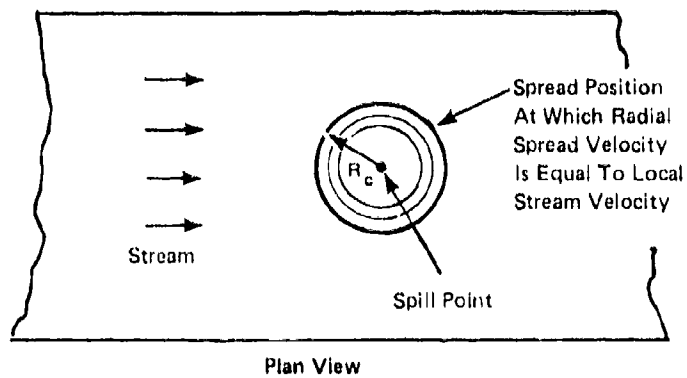
FIGURE 1-2a   Plan View of Spreading in the Gravity Inertia Region
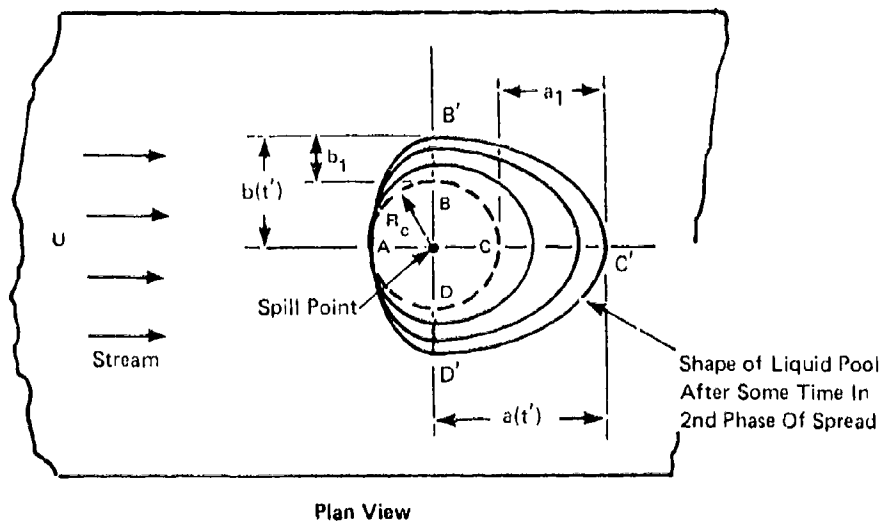
FIGURE I-2b   Plan View of Spreading During Stream Influence Stage

28

These are incorporated into a model to obtain the area of spread and the dimensions of the spread as a function of time. The spreading is assumed to stop when the liquid film thickness is equal to the mean bed roughness.

Gravity Spreading

We model the spreading of the liquid under the influence of gravity, assuming that during this spread process the stream has no influence. The termination of gravity spread in the streamwise direction is said to occur when the velocity of spread of the liquid front in the upstream direction is equal to the stream velocity at the mean thickness of the liquid at that instant. This situation is termed "critical."

The gravity spreading of a liquid on a plane solid surface has been treated in reference 1. The following result is taken from Table 8.1, page 110, of reference 1.

$$R(t) = 1.14 \ (G \ V)^{1/4} \ t^{1/2} \tag{9}$$

Also, the mean thickness of liquid film is given by

$$h_\ell(t) = \frac{V}{\pi \ R^2(t)} \tag{10}$$

Substituting equation 10 in equation 9 and differentiating, we can show that the velocity of spread of the liquid (in the gravity spread regime) is given by

$$u_{g,\ell} = \frac{dR}{dt} = c \ \sqrt{G \ h_\ell} \quad ^\dagger \tag{11}$$

From this equation, equating the left hand side to the stream velocity, expressed in terms of the height above the bed, we obtain a critical height h_ℓ^c. From this, the critical radius of spread R_c is calculated. This then gives the area of spread in the first stage, i.e.,

$$u(h_\ell^c) = c \ \sqrt{G \ h_\ell^c} = c \ \sqrt{G \ \frac{V}{A_c}} \tag{12}$$

---

† c has a magnitude equal to 1.152.

It is shown in the numerical example that even for very small distances above the river bed surface, the stream is fully turbulent. Hence, we use the 1/7th power law distribution to describe the velocity profile in the stream. Following Goldstein[5] we write

$$\frac{u(y)}{u_s} = (8/7) \ (y/d)^{1/7} \tag{13}$$

where

    d is the depth of the stream

    u_s is the mean stream velocity.

Equating 11 and 13, we get

$$\frac{h_\ell^c}{d} = 0.9783 \ F_D^{2.8} \tag{14a}$$

where F_D = Densimetric stream Froude number

$$= \frac{u_s}{\sqrt{G \ d}} \tag{14b}$$

Substituting 14a in 10, we get

$$R_c = 0.5704 \ \frac{1}{F_D^{1.4}} \sqrt{\frac{V}{d}} \tag{15}$$

and from 15 and 9 we get

$$t_c = \frac{0.2504}{F_D^{2.8}} \sqrt{\frac{V}{G \ d^2}} \tag{16}$$

Spreading Due to Stream Shear

The critical condition described above is based on the time at which the radial gravity spread velocity is equal to the stream velocity at the height of the film thickness. During the period following criticality, the downstream end (point c in Figure I-2b) is dragged at a velocity equal to the mean stream velocity existing at the height of liquid film thickness. Upstream, point A does not move because of viscous friction with the bed. Cross stream points B and D expand at velocity

30

of the gravity spread velocity corresponding to the film thickness. A schematic representation of the growth of the pool area with time is indicated in Figure I-2b for times after criticality.

The model proposed to determine this spread area after criticality assumes that the area can be divided into two semiellipses, AB'D' and D'B'C' (Figure I-2b). The rate of increase of the total area is correlated with the various velocities of the edges keeping in mind that the volume of the liquid in the pool is a constant. In this analysis, no account is taken of the possibility that during the spread the liquid may hit the edges of the river bank. The details of the mathematics of the model are indicated below.

Let

$t' = t - t_c$ = time period after the spread reaches criticality

$A(t')$ = area of the pool at time t'

a_1 = distance traveled by the downstream edge of the pool in t' (point c in Figure I-2b)

b_1 = distance traveled by cross stream pt (B) in time t' after criticality

b = $R_c + b_1$

a = $R_c + a_1$

Hence the area

$$A(t') = \underbrace{\frac{\pi R_c b}{2}}_{\substack{\text{area of semi-}\\\text{ellipse D'AB'}}} + \underbrace{\frac{\pi ab}{2}}_{\substack{\text{area of}\\\text{semiellipse B'C'D'}}} \qquad (17a)$$

i.e., $A(t') = \frac{\pi}{2} [R_c (R_c + b_1) + (R_c + a_1)(R_c + b_1)]$

$$= \pi (R_c + b_1) [R_c + \frac{a_1}{2}] \qquad (17b)$$

Substituting for b_1 and a_1 in terms of spread velocities, we have

31

$$A(t') = \pi R_c^2 \left[1 + \frac{1}{R_c} \int_0^{t'} u_{g,\ell} \, dt \right]\left[1 + \frac{1}{2R_c} \int_0^{t'} u \, dt \right] \tag{17c}$$

where $u_{g,\ell}$ is the liquid gravity spread velocity (see equation 11) and u is the stream velocity at the height corresponding to the liquid film thickness.

The thickness of the liquid film at any time is

$$h(t') = \frac{V}{A(t')} \tag{18}$$

Substituting 18 in 11, we get (with c = 1.152)

$$u_{g,\ell}(t') = c\sqrt{G\,h(t')} = c\sqrt{\frac{G\,V}{A(t')}} \tag{19}$$

Similarly, u, the stream velocity, is a function of the height (see equation 13). However, the variation of stream velocity from the height of film at criticality to final height is small (see specific example). Hence, to simplify the mathematical complexity, we use a mean velocity of spread for the downstream point. This is given by

$$\bar{u} = \frac{1}{(h_c - h_f)} \int_{y=h_f}^{h_c} u \, dy$$

Substituting equation 13 in 20 and integrating, we get

$$\bar{u} = u_s \frac{\left[\left(\frac{h_c}{d}\right)^{8/7} - \left(\frac{h_f}{d}\right)^{8/7} \right]}{\left[\left(\frac{h_c}{d}\right) - \left(\frac{h_f}{d}\right) \right]} \tag{21}$$

Substituting equation 19 and $\bar{u}$ from equation 21 for the u in the integral in equation 17c, we get

$$A(t') = \pi R_c^2 \left[1 + \frac{c\sqrt{V\,G}}{R_c} \int_0^{t'} \frac{dt}{\sqrt{A(t)}} \right]\left[1 + \frac{\bar{u}\,t'}{2R_c} \right] \tag{22a}$$

The above integral equation for A(t') is solved with initial condition

$$A(o) = \pi R_c^2 \tag{22b}$$

32

The solution to this equation is given in Appendix A.

$$\alpha = \frac{A}{\pi R_c^2} = \left[\frac{6}{v} \left[(1 + v\tau)^2 - (1 + v\tau)^{3/2} \right] + (1 + v\tau)^{3/2} \right]^{2/3} \quad (23a)$$

where

$$v = \frac{\bar{u}}{u(h_c)}$$

$$\tau = \frac{u(h_c)\ t'}{2R_c} \quad (23b)$$

Note also

$$a_f = R_c + a_1 = R_c \left[1 + \frac{a_1}{R_c} \right] = R_c \left[1 + \frac{\bar{u}\ t_f'}{R_c} \right]$$

i.e. $a_f = R_c [1 + 2v\ \tau_f]$ \quad (24a)

Therefore

$$L = R_c + a_f = 2R_c [1 + v\ \tau_f] = \text{Downstream length of spread} \quad (24b)$$

Similarly,

$$b_f = R_c \left[1 + \frac{1}{R_c} \int_0^{t_f'} u_{g,\ell}\ dt \right] = R_c \left[1 + 2 \int_0^{\tau_f} \frac{d\tau}{\sqrt{\alpha}} \right]$$

Using equation A-4 of Appendix A, we get

$$b_f = R_c \times \frac{\alpha_f}{[1 + v\ \tau_f]} \quad (25a)$$

i.e. cross stream spread $B = 2b_f = 2R_c \dfrac{\alpha_f}{1 + v\ \tau_f}$ \quad (25b)

Algorithm for Obtaining the Area of Spread

Given: (1) mass of liquid spilled and its density

(2) mean stream velocity, stream depth, stream width, and bed roughness dimension or Manning coefficient

Following is the sequence of calculations.

33

Item #	Obtain the Value of this Parameter	Using the Equation	Remarks
1	e	8	If "e" is not given, and "n" is given
2	Set $h_f = e$	--	
3	$V = \dfrac{M}{\rho_\ell}$	--	Volume of spill
4	$G = g\left(1 - \dfrac{\rho_w}{\rho_\ell}\right)$	--	Effective gravity
5	$A_f = \dfrac{V}{h_f}$	--	Final spread area
6	$F_D = \dfrac{u_s}{\sqrt{Gd}}$	14b	Densimetric Froude Number
7	R_c	15	Critical radius
8	t_c	16	Critical time
9	$A_c = \pi R_c^{\,2}$		Critical area
10	$h_c = \dfrac{V}{A_c}$	18	Critical film thickness
11	$\bar{u}$	21	Mean velocity of water close to the bed
11	$u(h_c) = 1.143\left(\dfrac{h_c}{d}\right)^{1/7} u_s$	13	
12	$v = \bar{u}/u(h_c)$		
13	$\alpha_f = A_f/A_c$		
14	Solve for τ_f iteratively	23	
15	$t_f' = \dfrac{2R_c\,\tau_f}{u(h_c)}$	--	
16	Final time of spread $t_f = t_c + t_f'$		
17	Longitudinal spread $L = 2R_c[1 + v\,\tau_f]$		
18	Lateral spread $B = 2b_f = \dfrac{2\alpha_f}{1 + v\,\tau_f}\,R_c$	25	

34

SPECIFIC EXAMPLE

Chemical Data

Chemical spilled:	CHLOROFORM

Volume of liquid spilled (assumed) $= V = 8,000$ gallons $= 30.28 \text{ m}^3$

Density of liquid $= \rho_\ell = 1490 \text{ kg/m}^3$

Viscosity of liquid $\mu_\ell = 0.47 \times 10^{-3} \text{ N s/m}^2$

River Data

Mean velocity $= u_s = 1 \text{ m/s}$

Width of river $= W = 150 \text{ m}$

Depth of river $= d = 8 \text{ m}$

Manning coefficient $= n = 0.025$

Water Data

Kinematic viscosity $= \nu_w = 10^{-6} \text{ m}^2/\text{s}$

Calculations

To show that for most of the river depth, the water flow is very turbulent.

Hydraulic radius $R_h = \dfrac{150 \times 8}{(8 \times 2 + 150)} = 7.23 \text{ m}$

Frictional velocity due to bed roughness $= u^* = \dfrac{3.124 \ u_s \ n}{R_h^{1/6}} = \dfrac{3.124 \times 1 \times .025}{(7.23)^{1/6}}$

$$= 5.62 \times 10^{-2} \text{ m/s}$$

The top of the laminar sublayer from the wall in a turbulent flow is given by:

$$y^+ = \frac{y u^*}{\nu_w} \approx 30$$

Hence $y = \dfrac{30 \times 10^{-6}}{5.62 \times 10^{-2}} = 5.34 \times 10^{-4} \text{ m}$

i.e., from this height above the river bed surface, up to the top of the water surface, the flow is very turbulent. This justifies the use of 1/7th power law in equation 13.

35

$$e = 10^{\left[3.8173 - \dfrac{8.571 \times 10^{-2}}{0.025}\right]}$$

$$= 2.45 \text{ inches}$$
$$= 6.22 \times 10^{-2} \text{m}$$

Effective gravity $= G = 9.8 \times (1 - \dfrac{1000}{1490}) = 3.223 \text{ m/s}^2$

Mean height of bed roughness $= h_f = e = 6.22 \times 10^{-2} \text{m}$
(See equation 8)

Final spread area $A_f = \dfrac{V}{h_f} = \dfrac{30.28}{6.22 \times 10^{-2}} = 486.8 \text{ m}^2$

Densimetric Froude number $F_D = \dfrac{1}{\sqrt{3.223 \times 8}} = 0.197$
(See equation 14b)

Critical height $h_c = .9783 \times (.197)^{2.8} \times 8 = 8.27 \times 10^{-2} \text{ m}$
(See equation 14a)

Critical radius $R_c = \dfrac{0.5704}{.197^{1.4}} \sqrt{\dfrac{30.28}{8}} = 10.8 \text{ m}$
(See equation 15)

Critical time $t_c = \dfrac{0.2504}{0.197^{2.8}} \sqrt{\dfrac{30.28}{8^2 \times 3.223}} = 9.07 \text{ s}$

Critical area $A_c = \pi R_c^2 = 366 \text{ m}^2$

Velocity of stream at $h_c = u_c = 1.143 \left(\dfrac{8.27 \times 10^{-2}}{8}\right)^{1/7} = 0.595 \text{ m/s}$
(See equation 13)

Mean velocity between height h_c and h_f
(See equation 21)

$$\bar{u} = 1.0 \times 8^{-1/7} \left[\dfrac{(8.27 \times 10^{-2})^{8/7} - (7.41 \times 10^{-2})^{8/7}}{(8.27 \times 10^{-2}) - (7.41 \times 10^{-2})}\right] =$$

$$= 0.590 \text{ m/s}$$

Hence (equation 23b) $v = \dfrac{0.590}{0.595} = 0.992$

and $\alpha_f = \dfrac{A_f}{A_c} = \dfrac{486.8}{366} = 1.329$

Solving for τ_f from equation 23a, we have

$$1.329^{1.5} = \left[\dfrac{6}{v} (Z^{4/3} - Z) + Z\right] \text{ where } Z = (1 + v\, \tau_f)^{3/2}$$

$$1.531 = 6.913 (Z^{4/3} - Z) + Z$$

z	$\frac{6}{v}(z^{4/3} - z) + z$
1.0	1.00
1.1	1.345
1.2	1.720
1.15	1.529
1.151	1.533
1.1505	1.531

Hence, $Z_f = 1.150$

$$(1 + v\,\tau_f) = (1.150)^{2/3} = 1.098$$

$$\tau_f = .0988$$

Hence, final spread time $t_f = t_c + \dfrac{.0988 \times 2 \times 10.8}{.593} = 9.07 + 3.585 = 12.66$ s

Longitudinal spread $L = 10.8 \times 2 \times 1.03765 = 23.73$ m

Lateral spread $B = 2 \times 10.8 \times \dfrac{1.117}{1.03765} = 26.13$ m
(see equation 25b)

The spread shape is almost a perfect circle.

DISCUSSION

Methods have been discussed to predict both the trajectory during sinking and the consequent spreading of a heavier than water liquid on the river bed surface. The impact time and locations of the sinking liquid with the river bed is determined assuming that the instantaneously released liquid is broken up into small liquid drops which later sink due to the action of gravity, at the same time being carried downstream by the stream current.

The model for spreading on the river bed is based on the assumption that the liquid spread ceases when the mean film thickness of the liquid is equal to the bed roughness. Once the liquid sinks into the crevices of the river bed, it is essentially held there, because the

37

water velocities below the roughness heights are small. This means
that further spreading of the liquid is either totally nonexistant
or is very small and can therefore be neglected.

It is needless to say that the final answer (such as duration of
spread and the final dimensions of spread) depends on the mean bed
roughness. An expression has been derived to connect the usual Manning
roughness coefficient n and the bed roughness e (equation 8). It
should be noted that the equation is a dimensional equation and has
limited applicability range. Equation 8 should be used only when no
direct data are available as to the river bed roughness dimension.
Where such roughness data are available, we recommend the use of that
data rather than equation 8.

The limitations of the model presented arise from the lack of
experimental data to compare the predicting with. For example, it
is not very clear whether all of the liquid spilled would be broken up
into liquid globules. Nevertheless, this is a key assumption for
finding the location at which the liquid reaches the river bottom.
The more serious limitation of the model is in the necessity to know
the mean bed thickness. This number is quite important in that a 50%
error in the evaluation of this results in a corresponding 50% error
in the estimation of the final area of spread. Since the total dis-
solution rate of a slowly soluble liquid is dependent on the surface
area exposed (Chapter II), wrong estimation of bed roughness would
result in serious errors in the hazard estimation.

It is, however, felt that notwithstanding the limitations alluded
to above, a reasonably simple model has been developed for studying
the spread of heavier than water liquid on the river bed. Such a model
was not available in the literature.

The model by itself has limited utility, but it is an essential input
for calculating the dissolution rate of slowly dissolving chemicals. The
latter phenomenon is treated in Chapter II.

38

CONCLUSIONS

A model has been worked out to obtain the duration of spread on the river bed of a heavier than water liquid. The model is based on a two-regime spread theory. In the first regime, the spread is essentially gravity inertia dominated with stream flow having no effect on the spread. In the second regime, the spread is determined by the velocity distribution in the river.

It is seen from the example that the spread takes place in relative'y short duration, and for the given example, the aspect ratio of spread is close to unity. It is concluded that the spread will be more skewed if the mean stream velocity is larger.

The model proposed for the descent of the heavy liquid released on the surface is similar to the ones proposed in an earlier report. The liquid is assumed to break up into liquid drops, sink, and finally coalesce to form the spreading pool on the river bed. Lack of experimental data precludes the development of any sophisticated analytical model at this stage.

To solve the equation

$$A(t') = \pi R_c^2 \left[1 + \frac{c \sqrt{VG}}{R_c} \int_0^{t'} \frac{dt}{\sqrt{A(t)}} \right] \left[1 + \frac{\bar{u} \, t'}{2 \, R_c} \right]$$

(A-1)

with $A(o) = \pi R_c^2$

(A-2)

Let

$$\alpha = \frac{A(t')}{A(o)} = \frac{A(t')}{\pi R_c^2} = \text{nondimensional area}$$

$$\tau = \frac{u(h_c) t'}{2 \, R_c} = \text{dimensionless time}$$

(A-3)

$$v = \bar{u}/u(h_c)$$

Hence $\alpha(\tau) = \left[1 + \frac{2 \, c \sqrt{VG}}{u(h_c) \sqrt{A(o)}} \int_0^\tau \frac{d\tau}{\sqrt{\alpha(\tau)}} \right] \left[1 + v \, \tau \right]$

From equation 12, we see that

$$\frac{c \sqrt{VG}}{u(h_c) \sqrt{A(o)}} = 1$$

Hence the equation reduces to

$$\alpha(\tau) = \left[1 + 2 \int_0^\tau \frac{d\tau}{\sqrt{\alpha(\tau)}} \right] \left[1 + v \, \tau \right] \quad \text{with } \alpha(o) = 1$$

(A-4)

Differentiating the LHS and RHS with respect to τ we get

$$\frac{d\alpha}{d\tau} = \left[1 + v \, \tau \right] \frac{2}{\sqrt{\alpha(\tau)}} + v \left[1 + 2 \int_p^\tau \frac{d\tau}{\sqrt{\alpha(\tau)}} \right]$$

40

Substituting for the second term on the RHS from equation A-4, we get

$$\frac{d\alpha}{d\tau} = \frac{2}{\sqrt{\alpha}} [1 + \nu \tau] + \frac{\nu \alpha}{[1 + \nu \tau]} \tag{A-5}$$

Let

$$\xi = 1 + \nu \tau$$
$$\eta = \alpha^{3/2} \tag{A-6}$$

Substituting A-6 in A-5 and simplifying we get

$$\frac{d\eta}{d\xi} = 3 \frac{\xi}{\nu} + \frac{3}{2} \frac{\eta}{\xi} \quad \text{with } \eta = 1 \text{ at } \xi = 1 \tag{A-7}$$

The solution to the above equation (Bernoulli form) is

$$\eta \, \xi^{-3/2} = \frac{3}{\nu} \int \xi^{-1/2} \, d\xi + \text{constant of integration}$$
$$\eta = \frac{6}{\nu} \xi^2 + \text{const } \xi^{3/2}$$

with $\eta = 1$ at $\xi = 1$ we get

$$\eta = \frac{6}{\nu} \left[\xi^2 - \xi^{3/2} \right] + \xi^{3/2} \tag{A-8}$$

i.e.,

$$\alpha(\tau) = \left[\frac{6}{\nu} \left[[1 + \nu \tau]^2 - (1 + \nu \tau)^{3/2} \right] + (1 + \nu \tau)^{3/2} \right]^{2/3} \tag{A-9}$$

NOMENCLATURE

All dimensional quantities are assumed to be in appropriate S.1. Units.

$A(o)$	= Area of spread of the pool at critical condition	m^2
$A(t')$	= Area of spread of the liquid at any time	m^2
A_c	= $A(o)$ = area of pool at criticality	m^2
A_f	= Final pool spread area	m^2
a	= Semi-major axis (in the stream direction) of the elliptical spread area during the shear flow induced spread (see Figure 1-2b)	m
a_1	= Distance traveled by the downstream edge	m
B	= Total length of spread of the liquid pool in the cross stream direction	m
b	= Semi-major axis in the cross stream direction (see Figure I-2b)	m
b_1	= Distance traveled by cross stream front of liquid in time t'	m
c	= Constant in equation 11 for the velocity of the front	
c_1, c_2	= Empirical constants obtained by fitting a best line to the results in Table I-1	
d	= River depth	m
e	= Mean height of the roughness of the river bed	m
F_D	= Densimetric Froude number (see equation 14a)	
G	= Effective gravitational acceleration for liquid spreading $$g(1 - \frac{\rho_w}{\rho_\ell})$$	m/s^2
g	= Acceleration due to gravity	m/s^2
$h(t')$	= Height of film at any time t'	m
h_c	= Liquid film height at critical condition	m
h_f	= Final height of the liquid film = e	m
h_ℓ	= Mean height of the liquid film of the spreading liquid at any time	m
L	= Total length of spread of the pool in the streamwise direction	m

42

n	= Manning friction factor for the river	
R	= Mean radius of the largest stable liquid drop (see equation 1)	m
R_c	= Radius of the pool at the end of gravity spread (critical condition) (see equation 15)	m
Re_d	= Flow Reynolds number based on depth = $\dfrac{U\,d}{\nu_w}$	
Rh	= Hydraulic depth of the river	m
t	= Time after spill	s
t'	= Time after the pool spread attains critical condition = $(t - t_c)$	s
t_c	= Time to critical condition (see equation 16)	s
t_{st}	= Settling time for the liquid drops (see equation 5)	s
U(R)	= terminal velocity of settling of the liquid drops in the river (see equation 2)	m/s
u(y)	= Stream velocity at height y from the bed surface	m/s
$\bar{u}$	= Average stream velocity over a height h_c from the bottom of the river (see equation 21)	m/s
$\overline{u'^2}$	= Mean square fluctuating velocity in the velocity in the river	$(m/s)^2$
u*	= Frictional velocity in river = $\dfrac{3.124\,u_s\,n}{R_h^{1/6}}$	m/s
$u_{g,\ell}$	= Gravity spreading velocity of liquid pool (see equation 11)	m/s
u_s	= Mean stream velocity	m/s
V	= Volume of liquid spilled	m^3
v	= $\dfrac{\bar{u}}{u(h_c)}$ = Dimensionless average velocity over o – h_c height (see equation A-3)	
W	= Width of the river	m
X	= Downstream distance at which the liquid drops released at the river surface would reach the bottom	m
y	= Vertical distance from the river bed	m
Z	= $(1 + v\,\tau_f)^{3/2}$	

Greek Letters

α = Ratio of liquid spread area at any time after criticality to the spread area at criticality (see equation A-3)

η = $\sigma^{3/2}$ (see equation A-6)

ν_w = Kinematic viscosity of water m^2/s

ξ = $1 + \nu \tau$ (see equation A-6)

ρ_ℓ = Density of liquid spilled kg/m^3

ρ_w = Density of water kg/m^3

σ = Interfacial tension between liquid and water N/m

τ = Dimensionless time = $\dfrac{u(h_c) \, t'}{2 \, R_c}$ (see equation A-3)

Subscripts

c = Critical condition

f = Final value

ℓ = Liquid

w = Water

Superscript

c = Critical

44

REFERENCES

1. P. Raj and A. S. Kalelkar, "Assessment Models in Support of the Hazard Assessment Handbook," (CG-446-3), January 1974, Chapter 12, page 171.

2. V. Streeter, "Handbook of Fluid Dynamics," McGraw-Hill, 1961, p. 18-6, equation 18.2.

3. F. S. Merrit, Editor, "Standard Handbook for Civil Engineers," McGraw Hill, New York, 1968, page 21-48, Table 21-11.

4. V. Streeter, "Handbook of Fluid Dynamics," McGraw-Hill, 1961, p. 3-17, equation 3.26.

5. S. Goldstein, "Modern Development in Fluid Mechanics", Dover Publications, New York.. 1965.

6. Dr. ING M. Selim Yalin, "Mechanics of Sediment Transport", Oxford Ed. 1972.

CHAPTER II

DISSOLUTION AND DISPERSION OF CHEMICALS OF FINITE SOLUBILITY

OBJECTIVES

The objectives of the analyses presented in this chapter are to predict the rate of dissolution of a low solubility chemical in water, the dispersion of the dissolved chemical, and the duration and extent of hazard.

INTRODUCTION

There are a number of chemicals, both solid and liquid, in the CHRIS chemicals list that have low solubility in water.[*] A list of such hazardous chemicals having solubility less than 1% is given in Appendix D.

When any of the chemicals in the above list is spilled on the waterway (as in a river for example), there exists a danger that the chemical will dissolve slowly, thereby presenting the hazard over an extended period of time. Even though low solubility leads to low levels of chemical concentrations in water, it does not automatically follow that the hazard is also small because some of these chemicals are hazardous to human health as well as toxic to aquatic life, even in extremely low concentrations. In addition, some of these chemicals may react with other dissolved chemicals in water producing very undesirable compounds. Therefore, there exists a need to understand and be able to predict the dissolution rates of slowly dissolving chemicals in streams. Also, it is necessary to know not only the rate of dissolution and the consequent pollutant concentration in water but also the duration and extent of the hazard zone. The latter is of particular importance when decisions have to be taken to initiate appropriate remedial measures following a spill into water (especially when the water is used for a city's drinking water needs).

---

[*]The term "solubility" denotes the saturation concentration of the given chemical in water at standard temperature and pressure. It is usually expressed in kg (chemical) per 100 kg of water at 15°C and 1 atm pressure. The term "low solubility" implies a less than 1% solubility.

The rate of dissolution of a chemical depends on the nature of the chemical itself (such as its solubility, density, viscosity, etc.) and the environmental conditions (such as stream velocity, turbulence level, bed structure, water temperature, and total water flow). Liquid chemicals which are heavier than water sink to the bottom when spilled on water surface, spread on the river bed, and may even percolate to interior of the bed soil. These will later dissolve slowly, polluting the river over a long period of time. The spill of a lighter-than-water chemical on the water surface results in the formation of a pool which moves with the stream current if there are no obstructions or dead zones in the streams. During this downstream movement of the chemical pool, the chemical dissolves slowly due to the action of the stream turbulence. A third type of the hazard is represented by solid chemicals of low solubility. Depending on the size and density of the solid particles, these may sink directly to the river bottom and then dissolve slowly (as in the case of heavy liquids) or may be in suspension in water. In the case of the latter, the situation is similar to the case of surface liquid pool.

In Section 1 of this chapter, a model is developed to predict the dissolution rate from a stagnant pool of heavy, liquid chemical at the bottom of a river. The part that deals with the spill, movement to the river bed, and the subsequent spreading, has been modeled and discussed in Chapter I.

In Section 2, the dissolution of lighter-than-water pool is modeled and discussed. Finally, in Section 3, the models are used to predict the chemical concentration using dispersion models. Specific examples for each section are given.

THEORETICAL DEVELOPMENT

Section 1: Dissolution of Stagnant Pool of Heavy, Slightly Soluble Liquid at the Bottom of a Moving Body of Water

In this section, a model is developed to predict the dissolution rate of a liquid chemical, which is heavier than water and which has low solubility. The liquid is assumed to be present on the river bed in the form of an immobile pool. The assumptions made in deriving the model are listed below.

47

Assumptions

- The liquid pool area exposed to water remains the same throughout the dissolution process.
- The liquid dissolution is controlled by the hydrodynamics in the river
- No gross movement of the pool occurs during the dissolution period.
- No interface between the liquid and water is relatively flat.
- Two-dimensional mass transfer model is used.
- The effect due to the edges in the dissolution process is small and hence neglected.

The dissolution of the liquid pool is modeled using the analysis of turbulent flow mass transfer on a flat plate.[1] The essential features of the model are shown schematically in Figure II-1. The liquid pool at the bottom of the river is of thickness "H," which is assumed to be the "mean thickness" of the bed roughness. Because of the flow of the water on top of the liquid pool, a concentration boundary layer is built up, and hence the pool is consumed at higher rates in the regions near the leading edge compared to the rates of dissolution at the trailing regions of the pool.

U = Mean Velocity

Concentration Boundary Layer

Liquid on the River Bed in the Form of a Pool

H

River Bed Roughness
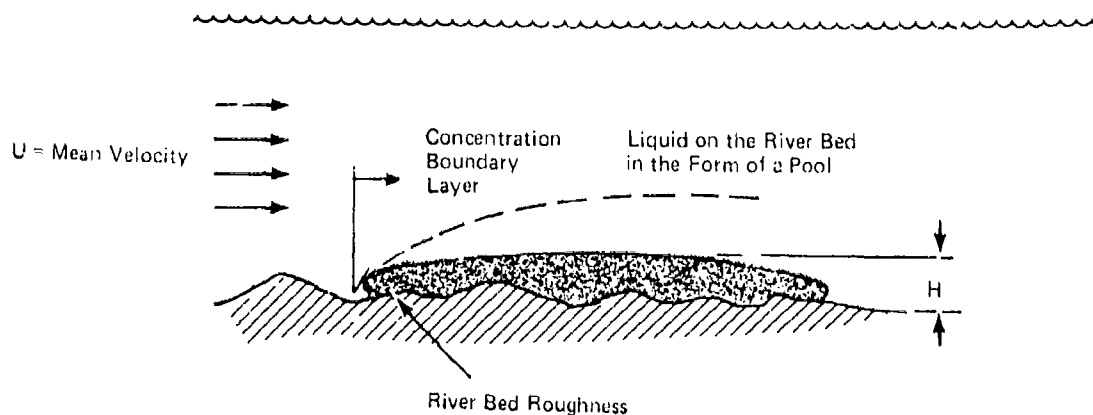
FIGURE II-1   Schematic Diagram Illustrating the Position of the Dissolving Chemical on the River Bed

48

We write the following rate of dissolution equation[*]

$$N = \bar{K} A \rho_w (C_{surf} - C_{bulk}) \tag{1}$$

Because of the large quantity of water flow rate in a navigable river and the generally slow dissolution rate of chemicals, we can assume, without loss of accuracy,

$$C_{bulk} = 0 \tag{2}$$

The equilibrium concentration of the chemical, on the surface of pool at the bottom of the river, namely, C_{surf}, is obtained from the solu-bility properties of the chemical. Specifically, we treat

$$C_{surf} = C_{sat}(T) \tag{3}$$

The mean mass transfer coefficient $\bar{K}$ in equation 1 is estimated from j factor analogies of heat and mass transfer.[2,3] The average j factor for turbulent flow over a flat plate is (for $Re_L > 1.5 \times 10^4$)

$$j_D = \left(\frac{\bar{K}}{u}\right) Sc^{2/3} = \frac{0.037}{Re_L^{0.2}} \tag{4}$$

where Re_L = Reynolds number based on the length of the pool = $\dfrac{uL}{\nu_w}$

In a river flow, and for the conditions of liquid spill and dissolution that might occur due to a barge accident, it is expected that the pool Reynolds number will by far exceed the value 1.5×10^4. In addition, actual data from the dissolution of solid flat plates indicate slightly higher j_D values than that given by equation 4. (However, when meticulously prepared experimental specimen were used, experimental j_D values were much closer to that predicted by equation 4.)

Substituting equation 4 in 1 and noting the conditions of equations 2 and 3, we get

---

[*]See the nomenclature for the definitions.

$$N = u\, C_{sat}\, A\, \rho_w\, \frac{0.037}{Sc^{2/3}}\, \frac{1}{Re_L^{0.2}} \qquad (5a)$$

$$N = 0.037\, C_{sat}\, DW\rho_w\, Sc^{1/3}\, Re_L^{0.8} \qquad (5b)$$

where W is the width of the pool.

In deriving the above equation it is assumed that the temperature of the liquid is the same as that of the stream and C_{sat} corresponds to this temperature.

It is recalled that equation 5b is strictly correct only for a rectangular pool of downstream length L and width W.
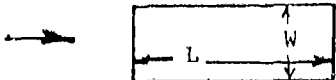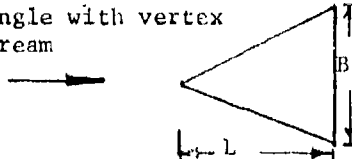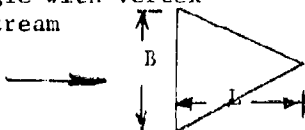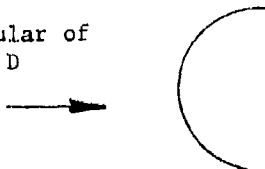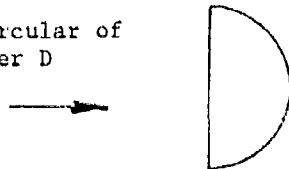
For other shapes of pool area (such as a circle or an ellipse or any other shape) a shape factor has to be introduced into the equation to take into consideration the nonrectangular shape of the liquid pool. The values of the shape factor to be used are given in Table 11-1 and derived in Appendix B. Based on the results of Appendix B, we rewrite equation 5b as

$$N = S[0.037\, C_{sat}\rho_w DW\, Sc^{1/3}\, Re_L^{0.8}] \qquad (6)$$

where now the width W is interpreted as the width of an _equivalent_ rectangular pool of length L and having the same area as the actual pool.

Equation 6 is valid only when both the hydrodynamic boundary layer and the concentration boundary layer grow from zero thickness at the leading edge (of the liquid pool). In a river, however, the hydrodynamic boundary layer is fully developed and the presence of a liquid pool does not affect it. An analysis considering this fully developed character of the hydrodynamic boundary layer and the developing concentration boundary layer is worked in Appendix C. The main result from this analysis is that the dissolution rate depends on the flow depth in the river. This is because of the dependence of the velocity profile on the depth of the river. The results from this modified analysis give

50

TABLE 11-1

Shape of the Pool	Value of W	w = W/L	Value of S
Rectangular L x W	W	w	1
Elliptical Major axis L Minor axis B	$\frac{\pi}{4} B$	$\frac{\pi}{4} \frac{B}{L} =$ $\frac{\pi}{4} b$	1.075
Circular of diameter D	$\frac{\pi}{4} D$	$\frac{\pi}{4}$	1.075
Triangle with vertex upstream	$\frac{B}{2}$	$\frac{B}{2L}$ $= \frac{b}{2}$	$= 1.111$ $\frac{1}{0.9}$
Triangle with vertex downstream	$\frac{B}{2}$	$\frac{B}{2L}$ $= \frac{b}{2}$	$= 1.111$ $\frac{1}{0.9}$
Semicircular of diameter D	$\frac{\pi}{4} D$	$\frac{\pi}{2}$	1.041
Semicircular of Diameter D	$\frac{\pi}{4} D$	$\frac{\pi}{2}$	1.041

mean S = 1.076

$$\overline{j_L} = \frac{\overline{K(L)}}{u_m} Sc^{2/3} = 0.0343 \frac{Sc^{2/27}}{Re_L^{2/9}} \left(\frac{L}{d}\right)^{1/9} \qquad (7)$$

and therefore N is given by

$$N = S[0.0343 \, \rho_w \, C_{sat} \, DW \, Sc^{11/27} \, Re_L^{7/9} \, \frac{L}{d}^{1/9}] \qquad (8)$$

It is seen by comparing equations 6 and 8 that the powers on the Sc and Re_L have not changed very much. In addition, the effect of depth appears in equation 8 with a 1/9th power, and therefore its effect is expected to be small. The example considered below illustrates the small differences obtained in the dissolution rates using equations 6 and 8.

Numerical Example for Section 1

Chemical

Chemical spilled	CHLOROFORM ($CHCl_3$)
Density of $CHCl_3$	$= \rho_{liq}$ = 1490 kg/m^3
Molecular weight	= M = 119.4 kg/kg mole
Solubility at 293°K	$= C_{sat} \begin{cases} = 0.8 \text{ kg/100 kg of water} \\ = 8 \times 10^{-3} \end{cases}$
Diffusion coefficient in water	D = 1.06×10^{-9} m^2/s

Water

Density of water	$= \rho_w$ = 1000 kg/m^3
Kinematic viscosity (at 293°K)	$= \nu_w$ = 10^{-6} m^2/s

Pool data [*]

Assumed length of pool	L	= 10 m
Width of pool	W	= 5 m
Depth of liquid pool	H	= 0.04 m

---

[*]Liquid pool dimensions are assumed for the sake of illustrating the calculation procedure.

Environmental Conditions

Stream velocity (mean) = u_s = 1 m/s

Stream depth = d = 5 m

Water temperature (mean) = T_w = 273°K

Hence, Schmidt number = Sc = $\dfrac{\nu_w}{D}$ = $\dfrac{10^{-6}}{1.06 \times 10^{-9}}$ = 943.4

Reynolds number (based on the length L) = Re_L = $\dfrac{1 \times 10}{10^{-6}}$ = 10^7

Shape factor (for rectangular pool) S = 1

Substituting Re_L, Sc, C_{sat}, W and D in equation 6, we get

$$N_{flat\ plate} = 1 \times .037 \times 8 \times 10^{-3} \times 10^3 \times 1.06 \times 10^{-9} \times 5 \times (943.3)^{1/3} (10^7)^{0.8}$$

$$= 6.125 \times 10^{-3} \text{ kg/s}$$

Total mass of liquid in the pool = ρ_{liq} LWH = 1490 × 10 × 5 × .04 = 2980 kg

Total time for dissolution = t_{total} = $\dfrac{2980}{6.125 \times 10^{-3}}$ ≃ 486530 secs ≃ 135 hours

If instead we use equation 8, we get

$$N = 10^3 \cdots .0343 \times 8 \times 10^{-3} \times 1.06 \times 10^{-9} \times 5 \ (943.4)^{11/27} (10^7)^{7/9} (10/5)^{1/9}$$

$$= 7.12 \times 10^{-3} \text{ kg/s}$$

Hence, t_{total} = $\dfrac{2980}{7.12 \times 10^{-3}}$ ≃ 418539 s ≃ 116.3 hours

The concentration boundary layer thickness δ at the trailing edge of the pool (see equation 8c of Appendix C)

$$\frac{\delta}{L} = \frac{0.3375}{Sc^{14/27} Re_L^{7/36}} \left(\frac{d}{L}\right)^{1/36} = \frac{0.3375 \ (5/10)^{1/36}}{(943.7)^{14/27} (10^7)^{7/36}} = 4.14 \times 10^{-4}$$

Hence, δ = 4.14 × 10^{-3} m

This is much smaller than the depth of the river. Hence, for calculating the stream pollutant level concentration downstream of the dissolving pool, we can assume that the source is a line source of width W and of total strength N (kg/s). This source is assumed to be located at the bottom of the river.

Section 2: Dissolution of Lighter Than Water, Low Solubility Chemical

There are several chemicals in the CHRIS list of chemicals which have low solubility and density lower than that of water. When any of these chemicals are spilled on water, in, say, a river, the chemical forms a surface pool, at the same time is carried downstream with the current. This pool of liquid slowly dissolves in water due to the action of stream turbulence. The ability of the pool of the chemical to remain as one continuous area depends on not only the chemical properties (such as the surface tension) but also on the hydrodynamics of flow in the river (such as intensity of turbulence in the stream, possibility of obstructions in the river like a bridge pier, etc.).

In this section, a model is developed to obtain the dissolution rate of a chemical as a function of stream hydrodynamic conditions. The model is based essentially on the surface renewal theory first developed by Higbie[4] and later modified by Danckwerts.[5] However, the model derived below uses the latest developments in the above theories.

Figure II-2 shows the essentials of the model. As the liquid chemical pool floats down river, it dissolves due to the action of the turbulent eddies. The eddies are assumed to "contact" the pool for varying time intervals depending on the eddy size and absorb the chemical. This absorption process is controlled by the molecular diffusivity of the chemical in water. These eddies are replaced by new ones after the elapse of a duration equal to a "mean renewal time." Those eddies that absorb the chemical from the pool are assumed to mix with the bulk flow in the river. Such an absorption is described by "eddy" cell models."

54
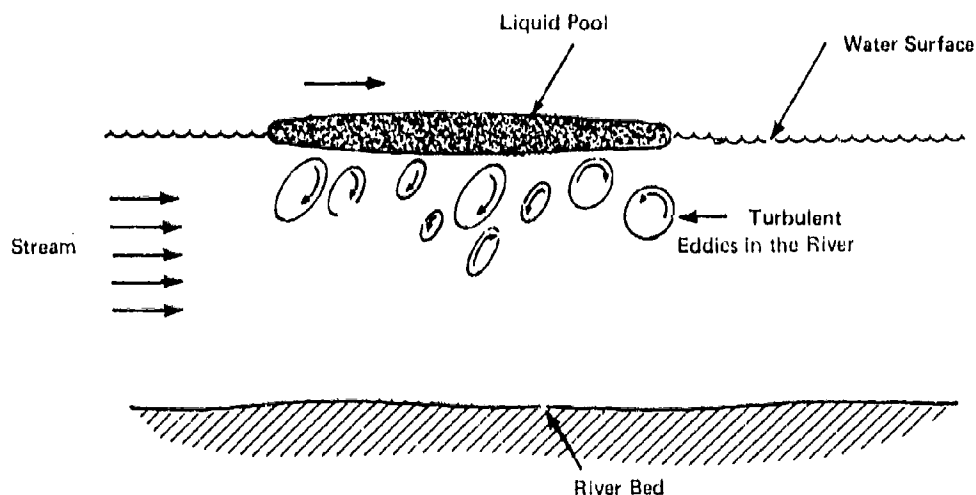
FIGURE II-2 Dissolution of Lighter Than Water Chemical
During Its Downstream Travel

Eddy cell models described above have been theoretically
investigated by Fortescue and Pearson[6] and Lamant and Scott.[7]
The primary aim in all of the above works has been to predict
the value of the mass transfer coefficient for gas absorption into a
turbulent liquid flow. The differences in the predicted results by
the above two groups arise due to the relative importance given to
large and small size eddies in the stream. It is found that Fortescue's
analysis agrees better with experimental data for both flow in tubes
and for flow in rivers (aeration of polluted water). As such, the
model given by Fortescue is given below and adopted for use in CHRIS.
An excellent review of the various surface renewal models in the
literature and their applicability to predicting the reaeration rates
in rivers is given by Kramer[8] and for gas absorption by turbulent
fluid in three different types of flow circumstances by Theofanous,
et al.[9]

Fortescue gives a correlation of the type

$$\bar{K} = 1.46 \left[D\sqrt{\overline{u'^2}} / \Lambda \right]^{1/2} \tag{9}$$

55

where

$$\sqrt{\overline{u'^2}} = \text{turbulent intensity (due to the fluctuating component) velocity (m/s)}$$

$$\Lambda = \text{mean eddy size or integral length scale (m)}$$

where the mass transfer coefficient is described by the equation

$$\dot{m}''_{dis} = \overline{K}\rho_w (C_{sat} - C_{bulk}) \tag{10}$$

where

$$\dot{m}''_{dis} = \text{rate of dissolution of the liquid in water per unit interface area (kg/m}^2\text{s)}$$

In order to use equations 9 and 10 to predict the dissolution rate of the liquid pool in the river, the river turbulence characteristics have to be known ($\overline{u'^2}$ and Λ). O'Connor and Dobbins[10] suggest the use of the following to estimate river turbulence:

$$(\overline{u'^2})^{1/2} = 0.1\ u \tag{11a}$$

$$\Lambda = 0.1\ d \tag{11b}$$

Using the above criteria and equation 9, Fortescue and Pearson[6] have shown that the experimental data on mass transfer coefficients for reaeration of natural streams and the theoretically predicted values agree quite well. The theoretical value is slightly greater than the observed value. Therefore, the use of equation 9 together with equations 11a and 11b result in an increased dissolution rate which is conservative from the point of view of pollution hazards in the river. An example is given below to illustrate the calculation procedure.

Numerical Example for Section 2

Chemical Properties from Reference 11

Chemical	ETHYL BUTANOL (EBT)
Density (liquid) at 293°K	= 834 kg/m^3
Viscosity ratio (μ_{liq}/μ_{water})	= 0.7
Solubility	= 0.43 kg/100 kg of water
Boiling temperature	= 419°K

56

Quantity of chemical spilled = 1000 tons
(instantaneously) $\approx 10^6$ kg

Diffusivity in water $\approx 0.78 \times 10^{-9}$ m^2/s
(calculated by the method given in
Reference 11)

Environmental Conditions

Water temperature 15°C = 288°K

River width $\approx$ 1000 m

River depth   = 15 m

Mean water velocity   = 2 m/s

Calculations

Using equations 11a and 11b, we have

$$\sqrt{\overline{u^2}} = 0.1\ u = 0.2 \text{ m/s}$$

Λ = integral length scale = 0.1 x d = 1.5m

Hence, K_L from equation 9 is

$$K_L = 1.46[0.78 \times 10^{-9} \times 0.2/1.5]^{0.5} = 1.489 \times 10^{-5}$$

The dissolution rate from equation 10 is

$$\dot{m}''_{dis} = 1.489 \times 10^{-5} \times 10^3\ [\frac{0.43}{100} - 0] = 6.41 \times 10^{-5}\ kg/s\ m^2$$

This is an extremely slow rate of dissolution in the stream.

The concentration of the pollutant in the river is calculated using the water dispersion models indicated in the next section.

Section 3: Water Dispersion of Slowly Dissolving Chemicals

The dissolution of slowly dissolving chemicals has been discussed in the first two sections of this report. It is seen that if the chemical is heavier than water, the source of pollution is fixed relative to the river bottom. (The chemical dissolves in water from a pool formed on the river bed.) The dispersion from such a case can be modeled as if the source were assumed to be a line source of pollutant, located on the river bed.

In the case of lighter than water chemical, the chemical pool (which may be expanding due to the action of buoyancy forces and

57

stream turbulence) is transported downstream by the water flow in
the river. The dissolution of such a chemical and the subsequent
dispersion of the chemical in the stream may be modeled using a
traveling, continuous source on the water surface. These two models
are derived below.

(i) Finite Width, Continuous Line Source at the Bottom of the River

The physical system modeled for dispersion is schematically illustrated
in Figure II-3. The source is considered to be a line source at the
downstream end of the pool.
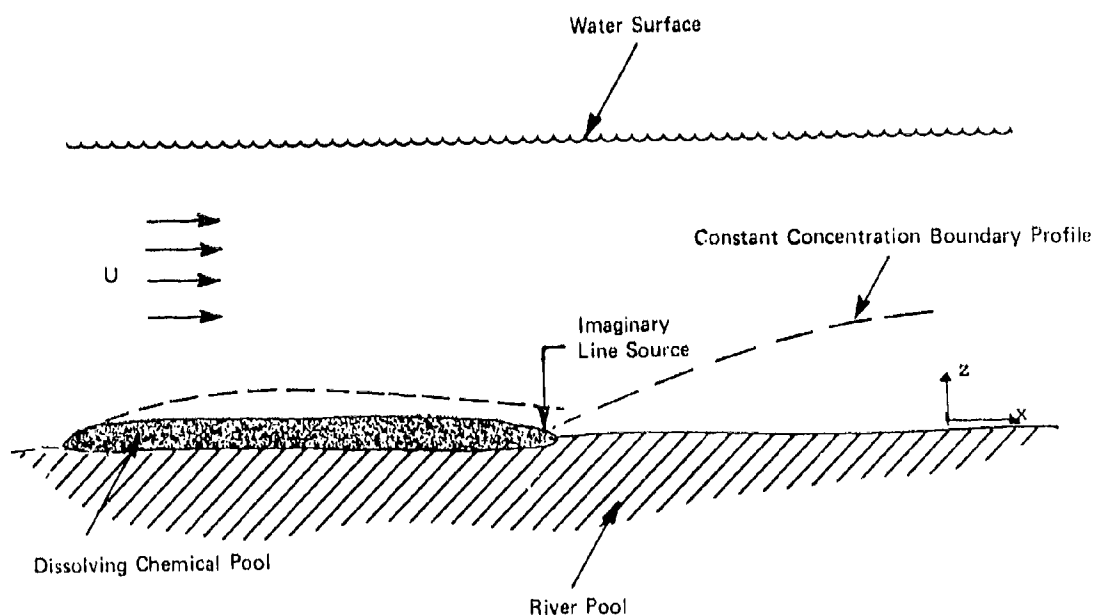
FIGURE II-3   Line Source Description of the Dispersion of Chemical
from a Stationary Pool

Two formulae are presented to calculate the river concentration.
The first is to be used when the location of the point at which con-
centration is to be known is close to the back edge of the pool
("nearfield"). The second formula is used when the observation point
is far off. An estimate of the critical distance beyond which the
"farfield" approximation is to be used is also given. The concentration
at any downstream position of the river is given by

Nearfield

$$C(x,y,z,t) = C_{max}\left[e^{-\left(\frac{z}{s_z}\right)^2} + e^{-\left(\frac{z-2d}{s_z}\right)^2}\right]\left[\text{erf}\left(\frac{y + B/2}{s_y}\right) - \text{erf}\left(\frac{y - B/2}{s_y}\right) + \epsilon\right] \quad (12)$$

where

$$C_{max} = \frac{\dot{m}'}{2\rho_w\sqrt{\pi u X e_z}}$$

$$s_z = \sqrt{\frac{4Xe_z}{u}} \qquad\qquad\qquad\qquad\qquad (13)$$

$$s_y = \sqrt{\frac{4Xe_y}{u}}$$

ϵ = correction term which takes into account the presence of the side walls of the channel

$$\epsilon = \left[\text{erf}\left(\frac{y - W_R + \frac{B}{2}}{s_y}\right) - \text{erf}\left(\frac{y - W_R - \frac{B}{2}}{s_y}\right) + \text{erf}\left(\frac{y + W_R + \frac{B}{2}}{s_y}\right) - \text{erf}\left(\frac{y + W_R - \frac{B}{2}}{s_y}\right)\right] \quad (14)$$

z = distance above the bottom of the river

Farfield

Average concentration under __steady state__ conditions is determined from the continuity equation

i.e. $$\bar{C} = \frac{\dot{m}}{W_R d \rho_w u} \qquad\qquad\qquad\qquad (15)$$

It can be shown that after a downstream distance X_{cri} given by

$$X_{cri} = \left(\frac{W_R}{B}\right)^2 \left(\frac{ud}{e_z}\right) d \quad \frac{1}{4\pi} \qquad\qquad (16)$$

the peak concentration given by equation 13 will be less than that given by 15. Hence, the dividing line between "nearfield" and "farfield" could be taken as $X_{critical}$.

The values of e_z and e_y etc. used in the above equations have to be evaluated for each river, using the conditions of velocity, bed

59

roughness, etc. These methods have been indicated in "Assessment Models in Support of the Hazard Assessment Handbook (CG-446-3)" (rep. # CG-D-65-74).

The width (B) of the line source could be considered equal to the width of the equivalent rectangular source (see Appendix A) for the water dispersion calculations.

(ii) Moving Source on the Surface of the River

A slowly dissolving and lighter-than-water chemical introduces the pollutant (chemical) into the water stream continuously. The location of the source changes every instant because the pool of chemical is floating downstream at the stream velocity. Because of this source motion, the concentration felt at any particular location of an observer in the stream changes with time. It first increases and then decreases if the observation location is downstream of the spill point.

The actual situation of water dispersion from an expanding pool (which stops expanding in the cross stream direction after its diameter becomes equal to the stream width) dissolving slowly and moving downstream is extremely difficult to model. Instead of considering all of the complications involved in the model, the analysis presented below uses a simpler approach of considering the source as a moving point source on the water surface. This approach is expected to yield a conservative number for the maximum concentration level reached at the bottom of the stream, compared to when the area source (of time dependent area) is used.

Let

$$\dot{m}(t) = \text{dissolution rate of the chemical (kg/s) at time t.}$$

This source strength is obtained by methods illustrated in Section 2 of this chapter.

$$X, Y = \text{coordinates (relative to the initial location of the}$$

spill) of the point within the stream at which concentration is needed as a function of time.

In developing the model, the following assumptions are made:

60

Assumptions

- The dissolution rate is so small that the mixing by turbulent eddies keeps the concentration within the zone affected (see Figure II-4) essentially a constant.

- This zone of pollution moves downstream at the velocity of the stream and also expands in volume due to the turbulent diffusion of the pollutant.

Two cases are possible; namely, (1) when the pool of liquid is small and diameter smaller than the width of the river, and (2) when the pool of liquid has expanded to such an extent that it cannot expand any more in the lateral direction and therefore behaves as a one-dimensional pool. Only the first case is considered below.

When the pool diameter is smaller than the stream width, the geometric shape of the zone (within the stream) affected by the pollutant after a duration of t from the moment of spill can be approximated by a parallelopiped. The dimensions of this parallelopiped are estimated by assuming a turbulent diffusion of the dissolved chemical into the bulk of the river.

Length (streamwise) of this affected zone

$$\ell_v = \begin{cases} 2R & \text{if } R > \sqrt{\pi e_x t} \\ 2\sqrt{\pi e_x t} & \text{if } R < \sqrt{\pi e_x t} \end{cases} \tag{17}$$

Breadth (cross stream) of the affected zone is estimated by

$$b_v = \begin{cases} 2R & \text{if } R > \sqrt{\pi e_y t} \\ 2\sqrt{\pi e_y t} & \text{if } R < \sqrt{\pi e_y t} \end{cases} \tag{18}$$

and depth (d) is estimated by

$$d_v = \sqrt{\pi e_z t} \tag{19}$$

Hence, the volume of the affected zone is

$$V(t) = \ell_v b_v d_v \tag{20}$$

and the mean concentration is

$$C_{mean}(t) = \frac{M(t)}{o \cdot V(t)} \tag{21}$$

61
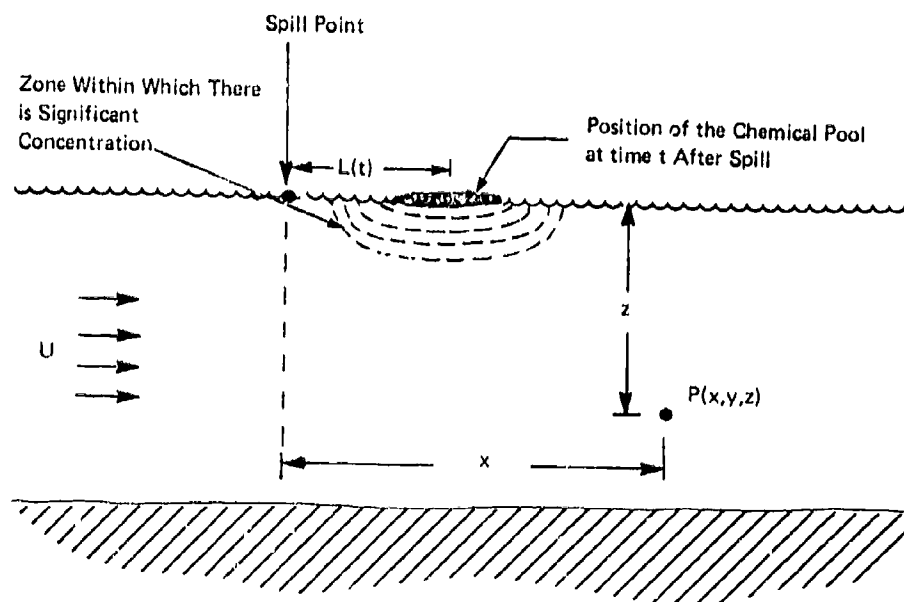
FIGURE II-4   DISSOLUTION AND DISPERSION OF FLOATING CHEMICAL

62

$$\text{where } M(t) = \int_0^t \dot{m} \, dt = \text{mass of dissolved chemical in duration } t \qquad (22)$$

The concentration at any point P (see Figure II-4) is smaller by an order of magnitude compared to the mean concentration (equation 21) if the point P is outside the affected zone. If, however, P is within the affected zone, the concentration could be as high as C_{sat} and as low as essentially zero.

An <u>approximate</u> way of calculating the concentration at any point P is given by

$$C(x',y',z',t) = C_{sat} \; e^{-\left(\frac{x'}{s_x}\right)^2} \left[e^{-\left(\frac{y'}{s_y}\right)^2} + e^{-\left(\frac{y'+W}{s_y}\right)^2} + e^{-\left(\frac{y'-W}{s_y}\right)^2} \right]$$

$$\times \left[e^{-\left(\frac{z'}{s_z}\right)^2} + e^{-\left(\frac{z'-2d}{s_y}\right)^2} \right] \qquad (23)$$

where x', y', z' are the coordinates of a point in the water relative to an origin located at the center of the pool of chemical on the water surface

$$\left. \begin{aligned} s_x &= 2\sqrt{e_x t} \\ s_y &= 2\sqrt{e_y t} \\ s_z &= 2\sqrt{e_z t} \end{aligned} \right\} = \text{Dispersion parameters in the three respective directions} \qquad (24)$$

Referring to Figure II-4, the coordinates (x', y', z') of the point P relative to 0 are

$$x' = -L(t) = X - ut$$
$$y' = \qquad Y \qquad\qquad (25)$$
$$z' = \qquad Z$$

63

Specific Example for Section 3

For the purpose of the illustration of the calculation procedure, we consider the data given in the example for Section 2. The formula and calculation procedure for obtaining the turbulent diffusion coefficients are elaborated in Reference 13.

Width to depth ratio for the river $= \dfrac{W_R}{d} = \dfrac{1000}{15} \simeq 67$

Therefore, the river can be assumed to be narrow.

Hydraulic radius of the river $= R_h = \dfrac{1000 \times 15}{(30 + 1000)} = 14.56$ m

(Assumed) Manning friction factor $n = 0.03$

Stream velocity $u = 2$ m/s

Distance of the observer $X = 500$ m

Observation point located on the ground at midstream

Hence, shear velocity (in S.I. Units) $u* = \dfrac{3.124\ n\ u}{R_h^{1/6}} = 0.12$ m/s

From equation 4.3 of Reference 13, we have

e_z = turbulent diffusion coefficient in z direction $= 0.067\ u* R_h$

$$= 0.117\ m^2/s$$

$e_x = 0.1\ e_z = 0.012\ m^2/s$

$e_y = 0.23\ u* R_h = 0.402\ m^2/s$

Line source strength obtained from the result in the example in Section 1 $= \dot{m}' = N/L = \dfrac{6.125 \times 10^{-3}}{10} = 6.125 \times 10^{-4}$ kg/ms

From equation 13, we have

$$C_{max} = \frac{6.125 \times 10^{-4}}{2 \times 1000 \times \sqrt{\pi} \times 2 \times 500 \times 0.117} = 1.597 \times 10^{-8} \text{ kg/kg of water}$$

$$s_z = \sqrt{\frac{4 \times 500 \times .117}{2}} = 10.82 \text{ m}$$

$$s_y = \sqrt{\frac{4 \times 500 \times .402}{2}} = 20.05 \text{ m}$$

$$\text{erf}\left(\frac{B}{2s_y}\right) = \text{erf}\left(\frac{5}{2 \times 20.05}\right) = 0.14032$$

64

From equation 14, we have

$$
\iota = \left[\mathrm{erf}\left(\frac{-1000 + 2.5}{20.05}\right) - \mathrm{erf}\left(\frac{-1000 - 2.5}{20.05}\right) \right] +
$$

$$
\left[\mathrm{erf}\left[\frac{1000 + 2.5}{20.05}\right] - \mathrm{erf}\left(\frac{1000 - 2.5}{20.05}\right) \right] < \frac{e^{-2500}}{3.554}
$$

Hence ι is very small

From equation 12, we have, therefore,

$$C(500 \text{ m, o, o, t}) = 1.597 \times 10^{-8} \times 2 \times 0.14032 = 0.4482 \times 10^{-8} \text{ kg of chemical/}$$
$$\text{kg of water}$$

A similar procedure can be used to calculate the concentration in the river when the chemical is dissolving while floating downstream.

DISCUSSION

In this chapter, three phenomena have been analyzed, each one in some way connected to the other two.

The first physical model considered is the dissolution rate of a pool of heavy liquid of low solubility present on the bottom of a river. The calculations have been made by assuming the immovable liquid pool to be a flat plate in an open stream. The result leads to equation 6. One of the major assumptions used in deriving equation 6 from flat plate theory is that both concentration and hydrodynamic boundary layers start at the leading edge (upstream end) of the pool. However, in a river flow, this is not true. The hydrodynamic boundary layer depth is essentially the depth of flow in a river because of the fully developed nature of the turbulent flow in the river. The concentration boundary layer, of course, begins at the leading edge as has been assumed. Because of this difference in treating the problem, equation 6 is expected to yield a lower dissolution rate.

An analysis taking into account the fully developed nature of the flow boundary layer and the developing concentration boundary layer is given in Appendix C. It is seen that the results obtained by a simple flat plate analysis (equation 6) and the refined analysis (equation 8) are not very different. In the latter case, however, the stream depth enters as a parameter. This is so since the velocity distribution in the stream is related to the depth of the river.

65

Another important result obtained in the analysis is the insensitivity of the total dissolution rate to the shape of the pool. The shape factor S given in Table II-1 for various simple geometrical shapes indicates that so long as the areas of the different pool are the same, the dissolution rate does not vary very much. (The maximum variation is about 11% compared with a rectangular geometry.) This is an extremely interesting and important result in that for calculating stream pollution levels, the pool shape need not be known very accurately.

In Section 2 of this chapter, the spreading downstream movement and the dissolution of a slowly soluble, lighter than water chemical has been analyzed. It is seen that because of the movement of the pool at essentially the same velocity as the water surface current, the mechanism of dissolution is primarily due to the river turbulence. Except for the random eddy motion which is a part of the turbulent structure of the river flow, no sustained dissolution of the chemical is possible. This can be explained from the fact that the dissolved chemical will also be in the neighborhood of the pool which would result in a continuous decrease in the solubility potential $(C_{sat} - C_{freestream})$. The example considered indicates the extremely small dissolution rate. Because of this, it is fair to surmise that the spilled chemical persists for a long time on the river surface.

The pollution hazard from such a traveling chemical pool seems to be limited to a size comparable to the size of the pool and traveling downstream. The lateral dispersion of the dissolving chemical is accomplished by the stream turbulence.

In Section 3 of this chapter, models are developed to predict the downstream concentration of the chemical dissolving slowly. Both stagnant pool and the travelling pool have been considered. It is seen that because of the small concentration boundary layer thickness (in the case of stagnant pools) at the trailing end of the pool, a line source description is more than adequate. The turbulent dispersion coefficients are obtained in a manner discussed in one of the CHRIS reports (Reference 13).

Equations 12 and 23 give the concentration in the river for a fixed line source and a moving surface point source, respectively.

66

In both the equations, the presence of the side and bottom walls of
the river channels have been accounted for. It should be noted that
these equations give the best estimate value of the concentrations
because of the gross simplifications made in describing the turbulent
diffusion process. The channel geometry is assumed to be rectangular,
the spill is assumed to occur in the center of the river, and charac-
teristics of the river are assumed to be similar in all locations (and
therefore identical turbulent diffusion coefficients). None of the
above is strictly true in an actual river. In addition, several other
complications such as secondary flows, nonuniform velocity distribution,
etc., in the river have not been considered. However, the concentrations
predicted would not be off by orders of magnitude compared to any realistic
value that may occur in a given spill.

Several other useful relations are derived, such as the size of
the affected zone (equations 17 through 19), mean concentration
(equation 21), and in the case of stationary source, the distance
downstream (X_{crit}) beyond which one-dimensional dispersion theories
are applicable.

CONCLUSIONS

Models have been developed to obtain the dissolution rate of a
chemical (which has low solubility in water) when it is spilled on
water. Both heavier than water and lighter than water liquid chemicals
have been considered. Also developed are the models to calculate the
downstream concentrations of the dissolved chemical as a function of
time and spatial location.

It is seen from the analyses that:

- The dissolution rate is very small for most river situations.

- For the heavier than water liquid (pools) dissolving, the total
  dissolution rate is essentially independent of the shape of
  the pool.

- For calculating the downstream dispersion from such stagnant
  pools, a line source description of the "source" is adequate.

67

APPENDIX B

Evaluation of Shape Factors for Turbulent Mass Transfer from Nonrectangular Shape Areas

Figure B-1 shows a liquid pool area from which mass is being transferred to the fluid flowing over it (turbulently).
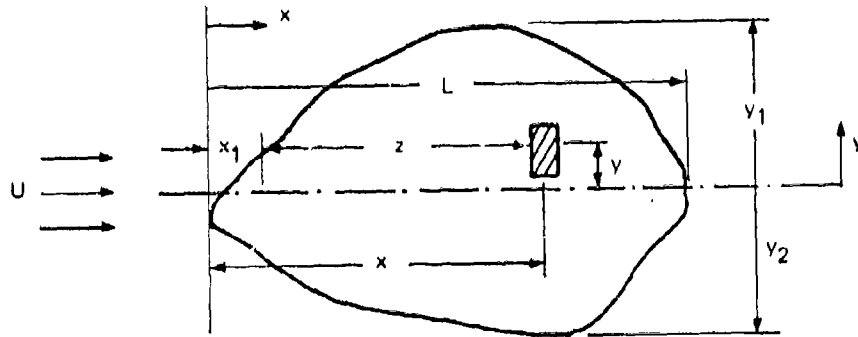
FIGURE B-1 EVALUATION OF SHAPE FACTOR FOR ARBITRARILY-SHAPED POOL

The mass transfer coefficient at any position on the pool can be expressed by[*] (See Ref. 2)

$$\frac{K(x,y)z}{D} = 0.0296 \left(\frac{Uz}{\nu_w}\right)^{0.8} Sc^{1/3} \tag{B-1}$$

where z is the distance from the leading edge to the elemental area under consideration. From equation B-1, it follows that the total mass transfer rate from the total area is given by

$$N = \int_A C_{sat} K(x,y) \, dA$$

$$N = C_{sat} D \times 0.0296 \left(\frac{U}{\nu_w}\right)^{0.8} Sc^{1/3} \int_{x=x_1(y)}^{x_2(y)} \int_{y=y_1}^{y_2} \frac{dxdy}{\left[x-x_1(y)\right]^{0.2}} \tag{B-2}$$

i.e

$$N = S(\frac{5}{4} \times 0.0296) \, C_{sat} \, D \, W \, Sc^{1/3} \, Re_L^{0.8} \tag{B-3}$$

68

where shape factor

$$S = \frac{4}{5} \quad \frac{L^{0.2}}{L\,W} \quad \int_{y_1}^{y_2} \int_{x=x_1(y)}^{x_2(y)} dy \quad \frac{dx}{\left[x-x_1(y)\right]^{0.2}} \qquad \text{(B-4)}$$

It is the object of this appendix to evaluate equation B-4 for various shapes of pool.

We can rewrite equation B-4 in dimensionless form by defining

$$\xi = \frac{x}{L}, \quad \eta = \frac{y}{L}, \quad \omega = \frac{W}{L} \qquad \text{(B-5)}$$

$$S = \frac{4}{5} \frac{1}{\omega} \int_{\eta_1}^{\eta_2} d\eta \int_{\xi_1}^{\xi_2} \frac{d\xi}{\left[\xi - \xi_1(\eta)\right]^{0.2}}$$

i.e.

$$S = \frac{1}{\omega} \int_{\eta_1}^{\eta_2} \left[\xi_2(\eta) - \xi_1(\eta)\right]^{0.8} d\eta \qquad \text{(B-6)}$$

1. **Rectangular Section**

$\xi_1 = 0, \; \xi_2 = 1, \; \eta_1 = 0, \; \eta_2 = \omega$

$$S = \frac{1}{\omega} \int_0^\omega 1^{0.8} \, d\eta = \frac{\omega}{\omega} = 1$$

Figure B-2

Hence

$$S = 1$$

2. **Elliptical Section**

Equation to the ellipse

$$\frac{\left(\xi - \frac{1}{2}\right)^2}{(1/2)^2} + \frac{\eta^2}{(b/2)^2} = 1$$

Figure B-3

Hence

$$\xi_2(\eta) - \xi_1(\eta) = \sqrt{1 - \frac{\eta^2}{(b/2)^2}}$$
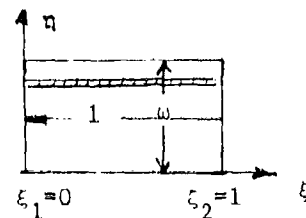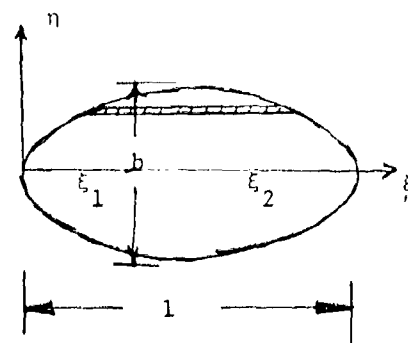
i.e.　$\omega = \dfrac{\pi}{4} \dfrac{LB}{L^2} = \pi/2 \, \dfrac{b}{2}$

$$S = \dfrac{2}{\pi/2 \ (b/2)} \int_{0}^{b/2} \left\{ \sqrt{1 - \left(\dfrac{\eta}{b/2}\right)^2} \right\}^{0.8} d\eta$$

i.e.,　$S = \dfrac{4}{\pi} \displaystyle\int_{t=0}^{1} (1-t^2)^{0.4} dt$

(see Ref. 14)

$$= \dfrac{2}{\sqrt{\pi}} \dfrac{\Gamma(1.4)}{\Gamma(1.9)}$$

$S = 1.075$

3. Circular Section

Since circle is a special case of an ellipse, and since the value of S does not depend on the eccentricity of the ellipse (see above), the value of the S for circle is the same as for an ellipse

$S = 1.075$

4. Triangular Section

$\xi_1 = \eta \cot \alpha$

$\xi_2 = 1.$

$\omega = \dfrac{b}{2} = \tan \alpha$

Figure B-4

70
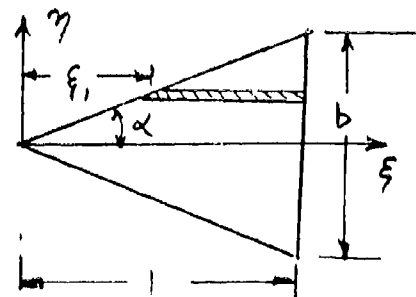
Therefore, substituting in equation B-6

$$S = \frac{2}{(b/2)} \int_{y=0}^{(b/2)} (1-\eta \cot\alpha)^{0.8} \, d\eta$$

$$= 2 \int_0^1 (1-t)^{0.8} \, dt = 2 \frac{\Gamma(1.8) \, \Gamma(1.0)}{\Gamma(1+1.8)}$$

$$S = \frac{1}{0.9} = 1.111$$

It can be shown that the above result holds good even when the base of the triangle is upstream and the vertex downstream.

5. Semicircular Section

$$\xi_1 = 1-\cos\theta \qquad \eta = \sin\theta$$

$$\xi_2 = 1 \qquad d\eta = \cos d\theta$$

$$\omega = \frac{\pi}{2}$$
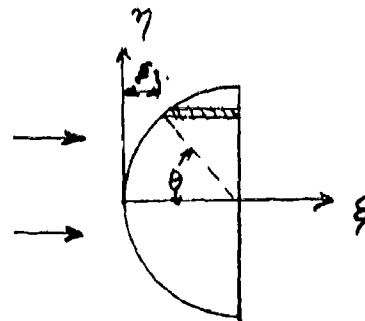
Figure B-5

From equation B-6 we have

$$S = \frac{2}{(\pi/2)} \int_{\theta=0}^{\pi/2} [\cos\theta]^{1.8} \, d\theta = \frac{4 \times 1.8}{2^{2.8}} \cdot \frac{\Gamma(1.8)}{[\Gamma(1.9)]^2} \qquad \text{(See Ref. 14)}$$

71

It can be shown that the same result as above holds good even when the semicircular section is such that the curved edge is on the downstream side.

APPENDIX C

ESTIMATION OF THE RATE OF DISSOLUTION
INTO THE STREAM OF A CHEMICAL
SPREAD OUT ON A RIVER BED

The objective of the analysis presented below is to estimate the rate of dissolution of the chemical into the stream.

The following physical description of the various phenomena relative to the dissolution are known: (see Fig. C-1)

- The flow in the stream is turbulent.

- The flow is fully developed, i.e., the velocity profile has developed fully and the entire depth of flow represents the turbulent boundary layer.

- The velocity profile (time averaged) is unvarying with x direction. This is because the velocity profile is fully developed and the shear stress from the walls exactly balances the acceleration due to the bed slope.

- When this hydrodynamically fully developed stream comes in contact with the chemical pool on the bed, a turbulent concentration boundary layer results.

- The problem cannot be solved by using the results of mass transfer from a semi-infinite flat plate because in the latter case, the hydrodynamic boundary layer is also developing.

- Hence, this problem has to be solved either using the penetration model (Higbie-Danckwerts model) or an equivalent turbulent Graetz problem for channel flow.

73

FIGURE C-1 Illustration of the physical Condition of Turbulent
River Flow on the Liquid Pool

74

The objective of the analysis presented below is to estimate the rate of dissolution of the chemical into the stream.

The following physical description of the various phenomena relative to the dissolution problem are known.

- The flow in the stream is turbulent.

- The flow is fully developed, i.e., the velocity profile has developed fully and the entire depth of flow represents the turbulent boundary layer.

- The velocity profile (time averaged) is unvarying with x direction. This is because the velocity profile is fully developed and the shear stress from the walls exactly balances the acceleration due to the bed slope.

- When this hydrodynamically fully developed stream comes in contact with the chemical pool on the bed, a turbulent concentration boundary layer results.

- The problem cannot be solved by using the results of mass transfer from a semi-infinite flat plate because in the latter case, the hydrodynamic boundary layer is also developing.

• Hence, this problem has to be solved either using the penetra-
tion model (Higbie-Danckwerts model) or an equivalent turbulent
Graetz problem for channel flow.

The analysis given below is based on a turbulent Graetz model
where the fully developed velocity profile is assumed, and this is
used to obtain a concentration profile and concentration boundary
layer thickness. The results are later compared with flat plate model
and similarities and divergences discussed.

Integral Technique to Solve a Turbulent Graetz Problem (2-D Problem)
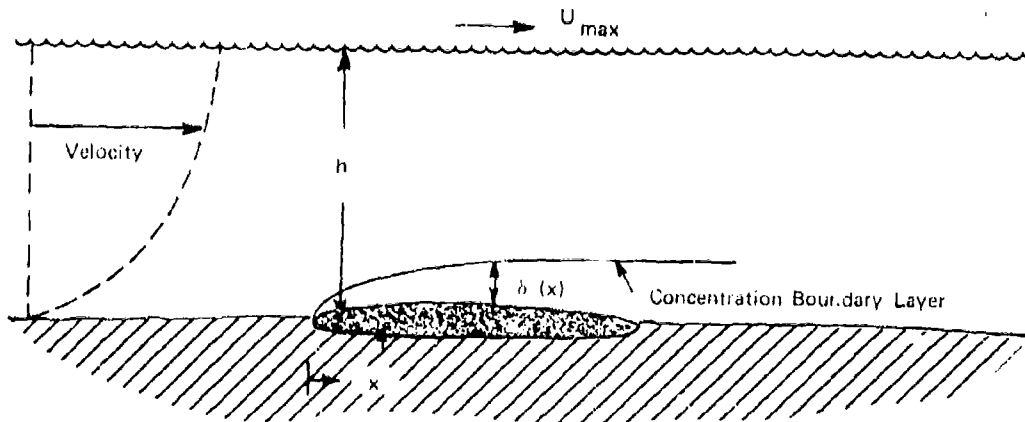
FIGURE C-2: Schematic Diagram for the Derivation of the Dissolution
Rate When the River Hydrodynamics are Fully Developed

Let $\delta(x)$ be the thickness of concentration boundary at any distance x
from the leading edge of the pool.

We assume:

1. Concentration of chemical in water is so small as <u>not to affect</u>
   the water density.

2. Evaporation rate is small and hence the hydrodynamics of the
   flow are not affected.

3. The velocity profile is given by[1]

$$\frac{u}{u_*} = 8.7 \left(\frac{y u_*}{\nu_w} \right)^{\frac{1}{7}} \tag{C-1}$$

---

[1]"Modern Developments in Fluid Dynamics," Goldstein, Volume 2, p. 340,
equation 25.

and

$$\frac{u_{mean}}{u_*} = 7.612 \left(\frac{u_* h}{\nu_w}\right)^{\frac{1}{7}} \qquad (C-2)$$

i.e.,
$$\frac{u}{u_{mean}} = 1.143 \ (y/h)^{\frac{1}{7}} \qquad (C-3)$$

a. Mass Balance to Layer Within the Concentration Boundary Layer

$$\frac{d}{dx} \int_0^{\delta(x)} \rho_w \ u \ dy = \dot{m}''_{in} \qquad (C-4)$$

b. Specie Balance to Layer Within the Boundary Layer

Let ρ_ℓ be the concentration (in density units) at any location. Then

$$\frac{d}{dx} \int_0^{\delta(x)} u \rho_\ell \ dy = \dot{m}''_{dis} + \dot{m}''_{dis} \qquad (C-5)$$

Substituting C-4 in C-5 and assuming $\rho_\ell = \rho_w c$, where c is concentration, we get

$$\frac{d}{dx} \int_0^{\delta(x)} \rho_w \ u \ (c - c_\infty) \ dy = \dot{m}''_{dis} \qquad (C-6)$$

Assuming that the turbulent dissolution rate can be predicted using the analogy, we have

$$\frac{\dot{m}''_{dis}}{\rho_w} = 0.0225 \ (c_{sat} - c_\infty) \ u(\delta) \left[\frac{\nu_w}{\delta u(\delta)}\right]^{\frac{1}{4}} Sc^{-\frac{2}{3}} \qquad (C-7)$$

Substituting C-7 in C-8, we get

$$\frac{d}{dx} \ u(\delta) \int_0^\delta \frac{u}{u(\delta)} \left(\frac{c - c_\infty}{c_{sat} - c_\infty}\right) \ dy = 0.0225 \left[\frac{\nu_w}{\delta \ u(\delta)}\right]^{\frac{1}{4}} u(\delta) \ Sc^{-2/3}$$

77

Let us assume

$$\frac{C - C_\infty}{C_{sat} - C_\infty} = 1 - (y/\delta)^{\frac{1}{7}}$$

and

$$\frac{u}{u(\delta)} = (y/\delta)^{\frac{1}{7}}$$

Hence, we get

$$\frac{d}{dx} \; \delta u(\delta) \int_0^1 \eta^{\frac{1}{7}} (1-\eta^7) \, d\eta = 0.0225 \, u(\delta) \left[\frac{\nu_w}{\delta \, u(\delta)} \right]^{\frac{1}{4}} Sc^{-2/3}$$

i.e., $\dfrac{d}{dx} \left[\delta u(\delta) \right] = (\dfrac{72}{7} \times .0225) \, Sc^{-2/3} \, u(\delta) \left[\dfrac{\nu_w}{\delta u(\delta)} \right]^{\frac{1}{4}}$

Using equation C-3, we get

$$h \, u_m \; \frac{d}{dx} \left[\frac{\delta}{h} \; \frac{u(\delta)}{u_m} \right] = 0.231 \; Sc^{-2/3} \; u_m \left(\frac{u(\delta)}{u_m} \right) \left[\frac{\nu}{h u_m} \right]^{\frac{1}{4}} \frac{1}{\left[\frac{\delta}{h} \frac{u(\delta)}{u_m} \right]^{\frac{1}{4}}}$$

Let $\zeta = \dfrac{x}{h}$, $\eta = \delta/h$

Hence

$$\eta^{\frac{1}{7}} \frac{d}{d\zeta} (\eta \, \eta^{\frac{1}{7}}) = 0.22 \; Sc^{-2/3} \; Re_h^{-\frac{1}{4}}$$

Hence, integrating we get

$$\eta^{\frac{9}{7}} = 0.248 \; \zeta \; Sc^{-\frac{2}{3}} \; Re_h^{-\frac{1}{4}} \tag{C-8a}$$

i.e., $\eta^{\frac{1}{7}} = 0.3376 \left[Sc^{-\frac{2}{3}} \; Re_h^{-\frac{1}{4}} \right]^{\frac{1}{9}} \zeta^{\frac{1}{9}}$ (C-8b)

i.e., $\dfrac{\delta}{x} = \dfrac{0.33755}{Sc^{\frac{14}{27}} \, Re_x^{\frac{7}{36}}} \; (h/x)^{\frac{1}{36}}$ (C-8c)

Using the definition for mass transfer coefficient K_L, we have with equation C-7 and C-3,

$$K_L = \frac{\dot{m}''_{diss}}{\rho_w (C_{sat} - C_\infty)} = 0.0225 \; u(\delta) \left[\frac{\nu}{\delta u(\delta)} \right]^{\frac{1}{4}} Sc^{-2/3}$$

$$K_L = 0.026 \; u_m \; Re_h^{-\frac{1}{4}} \; Sc^{-\frac{2}{3}} \; \frac{1}{\eta^{\frac{1}{7}}} \tag{C-9a}$$

78

(Modified Sherwood Number) Sh is given by

$$Sh = \frac{KL}{u_m} = 0.026 \frac{Re_h^{-\frac{1}{4}} \, Sc^{-2/3}}{\eta^{1/7}} \tag{C-9b}$$

Substituting for $\eta = \delta/h$ from equation C-8b, we have

$$Sh(\xi) = 0.0305 \left[Re_n^{-\frac{1}{4}} \, Sc^{-2/3} \right]^{\frac{8}{9}} \xi^{-\frac{1}{9}} \tag{C-9c}$$

Hence, mean Sherwood number over a length "L" of the pool is given by

$$\overline{Sh}(L) = \frac{1}{L} \int_0^L Sh(x) \, dx = \frac{1}{\xi_{max}} \int_0^{\xi_{max}} Sh(\xi) \, d\xi = \frac{9}{8} \, Sh(\xi_{max})$$

i.e., $\overline{Sh}(L) = 0.0343 \left[\frac{\nu}{u_m h} \right]^{\frac{2}{9}} Sc^{-\frac{16}{27}} \left(\frac{h}{L} \right)^{\frac{1}{9}}$

$$\overline{j}(L) = -\frac{\overline{k(L)}}{u_m} \, Sc^{2/3} = 0.0343 \frac{Sc^{2/27}}{Re_L^{2/9}} \left(\frac{h}{L} \right)^{-\frac{1}{9}} \tag{C-10}$$

Compare this equation to the flat plate equation which is

$$\overline{j}(L) = 0.037 \Big/ Re_L^{\frac{2}{10}} \tag{C-11}$$

Comparing equations C-10 and C-11, we see that the dependence of the j factor on the Reynolds number is almost identical (if we neglect the small difference between 2/9 and 2/10). However, the present analysis gives a Schmidt number and depth to pool length dependent result. However, the values of the fractions in the indices of Sc and (h/L) are very small compared to unity. Hence, it is expected that the results obtained for the value of the mass transfer coefficient by using the present method will differ very little compared with that shown in the following way:

Let $\quad R = \dfrac{(K)_{\text{this analysis}}}{(K)_{\text{flat plate}}}$

79

Using equations C-10 and C-11, we get

$$R = \frac{(\bar{j}_L) \text{ this analysis}}{(j_L) \text{ flat plate}} = 0.927 \; \frac{Sc^{2/27}}{Re_L^{\frac{1}{45}} \left(h/L\right)^{1/9}}$$

Value of R is given in the table below for certain variations of the parameters

h/L	Re_L	Sc = 1.0	Sc = 100	Sc = 1000
	10^4	0.755	1.062	1.259
1.0	10^5	0.718	1.010	1.198
	10^6	0.682	0.959	1.138
	10^4	0.756	1.063	1.261
0.5	10^5	0.719	1.011	1.200
	10^6	0.683	0.961	1.139
	10^4	0.904	1.272	1.508
0.1	10^5	0.860	1.210	1.435
	10^6	0.817	1.149	1.363

Discussion

The above table shows that the maximum variation in the ratio of the two j factors will be by about a factor of $(1.508/0.682) \simeq 2$ within the range of flow and other physical conditions that may be encountered in actual practice. It is impossible to say whether the model derived in the present analysis is any superior to that of a flat plate flow model. It is to be kept in mind that in reality under turbulent flow conditions in a river there may be other phenomena which may have strong influences on the dissolution rates (like swirls, wavy bed, large protrusions at the bed, etc.). All these will certainly contribute towards increasing the mass transfer.

80

It may also be pointed out that the results obtained in the model (equation C-10) would be slightly different if instead of using the 1/7th power law velocity profile (equation C-3), the logarithmic velocity profile was used. However, the result will not be significantly different from that obtained in equation C-10.

Sample Calculations: Data same as that used by Robert Reid.

Chemical   CHLOROFORM

$Sc = 943.4$ Solubility $= c_{sat} = 8 \times 10^{-3}$ kg/kg

$Re_L = 10^7$ Density $= \rho_\ell = 1490$ kg/m^3

$L = 10$ meters

$h = 5$ meters (say)   Thickness of
                                liquid film $= 0.04$ m

$u_{mean} = 1.05$ m/s

$\bar{j}_L$ from equation C-10 $= 1.712 \times 10^{-3}$

Hence $\bar{K}_L = Sc^{-2/3} u_{mean} \bar{j}_L = 1.869 \times 10^{-5}$ m/s

Mean dissolution rate $= \bar{K}_L \rho_w (C_{sat} - C_\infty) = 1.869 \times 10^{-5} \times 10^3 \times 8 \times 10^{-3}$
per unit area

$$= 1.495 \times 10^{-4} \text{ kg/m}^2\text{s}.$$

Mass of chloroform $= 1490 \times 0.04 = 59.6$ kg/m^2
spilled/unit area

Time for complete dissolution $= \dfrac{59.6}{1.495 \times 10^{-4}} = 110.7$ hrs.

81

APPENDIX D

Slowly Dissolving Chemicals

CHRIS Chemical Code	Chemical Name	Solubility in Water kg/100 kg	Viscosity Ratio $\frac{\mu_{liq}}{\mu_w}$	$\frac{\rho_{\ell}}{\rho_w}$ Density Ratio	State at STP
ACP	Acetophenone	.55	1.99	1.028	L
ALC	Allyl Chloride	.33	.33	.938	L
AML	Amyl Acetate	.2	1.02	.876	L
BAI	Iso-Butyl Acrylate	.2	.83	.889	L
BNZ	Benzene	.18	.65	.879	L
BTC	N-Butyl Acrylate	.2	.9	.899	L
BZD	Benzaldehyde	.3	1.4	1.046	L
CAF	Calcium Chloride	.018	--	3.18	S
CAH	Calcium Hydroxide	.13	--	2.24	S
CBT	Carbon Tetrachloride	.08	.952	1.59	L
CHX	Cyclohexane	.015	1.043	.779	L
CRB	Chlorobenzene	.049	.8	1.11	L
CRF	Chloroform	.8	.57	1.49	L
DBC	Di-isobutyl Carbinol	.06	14.3	.812	L
DBO	O-Dichlorobenzene	.015	.7	1.306	L
DCP	2,4-Dichlorophenol	.46	--	1.4	S
DOP	Dioctyl Phthalate	.005	6.0	.98	L
DPP	Dichloro Propane	.26	.99	1.158	L
DPT	Dicyclopentadiene	.02	.7	.978	L
DTH	Dowtherm	.00138	3.2	1.06	L
EBT	Ethyl Butanol	.43	.7	.834	L

Slowly Dissolving Chemicals

CHRIS Chemical Code	Chemical Name	Solubility in Water kg/100 kg	Viscosity Ratio $\frac{\mu_{liq}}{\mu_w}$	$\frac{\rho_\ell}{\rho_w}$ Density Ratio	State at STP
ECL	Ethyl Chloride	.6	.3	.906	L
EDB	Ethylene Dibromide	.27	1.7	2.18	L
EDC	Ethylene Dichloride	.8	.86	1.253	L
EDT	Ethylenediamine-Tetracetic Acid	.5	--	.86	S
EHX	2-Ethyl Hexanol	.07	9.8	.834	L
ETB	Ethyl Benzene	.02	.68	.867	L
IBA	Isobutyl Acetate	.6	.724	.871	L
IOA	Iso-octyl Alcohol	.07	10.0	.832	L
ISA	Isodecyl Alcohol	.01	6.0	.841	L
MAC	Methyl Amyl Acetate	.1	2.0	.86	L
MFA	Motor fuel anti-knock compounds	10^{-5}	6.0	1.5	L
MLT	Malathion	.0145	36.8	1.235	L
MPT	Methyl Parathion	.0025	6.0	1.22	L
MTB	Methyl Bromide	.09	--	1.68	L (cryogen)
MTC	Methyl Chloride	.6	.31	.997	L (cryogen)
NTB	Nitrobenzene	.19	2.01	1.204	L
NTM	Molten Napthlane	.3	.88	1.145	L
OTA	Octanol	.6	8.9	.829	L
PCP	Pentachlorophenol	.1	--	1.98	S
STY	Styrene	.3	.75	.906	L

83

Slowly Dissolving Chemicals

CHRIS Chemical Code	Chemical Name	Solubility in Water kg/100 kg	Viscosity Ratio $\frac{\mu_{liq}}{\mu_w}$	$\frac{\rho_\ell}{\rho_w}$ Density Ratio	State at STP
TCE	Trichloroethane	.07	.86	1.31	L
TCF	Trichlorofluoromethane	.11	--	1.49	L (cryogen)
TCL	Trichloroethylene	.11	.58	1.46	L
TCP	Tricresyl Phosphate	3E-4	80.0	1.16	L
TOL	Toluene	.05	.587	.867	L
TPH	Trichloro Phenol	.1	--	1.7	S
TTE	Tetrachloroethylene	.0165	.841	1.63	L
TXP	Toxaphene	3E-4	--	1.6	S (for solid)
VCI	Vinylidenechloride, Inhibited	.5	.33	1.21	L
VCM	Vinyl Chloride	.6	.27	.969	L (cryogen)
VNT	Vinyl Toluene	.0089	.837	.897	L

NOMENCLATURE

A $\qquad$ = Surface area of the liquid pool (m^2)

B $\qquad$ = Width of line source at the river bottom

C, c $\qquad$ = Concentration of liquid in water (kg/kg of water)

D $\qquad$ = Diffusivity (molecular) of the chemical in water (m^2/s)

d $\qquad$ = Depth of the stream (m)

e_x, e_y, e_z = Turbulent diffusion coefficients (m^2/s)

H $\qquad$ = Mean film thickness of the pool at the riverbed (m)

j_D $\qquad$ = Dimensionless mass transfer coefficient (colburn j factor)

$\dfrac{\bar{K}}{u} Sc^{2/3}$ (equation 4)

$\bar{K}$ $\qquad$ = Mean mass transfer coefficient over the length of the pool (kg/m^2 s) (see equations 1 and 10)

L $\qquad$ = Maximum extent of the pool in the stream flow direction (m)

L(t) $\qquad$ = The downstream distance of travel of the center of the floating pool in time t

M $\qquad$ = Mass of chemical dissolved in a time period t (kg)

$\dot{m}'$ $\qquad$ = Line source strength in kg/m s

$\dot{m}''_{dis}$ $\qquad$ = Rate of dissolution of the liquid in water per unit interface area (kg/m^2 s)

N $\qquad$ = Total dissolution rate (kg/s) of the liquid

R $\qquad$ = Radius of the floating pool as a function of time (m)

Re_L $\qquad$ = Reynolds number based on stream mean velocity and length of liquid pool $= \dfrac{u\,L}{\nu_w}$

S $\qquad$ = Shape factor (see equation 6 and Appendix B)

Sc $\qquad$ = Schmidt number of the chemical $= \dfrac{\nu_w}{D}$

T $\qquad$ = Temperature of water (K)

u $\qquad$ = Mean velocity of the stream (m/s)

85

$\overline{u'^2}$ = Mean square fluctuating velocity in the river (m^2/s^2)

V = Volume of the water affected by the dissolving pool in floating pool case (m^3)

W = Equivalent width of a rectangular pool of length L and having the same area as the actual pool (m)

W_R = Width of the river (m)

w = Aspect ratio of pool = W/L

X = Downstream distance from the trailing edge of the pool

y = Cross stream distance from the middle of the river

z = Vertical distance above the river bed

Subscripts

bulk = The condition in the free stream of the river

surf = The waterside conditions at the surface of the liquid pool

w = Water

sat = The saturated condition of the liquid in water

GREEK

δ	=	Boundary layer thickness	(m)
η	=	Dimensionless crossstream distance (also see Equ. C-8a)	See Equ. B-5
Λ	=	Mean eddy size (see Equ. 9)	(m)
ν_w	=	Kinematic viscosity of water	(m^2/s)
ξ	=	Dimensionless stream wise distance (Also see Equ. C-8a)	See Equ. B-5
ρ_ℓ	=	Density of liquid	(Kg/m^3)
ρ_w	=	Density of water	(kg/m^3)
ω	=	Dimensionless width of liquid pool	See Equ. B-5

REFERENCES

1. A. F. Skelland, "Diffusional Mass Transfer," Chapter 6, p. 271, Wiley (Interscience), NY, 1974.

2. Rohsenow and Choi, "Heat Mass and Momentum Transfer," Prentice Hall, p. 416, 1964. Also page 203, equation 8.57.

3. T. K. Sherwood, "A Review of the Deveopment of Mass Transfer Theory", Proc., 20th Ann. Symp., Mass Transfer and Diffusion, Univ. of Houston, 1973.

4. R. Higbie, Trans A.I.Ch.E., Volume 31, p. 65, 1935.

5. P. V. Danckwerts, "Significance of Liquid Film Coefficients in Gas Absorption," Ind. Eng. Chem., Volume 43, n6, p. 1460, 1951.

6. G. E. Fortescue and J. R. A. Pearson, "On Gas Absorption into a Turbulent Liquid," Chem. Eng. Sci., v22, pp. 1163-1176, 1967.

7. J. C. Lamant and D. S. Scott, "An Eddy Cell Model of Mass Transfer into the Surface of a Turbulent Liquid," A.I.Ch.E., v16, n4, pp. 513-519, July 1970.

8. G. R. Kramer, "Predicting Reaeration Coefficients for Polluted Estuary," Journal of the Environmental Engineering Division, Transactions ASCE, EE1, Paper No. 10351, pp. 77-92, February, 1974.

9. T. G. Theofanous, R. N. Houze, and L. K. Brumfield, "Turbulent Mass Transfer at Free, Gas-Liquid Interfaces, with Applications to Open-Channel, Bubble, and Jet Flows," AIAA/ASME Thermophysics and Heat Transfer Conference, Boston, Massachusetts, Paper No. 74-HT-57 (also AIAA No. 74-763), July, 1974.

10. D. J. O'Connor and W. E. Dobbins, Trans A.S.C.E., v123, p.641, 1968.

11. CHRIS Manual 2 - Property data on the computer.

12. R. C. Reid and T. C. Sherwood, "The Properties of Gases and Liquids," McGraw-Hill, Second Edition, p. 550, equation 11-49, 1966.

13. P. Raj and A. S. Kalelkar, "Assessment Models in Support of the Hazard Assessment Handbook (CG-446-3), NTIS AD776617, Report to USCG from Arthur D. Little, Inc., January 1974.

14. "Table of Integrals, Series and Products," I.S. Gradshteyn and I.M. Ryzhik, Academic Press, page 294, equation 3.249-5, New York, 1965.

CHAPTER III

DISSOLUTION OF COLD AND SOLUBLE CHEMICALS UNDER WATER

OBJECTIVE

The objective of the analysis presented in this chapter is to obtain an estimate of the fractional mass dissolved and the fractional mass escaping into the atmosphere in the form of vapor when a cold, soluble chemical is released at large depths in a water body.

INTRODUCTION

Some marine accidents may be visualized in which a volatile, yet soluble, chemical is released under water. Simultaneous boiling and dissolution can be expected to occur under these circumstances. However, several other phenomena may also result depending on the properties of the released chemical and the environmental conditions. The fraction of the released chemical that escapes into the atmosphere is expected to be a strong function of both the solubility and the depth of release. If the chemical is released at large depths, the hydrostatic pressure may be sufficient to inhibit boiling. Under these conditions the chemical simply dissolves in water. If the water temperature is higher than that of the released chemical, transfer of heat occurs and this results in a temperature rise of the liquid. Boiling of the chemical is initiated when its temperature reaches the saturation temperature corresponding to the local pressure. One other important phenomenon that has to be considered in a liquid-liquid boiling system is the liquid superheat. In the absence of nucleation sites for boiling, a liquid will not boil even if its temperature is equal to or exceeds the saturation temperature corresponding to the pressure at the location of the liquid drop. Any heat transfer from the ambient fluid to the volatile liquid results in its superheating. It has, however, been found experimentally (and predicted theoretically) that there is a limit-temperature up to which the liquid can be

89

superheated at any given pressure. If the temperature of the liquid drop reaches this superheat limit-temperature, spontaneous (and in many cases violent and explosive) boiling occurs, whether nucleation sites exist or not.

A thorough and completely general analysis of the consequences of an accident involving underwater release of a cold, soluble chemical is exceedingly difficult. Dissolution and boiling rates are strong functions of the initial drop size. A release accident results in the formation of a spectrum of liquid drop sizes. The relative abundance (or distribution) of these drop sizes depends to a large extent on the mode of release (i.e., the dynamics of the accident). The properties of the released chemical are also important. There is no way of quantifying the accident dynamics at the present time, nor is there information in the literature on the expected initial size distribution resulting from a liquid release at large depths under water.

The effect of hydrostatic pressure on the solubility of the chemical during the dissolution of the liquid drop in water merits consideration. It is well known that the solubility of gases depends on the pressure as well as on the temperature. In the case of a liquid drop dissolving in water during its ascent or descent, the hydrostatic pressure changes. Also, for a release at large depths, the total pressure itself is high. The problem of dissolution can be treated in this case only on a quasi-steady basis - that is, assuming that at every instant the concentration of the solute at the liquid drop-water interface is equal to the saturation concentration corresponding to the local total pressure.

Another important issue relates to the effect of initial liquid density. If it is less than that of water, there is no question -- the volatile liquid will rise to the surface and vaporize. However, if the initial liquid density is higher than that of water, the liquid will tend to settle and at the same time (possibly) vaporize. Should there be little or no disengagement between the residual liquid and

evolved vapor, then the net density of the drop will, of course, decrease and the drop/bubble may even rise. If, on the other hand, vapor can move away from the drop, the liquid portion will sink, whereas the vapor portion will rise. Most data available in the literature have centered upon liquids which are _less_ dense than water (e.g., ethyl chloride, density $\sim$ 0.90 g/cm^3). An analysis of this case may not be applicable to sulfur dioxide (density $\sim$ 1.45 g/cm^3) or chlorine (density $\sim$ 1.47 g/cm^3). In a preliminary study of liquid chlorine spills in water [1] for spills up to 10 gallons, the dense chlorine liquid was never seen to sink; it was buoyed up by the rapid vapor evolution, and boiling occurred on the surface.

This brief description of the behavior of a cold, soluble chemical released in water indicates that several aspects of the problem have to be considered in a theoretical analysis. Figures III-1 and III-2 indicate schematically the possible events that can occur. In Figure III.1-a, a simple case is illustrated. A liquid drop rises to the surface, is warmed by heat transfer and reduced in size by dissolution. Although the ambient pressure decreases during the ascent, boiling does not occur until the liquid reaches the surface. In Figure III.1-b, the same sequence is described, but in this case, the drop attains the superheat limit temperature, T_{SH}, before reaching the surface. When this occurs, the drop fragments and boils violently. The residual vapor bubbles then will rise and dissolve further.

In Figure III.2 similar scenarios are described for a liquid drop that is more dense than water. Not shown is the case where the liquid drop, upon entering the water, entrains a small amount of vapor. This vapor will grow by vaporization and can lead to a buoyant force sufficient to lift the vapor-liquid ensemble back to the surface. Vapor is then partially shed out of the liquid, and the vapor bubble-liquid drop ensemble again falls. The sequence may be repeated until the drop is completely evaporated or dissolved.

Figure III-1 (a)

Sequence of possible events when a lighter
than water, cold, soluble liquid is
introduced at depth H

Drop reaches surface without
attaining T_{SH}. All remaining
mass goes as vapor

Pressure decreases
as drop rises

Mass loss from dissolution
changes diameter

Temperature rises
from water heat
transfer

Drop at depth H

Figure III-1 (b)

Bubbles escape to air

Vapor bubbles dissolve

Bubbles rise, lose
mass, pressure and
diameter decrease

When drop reaches T_{SH}; drop
explodes into N
identical bubbles of
radius r_c, pressure p,
temp. T_{SH}

Pressure decreases as drop
rises

Mass loss from dissolution
changes diameter of drops

Temperature rises due
to heat transfer from
water

Drop at depth H

93

Figure III-2

Sequence of possible events when a heavier
than water, cold, soluble liquid is
introduced at depth H

(a)

Drop at H

Sinks and dissolves; the
diameter decreases

Temperature increases

Disolves completely before
$T = T_{SH}$ _and_ before reaching
bottom

(b)

Sinks and dissolves, diameter
decreases

Temperature increases

Reaches bottom; new h, k_L

Dissolves before $T = T_{SH}$
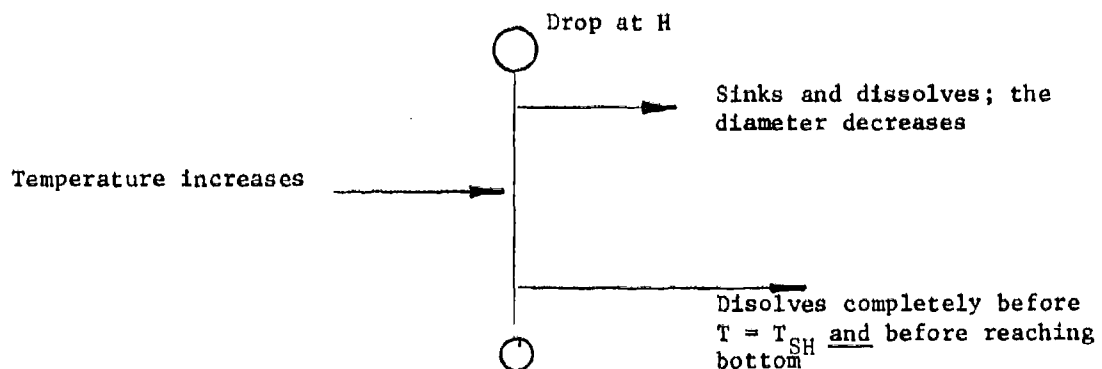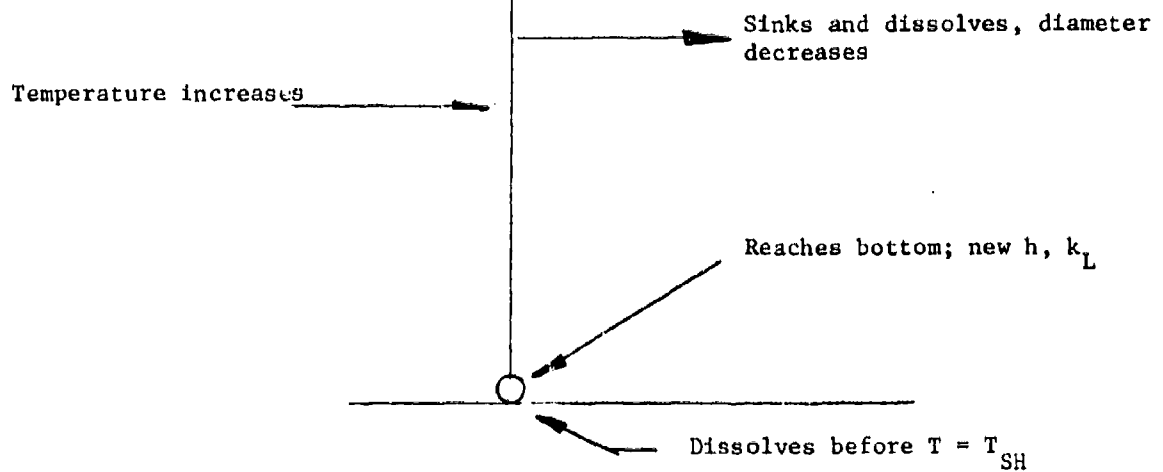
Bubbles escape
releasing vapor
to air

Drop at H

(c)

Bubbles dissolve be-
fore reaching sur-
face

Sinks and dissolves;
diameter decreases

Pressure decreases,
diameter becomes smaller

Temperature
increases

Dissolve--mass loss

Reaches $T = T_{SH}$ before
reaching bottom; explodes
into N bubbles of $r = r_c$, $T = T_{SH}$,
pressure

Bubbles rise at
terminal velocity

Drop at H

(d)

Sinks and dis-
solves; diameter
changes

Reaches bottom before
$T = T_{SH}$; new h, k_L values

Temperature
increases

then reaches T_c and
explodes as in (c)

95

ANALYSES

In order to formulate properly the dissolution problem, it is necessary to know the physical properties of the chemicals. Therefore, a list of commonly transported chemicals whose boiling points at atmospheric pressure are lower than 293 °K has been compiled and is given in table III-1. The data in table III-1 has been taken from the initial list of 450 chemicals in CHRIS[2]. It is seen from this list that the hydrocarbons generally have lower solubility (less than 1 Kg in 100 Kgs of water). In addition, all the hydrocarbon liquids are lighter than water. The halogenated compounds have reasonably high solubility in water. Some of them, such as vinyl chloride, cyanogen chloride, chlorine, etc. are also highly toxic. Most of the nitrogen – and sulphur-based compounds in table III-1 are either reactive or are highly soluble in water. The behavior in water of some of these chemicals (such as ammonia) has been analyzed elsewhere;[3] that of phosgene is discussed in another chapter in this report.

DYNAMICS OF VAPOR BUBBLE AND LIQUID DROP MOTIONS

(a) Vapor Bubbles

The determination of the dynamics of gas bubble motion in water (due to buoyancy forces) from purely theoretical considerations is extremely difficult because of the internal circulations within the gas bubble, the effect of surfactants (if any), the deformation of the bubble, etc. If one observes a rising air bubble in water, it is seen that in relatively large bubbles (mean diameters of 1 to 2 cms), the motion is pulsating; the bubble moves with a tumbling motion and the shape of the bubble is far from being spherical. The dynamics of the bubble are significantly affected by the bubble Reynolds number (Re_b). As Levich[4] points out, for a $Re_b < 700$ (bubbles less than ~ 0.2 to 0.3 cm in diameter), the shape is nearly spherical, and in water they rise almost vertically. Above this Re_b value, bubbles tend to become flattened ellipsoids with irregular boundaries. The rise of such bubbles resembles a spiral and, surprisingly, the rise velocity

Table III-1:   List of Liquid Chemicals whose Boiling Points
are below the ambient temperature

	ρliq/ TEMP	BOILING TEM-PERATURE AT ATMOS PRES	CRITICAL TEMP. K	SOLUBILITY kg IN 100 kg OF WATER	c_1	c_2	c_3 (See foot note)
HYDROCARBONS							
ACE ACETYLENE	613/193	189	309.4	-	9.22	709.1	-19.96
BDI BUTADIENE	621/293	269	425.0	-	8.984	935.5	-33.56
BTN BUTYLENE	595/293	267	419.6	-	9.503	1200.	0.04004
BUT BUTANE	600/273	273	425.	-	8.955	945.9	-33.16
ETH ETHANE	546/185	185	305.5	-	9.336	800.	0.04004
ETL ETHYLENE	569/169	169	283.1	-	8.872	585.	-18.16
IBL ISOBUTYLENE	590/293	266	417.9	-	9.501	1197.	0.04004
IBT ISOBUTANE	557/293	261	408.	-	8.873	882.8	-33.16
MTH METHANE	422/113	111	190.7	-	8.737	389.9	-7.16
PPL PROPYLENE	609/226	225	365.	-	8.945	785.0	-26.16
PRP PROPANE	590/223	231	176.5	-	8.955	813.2	-25.16
HALOGENATED COMPOUNDS							
CCL CYANOGEN CHLORIDE	1222/273	286.	-	-	10.9	1430.	-
CLX CHLORINE	1424/288	239.	417.	0.65/298	9.543	1086.	0.04004
DCF DICHLORO FLUORO-METHANE	1350/288	243.	385.	-	-	-	-
ECL ETHYLCHLORIDE	906/285	285.	460.4	0.6/293	9.816	1375.	0.04004
FXX FLUORINE	1500/85	85.	144.6	-	8.896	331.	0.04004
HDC HYDROGEN CHLORIDE	1191/188	188.	324.6	-	9.554	856.	0.04004
HFX HYDROGEN FLOURIDE	992/293	293.	503.8	-	9.519	1317.	0.04004
MCF MONOCHLORO-DIFLUOROMETHANE	1410/233	233.	369.2	0.3/298	9.75	1104.	0.04004

MTB	METHYL BROMIDE	1680/293	277.	464.	0.09/293	9.085	986.6	-34.86
MTC	METHYL CHLORIDE	997/244	249.	416.8	0.6/293	9.606	1148.	0.04004
TCF	TRICHLORO FLUOROMETHANE	1490/293	297.	471.	0.11/298	9.649	1380.	0.04004
VCM	VINYL CHLORIDE	969/260	259.	431.6	0.6/293	9.566	1183.	–

NITROGEN SULFUR

MISC. COMPOUNDS

	AMMONIA	682/240	280.					
DMA	DIMETHYLAMINE	671/280	280.	437.8	–	10.42	1517.	0.04004
EOX	ETHYLENE OXIDE	869/293	284.	469.	–	9.797	1359.	0.04004
HCN	HYDROGEN CYANIDE	689/293	299.	456.7	–	9.916	1467.	0.04004
HDS	HYDROGEN SULFIDE	916/213	213.	373.6	–	9.559	970.	0.04004
NOX	NITROGEN TETRA- OXIDE	1450/293	294.	431.4	–	11.04	1799.	3.64
NTC	NITROSYL CHLORIDE	1360/267	267.	441.	–	9.972	1328.	0.04004
PHG	PHOSGENE	1380/293	281.	455	–	9.636	1303.	0.04004
SFD	SULFUR DIOXIDE	1450/263	263.	430.	10/293	9.407	999.9	-35.96
TMA	TRIMETHYLAMINE	633/293	276.	433.3	–	9.725	1303.	0.04004

Note: Saturation temperature T_s at any pressure p is calculated by

$$T_s = \frac{C_2}{C_1 - \log_{10} p_{vap}} - C_3$$

where T_s is in deg K

p is in N/m^2

98

becomes relatively insensitive to diameter. In water, bubbles of this size rise at about 1 ft/s ($\sim$ 30 cm/s). Large bubbles (d > 2 cm) tend to break down into smaller bubbles.

The constant rise velocity of large bubbles (of radii larger than about 0.1 cm) is given by Levich[4] as:

$$u_b = \left[\frac{4\sigma^2 g}{30 \rho_w \mu_w} \left(1 - \frac{\rho_{vap}}{\rho_w} \right) \right]^{\frac{1}{5}} \tag{1}$$

For radii less than 0.1 cm, the experimental data reported by Levich[4] can be correlated by the equation*

$$u_b = \frac{1}{28} \frac{r_b^2}{\nu_w} g \left(1 - \frac{\rho_{vap}}{\rho_w} \right) \tag{2}$$

---

* The dependence of rise velocity on the square of the diameter (as indicated in equation 2) implies that most of the drag on the bubble results from viscous friction rather than turbulent form drag. This is a rather unexpected result considering that the Reynolds numbers are about 300 to 400 (so that Stokes Law of Resistence is not valid). Levich[4] argues that even at these high Reynolds numbers, the wake behind the bubble is very small because of the gas circulation within the bubble; therefore, the main resisting force is due to the viscous friction (dissipation) in water. Based on these ideas, Levich[4] in fact derives theoretically an equation for gas-bubble rise which differs from equation 2 only in a constant factor, but which has the correct bubble radius dependency.

Large bubbles tend to break up into smaller bubbles due to the dynamic pressure forces acting on the bubbles during their motion. The critical radius of the largest size bubble that is stable is given by Levich[4]

$$(r_b)_c = \left(\frac{3}{\kappa_f'}\right)^{\frac{1}{3}} \left[\frac{\sigma}{\rho_w u_b^2 \left(\frac{\rho_{vap}}{\rho_w}\right)^{\frac{1}{3}}}\right] \tag{3}$$

Where κ_f' is the turbulent drag fluctuation factor (due to internal gas motion within the bubble) and is generally of magnitude ≈ 0.5.

(b) Liquid Drop Motion

The motion of liquid drops in water has been treated in detail in the Hazard Assessment Handbook[5]. Here we quote the results.

For a non-deformable drop moving at its terminal velocity such that the Reynolds number is $400 < Re_d < 5000$ (i.e., turbulent motion), the terminal velocity is given by

$$v_d = \left[\frac{8r_d}{3C_D} \; g \; \left(1 - \frac{\rho_\ell}{\rho_w}\right)\right]^{\frac{1}{2}} \tag{4}$$

For a deformable drop the terminal velocity is

$$u_d = v_d \left[(1-\delta) \; \frac{1+A(1-\delta)^{3/2}}{(1+A)}\right]^{\frac{1}{2}} \tag{5}$$

where $\delta = 0.056$ We (6a)

$A = 1.778$ a constant (6b)

$$\text{We} = \rho_w \frac{u_d^2 \, r_d}{\sigma} = \text{Weber number} \tag{6c}$$

C_D = drag coefficient $\simeq 0.5^*$ (6d)

Therefore for a given drop radius (r_d) the terminal velocity u_d must be obtained by a trial and error procedure using equation 4, 5 and 6.

Large liquid drops tend to break up at Weber numbers of the order of $10.^+$ Based on this critical Weber number criterion, the maximum size of stable liquid drops is given by

$$(r_d)_c = 2.79 \sqrt{\frac{\sigma}{g \rho_w \left(1 - \frac{\rho_a}{\rho_w} \right)}} \tag{7}$$

---

*In general the drag on a liquid drop due to its motion through pure water is less than that of a solid body of equivalent diameter. This results because of the flow circulation that develops in the liquid drop. However, in the presence of surface active materials (which can be expected to be present in natural stream rivers and lakes), the circulation in liquid drops is inhibited to a considerable degree with the consequence that the motion of the liquid drop is more like that of a solid body than that of a liquid drop. For details see Levich [4], Sections 73 and 74.

$^+$Levich's theoretical criterion (Section 79 of Reference 4) is $\text{We}_c = 2$. However, experiments indicate that drops are stable for higher values of the Weber number than the above. [19]

SOLUBILITY

In general all chemicals can be classified (qualitatively) according to their solubility limits in water as very slightly soluble, slightly soluble and very highly soluble. It is however, difficult to establish precisely the category to which a given chemical may belong.

Slightly Soluble Chemicals may be defined, somewhat arbitrarily, as those whose equilibrium liquid concentration in water (at 1 atmosphere pressure) is less than 1% by mass. Ethyl chloride (S = 0.6%) and Vinylchloride (S=0.6%) would then belong in this group. In order to take into account the variation of solubility with pressure, the solution effects have to be considered. Henry's Law indicates that under equilibrium conditions

$$p_i = H_i(T) \; X_i \qquad\qquad (8a)$$

and $\quad p_i = PY_i = $ partial pressure of ith specie
in the vapor $\qquad\qquad (8b)$

where $\quad X_i = $ mole fraction of ith specie in water

$Y_i = $ mole fraction of ith specie in vapor

$P \;\; = $ total pressure

$H_i(T) = $ Henry's Law constant for the ith specie (a function of temperature but assumed to be independent of the liquid composition)

Often, instead of using the mole fraction X_i in water, the liquid concentration C_i^L (moles or mass/volume) is employed. For a single component chemical dissolved in water we can write

$$p_i \simeq \frac{C_i^L \, H_i(T)}{\rho^L} \qquad\qquad (9)$$

where ρ^L is the molar density of pure solvent.

In the case of Highly Soluble Chemicals (ammonia, hydrogen sulphide, etc.), the solubility relation is more complex:

$$P_i = \phi_i \, P \, Y_i = \gamma_i \, P_{vp_i} \, X_i = \gamma_i^\infty \, H_i^\infty X_i \tag{10}$$

where ϕ_i is the fugacity coefficient of i in the vapor phase (in ideal gases it is unity) and γ_i is the activity coefficient of i in the liquid (a function of P, T and X_i, though the effect of P is small). The activity coefficeint is based on pure liquid solute at T (i.e., $P \equiv P_{vp_i}$ (T)). γ_i^∞ is also a liquid activity coefficoint, but it is based on a standard state of infinite dilution, $P = H_i^\infty$ (ideal gas). Normally, for dilute solutions, the infinite dilution standard state is preferable; in any case, γ must be known as a function of composition and temperature.

Figure III-3 schemetically illustrates the variation of vapor partial pressure of a given solute over a solution, as a function of the molar concentration of the solute in the solution. Most of the chemicals considered in this chapter have relatively low solubility (and therefore the activity coefficient γ_i'' can be considered to be unity). Table III-2 gives the solubility of various hydrocarbon gases. The table indicates that the solubility increases with an increase in temperature.

HEAT AND MASS TRANSFER BETWEEN WATER AND VAPOR BUBBLE OR LIQUID DROP

(a) Vapor Bubble

The mass transfer rates from single vapor bubbles moving in water are reasonably well established by experiments. Several correlations are discussed by Raymond and Zreminski[6] (for the dissolution of CO_2 in water) and by Johnson et al[7]. Sherwood et al[8] have reviewed the

Logarithm of the ith specie partial pressure in vapor

$\ln p_i$

$\ln H_i^\infty$

$\ln \gamma_i^\infty$

$\ln p_{vp_i}$

$\ln \gamma_i$

Real Data

0

X_i

1

Mole fraction of ith specie in the solution
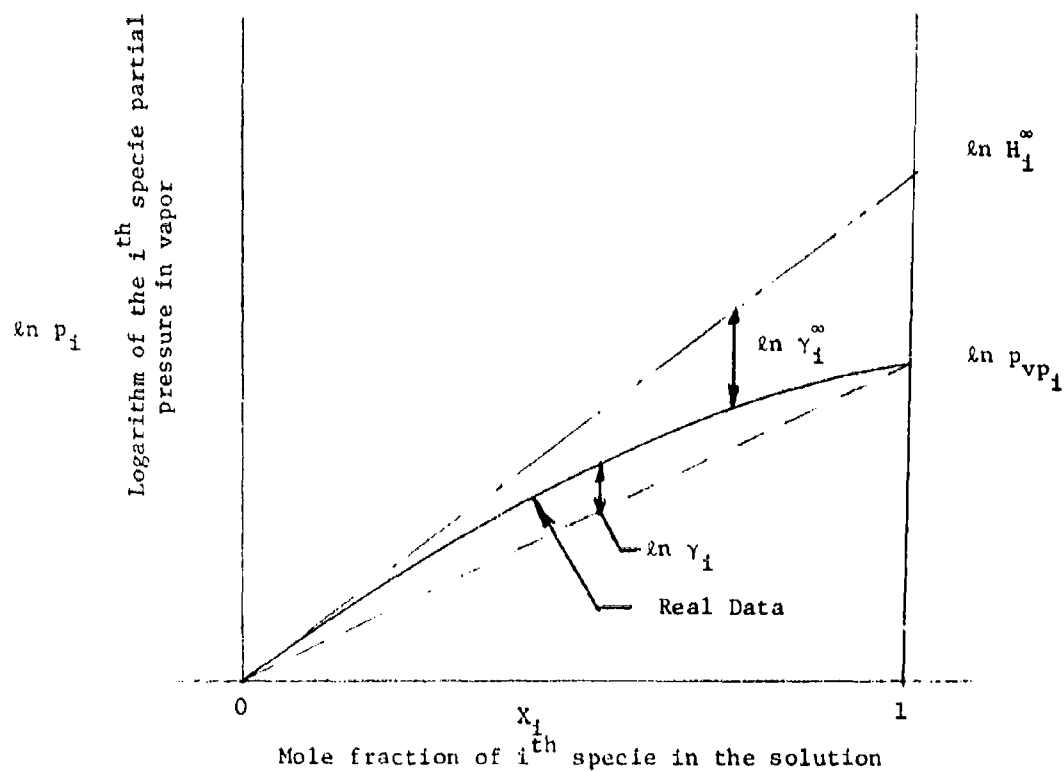
Figure III-3:   Variation of the vapor partial pressure
of a specie (i) with its concentration
in a liquid mixture.

104

Table III-2

Solubility of Hydrocarbon Gases in Water
at Atmospheric Pressure

Note: Solubility is expressed by the relationship

p (mm H_g) = K X (mole fraction in solution)

COMPOUND	T (°C)	K (mm H_g)	REFERENCE
ACE, Acetylene	0	0.54×10^6	
	10	0.73×10^6	(13)
	20	0.92×10^6	
	30	1.11×10^6	
BDI, Butadiene	20	3.1×10^6	(14)
	37	6.0×10^6	(15)
BTN, Butylene	20	1.1×10^7	(14)
BUT, n-Butane	19.8	2.89×10^7	(16)
	29.8	4.06×10^7	
ETH, Ethane	1.5	1.01×10^7	(16)
	10.5	1.44×10^7	
	19.8	1.91×10^7	
	29.8	2.52×10^7	
ETL, Ethylene	0	4.2×10^6	(13)
	10	5.8×10^6	
	20	7.7×10^6	
	30	9.6×10^6	
IBL, Isobutylene	20	9×10^6	(14)
IBT, Isobutane	5	2.1×10^7	(17)
	25	4.5×10^7	
	45	7.3×10^7	

MTH, Methane	2.0	1.76×10^7	(16)
	10.5	2.21×10^7	
	19.8	2.69×10^7	
	30.4	3.27×10^7	
PPL, Propylene	2	2.3×10^6	(13)
	10	3.39×10^6	
	18	4.32×10^6	
PRP, Propane	19.8	2.4×10^7	(16)
	29.8	3.28×10^7	

literature in detail and suggest the use of

$$\frac{\kappa \; r_b}{D} = 0.8 \; Re_b^{\frac{1}{2}} \; Sc^{\frac{1}{2}} \tag{11}$$

$$\text{for} \; r_b > 0.25 \; \text{cm}$$

$$\frac{\kappa \; r_b}{D} = 0.63 \; Re_b^{\frac{1}{3}} \; Sc^{\frac{1}{3}} \tag{12}$$

$$\text{for} \; r_b < 0.05 \; \text{cm}$$

For the purposes of this study we assume that the first formula is
valid for bubbles of radii $r_b > 0.1$ cm and (12) for $r_b < 0.1$ cm.

(b) Liquid Drop

The mass transfer coefficient due to the motion of a liquid drop-
in-water depends on both the velocity and the properties of the fluids.
Since the magnitude of the circulation velocities in the drop depend
on the viscosity ratios of the two fluids and the concentration of
surfactants, it is reasonable to expect that the mass transfer co-
efficient (or the Sherwood number, $\frac{\kappa \; r_b}{D}$) also would depend on the

viscosity ratio and the surfactant presence. Unfortunately, there
do not seem to be any experimental data available to quantify the above
effects. All of the available experimental information has been
reviewed by Sherwood et al.[8]   The most reasonable correlation available
for mass transfer between single drops of liquids and water is
(Sherwood et al[8], Chapter 6)

$$\frac{\kappa \; r_d}{D} = 0.424 \; Re_{r_d}^{\frac{1}{2}} \; Sc^{\frac{1}{2}} \tag{13}$$

where Re_{r_d} is the Reynolds number based on drop radius. In an

analogy with vapor bubble mass transfer, we assume that this correlation

107

is applicable to all drop radii greater than 0.1 cm. Similarly for $r_d < 0.1$ cm we use the correlation

$$\frac{\kappa \, r_d}{D} = 0.63 \, Re_{r_d}^{\frac{1}{3}} \, Sc^{\frac{1}{3}} \tag{14}$$

When a drop of liquid of density $\rho_\ell > \rho_w$ settles to the bottom of the river, the heat and mass exchange between the liquid and water is reduced considerably because there is no relative vertical motion. Should there be a water current laterally (as in a river), the drop may be carried down stream. It is also possible that all of the liquid drops that reach the bottom coalesce and form a liquid pool. The dissolution from such a pool has been treated in an earlier chapter in this report. However, if we assume that the drop remains stationary and retains its geometrical integrity, then the mass transfer rate can be determined using the low Reynolds number limit value. That is,

$$\frac{\kappa \, r_d}{D} = 1 \tag{15}$$

The heat transfer coefficients for the transfer of heat from water to the liquid drops are obtained from the Hazard Assessment Handbook[5], where

$$\frac{h \, r_d}{K} = 0.79 \, Re_d^{0.4} \, Pr^{0.33} \tag{16}$$

This equation was applied for drops of all sizes. In the limit of zero velocity (the drop rests on the bottom of the water body), the heat-mass transfer analogy is applied; the result is parallel to equation (15):

$$\frac{h \, r_d}{K} = 1 \tag{17}$$

SUPERHEATED LIQUIDS

Should a liquid be at a temperature which exceeds the boiling point (at the existing pressure), it is called a superheated liquid. There exists a thermodynamic potential to cause vaporization, but if there are kinetic or rate limitations, then vaporization may be delayed.

In the context of the present project, superheated liquids may be important since it is well known that vaporization is inhibited if a volatile liquid is heated and contact is made only with other liquids. Thus, if a low-boiling chemical is spilled into water (whose temperature exceeds the boiling point), there is good reason to assume that boiling may be delayed. For chemicals less dense than water and released at the surface, superheating would not normally occur as heating would occur while the spilled chemical floated on the surface and therefore was in contact with vapor. On the other hand, if the spilled chemical is more dense than water, it would sink while being heated. As noted above, if there were no vapor phase initially, we would expect the liquid to warm to the temperature of the water without boiling -- provided that a certain critical value of the temperature were not exceeded. This critical value is termed the super-heat-limit temperature and will be discussed later.

Experimental observations at M.I.T. verify these contentions[9]. For example, when a Freon-flourinated hydrocarbon was spilled into water which was about 30-40 °C above the boiling point of the Freon, no boiling was observed except in some drops which entrained an air bubble as they broke the water surface.* The others are reported to have fallen into the bottom of the water and formed a layer of liquid

---

*An interesting behavior of the Freon drops is reported to have been observed. As the drops fell through the water, vaporization occurred into the initial gas bubble. Soon the bubble provided sufficient buoyancy for the Freon drop to rise to the surface. Normally, it shed only a part of the gas bubble after reaching the surface and began to descend once more. This "yo-yo" effect was observed to occur over several cycles until complete vaporization resulted.

Freon which "superheated" by 30-40 °C. When this layer was stirred vigorously or if some sand were poured into the vessel, boiling was observed to occur rapidly and vigorously-within seconds, all the Freon had vaporized.

The cause of this interesting behavior is that, to initiate boiling, contact must be made between the superheated liquid and some vapor so as to allow further vapor to be formed. Solids, such as metals, sand, etc. have numerous microscopic concavities which entrap gas. These act as vapor nuclei suppliers. If, however, a liquid is surrounded by another liquid, there are no vapor embryos and the initiation of boiling is hindered.

As noted above, there does exist a critical limit beyond which it is impossible to superheat a liquid. This superheat-limit temperature results from the spontaneous formation of vapor in the <u>bulk</u> of the superheated liquid. If a liquid should attain this superheat limit temperature, both theory and experiment agree that vapor is formed so very rapidly that the process resembles an explosion. The phenomenon has been dubbed a "vapor explosion".

To estimate the superheat limit temperature of a pure chemical, thermodynamic stability theory indicates that the criterion is

$$\left(\frac{\partial p}{\partial V}\right)_T = 0 \tag{18}$$

That is, given a function ϕ (p, V, T) which describes the volumetric behavior of a liquid, $(\partial p/\partial V)_T$ is determined and, knowing the system pressure, one can determine T_{SH}; the superheat-limit temperature. Most equations of state lead to the simple rule that

$$T_{SH} \sim 0.89 \ T_c \tag{19}$$

where T_c is the critical temperature of the material.

110

For example, if one chooses the Redlich-Kwong equation 18

$$p = \frac{RT}{(V-b)} - \frac{a}{T^{0.5} V (V+b)} \qquad (20)$$

to represent the volume V of a liquid as a function of T and P, then with equation (18) one obtains a relation between T_{SH} and V_{SH}. Substituting these in equation 20 with P equal to the existing pressure, V_{SH} can be eliminated and T_{SH} found in terms of the parameters a and b. However, a and b are related to the critical constants and if these are employed, with P ∽ 1 bar, equation (19) is obtained.

An alternate approach to thermodynamics is through kinetic theory. No simple equation results, but predictions of T_{SH} are in excellent agreement with equation (19).

As an example, for liquid chlorine, the critical temperature is 417 K. Then from equation (19)

$$T_{SH} \sim 371 \ K$$

Liquid chlorine boils at 240K at atmospheric pressure. If it should be spilled into water at 293K, it is possible for this material to superheat over 50°C but it could not attain the T_{SH} limit and no vapor explosion would result.

In mixtures, the theory is considerably more complicated. In a n-component system, equation (18) is replaced by

$$Y^{(n)}_{(n+1),(n+1)} = 0 \qquad (21)$$

where $Y^{(n)}$ is the n-th Legendre transform of the energy and the subscripts refer to a double-differentiation with respect to the n+1 variable. In a binary mixture of A and B, equation (21) becomes

$$\left(\frac{\partial^2 G}{\partial N_A^2} \right)_{T, P, N_B} = 0 \qquad (22)$$

111

or
$$\left(\frac{\partial \mu_A}{\partial X_A}\right)_{T,P} = 0 \tag{23}$$

Where $\underline{G}$ is the total Gibbs energy of a system with N_A moles of
A and N_B of B, μ_A is the chemical potential of A and X_A the mole
fraction.

No kinetic theory results have yet been developed for mixtures.

In summary, liquids whose density exceeds that of water -- and
whose boiling points are less than the ambient water temperature --
may not boil when spilled into water. Rather, the liquids will super-
heat and, unless nucleated by sediment in the water or on the stream
bottom, will remain in this superheated state for indefinite periods
of time. In the rare cases where the water temperature exceeds
T_{SH}, a vapor-explosion may result. Vapor explosions can occur even
if the density of the spilled chemical is less than that of water.

Superheated liquids and their properties are reviewed in
reference (10).

MODELLING THE DISSOLUTION PROCESS

(a) Dissolution of Vapor Bubble Released at Depth H

When a vapor bubble is released at a depth H in water, it rises
through the water column essentially at a constant velocity equal
to its terminal velocity. The dynamics of motion of the bubble have
been discussed in an earlier section. For bubbles of size larger
than about 0.1 mm diameter, the gas pressure inside the bubble can be
assumed to be equal to the local (total) pressure at any water depth.
The vapor within the bubble consists of both water vapor and the
chemical vapor. Since the vapor pressure of water at ambient
temperatures (in the zero to 20 °C range) is small compared to gas pressure
in the bubble we can assume that the gas in the bubble essentially

112

consists of pure vapor. Subject to this assumption we write,

$$C = \alpha(T) \; \frac{p}{R_u T} \tag{24}$$

where C = molar density of solute in water at the vapor-
      liquid interface

   $\alpha(T)$ = Ostwald coefficient

   R_u = universal gas constant

   T = ambient water temperature

   p = local total pressure of water at any depth

Equation 24 is identical to equation 9 except that the proportionality
constant is the Ostwald coefficient instead of the Henry constant
(in equation 9).

The total pressure p at any depth $(H-z)$ can be written as*

$$p = p_a + \rho_w \, (H-z) \tag{25}$$

where p_a is the atmospheric pressure above the water surface

We now write the mass balance equation for the dissolution of
vapor in water from a single bubble.

$$\frac{d}{dt} \, (N) = - \, \kappa A_b \, (C-C_\infty) \tag{26}$$

where N is the total number of moles of the chemical in the vapor
bubble and C_∞ is the dissolved vapor concentration in water at distances
far removed from the vapor bubble. In general, it can be assumed
that $\quad\quad\quad\quad C_\infty = 0 \tag{27}$

In equation 26, N is a function of the bubble volume, total
pressure and temperature of vapor; κ (the mass transfer coefficient)
depends on the velocity of rise and bubble size; and C (the dissolved
concentration) is also a function of pressure (see equation 24). For
a constant velocity of rise of the bubble, the time derivative can be
replaced by a space derivative $(dz = u_b \, dt)$. Hence equation 26 becomes

---

*Note that $z = H$ represents the water surface and $z = 0$ represents
the release point under water.

113

$$\frac{d\ (N/N^{(i)})}{d(z/H)} \ = \ -\left[\frac{\kappa^{(i)}\ A_b^{(i)}\ C^{(i)}\ H}{N^{(i)}\ u_b}\right]\left(\frac{\kappa}{\kappa}^{(i)}\right)\left(\frac{C}{C}^{(i)}\right)\left(\frac{A_b}{A_b}^{(i)}\right) \qquad (28)$$

where the superscript i represents the initial value.

The solution of equation 28, gives the fraction $(N/N^{(i)})$ of vapor remaining in the bubble as a function of location of the bubble. By noting this value at the water surface the fraction of the vapor mass dissolved in water can be calculated. In order to perform such a calculation, the dependence of the mass transfer coefficient κ on velocity and bubble radius is obtained from either equation 11 or equation 12.

For example, in the case of large vapor bubbles, we use equation 11. That is

$$\frac{\kappa}{\kappa}^{(i)} \ = \left[\frac{r_b}{r_b^{(i)}}\right]^{-\frac{1}{2}} \qquad (29a)$$

Similarly using equations 24 and 25 we have

$$\frac{C}{C^{(i)}} \ = \ \frac{p_a + \rho_w g\ (H-z)}{p_a + \rho_w gH} \qquad (29b)$$

$$\frac{A_b}{A^{(i)}} \ = \ \left[\frac{r_b}{r_b^{(i)}}\right]^2 \qquad (29c)$$

and $\qquad \dfrac{N}{N^{(i)}} \ = \ \dfrac{\rho_v\ r_b^3}{\rho_v^{(i)} (r_b^{(i)})^3}$

assuming perfect gas the above becomes

$$= \ \frac{p_a + \rho_w g(H-z)}{p_a + \rho_w gH}\ \left(\frac{r_b}{r_b^{(i)}}\right)^3 \qquad (29d)$$

114

The solution to equation 28 using the equations 29a through 29d is given in appendix E. Only the final result is quoted here; the fraction of released mass that escapes into the atmosphere is

fraction of mass escaping into the = atmosphere

$$\left[1 - \frac{1}{3p^* \tau_1} \left\{ 1 - (1-p^*)^{\frac{3}{2}} \right\} \right]^2$$

for $\tau_1 \geq \frac{1}{3p^*} \left(1 - (1-p^*)^{3/2} \right)$ (30)

$= 0$, otherwise

where p^* is a dimensionless release depth pressure and τ_1 is a dissolution parameter defined in the nomenclature. A similar result has also been derived in <u>appendix E</u> for the dissolution of small vapor bubbles. The dimensionless equations and the solutions are given comprehensively in Table III-3.

The transfer of heat from water to the vapor has very little effect on the solubility since the solubility is a function of the water temperature. For the calculation made above it is assumed that the heat transfer to the vapor is negligible and that the vapor temperature within the bubble remains a constant throughout the rise time of the bubble. This temperature is equal to the saturation temperature at the release pressure if the bubbles are formed immediately after the liquid release or is equal to the superheat limit temperature, if the vapor bubbles are formed by superheat explosion of a liquid drop.

Dissolution of Drops

During the rise or fall of a drop, there are two simultaneous phenomena that take place -- dissolution into water and heat transfer from water to the drop. Dissolution is modeled in a way identical to the vapor bubble dissolution. However, unlike the case of vapor bubbles, the terminal velocity of a drop changes continuously with drop size.

115

Table III-3: Summary of formulae used in estimating the
dissolution of drops and bubbles released
at large depths in water

	Drops		Bubbles	
Critical Radius	$r_{c_d} = 2.79 \sqrt{\dfrac{\sigma}{\rho_w G}}$		$r_{c_b} = 1.82 \left[\dfrac{\sigma}{u^2 \left(\rho_w^2 \rho_v\right)} \, \tfrac{1}{3}\right]$	
Change Over Radius $^+$	$r_{ch_d} = 3.95 \left[\dfrac{\rho_w \nu_w^2}{G}\right]^{\frac{1}{3}}$		$r_{ch_b} = 4.2 \left[\dfrac{\sigma^2 \nu_w^4}{g^4 \rho_w^2}\left(1 - \dfrac{\rho_\ell}{\rho_v}\right)\right]^{\frac{1}{10}} \approx 4.2 \left[\dfrac{\sigma \nu_w^2}{g^2 \rho_w}\right]^{\frac{1}{5}}$	
	For $r_{ch_d} \le r \le r_{c_d}$ (large)	For $0 \le r \le r_{ch_d}$ (small)	For $r_{ch_b} \le r_b \le r_{c_b}$ (large)	For $0 < r_b < r_{ch_b}$ (small)
Terminal velocity (u)	$1.13\sqrt{G\,r}$	$0.144 \left[\dfrac{G\,r^2}{\nu_w}\right]$ [Modified Stokes Law]	$0.668 \left(\dfrac{\sigma^2 G}{\nu_w \, \rho_w}\right)^{\frac{1}{5}}$	$0.037 \left(\dfrac{G\,r^2}{\nu_w}\right)$
Mass transfer Coefficient (κ)	$0.424 \dfrac{D}{r}(Re\,Sc)^{0.5}$	$0.63 \dfrac{D}{r}(Re\,Sc)^{0.33}$	$0.799 \dfrac{D}{r}(Re\,Sc)^{0.5}$	$0.63 \dfrac{D}{r}(Re\,Sc)^{0.33}$
Heat Transfer Coefficient (h)	$\longrightarrow$ $\qquad 0.79 \dfrac{K}{r} Re^{0.4} Pr^{0.33} \qquad$ $\longrightarrow$			
ϕ	$\left[1 + \dfrac{(1-p^*n)^2 - 1}{\frac{24}{7} p^* \tau_1}\right]^{\frac{6}{7}}$	$\left[1 + \dfrac{(1-p^*n)^2 - 1}{2p^* \tau_1}\right]^{\frac{1}{2}}$	$\left[1 + \dfrac{(1-p^*n)^2 - 1}{3p^* \tau_1}\right]^{3/2}$	$\left[1 + \dfrac{(1-p^*n)^2 - 1}{2p^* \tau_1}\right]^{\frac{1}{2}}$

Note: $G = g\left|(1 - \dfrac{\rho_\ell}{\rho_w})\right|$

$^+$ Change over radius is that radius of bubble or drop at which the regime of motion changes. At
the change over radius the terminal velocity calculated by the two equations applicable to the
two regimes is the same.

The mass transfer equation for a dissolving liquid drop is written as

$$\frac{u_d}{u_d^{(i)}} \quad \frac{d(N/N^{(i)})}{d(z/H)} = - \left[\frac{\kappa^{(i)} A_d^{(i)} C^{(i)} H}{N^{(i)} u_d^{(i)}} \right] \left(\frac{\kappa}{\kappa^{(i)}}\right) \left(\frac{C}{C^{(i)}}\right) \left(\frac{A_d}{A_d^{(i)}}\right) \quad (31)$$

Similarly the heat transfer equation is

$$\frac{d}{dt} (m\, c\, T_\ell) = h\, A_d\, (T_w - T_\ell) \tag{32}$$

where m is the mass of liquid in the drop, h the heat transfer coefficient, T_w and T_ℓ are respectively the water bulk temperature and the liquid drop temperature. The value of the heat transfer coefficient h is obtained from heat/mass transfer correlations discussed earlier in this section.

In the case of liquid drops, there results a spontaneous boiling when the drop reaches the water surface (in the case of a lighter-than-water liquid) or when the critical superheat temperature is attained. The calculations of drop dissolution using equations 31 and 32 are then stopped and vapor bubble dissolution equations are used for subsequent calculations. Alternatively boiling can be assumed to occur (resulting in vapor bubble formation) when the temperature of the liquid drop attains the saturation temperature corresponding to the local pressure. The latter will occur when there are nucleation sites availble for boiling to start.

It is expected that a spectrum of drop sizes will be formed during the process of accidental release of a large amount of liquid chemical under water. To date there have been no experiments to correlate the drop size distribution with the dynamics of the accident. However, certain reasonable drop size distributions can be assumed. Two such distributions are schematically illustrated with their distribution equations, in figures III-4a and III-4b.

117

The Beta Distribution

$$f_X(y) = \begin{cases} \dfrac{\Gamma(\alpha + \beta)}{\Gamma(\alpha)\Gamma(\beta)} y^{(\alpha-1)}(1-y)^{(\beta-1)}, & \text{for } 0 \le y \le 1 \\ 0, & \text{elsewhere} \end{cases}$$

Fraction of drops with radii between r and r + dr

$$y = \frac{r}{r_{max}}$$
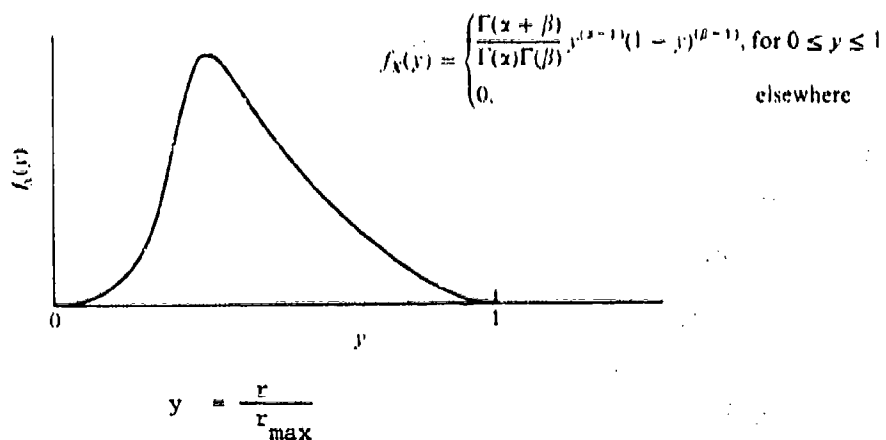
Figure III-4.a: A possible distribution when there is a maximum size drop determined by a physical constraint.

The Rayleigh Distribution

$$f(r) = \frac{r}{\overline{r^2}} \, \text{Exp} \left[- \frac{r^2}{2\overline{r^2}} \right]$$

Fraction of drops with radii between r and r + dr

$$r = \sqrt{\overline{r^2}}$$

r → drop radius
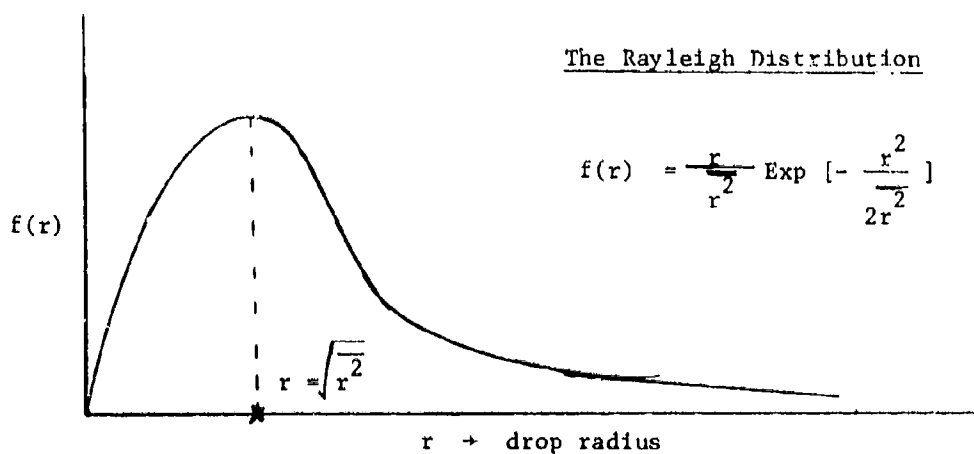
Figure III-4.b: Possible distribution when there is no physical constraint on maximum drop size.

The equations 31 and 32 are expressed in dimensionless form and solved for the mass of liquid escaping and temperature. This procedure is illustrated in appendix E. The resultant equations and any solutions which are expressible in closed form are indicated in Table III-3. Also indicated in Table III-3 are the formulas for critical size of bubbles and drops and the heat/mass transfer formulae.

SPECIFIC EXAMPLE

In order to illustrate the calculation procedures, a specific numerical example is worked. The final answer that is sought in the example is the mass fraction that escapes into the air when vinyl chloride liquid is released at a reasonably large depth.

WATER PROPERTIES

Density	ρ_w	1000	kg/m^3
Temperature	T_w	293	K
Kinematic viscosity	ν_w	10^{-6}	m^2/s
Prandtl number	P_r	7	

VINYL CHLORIDE PROPERTIES

Density	ρ_ℓ	969	kg/m^3
Solubility in water at atmospheric pressure	S	.006	$kg/kg \ H_2O$
Molecular weight	M	62.5	kg/kgmol
Diffusivity	D	10^{-9}	m^2/s
Heat capacity	C_p	1270	J /kg K
Thermal conductivity (estimated)	K	.597	W/m K
Surface tension	σ	.07	N/m
Release temperature	T_1	259.4	K
Vapor pressure correlation constants where $T_{vap} = \dfrac{C_2}{C_1 - \log_{10} P_{vap}} - C_3$	C_1	1183	k
	C_2	9.566	
	C_3	0.	K
Critical temperature	T_c	431.6	K
Schmidt number	Sc	10^3	

ENVIRONMENTAL PARAMETERS

Release depth	H_0	15	m
Ambient pressure	P_a	101325	N/m^2

Parameter	Equation	Formula	Calculation	Value
Effective gravity		G	$g \left(1 - \dfrac{\rho_\ell}{\rho_w}\right) = 9.8 \times (1 - 0.969)$	$0.304 \ \text{m/s}^2$
Temperature above which violent boiling occurs	19	T_{SH}	0.89×413.6	$= 368 \ \text{K}$
Critical drop radius (also the initial radius)	7	$r_{c_d} = r^{(i)}$	$2.79 \times \left[\dfrac{0.07}{1000 \times 0.304}\right]^{\frac{1}{2}}$	$= 0.0424 \ \text{m}$
Saturation concentration in water at atmospheric pressure		C	$= \dfrac{S \ \rho_w}{M} = \dfrac{0.006 \times 1000}{62.5}$	$= 0.096 \ \text{kmol/m}^3$
Equilibrium concentration at 15 m depth in water	24	$C^{(i)}$	$= 0.096 \ \dfrac{2.48 \times 10^5}{1.01 \times 10^5}$	$0.235 \ \text{kmol/m}^3$
Total pressure at 15 m depth of water	25	$p^{(i)}$	$= 101325 + 9.8 \times 1000 \times 15$	$2.48 \times 10^5 \ \text{N/m}^2$
Schmidt Number		$Sc = \dfrac{\nu_w}{D}$	$10^{-6} / 10^{-9}$	1000
Terminal velocity of non deformable drop	4	v	$2.31 \sqrt{0.0424 \times 0.304}$	$0.262 \ \text{m/s}$
Terminal velocity of a deformable drop	5	u_i	$0.262 \left[(1-0.56) \ \dfrac{1 + 1.78 \ (1-.56)^{3/2}}{1 + 1.78}\right]^{\frac{1}{2}}$	$0.129 \ \text{m/s}$
Reynolds number		$Re = \dfrac{u_i \ r_{c_d}}{\nu_w}$	$= \dfrac{0.129 \times 0.0424}{10^{-6}}$	$= 5450$
Initial mass transfer coefficient	13	$\kappa^{(i)}$	$0.424 \times \dfrac{10^{-9}}{0.0424} \sqrt{5450 \times 1000}$	$= 2.34 \times 10^{-5} \ \text{m/s}$
Initial heat transfer coefficient	16	$h^{(i)}$	$= 0.79 \times \dfrac{0.597}{0.0424} \ (5450)^{0.4} \ 7^{0.33}$	$= 660 \ \text{W/m}^2 \ \text{K}$
Initial molar content of the drop		$N^{(i)}$	$= \dfrac{969}{62.5} \ \dfrac{4 \times \pi \times (0.0424)^3}{3}$	$= 4.95 \times 10^{-3} \ \text{kmol}$

120

Initial surface area of drop	A_i	$4 \times \pi \times (.0424)^2$	$0.0226\ m^2$
Characteristic dis-solution time	E.2 t_d =	$\dfrac{0.00495}{0.0226 \times .235 \times 2.34 \times 10^{-5}}$	$=3.98 \times 10^4$ s
Characteristic rise time	E.2 t_r	$\dfrac{15}{0.129}$	116 s
Characteristic heat up time	t_h	$= \dfrac{0.00495 \times 1270 \times 62.5}{660 \times .0226}$	26.35 s
Dimensionless mass transfer time scale	E.2 $\tau_1 = \dfrac{t_d}{t_r}$	$= 3.98 \times 10^4/116$	343
Dimensionless heat transfer time scale	E.19 $\tau_2 = \dfrac{t_h}{t_r}$	$= \dfrac{26.35}{116}$	0.227
Dimensionless hydro-static pressure at depth H_0	E.2 $p^* = \dfrac{\rho_w g H_0}{p^{(i)}}$	$\dfrac{1000 \times 9.8 \times 15}{2.48 \times 10^5}$	0.593
Changeover radius	r_{ch_d} Table III-3	$= 3.95 \times \left[\dfrac{1000 \times 10^{-12}}{.304}\right]^{1/3}$	$=5.88 \times 10^{-3}$ m

Since the initial drop radius is larger than the r_{ch_d} we use the results from column 1 of Table III-3. By a numerical integration of the equation for the temperature and comparing the liquid drop temperature at every depth with the local saturation temperature for boiling we find that

$$\text{at } \eta = 0.211 \ ; \ T_\ell = T_{vap}$$

The following results are also obtained

Depth at which $T_\ell = T_{vap}$	H	$(1-0.211) \times 15$	11.84 m
Radius of drop	r_d		0.0424 m
Liquid boiling temperature at this depth	T_{vap}		279.7 K

Fraction of mass of liquid remaining   E.2 $\phi^2 = \left[\dfrac{0.04237}{0.0424}\right]^3$ = 0.9994

In this example, it is assumed that when the liquid temperature reaches the local saturation temperature boiling ensues and vapor bubbles of critical size are formed. We now proceed to calculate the fraction of bubble mass that is dissolved.

Pressure at 11.84 m depth $p^{(i)}$ 2.17×10^5 N/m²

Local vapor density $\rho_v = \dfrac{p^{(i)} M}{R_u T_{vap}} = \dfrac{2.17 \times 10^5 \times 62.5}{8.31 \times 10^3 \times 279.7}$ = 5.83 kg/m³

Effective gravity for bubble rise   G $= (1 - \dfrac{\rho_v}{\rho_w})\, g = 9.8 \times [1 - \dfrac{5.83}{1000}]$ = 9.743 m/s²

Terminal velocity of initial size bubbles   1 $u_b^{(i)}$ $0.668 \times \left[\dfrac{0.07^2 \times 9.743}{1000^2 \times 10^{-6}}\right]^{1/5}$ = 0.3635 m/s

Critical bubble radius (this is also assumed to be initial bubble radius)   3 r_{c_b} $1.82 \times \dfrac{0.07}{.3635^2\,[1000^2 \times 5.83]^{\frac{1}{3}}}$ = 5.36×10^{-3} m

Initial equilibrium concentration at depth 11.84 m $C^{(i)}$ 0.206 kmol/m³

Bubble Reynolds number $Re^{(i)} = \dfrac{u_b^{(i)} r_b^{(i)}}{\nu} = \dfrac{0.3635 \times 5.36 \times 10^{-3}}{10^{-6}}$ = 1950

Mass transfer coefficient Table III-3 $\kappa^{(i)}$ $= \dfrac{0.799 \times 10^{-9} \times \sqrt{1950 \times 1000}}{5.36 \times 10^{-3}}$ = 2.08×10^{-4} m/s

Initial molar content of bubble $N^{(i)}$ $= \dfrac{4}{3}\pi \times (5.36 \times 10^{-3})^3 \times \dfrac{5.83}{62.5}$ = 6.02×10^{-8} kmol

Initial surface area of bubble $A_b^{(i)}$ $4 \times \pi\,(5.36 \times 10^{-3})^2$ = 3.61×10^{-4} m²

122

Characteristic dissolution time   E.2 t_d $= \dfrac{6.02 \times 10^{-8}}{(2.08 \times 10^{-4} \times 3.61 \times 10^{-4} \times 0.206)}$ $= 3.88$ s

Characteristic rise time   E.2 t_r $= \dfrac{11.84}{0.3635}$ $= 32.5$ s

Dimensionless time scale for mass transfer   E.2 τ_I $= 3.88/32.5$ $= 0.119$

Dimensionless local pressure   E.2 p^* $= \dfrac{1000 \times 9.8 \times 11.84}{(1000 \times 9.8 \times 11.84 + 101325)}$ $= 0.534$

From Table III, Column 1, the value of ϕ for any depth can be calculated. Noting ϕ and the relationship given by Equation E5, the radius of bubble vs. depth can be evaluated.

Change over radius of bubble (from "large" to "small") ** r_{ch_b} $= 4.2 \times \left[\dfrac{0.07 \times 10^{-6} \times 10^{-6}}{9.8^2 \times 1000} \right]^{\frac{1}{5}}$ $= 9.9 \times 10^{-4}$ m

A step wise calculation of ϕ as a function of η (and therefore r_b as a function of η) for the above values indicates that at

$$\eta = 0.199 \quad r_b = r_{ch_b}$$

Depth at this stage   H $= (1-0.199) \times 11.84$ $= 9.48$ m

Undissolved mass ϕ^2 $= N/N^{(i)}$ $= 0.0057$

Radius of the vapor bubble r_b $= r_{ch_b}$ $= 9.9 \times 10^{-4}$ m

Saturation temperature corresponding to this depth T_{vap} $= 279.7$ K

** Note that change over radius is defined as that bubble radius at which the bubble terminal velocity given by equations for small and large bubbles from Table III-3

123

Small bubble Rise Calcutation

Description	Symbol		Value
Depth at which small bubble calculations start	H		9.48 m
Initial pressure (at depth 9.48 m)	$p^{(i)}$	$= (\rho_w\, g\, H + p_a)$	1.94×10^5 N/m^2
Dimensionless hydro-static pressure	p^*		0.478
Initial equilibrium concentration	$c^{(i)}$		0.184 kmol
Initial terminal velocity	$u^{(i)}$	$= 0.364$ m/s	0.364 m/s
Reynolds number	$Re^{(i)}$		361
Initial Mass transfer coefficient (12)	$\kappa^{(i)}$	$= \dfrac{0.0378 \times 9.8 \times (9.9 \times 10^{-4})^2}{10^{-6}}$	
		$= \dfrac{0.364 \times 9.9 \times 10^{-4}}{10^{-6}}$	
		$= \dfrac{0.63 \times 10^{-9}}{9.9 \times 10^{-4}} \times (361 \times 1000)^{\frac{1}{3}}$	4.51×10^{-5} m/s
Initial molar content	$N^{(i)}$		3.4×10^{-10} kmol/m^3
Initial surface area	$A_b^{(i)}$		1.24×10^{-5} m^2
Characteristic disso-lution time	t_d		3.44 s
Characteristic rise time	t_r		26.0 s
Dimensionless mas transfer time scale	τ_1		0.132

We use now the ϕ equation given in Column 4 of Table III-3. It is found that the bubble dissolves completely at a η value of

Hence, η = 0.107

the depth at this η value H = $(1-0.107) \times 9.48$ 8.47 m

Therefore, by the time the vapor bubbles reach about half the liquid release depth, all of the vinyl chloride is dissolved.

DISCUSSION

Two facts should be apparent from the preceding theory and example, i.e.,

- little experimental data are directly applicable to act either as a guide or check on the theory.

- the calculation of the fraction mass dissolved in the water is not readily accomplished; a number of calculations need to be made and judgment is necessary in some instances.

Still, each of the steps in the calculations is based on experimental data or theory; it was, however, necessary to employ these in a far more complex situation than for the one applicable in the original investigation. To be more specific, suppose the example problem could be simplified to one such as, given a vinyl chloride bubble of a known size injected at a depth Z, calculate the fraction dissolved before the bubble reaches the surface. This calculation could be readily made using the equations given in this report -- and with some degree of confidence. On the other hand, if the total amount of gaseous vinyl chloride were, instead, specified, then accurate predictions become much more difficult. Stability theory must be invoked to estimate the "initial" bubble sizes. The results are critically dependent on the chosen distributions. Very small bubbles will dissolve far more rapidly than if the vinyl chloride vapor were in a few large bubbles.

If the initial statement were modified so that liquid vinyl chloride were present, then the problem definition is vague. Break-up of large liquid masses would be expected, but the distribution can only be approximated. Worse, it is not known if the liquid fragments would boil -- even though the water temperature exceeds the boiling temperature at the specified depth. Superheating can occur so readily that one may be faced with a mass of metastable liquid drops (of unknown distribution) which will boil (and violently) when they contact a suitable nucleation site.

125

Desperately needed are data to provide guidelines in this
interesting but undefined problem.

However, assuming the calculational procedure does provide a
valid (but approximate) estimation of the fraction mass boiled, it
would be very interesting to select several trial chemicals and examine
parametrically what would be expected if they were "spilled" into
water at various depths. Would the results of this exercise yield
results which could be generalized to provide conservative results
applicable to real accidents? If so, they would be of real value in
indicating to Coast Guard personnel whether most of the spill would
end in the water or, alternatively, in the air.

CONCLUSIONS

1. A theoretical analysis was carried out to indicate the
fraction mass dissolved from cold, soluble chemicals injected into
water at any specified depth.

2. The analysis assumes knowledge of the liquid (or gas) drop-size
distribution; heat and mass transfer considerations then indicate the
temperature change and fraction dissolved as the liquid (or gas)
rises (or falls).

3. Superheating of liquid drops is discussed and a criterion
presented to allow one to estimate if a superheat-limit vapor explosion
would result. In all cases of cold, soluble chemicals considered,
none would lead to a vapor explosion at typical sea-water temperatures.
Some superheating would be expected for liquids in contact with
water above the local boiling point; onset of boiling is, however,
difficult to predict.

4. An example problem was presented in detail to illustrate
the method of calculation. Vinyl chloride was assumed to be released
at a depth of 15 m. The initial liquid drop size was estimated
to be about 0.042 m (4.2 cm). Vaporizations began at about 11.8 m
and dissolution was completed before any of this chemical reached
the surface.

RECOMMENDATIONS

1.   Experimental data be obtained to verify the theoretical
methods outlined in this report -- or to provide a guide for modi-
fications.

2.   A parametric study be carried out with about six typical
cold, soluble chemicals with different boiling temperatures,
solubilities, and densities. (Some may be hypothetical.) From a
sensitivity analysis of the results, attempt to prepare broad
guidelines of value to Coast Guard personnel to allow rapid evaluations.
of the fraction mass dissolved in real release situations. This
study would be of value if it can be shown that some of the
independent variables were relatively unimportant in specifying
the final results.

127

APPENDIX E

In this appendix, the procedures for obtaining the solutions to the heat and mass transfer equations vapor are illustrated for both vapor bubble dissolution and liquid drop dissolution. The procedures involve writing the equations in dimensionless form and solving the resulting differential equations. Wherever possible, analytical solutions are given. When analytical solutions are not possible, brief statements are included for numerical solution procedure

(i) Vapor Bubble Dissolution

a) Large Bubbles

The equation to be solved is given in equation 28 and is

$$\frac{d \ (N/N^{(i)})}{d \ (z/H)} = - \left[\frac{K^{(i)} \ A_b^{(i)} \ C^{(i)} \ H}{N^{(i)} \ u_b} \right] \frac{K}{K^{(i)}} \ \frac{C}{C^{(i)}} \ \frac{A_b}{A_b^{(i)}} \qquad (E.1)$$

We define the following parameters

$$t_d = \frac{N^{(i)}}{K^{(i)} \ A_b^{(i)} \ C^{(i)}} \qquad = \ \begin{array}{l} \text{Characteristic} \\ \text{dissolution time} \end{array} \qquad (E.2)$$

$$t_r = \frac{H}{u_b} \qquad = \ \begin{array}{l} \text{Rise time of the} \\ \text{bubble} \end{array}$$

$$t_r = \frac{H}{u_d} \qquad = \ \text{Rise time of drop}$$

u_b and u_d are respectively the bubble and drop terminal velocities (upward). Because of the fact that the sizes of these bubbles and drops

128

vary during their motion in water, the terminal velocity changes from one regime to another. In such cases the above $u_b^{(i)}$ and $u_d^{(i)}$ should be interpreted as the initial velocities for the given regime:

$$\tau_1 = \frac{t_d}{t_r} \qquad\qquad = \text{Dimensionless time for mass transfer}$$

$$\eta = \frac{z}{H} \qquad\qquad = \text{Dimensionless upward distance*}$$

$$p^* = \frac{\rho_w \, g \, H}{p^{(i)}} = \frac{1}{1 + (p_a/\rho_w \, g \, H)}$$

$$\phi^2 = \frac{N}{N^{(i)}} = \left[\frac{r}{r^{(i)}}\right]^3 = \frac{\text{Moles of vapor in the bubble or drop of liquid}}{\text{Moles of vapor initially in the bubble or drop of liquid}}$$

$$\left.\rule{0pt}{11em}\right\} \text{(E.2)}$$

Also we note

$$\frac{A_b}{A_b^{(i)}} = \left(\frac{r_b}{r_b^{(i)}}\right)^2$$

$$\frac{\kappa}{\kappa^{(i)}} = \left[\frac{r_b}{r_b^{(i)}}\right]^{-\frac{1}{2}} \qquad\qquad \text{(See Equation 29a)} \qquad\qquad \text{(E.3)}$$

---

*$\eta = 1$ represents water surface

$\eta = 0$ represents the location of release of vapor bubble

$$\frac{C}{C^{(i)}} = \frac{p}{p^{(i)}} = (1 - p^* n) \tag{E.4}$$

$$\frac{N}{N^{(i)}} = \frac{p}{p^{(i)}} \left[\frac{r_b}{r_b^{(i)}} \right]^3 = \phi^2 \tag{E.5}$$

(See Equation 29d)

Hence

$$\left[\frac{r_b}{r_b^{(i)}} \right]^3 = \frac{\phi^2}{[1-p^* n]} \tag{E.6}$$

Substituting the parameters from equation E.2 and equations E.3, E.4, E.5, and E.6 in E.1, we get

$$\tau_1 \frac{d \phi^2}{d n} = - \phi (1 - p^* n)^{\frac{1}{2}} \tag{E.7}$$

with $\qquad \phi = 1$ at $\eta = 0$ $\tag{E.8}$

The solution of E.7 with E.8 is given by

$$\phi(n) = 1 - \frac{1}{3p^* \tau_1} \left[1 - (1 - p^* n) \right]^{\frac{3}{2}} \tag{E.9}$$

130

b) Small Bubbles

For small bubbles the terminal velocity of rise is no longer a constant but depends on the bubble radius (see Table III-3). The size at which bubbles are considered to be small is indicated in Table III-3.

$$\text{i.e.,} \quad \frac{u_b}{u_b^{(1)}} = \left[\frac{r_b}{r_b^{(1)}} \right]^2 \tag{E.10}$$

Also it is noted that the mass transfer coefficient's dependence on bubble radius is different from that of large bubble.

$$\text{i.e.,} \quad \kappa \propto u^{\frac{1}{3}} r_b^{-\frac{2}{3}} \tag{E.11}$$

Hence from E.10 and E.11

$$\kappa = \kappa^{(1)} = \text{constant}$$

Substituting E.10, E.11 and other equations as before in E.1, we get*

$$\tau_1 = \frac{d \phi}{d \eta} = - (1 - p^* \eta) \tag{E.12}$$

with $\phi = 1$ at $\eta = 0$

The solution to the above is

$$\phi (\eta) = \left[1 - \frac{\langle 1 - (1 - p^* \eta)^2 \rangle}{2 p^* \tau} \right]^{\frac{1}{2}} \tag{E.13}$$

---

*Note that η is defined with the depth at which small bubbles are said to be formed.

131

(ii) Liquid Drops

A) Dissolution of large drops: drops moving through the
water column

We note from equations 4 and 5 that the terminal velocity for
large drops is proportional to the square root of the radius

$$\text{i.e.,} \quad u_d \ \alpha \ r_d^{\frac{1}{2}} \tag{E.14}$$

Also from equation 13

$$\kappa \ \alpha \ r_d^{-\frac{1}{4}} \tag{E.15}$$

Substituting E.14 and E.15 in the drop mass transfer equation (28)
and using the definitions of parameters given in equation E.2, we can
write equation 28 as

$$\phi^{-\frac{5}{6}} \ \frac{d\phi}{d\eta} \ = \ -\frac{(1-p^* \ \eta)}{\tau_1} \tag{E.16}$$

with condition

$$\phi \ = \ 1 \text{ at } \eta \ = \ 0$$

[Note: for $\rho_\ell > \rho_w$, u_d the terminal velocity is directed
downwards; hence η values should be considered
negative and t_r less than zero.]

132

The solution to E.16 is given by

$$\phi(\eta) = \left[1 - \frac{1 - (1 - p^* \eta)^2}{\frac{24}{7} p^* \tau_1} \right]^{\frac{6}{7}} \tag{E.17}$$

The heat transfer process is described by equation 32 and is

$$m \frac{d}{dt} (c\, T_\ell) = h\, A_d\, (T_w - T_\ell) \tag{E.18}$$

To solve for the temperature of the liquid drop as it rises (or falls) through the water, equation E.18 has to be solved with appropriate conditions. In order to do so, the above equation is written in dimensionless form. The following parameters are defined

$$d\,\eta = \frac{u_d\, dt}{H}$$

$$\Delta T = (T_\ell - T_w) \qquad = \quad \text{Temperature difference between liquid and water}$$

$$\psi = \frac{T_\ell}{T_\ell^{(i)} - T_w} = \frac{T_\ell}{\Delta T^{(i)}} \qquad = \quad \text{Dimensionless liquid temperature}$$

$$[\text{Therefore,} \quad \psi^{(i)} = \frac{T^{(i)}}{\Delta T^{(i)}}, \quad \psi_w = \frac{T_w}{\Delta T^{(i)}}]$$

133

$$t_h = \text{characteristic drop heat up time} = \frac{m\, c\, N^{(i)}}{h^{(i)}\, A_d^{(i)}}$$

$$\tau_2 = \frac{t_h}{t_r} = \text{dimensionless heat up time}$$

We also note from equation 16 that

$$h \;\alpha\; r_d^{-0.6}\, u_d^{0.4} \tag{E.20}$$

Substituting E.19, E.20 and other parameters from E.2 into equation E.18, we get

$$\phi^2\, \frac{d\,\psi}{d\,\tau} = \frac{1}{\tau_2}\, \phi^{\frac{11}{15}}\, (\psi_w - \psi) \tag{E.21}$$

with $\psi = \psi^{(i)}$ for $\eta = 0$

It is noted that in the above equation ϕ is a function η given by equation E.17. E.21 has to be solved numerically. The solution will be given by

$$\psi = \psi_w + (\psi^{(i)} - \psi_w)\; e^{\left[-\frac{1}{\tau_2} \int_0^{\eta} \frac{d\,\eta}{[1 + \frac{7}{24}\, \frac{(1 - p^*\,\eta)^2 - 1}{\tau_1}]^{\frac{38}{35}}} \right]} \tag{E.22}$$

The solution procedure involves starting the numerical calculation at H (i.e., $y = \eta = 0$) and increase y in steps (for $\rho_\ell < \rho_{(w,}$ the drop rises).

(1) At each step the drop radius r_d (ϕ in dimensionless variable) and temperature T_ℓ (ψ in dimensionless variables) are calculated using equation E.17 and E.22.

(2) At each calculation point three conditions are checked, viz.

a) is
$$\begin{bmatrix} T_\ell > T_v \\ T_\ell \geq T_{SH} \end{bmatrix}$$
if yes, the height is noted and calculation of bubble dissolution started

b) is $r \leq r_{c_d}$
if yes, the calculations are further carried out using small drop dissolution theory (see below)

c) is $\eta = 1$
i.e., has the water surface been reached

B) Dissolution of Small drops: Drops moving through the water column

The starting condition, represented by the superscript (i) for the small drop will be the end condition of the large drop dissolution (case b above). Because of the different functional dependence of u_d and κ on drop radius, the form of the equations of mass and heat transfer will be different.

$$u_d \propto r_d^2$$
(See Table III-3; also Ref. 8)

$$\kappa \propto r_d^{-2/3} u_d^{1/3}$$
(See equation 14)

(E.23)

135

Substituting the above in the heat and mass transfer equations and noting that $\eta = 0$ is the water depth at which the small size liquid drops result from the dissolution of large drops, we can show that the equations become

$$\phi(\eta) = \left[1 - \frac{1 - (1 - p^* \eta)^2}{2 \, p^* \, \tau_1} \right]^{\frac{1}{2}} \tag{E.24}$$

$$\psi = \psi_w + (\psi^{(i)} - \psi_w) \, \text{Exp} \left\{ -\frac{1}{\tau_2} \int_{\eta = 0}^{\eta} \frac{d\eta}{\left[1 + \frac{[(1 - p^* \eta)^2 - 1]}{2 \, p^* \, \tau_1} \right] \frac{17}{15}} \right\} \tag{E.25}$$

^) Liquid Drop Resting on the Bottom of the Water Body

In the case $\rho_\ell > \rho_w$ the liquid drop probably falls to the bottom of the water body. If during this fall, the drop temperature does not reach either the local boiling temperature or in pure water the super-heat limit temperature, the drop settles down on the bottom surface. Assuming that the drop retains its shape and identity we derive the following dissolution rate equations.

Since there is no relative vertical motion between water and the drop we can make the following estimates for heat and mass transfer coefficients (Sherwood et al[8])

$$\frac{\kappa \, r_d}{D} = 1 \; ; \quad \frac{h \, r_d}{K} = 1 \tag{E.26}$$

136

Also since the pressure is a constant, at the bottom of the water body

$$C = \text{constant} = C^{(i)} \qquad (E.27)$$

Defining further

$$t_d = \frac{N^{(i)}}{\kappa^{(i)} A_d^{(i)} C^{(i)}} \qquad \text{as in E.2}$$

$$\tau = t/td \qquad\qquad\qquad\qquad \left.\begin{array}{c} \\ \\ \\ \end{array}\right\} \quad E(28)$$

$$t_h = \frac{N^{(i)} M c}{h^{(i)} A_d^{(i)}}$$

where M is the molecular weight of the liquid

We write the mass transfer equation where M is the molecular weight of the liquid

$$\frac{dN}{dt} = - \kappa A C \qquad (E.29)$$

as

$$\frac{N^{(i)}}{t_d} \frac{d}{d\tau} [N/N^{(i)}] = - \kappa^{(i)} A_d^{(i)} C^{(i)} \frac{\kappa}{\kappa^{(i)}} \frac{A_d}{A_d^{(i)}} \qquad (E.30)$$

i.e.,

$$\frac{d\phi^2}{d\tau} = - \left[\frac{r_d}{r_d^{(i)}}\right]^{-1} \left[\frac{r_d}{r_d^{(i)}}\right]^2 \qquad (E.31)$$

Because of constant pressure, we have

$$\phi^2 = \frac{N}{N^{(i)}} = \left[\frac{r_d}{r_d^{(i)}}\right]^3 \qquad (E.32)$$

137

Hence E.31 becomes

$$\phi^{-\frac{2}{3}} \frac{d\phi^2}{d\tau} = -1; \quad \phi = 1 \text{ at } \tau = 0 \tag{E.33}$$

Hence

$$\phi(\tau) = [1 - \frac{2\tau}{3}]^{3/4} \tag{E.34}$$

Similary for heat transfer we have

$$m \frac{d(c\, T_\ell)}{dt} = h\, A\, (T_w - T_\ell)$$

where m is the mass of each drop of liquid.

i.e.,

$$\frac{N}{N^{(1)}} \frac{\Delta T^{(1)}\, N^{(1)}\, M\, c}{t_d} \frac{d\psi}{d\tau} = \left(\frac{t_d}{t_h}\right) \phi^{2/3} (\psi_w - \psi) \tag{E.35}$$

where the definitions in equations E.19 have been used.

Hence E. 35 becomes

$$\phi^2 \frac{d\psi}{d\tau} = \frac{t_d}{t_h} \phi^{2/3} (\psi_w - \psi) \tag{E.36}$$

The solution to which is

$$\psi = \psi_w + (\psi^{(1)} - \psi_w) (1 - \frac{2}{3}\tau)^{\frac{3}{2} \frac{t_d}{t_h}} \tag{E.37}$$

138

i.e.,

$$T_\ell = T_w + (T_\ell^{(i)} - T_w)(1 - \frac{2}{3}\frac{t}{t_d})^{\frac{3}{2}\frac{t_d}{t_h}} \tag{E.38}$$

From these results the drop radius and its temperature can be determined. If the boiling temperature of the liquid corresponding to the bottom pressure is less than the water temperature then the liquid is likely to boil. The time at which this will happen can easily be calculated from equation E.38 provided that the boiling temperature at that depth is known.

NOMENCLATURE

A_1	Initial surface area	m^2
c	Specific heat of liquid	J/kg K
C	Equilibrium concentration of the solute in water at any pressure	$kmol/m^3$
$c^{(i)}$	Equilibrium concentration at the pressure corresponding to the initial depth of the bubble or drop	$kmol/m^3$
C_1	First constant of vapor pressure correlation	

$$T_{vap} = \frac{C_2}{C_1 - \log_{10} P_{vap}} - C_3$$

C_2	Second constant of vapor pressure correlation	K
C_3	Third constant of vapor pressure correlation	K
D	Diffusivity of chemical in water	m^2/s
g	Gravitation constant (9.8)	m/s^2
G	Reduced gravity $g(1 - \frac{\rho_v}{\rho_w})$ or $g(\frac{\rho_\ell}{\rho_w} - 1)$	m^2/s
h	Heat transfer coefficient	W/m^2 K
H	Depth at which the drop or bubble is formed	m
H_0	Release depth of the liquid chemical	m
K	Thermal conductivity	W/m K
m	Mass of liquid in a drop of liquid	kg
M	Molecular weight	kg/kmol
N	Molar content	kmol
N_1	Initial molar content	kmol
P_a	Ambient pressure	N/m^2
p	Total thermodynamic pressure at any depth	N/m^2
Pr	Prandtl number	
P_{vap}	Vapor pressure	N/m^2

140

p^*	Dimensionless pressure (Equation E.3) $=$	$\dfrac{\rho_w\, g\, H_0}{p_1}$
r	radius	m
r_{cb}	Critical bubble radius	m
r_{c_d}	Critical drop radius	m
r_{ch_b}	Changeover bubble radius	m
r_{ch_d}	Changeover drop radius	m
Re	Reynolds number $\dfrac{u\,r}{\nu_w}$	
R_u	Gas constant (8314)	J/kmol
S	Solubility	kg/kg H_2O
Sc	Schmidt number	
T	Temperature	K
T_c	Critical temperature	K
t_d	Characteristic dissolution time	s
t_h	Characteristic heat up time	s
t_r	Characteristic rise time	s
T_1	Initial temperature	K
T_{SH}	Critical superheat temperature	K
T_{vap}	Temperature corresponding to vapor pressure p_{vap}	K
T_w	Water temperature	K
u	Terminal velocity	m/s
v	Terminal velocity of non-deformable drop	m/s
V	Volume of a liquid drop	m^3
z	Vertical distance coordinate	m

GREEK

η Dimensionless rise distance $= \dfrac{z}{H}$

κ Mass transfer coefficient   m/s

ν Kinematic viscosity m^2/s

ρ_ℓ Density kg/m^3

ρ_v Vapor density kg/m^3

ρ_w Water density kg/m^3

σ Surface tension   N/m

τ_1 Dimensionless time scale for mass transfer $= t_d/t_r$

τ_2 Dimensionless time scale for heat transfer $= t_h/t_r$

ϕ Dimensionless molar content in a bubble or drop $= \left(\dfrac{N}{N^{(i)}}\right)^{\frac{1}{2}}$

ψ Dimensionless temperature $= \dfrac{T_\ell}{(T_\ell^{(i)} - T_w)}$

$\psi^{(i)}$ Dimensionless initial temperature $= \dfrac{T_\ell^{(i)}}{T_\ell^{(i)} - T_w}$

ψ_w Dimensionless water temperature $= \dfrac{T_w}{(T_\ell^{(i)} - T_w)}$

SUPERSCRIPTS

i   =   Initial value (refers to the value of the parameter at the location of the formation of drop or liquid).

SUBSCRIPTS

    b   =   bubble

    d   =   drop

    ch   =   characteristic
                also change over

    w   =   water

    ℓ =   liquid

    v   =   vapor

REFERENCES

1. "Hazards of Marine Transportation of Liquid Chlorine", U.S. Bureau of Mines, MIPR Z-70099-9-9374, March 1970.

2. "CHRIS-Hazardous Chemical Data", U.S. . t Guard CG-446-2, January 1974 (chemical properties file in Hazard Assessment Computer System).

3. "Prediction of Hazards of Spills of Anhydrous Ammonia on Water", U.S.C.G., Washington, January 1974, NTIS # AD779400.

4. Levich, V.G., "Physico-Chemical Hydrodynamics", Prentice Hall, New York, 1962, pp. 433 and 452.

5. "Assessment Models in Support of the Hazard Assessment Handbook (CG-446-3)", U.S.C.G, Washington, January 1974. NTIS #AD776617

6. Raymond D.R. and Zreminski, S.Z. AICHE Journal, V. 17, n 57, 1971.

7. A.I. Johnson, F. Besik, and A.E. Hemelec, "Mass Transfer from a Single Rising Bubble," The Canadian J. Chem. Eng., v 47, December 1969, pp. 559-564.

8. Sherwood, T.K., Pigford, R.L. and Wilke, C.R., "Mass Transfer"; McGraw-Hill Co., New York, 1975, Chapter 6.

9. Reid, R.C. - Private Communication - Department of Chemical Engineering, M.I.T., Cambridge (Mass), May 1976.

10. Reid, R.C., "Superheated Liquids" - American Scientist, Mar/Apl 1976, pp. 146-156.

11. S. Sideman, G. Hersch, and H. Gat, AICE Journal, 11, 1081, 1965.

12. D.H. Klipstein, Sc. D. Thesis, Dept. of Chem. Eng., MIT, 1963.

13. International Critical Tables, McGraw-Hill, 1927, Col. III, p. 260.

14. McAuliffe, C., J. Phys. Chem. 70, 1267 (1966)

15. Reed, D., and J. J. McKetto, J. Chem. Eng. Data 4, 294 (1959)

16. Claussen, W.F. and M.F. Polglase, J. Am. Chem. Soc., 74, 4817 (1952).

17. Wetlaufer, D.B., S.K. Malik, L. Stoller, and R.L. Coffin, J. Am. Chem. Soc. 86, 508 (1964).

18. Reid, R.C. and Sherwood T.K., "The Properties of Gases and Liquids", Chap. 3, p. 75, 2nd edition, McGraw Hill, New York, 1966.

REFERENCES (Continued)

19. Kalelkar A.S., and Kung, H.C., "Generalized Terminal Velocities of Large Drops", Report RC 70-T-10, Factory Mutual Res. Corp., Norwood, Mass 1970.

CHAPTER IV

SPREADING ON THE WATER SURFACE OF A CONTINUOUSLY RELEASED
LIGHTER THAN WATER, IMMISCIBLE LIQUID

OBJECTIVES

The objectives of the work presented in this chapter are:

- To experimentally investigate and understand the phenomenon of spread of a lighter than water liquid when released continuously;

- To develop a theoretical model to explain the above phenomenon and extend it to the case of spread of continuously released volatile liquid.

INTRODUCTION

One of the main pollutants of the waterways in and off the coastal waters of the United States is oil. There have been numerous instances in which large quantities of oil have leaked from damaged ships over considerable durations of time, sometimes extending over a few days.[1] Similar spills have been caused by offshore oil wells.[2] In such cases, it is imperative to know how much time would be available to fight the oil spread before it starts polluting the shorelines. In addition, one needs to know the extent of spread at various times to muster enough fighting equipment (booms and chemicals) to contain or minimize the spread of the spill.

Also, for analyzing the development of pool fires from a continuously released cold, liquefied flammable gas, it is essential to have the knowledge of the spread rates of liquids on water which are released continuously but which do not lose any mass (by evaporation or burning). Hence, there exists a need to understand the above problem of spread when the liquid is released continuously.

Only very few theoretical analyses exist in the literature which have studied the continuously released spread problem. Most analyses assume that the oil is released instantaneously. To the best of our knowledge, no scale experiments have been performed to understand this problem in any detail whatsoever.

146

Several workers (Fay,[3] Hoult,[4] Fannelop and Waldman[5])
have analyzed the instantaneous release problem. Fay[3] and Murray[6] have
also treated the problem of spread on a flowing water body. Fay has
analyzed the problem as a normal spread problem with a superimposed
water current, while Murray has used the idea of turbulent diffusion of
oil on the water surface. Murray's model seems to agree with the data
from a large oil spill, but its predictive capacity is dependent to a
large extent on the knowledge of "turbulent diffusion coefficient" for
oil on water. This coefficient has to be determined from experimental
data, and at the present time nothing is known of its dependence on the
current velocities, the properties of the oil, the turbulence level in
the water body, and so on. In short, there does not exist, at the present
time, a completely valid analysis of the spread for the continuous release
case.

Abbot and Hayashi[7] have theoretically studied the no mass loss-
continuous release problem and arrived at a result which indicates that
the spread rate is essentially at a constant velocity (radius of the slick
front proportional to the time). Their results are questionable because
their analysis omits certain terms in the momentum equation while retain-
ing other terms of the same magnitude.

It is clear from the above brief survey of literature that the
continuous release and spread problem has received very little attention,
and proper analyses are not available and far from being complete.
Besides, there does not seem to be any data available on a controlled
experiment. It is therefore with a view to obtaining lab-scale experimental
data on the spreading of non-volatile, lighter than water liquids on water
and developing a proper theory to explain the spread that the present
program was undertaken. In addition, the goal was to extend the analysis
to the case of spread with mass loss as in the case of cryogenic liquids
released continuously.

In part 1 of this chapter, the experimental program conducted and the
results obtained are described in detail. Three different oils were used
in the experiments. Several release rates were also investigated.

When a cold, liquefied gas such as the LNG is released on water, it boils off rapidly. The extent of spread of the liquid depends on the rate of release, the properties of liquid (and to some extent those of water), the evaporation rate, etc. Raj and Kalelkar[8] and more recently Mascari[9] have analyzed the problem of spread of instantaneously released cryogen on water. They have given formulae to predict the maximum radius of spread and time for complete evaporation. However, the problem of continuous release has not been analyzed. In the continuous release case, the "pool" size increases at first and reaches a maximum diameter which does not change with time provided the evaporation rate per unit of surface area of the liquid remains a constant (as in a fire or in the case of boiling on water which does not freeze and in which circulation patterns become well established).

The analytical model describing the spread in the non-volatile spreading case is developed in part 2. In part 3, the same analysis is extended to the case of a cryogenic spill. In part 4, the results obtained in part 3 are applied to the calculation of thermal radiation from an expanding pool of LNG. A specific example is worked out to illustrate the calculation procedure.

Part 1 - Experimental Investigation of the Spread of Oil Released at a Uniform Rate on the Water Surface

THEORETICAL DEVELOPMENT

1. Principle

The basic design concept of the experiment is to release oil from a small nozzle at a uniform rate on the surface of the body of water and record on a movie film the process of spread. The detailed spread data are obtained later from an analysis of the movie film.

2. Apparatus

Figure IV-1 shows schematically the details of the equipment used to achieve the above purpose. The apparatus consists of a 3 ft ⅹ 3 ft x 1 ft tank filled with water. Oil stored in a remodeled stainless steel fire extinguisher tank is forced out by pressurized nitrogen into the outlet nozzle. The flow rate is controlled by a valve in the oil flow line. The nozzle is a bent copper pipe attached to the oil flow pipeline by a quick release coupling so that nozzles of different diameters can be used

148

Pressure
Gauges

Head Valve

Regulator

Bleed Valve

Screw
Control

Butterfly
Valve

Gate Valve

0.25" I.D.

0.5" I.D.

Nitrogen Cylinder

Ruler

Drip Plate

Pressurized Vessel
Containing Oil

Tank
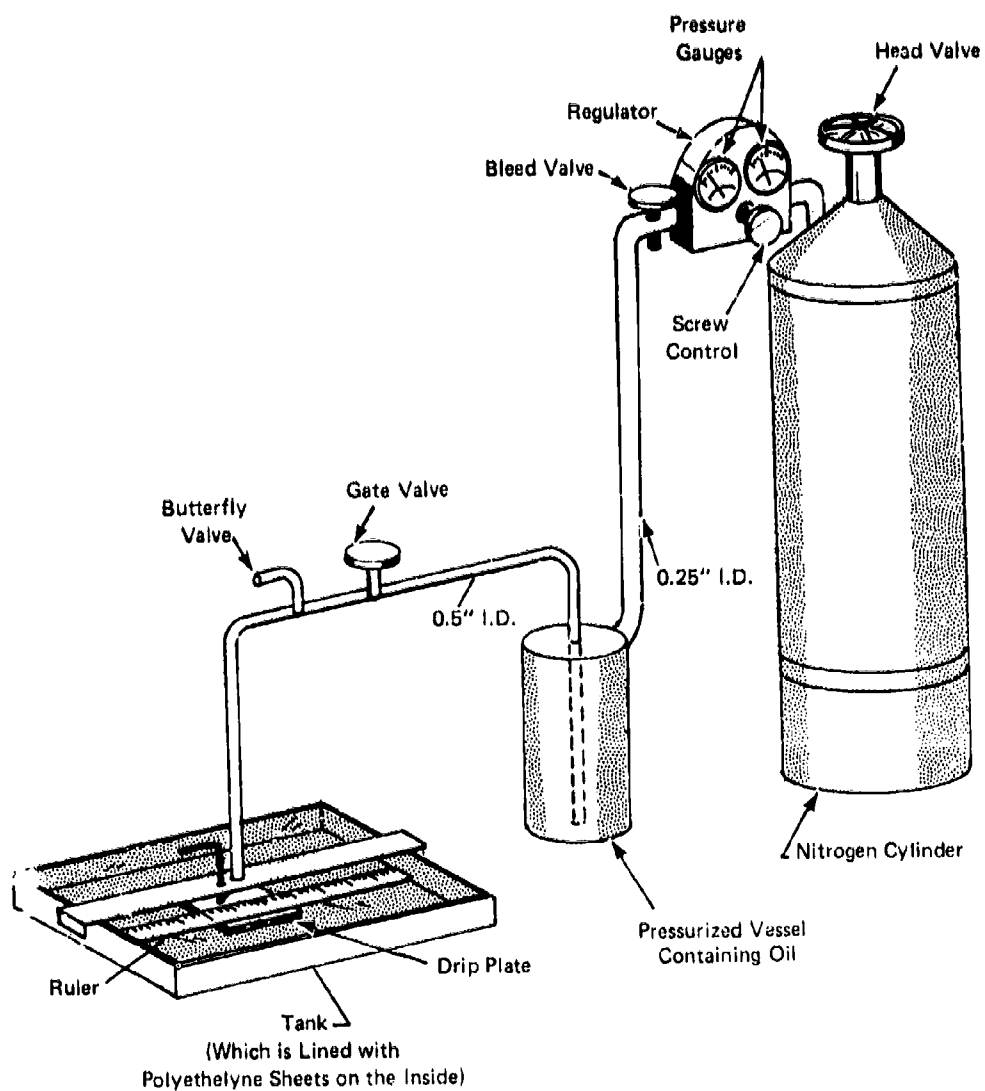(Which is Lined with
Polyethelyne Sheets on the Inside)

FIGURE IV-1

149

easily. The axis of the nozzle is kept normal to the water surface. There is provision to move the nozzle up or down so that the height of the mouth of the nozzle above the water surface can be altered. The oil spread is recorded on a movie film by a camera located above the water tank.

3. Experimental Procedure

A. Calibration

During the initial phases of the experiment, a calibration series is conducted to determine the relationship between the regulator pressure and the flow rate of oil. The oil flow rate is measured directly by timing the flow to fill a given volume. The calibration is conducted for all the nozzle diameters and oil used. These calibration tests were made with a view to obtaining a preset flow rate by simply setting the appropriate throttle valve pressure on the nitrogen cylinder regulator.

B. Test Procedure

After filling the water tank with pure water from a tap and allowing the water to settle, the height of the nozzle is adjusted to the proper height above the water surface. The temperature of the water is recorded. Regulator pressure is adjusted to a preset value depending on the flow rate of oil for the test. That the flow rate is indeed equal to the desired value is checked by letting the oil flow into a graduated beaker (this is done by opening the shut-off valve) and measuring the volume collected in a given time.

Prior to the test, when the nozzle is in position over the water surface, spills of oil drops dripping from the mouth of the nozzle are prevented from polluting the water surface by the drip plate shown in Figure IV-1.

The drip plate is removed from position, the camera is started, and the oil flow is started by opening the shut off valve. The flow is continued until the front of the oil slick reaches the wall of the tank.

After the test, the flow rate is checked again. The temperature of oil is recorded. The water from the tank is dumped to a sump and the liners (for the tank) are thrown out. The whole procedure is repeated for further tests after relining the water tank walls with a set of new liners.

After the movie film is processed, the radius vs. time data is obtained from it. It is recalled that a graduated ruler is provided (see Figure IV-1) on top of the water surface. This facilitates easy reading of the radius of the oil slick in the movie film.

SPECIFIC EXAMPLE

A series of 27 experiments was conducted which included three types of oil (SAE 30 motor oil - detergent and nondetergent variety, and castor oil), three different nozzle diameters (1/8", 1/4", and 1/2") and several flow rates (varying from as low as 0.8 ml/sec to as high as 125 ml/sec). Table IV-1 gives a summary of the tests conducted in this series of experiments. Table IV-2 gives the properties of the oils used.

Not all of the experiments yielded useful data (more about these problems can be found in the section on "discussions"). The data from those experiments which were considered successful are plotted in Figures IV-2-a, 2-b, and 2-c respectively for the three different oils used. These figures represent the radius of the slick as a function of time. The coordinates in these figures are in dimensionless units so that results from experiments with different nozzle diameters and flow rates could be presented on a single graph paper (for each oil).[†] These dimensionless quantities are defined by

$$\chi = \frac{r}{a} = \text{dimensionless radius}$$

$$\tau = \frac{t}{t_{ch}} = \text{dimensionless time}$$

where $a = $ nozzle diameter

$$t_{ch} = \text{characteristic time} = \left[\frac{a^4}{GQ} \right]^{1/3}$$

$$G = \text{effective gravity} = g \left(1 - \frac{\rho_{oil}}{\rho_{water}} \right)$$

$$\dot{Q} = \text{volumetric flow rate of oil.}$$

[†] Detailed radius vs time (in dimensional units) are not given with a view to saving space.

TABLE IV-1

Exp. #	Type of Oil	Date	Flow Rate (ml/sec)	Nozzle Dia. In.	Used In Plot	Remarks
1	?	1/2/75	99.0	0.50	No	Outside of room expts.
2	SAE 30	1/2/75	97.0	0.50	No	Outside
3	?	1/3/75	8.14	0.125	No	Outside
4	SAE 30 H.D.	1/21/75	4.65	0.125	No	Outside
5	SAE 30 H.D.*	1/29/75	?	0.125	No	Flow Not Steady
6	SAE 30 H.D.	1/30/75	1.0	0.125	Yes	Not Sharp Edge
7	SAE 30 H.D.	1/30/75	10.26	0.50	No	Globules
8	SAE 30 H.D.	1/30/75	125.0	0.50	No	Film Not Processed
9	SAE 30 H.D.	2/4/75	2.5	0.25	Yes	
10	SAE 30 H.D.	2/4/75	30.0	0.25	No	Globules
11	SAE 30 H.D.	2/4/75	21.43	0.25	No	Globules
12	SAE 30 H.D.	2/5/75	23.81	0.50	Yes	Flow Not Steady
13	SAE 30 H.D.	2/5/75	11.1	0.50	Yes	Not Sharp Edge
14	SAE 30 N.D.	2/6/75	42.86	0.50	Yes	Slick Drifted Away From Center
15	SAE 30 N.D.	2/7/75	9.84	0.50	Yes	Camera Trouble
16a	SAE 30 N.D.	2/7/75	3.51	0.25	Yes	Excellent Test
16b	SAE 30 N.D.	2/10/75	32.05	0.25	No	
17	SAE 30 N.D.	2/10/75	13.58	0.25	No	Globules
18	SAE 30 N.D.	2/10/75	.847	0.125	No	Did Not Form Circle
19	SAE 30 N.D.	2/10/75	8.33	0.125	Yes	Slick Drifted Forward
20	SAE 30 N.D.	2/11/75	0.78	0.125	Yes	Excellent Test
21	SAE 30 N.D.	2/11/75	21.28	0.25	No	Globules

*H.D. means high detergent motor oil

N.D. means nondetergent motor oil

TABLE IV-1 (Cont'd)

Exp. #	Type of Oil	Date	Flow Rate (ml/sec)	Nozzle Dia. In.	Used In Plot	Remarks
22	Castor	2/18/75	0.80	0.125	No	Edge Hard to See
23	Castor	2/19/75	0.732	0.125	No	Edge Hard to See
24	Castor	2/20/75	7.81	0.125	Yes	Globules at Beginning
25	Castor	2/21/75	3.57	0.25	Yes	Good Test
26	Castor	2/21/75	20.0	0.25	No	Air was in the Lines
27	Castor	2/25/75	26.7	0.25	Yes	Globules at Beginning

Type of Oil	Total # Exps. Proposed	Total # Exps. Conducted	Total # Exps. Successful
SAE 30 H.D.	-	13	4
SAE 30 N.D.	6	9	5
#1 Castor	4	6	3

TABLE IV-2

PROPERTIES OF THE OILS USED

Type of Oil	Density g/cm^3	Viscosity Stokes	Temp. at Which the Properties Are Specified °C
SAE 30, High Detergent	0.861	2.0	25.0
SAE 30, Non-Detergent	0.913	5.0	25.0
Castor Oil #1	0.939	6.3	25.0

154

FIGURE IV 2-a

LEGEND

#1 CASTOR OIL

	Exp. #	Flow Rate (ml/sec)	Nozzle Dia. (in.)	Date
⊙	24	7.81	0.125	2/20/75
▲	27	26.70	0.25	2/25/75
⊘	25	3.57	0.25	2/21/75

Least Square
St. Line

$X = 0.47 \, \tau^{0.64}$

$\tau = time/t_{CH}$

$X = R/a$

155
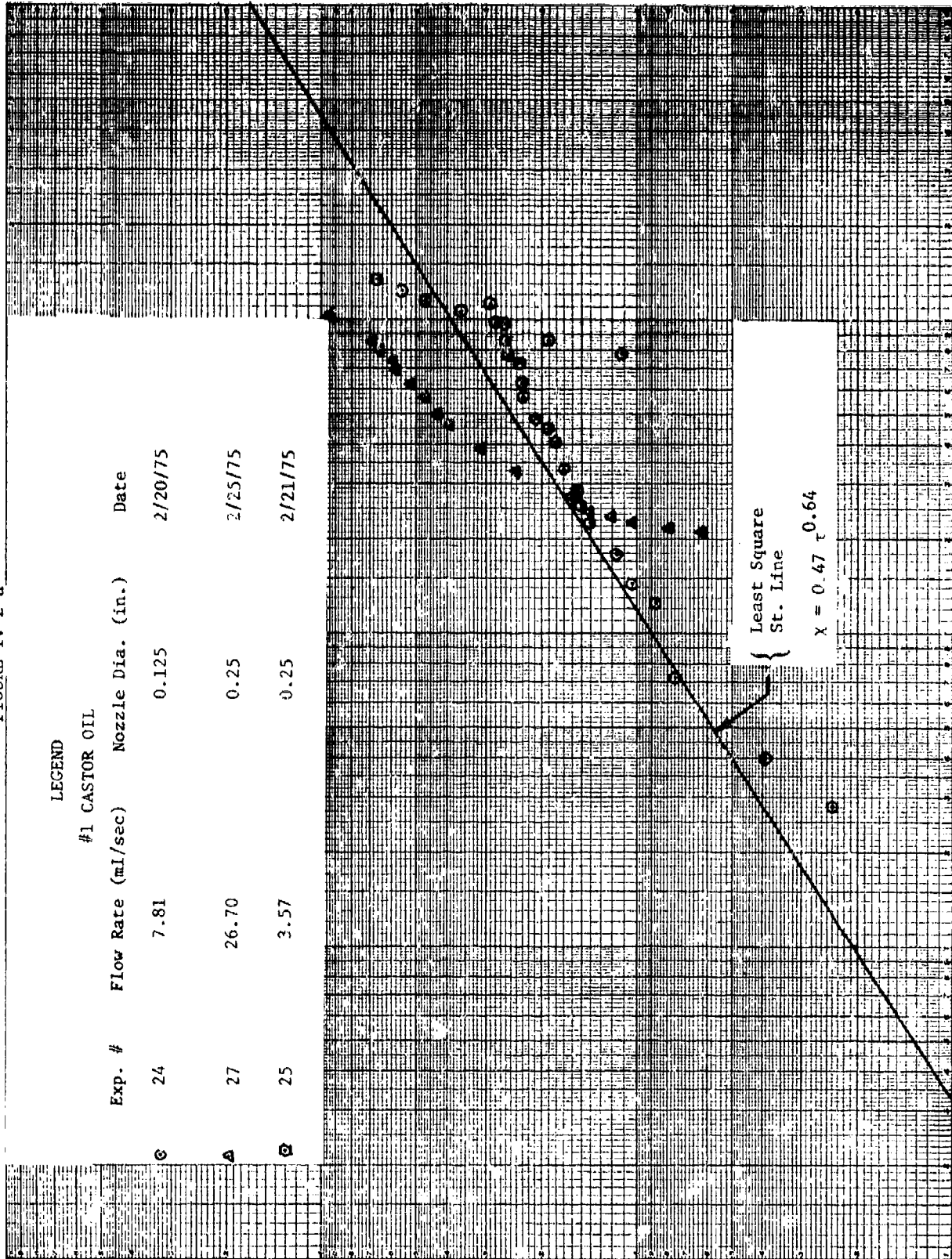
FIGURE IV 2-b

LEGEND

SAE 30 HIGH DETERGENT MOTOR OIL

Exp. #	Flow Rate (ml/sec)	Nozzle Dia. (in.)	Date
⊖	6	1.00	0.125	1/30/75
⊘	9	2.50	0.25	2/4/75
⊕	13	11.11	0.50	2/5/75
⊞	12	23.81	0.50	2/5/75

Least Square
St. Line
$X = 1.152 \, \tau^{0.49}$

$\tau = time/t_{CH}$

$X = R/a$

156

FIGURE IV 2-c

LEGEND

SAE 30 NONDETERGENT MOTOR OIL

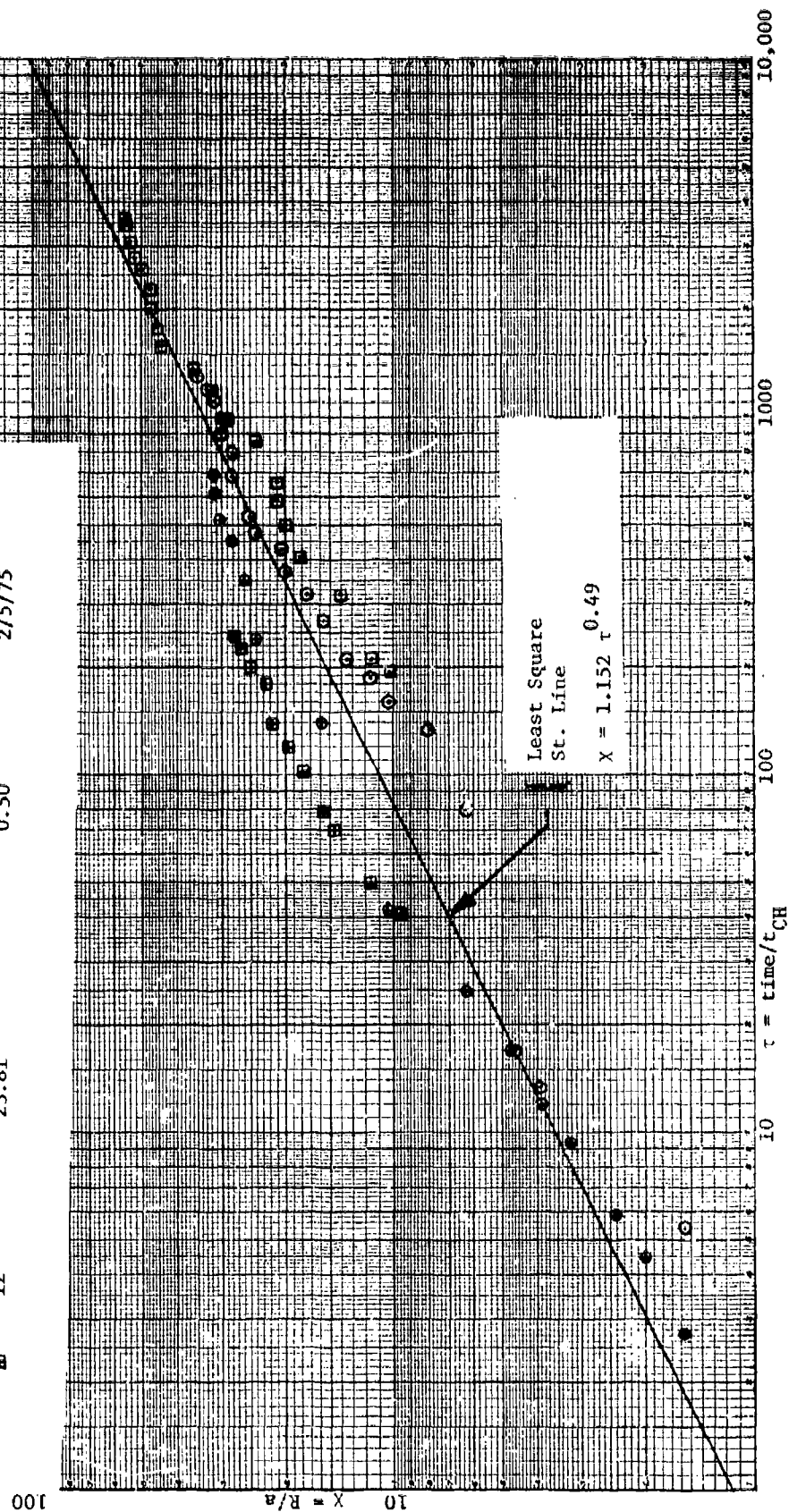|	Exp. #	Flow Rate (ml/sec)	Nozzle Dia. (in.)	Date
⊙	19	8.33	0.125	2/10/75
⊟	20	.78	0.125	2/11/75
⬡	16a	3.51	0.25	2/7/75
⊕	15	9.84	0.50	2/7/75
⊞	14	42.86	0.53	2/6/75

Least Square
St. Line
$X = 0.68 \, \tau^{0.54}$

$X = R/a$

$\tau = time/\tau_{CH}$

157
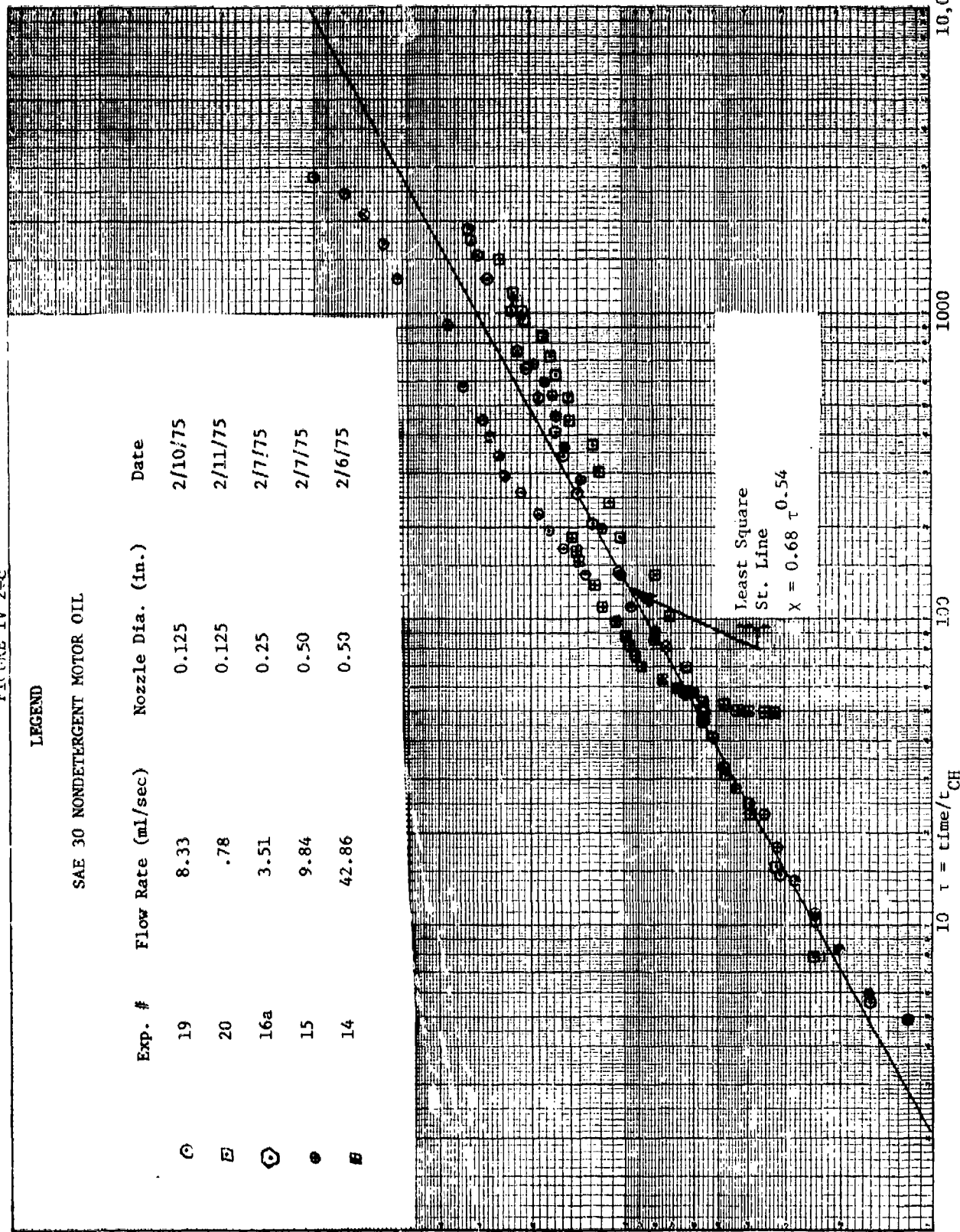
The results indicate considerable scatter, but still a reasonable trend is noticeable. A least square straight line fit obtained to the data plotted on log-log graph paper, is indicated in each of the Figures IV 2-a, 2-b, and 2-c. The least square straight line correlations obtained are in the form

$$\chi = A \, \tau^B \tag{0}$$

The values of A to B obtained from the least square fit are indicated in Table IV-3.

DISCUSSION ON THE EXPERIMENTAL INVESTIGATION

Though in all 27 experiments were conducted, it was not possible to obtain the data from each of the experiments. This was because in those experiments in which detergent oil was used, the oil slick was never formed in most experiments. Instead globules of oil were formed under the water surface, rose to the surface and spread out in clusters of small slicks. This is shown in Plate IV-1. Therefore, there was no definite "slick radius" that could be obtained. Another phenomenon that was observed when detergent oil was used was the rapid spreading of a monomolecular layer at a very high velocity (covering the entire water surface within a matter of 5 seconds) as soon as the first few drops of oil hit the water surface. It is presumed that this monomolecular layer is caused by and spreads as a result of the change in the water/oil interface characteristics brought about by the detergent in the oil. Presumably the surface tension of oil is changed considerably by the detergent. To avoid the formation of the monomolecular layer, it was decided to use non-detergent oil in all subsequent experiments, however, keeping the same oil properties as far as possible.

Experiment Nos. 14 through 21 used non-detergent oil. Although in using this oil the problem of spread with clusters of small slicks was eliminated, yet when either high flow rate was used or when the mouth of the nozzle was far above the water surface (greater than 2" to 3" in these experiments) globules of oil were formed in the water underneath jet entry. Although some relief from this was achieved at low flow rates when

TABLE IV-3

Least Square Straight Line Correlations for the Radius as a Function of Time

$$\chi = A \, \tau^B$$

Type of Oil	A	B
SAE 30 H - D	1.15	0.49
SAE 30 N - D	0.68	0.54
Castor Oil	0.47	0.64

the mouth of the jet was placed almost touching the water surface, at high flow rates this globule formation persisted. Plate IV-2 shows the spreading under one such high flow rate conditions. The spotty spreading can be seen clearly.

The behavior of the castor oil was similar to the motor oil during the spreading process. However, the castor oil was barely visible during the spread because both the oil and the water are almost colorless and the refractive indices of both are about the same. Therefore, the "front" of the slick is almost invisible in the movie film. The difficulty of recognizing the position of the front can be seen on Plate IV-3.

Considering the above difficulties, it is felt that the amount of data obtained from the experiments are quite large. What is more, all the data fall on the same graph papers when expressed in dimensionless form. Although there is considerable scatter in the data, it is seen that the mean square straight line on the log-log plot (of dimensionless radius as a function of dimensionless time) has a positive slope which varies between 0.49 and 0.64. These values are close to the theoretically predicted value of 0.5, which is derived in part 2. It is, however, felt that since the scatter in the data is considerable, the different values for A (from Table IV-3) may be just an accident. It may be a weak function of the type of oil (properties such as viscosity and density). To generalize to any oil, it may be appropriate to use a mean value of 0.75 for A.

CONCLUSIONS

Experiments have been conducted to measure the spread rates on water of oils released continuously. Three types of oils were used, and different flow rates form 3 different nozzle diameters. The results indicate that the radius of the spread varies as a 0.5th to 0.6th power of the time.

Part 2 - Continuous Spread Without Mass Loss

THEORETICAL DEVELOPMENT

1. Physical Picture of the Spread Phenomenon

When an immiscible, lighter-than-water liquid is released at reasonably low velocities in the form of a vertical jet onto the water surface, the liquid jet penetrates the water surface, sinks in to a certain depth, rises
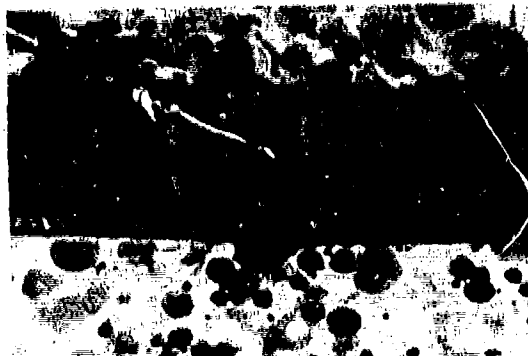
PLATE 1: GLOBULAR SPREADING OF DETERGENT OIL

PLATE 2: SPREADING OF NON-DETERGENT OIL WHEN RELEASED AT HIGH FLOW RATES. SPOTTY GLOBULAR SPREADING CAN BE SEEN.

PLATE3: SPREADING OF CASTOR OIL. THE OIL FRONT IS HARDLY VISIBLE. THE POSITION OF THE SPREADING FRONT IS INDICATED BY THE FINGER.

161

due to buoyancy force, and then spreads out radially. This is shown
schematically in Figure IV-3. However, if the jet velocity is large, the
liquid jet breaks up into globules of liquid. These globules then float
up to the water surface, break up, and coalesce to form an expanding pool.*
This qualitative description indicates that a mathematical description
of the phenomenon very close to the region of jet entry into water is
extremely difficult. As such, the analysis presented below is valid for
regions which are out of the zone of jet disturbance (say, beyond 4 or
5 jet radii).

During the radial spreading of the liquid, there exists a possibility
that a hydraulic jump will occur (as shown by dotted lines in Figure IV-3)
Hydraulic jump occurs when the radial velocity at any location is equal
to or exceeds the local small disturbance wave velocity. This wave
velocity is dependent on the liquid to water density difference, the
thickness of the liquid film, and gravitational acceleration. On the
outer side (downstream side) of the radial hydraulic jump, the thickness
of the liquid film is larger and the flow velocity lower than on the
inner side. Also, because the liquid velocity is higher than wave velo-
city at the inner side of the jump, this inner region is not
affected by what happens on the outer side. In effect, the region
between the jet and the hydraulic jump will have attained steady pro-
files, even though the liquid is spreading beyond the hydraulic jump.
This is an extremely important observation. In our analysis, we have
assumed that such a situation exists (i.e., the constancy of the velocity
and film thickness at a given radius corresponding to the position of a
hydraulic jump). The same assumption has been made by Abbot and Hyashi[7]
in their analysis of the radial spread problem. Watson,[10] Sabersky and Acosta[11]
have given the relationships between the upstream and downstream velocity
and height values for a radial hydraulic jump. These relations are given
later.

---

*
Refer to the photographs in Part I.

162
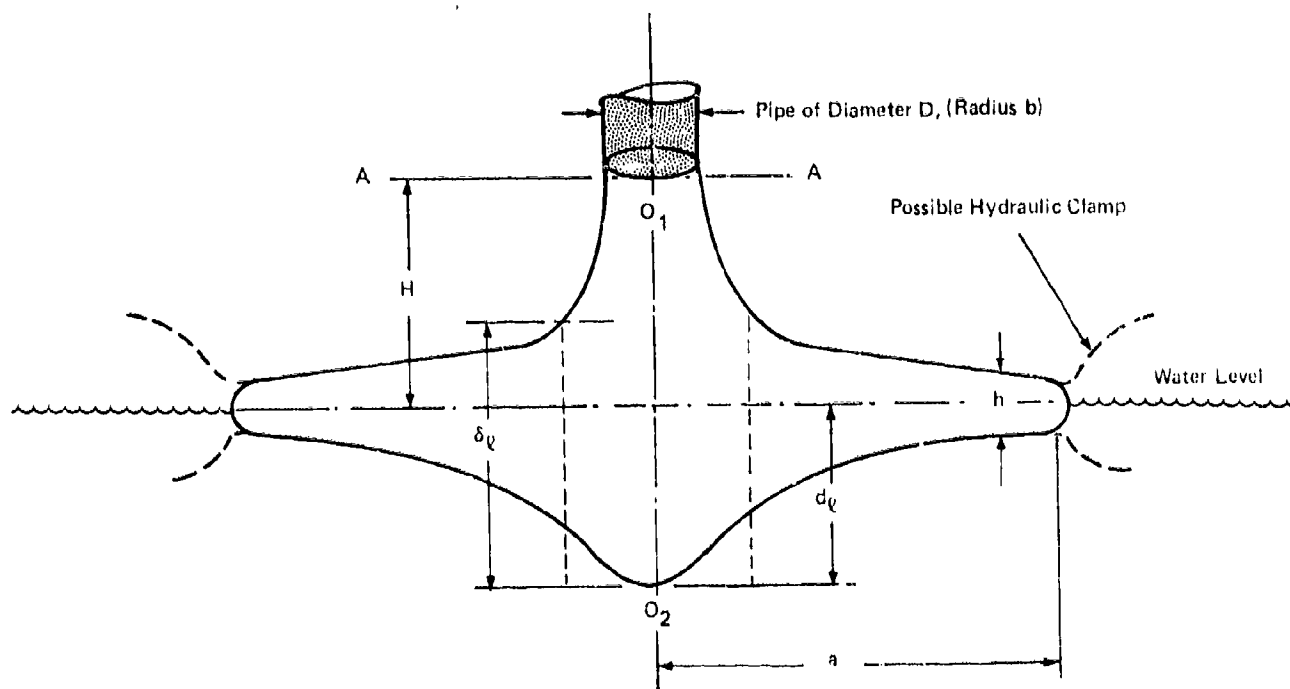
FIGURE IV-3   Schematic Diagram to Illustrate the Physics of a Liquid
Jet Impingement into Another Liquid

163

For understanding the spreading phenomenon during the initial
phases of spread, it is important to understand the physics of the flow
beneath the impinging jet. This is done in section A. In section B,
the radial spread problem is considered. The relevant equations are
written, simplified to the extent possible (without losing the physics
of the situation), and solutions obtained.

Section A: Analysis of Flow Near the Jet Entry and the Hydraulic Jump

When the jet velocity (vertical) is small, the jet liquid penetrates
the water surface to a depth d_ℓ (see Figure IV-3), rises up, and spreads
radially out. To determine this depth d_ℓ we have (see Figure IV-3):

Pressure at the stagnation point O_2 = pressure due to pure water at   (1)
depth d_ℓ

i.e., by applying Bernoulli equation to the vertical stream line $O_1 O_2$,
we have

$$\frac{P_{O_1}}{\rho_\ell} + g(H + d_\ell) + \frac{v^2}{2} = \frac{P_{O_2}}{\rho_\ell} \tag{2}$$

where P_{O_1} = barometric pressure at O_1 = P_{atm}

P_{O_2} = stagnation pressure (total) at O_2

Applying equation 1, we have

$$P_{O_2} = P_{atm} + \rho_w \, g \, d_\ell \tag{3}$$

where P_{atm} = ambient (atmospheric) pressure.

If the pressure at the nozzle exit is equal to the ambient pressure
(i.e., $P_{atm} = P_{O_1}$) then from equations 2 and 3 we get

$$\frac{d_\ell}{b} = \left(\frac{\rho_\ell}{\rho_w}\right)\left(\frac{\frac{v^2}{2 \, g \, b} + \frac{H}{b}}{(1 - \rho_\ell/\rho_w)}\right) \tag{4}$$

where b is the radius of the nozzle outlet.

164

Equation 4 gives the relationship between the depth of penetration and the velocity of liquid, the density of liquid and the height of the nozzle above the water surface. The velocity of the liquid as it hits the water surface is larger than when it leaves the nozzle because of the gravitational acceleration.

It is also noticed from equation 4 that as $\rho_\ell \rightarrow \rho_w$, the depth d_ℓ increases for a given inlet condition. As a matter of fact, if water is jetted into water ($\rho_\ell = \rho_w$), equation 4 indicates that the depth of penetration would be infinite. This, of course, is untrue. The reason that such an answer results from equation 4 is that in the derivation:

- The entrainment of water into the liquid jet was neglected;

- Even in the case of absolutely immiscible liquids, there is always friction at the jet-water interface. This was neglected in deriving equation 4.

In the case of liquids whose density is very close to that of water, the limiting factor in determining the depth of penetration is the liquid plume to water friction. Therefore, equation 4 should be used with caution.

It has been shown by Birkoff and Zorantonello[10] that for the inviscid flow of a jet impinging on a flat plate, the velocity of the radial flow is the same as the vertical velocity in the jet. Assuming that the effect of water (viscous) shear is small very close to the jet impingement region, we can model the radial flow to originate from a cylindrical source as shown in Figure IV-4, the radius of the cylindrical source being equal to the jet radius. Therefore,

$$u_b = U \tag{5}$$

where U is the vertical velocity of the jet liquid at the level of the water. The height h_b of this source of radius "b" is determined from the relationship

$$\dot{Q} = 2\pi\, h_b\, u_b\, b = \pi\, b^2\, U \tag{6}$$

Using equation 5 in equation 6, we get

165
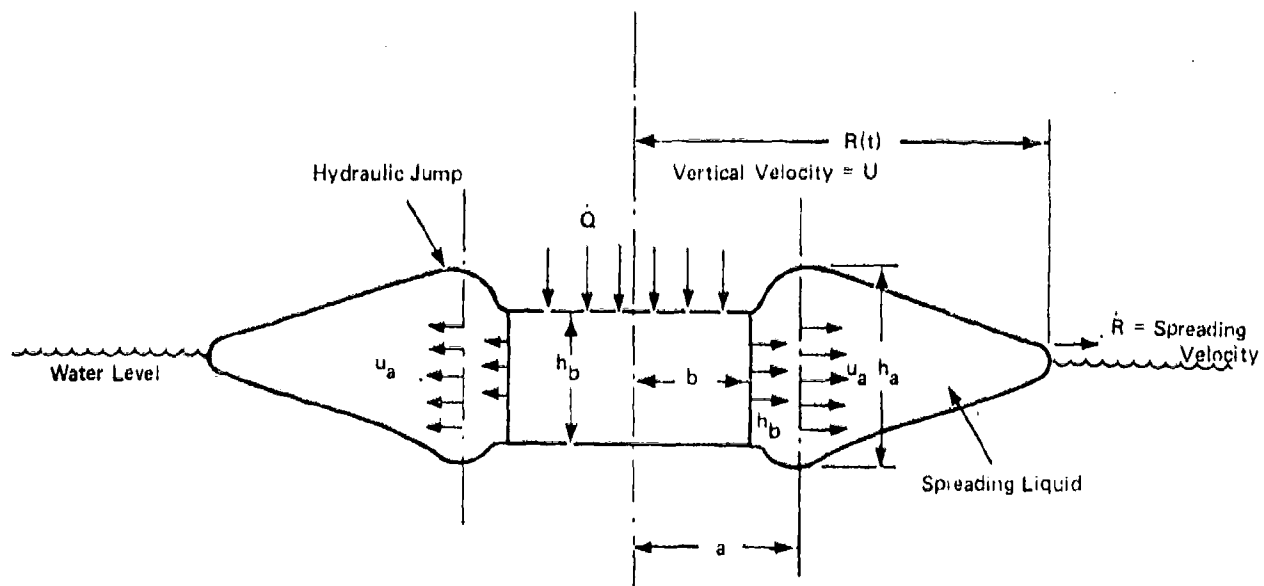
FIGURE IV-4 Schematic Diagram Illustrating the Spreading System

$$h_b = \frac{b}{2} \tag{7}$$

With F_b = Froude number at radius b = $\frac{u_b^2}{G\,h_b}$ (8a)

we have

$$F_b = \frac{u_b^2}{G\,h_b} = \frac{2U^2}{G\,b} \tag{8b}$$

where G = effective gravity = $g(1 - \rho_\ell/\rho_w)$ (9)

In general, $F_b \gg 1$. Hence, we can assume that right at the edge of the jet radius itself there occurs a hydraulic jump. If we represent the conditions of parameters after the hydraulic jump by a subscript "a" we have, using the formula in Sabersky and Acosta[11]

$$F_a = \frac{8F_b}{[\sqrt{8F_b + 1} - 1]^3} \tag{10}$$

$$\frac{h_a}{h_b} = \left[\frac{F_b}{F_a}\right]^{1/3} = \frac{[\sqrt{8F_b + 1} - 1]}{2} \tag{11}$$

and $\quad \frac{u_a}{u_b} = \frac{h_b}{h_a} = \frac{2}{[\sqrt{8F_b + 1} - 1]}$ (12)

The values of u_a, h_a, and F obtained by the above analysis are used in evaluating the spread rates. These are illustrated in the next section.

Specific Example for Section A

We use the data from one of the experiments described in Part 1 and illustrate the procedure for calculating the various quantities derived in this section.

Data from experiment #14

Type of oil used	= SAE 30 nondetergent
Density of oil	= ρ_ℓ = 0.913 gm/cm^3
Volume flow rate	= $\dot{Q}$ = 42.86 ml/sec
Diameter of nozzle	= D = 1.27 cm
Height of nozzle above the water line	= H = 0.5 cm

Calculation

Velocity at the exit of the nozzle: $V = \dfrac{42.86}{(\pi/4)(1.27)^2} = 33.83$ cm/sec

Effective gravity $= G = 980 (1 - 0.913) = 85.26$ cm/s^2

Radius of the nozzle $= D/2 = 1.27/2 = 0.635$ cm

Jet Froude number $= F_j = \dfrac{2V^2}{G\,D} = \dfrac{33.83^2}{85.26 \times .635} = 21.14$

Vertical velocity of the jet at the level of the water

$= U = \sqrt{V^2 + 2gH} = 46.09$ cm/s

Hence, the jet radius at the level of water $= b = \dfrac{D}{2}\sqrt{V/U} = 0.54$ cms

From equation 7, we have $h_b = \dfrac{b}{2} = 0.27$ cm

Froude number for radial flow at the jet radius (from equation 8b) $F_b = \dfrac{2 \times 46.09^2}{85.26 \times 0.54} = 92.28$

Since this Froude number is much larger than unity, there will be a radial hydraulic jump at the position where the jet strikes the water surface.

Radial velocity just before the jump $= u_b = U = 42.86$ cm/s

Radius at which hydraulic jump occurs $= b = 0.54$ cms

Height (thickness of liquid film before the jump) $= h_b = 0.27$ cms

Froude number before the jump $= F_b = 92.28$

From equation 10, $F_a = \dfrac{8 \times 92.28}{[\sqrt{8 \times 92.28 + 1} - 1]^3} = 0.0411$

From equation 11, $h_a = 0.27 \times \left[\dfrac{92.28}{0.0411}\right]^{1/3} = 3.536$ cms

From equation 12, $u_a = 42.86 \times \dfrac{0.27}{3.536} = 3.273$ cm/sec

The radius outside of the jump is assumed to be the same as b, i.e. outside radius of hydraulic jump $= a = 0.54$ cms.

These values are used as input parameters to the spreading model.

Figure IV-4 schematically illustrates the physical model used for developing the theory of spread.

It is assumed that liquid is issuing radially at a constant velocity u_a, at a radius "a" over a height h_a. These values remain constant in time. The liquid released on water spreads to an extent $R(t)$ in a time t (reckoned from the instant when $R(t) = a$). It is required to obtain a functional relationship between radius $R(t)$ and time t.

The radius "a" can be construed to be the radius of the outer side of a possible hydraulic jump in the liquid. In section A, we have indicated a method of estimating both the jump radius as well as velocity and height. Because of the hydraulic jump, these quantities do not change with time.

In performing the analysis given below, the following assumptions are made:

- The flow is steady and maintained at a constant value;
- The viscosity of the liquid is very high compared to that of water;
- Properties of oil are constant;
- The region of interest (spreading front) is far removed from the jet axis.

Analysis

We write the continuity, momentum, and global conservation equations for the spreading liquid and solve for the relationship between the radius of the spread front and time after release. These are illustrated below.

With reference to Figure IV-4, we write

Continuity: $\quad \dfrac{\partial(hr)}{\partial t} + \dfrac{\partial}{\partial r}(hru) = 0$ $\hspace{2cm}$ (13)

Global Continuity: $\quad \displaystyle\int_{r=a}^{R(t)} 2\pi h r \, dr = \dot{Q} t$ $\hspace{2cm}$ (14)

169

In writing equation 14, it is implicitly assumed that time is reckoned from the instant the spread radius is equal to "a." This radius "a" may be equal to the radius at which the hydraulic jump is located if it occurs at all. Otherwise, "a" could be considered to be equal to the radius of the impinging jet.

Momentum: $\dfrac{\partial u}{\partial t} + u \dfrac{\partial u}{\partial r} = \underbrace{- G \dfrac{\partial h}{\partial r}}_{\substack{\text{gravitational} \\ \text{force}}} + \underbrace{\dfrac{\sigma}{\rho h}}_{\substack{\text{viscous} \\ \text{shear} \\ \text{force}}}$ (15)

where σ is the shear stress at the liquid-water interface acting in the outward radial direction, and G is the effective gravity defined in equation 9.

Kinematic Condition: at $r = R(t)$; $u\,[R(t)] = \dfrac{dR(t)}{dt}$ (16)

Initial Condition

at $t = 0$; $R(0) = a$ (17)

and no liquid exists in the region $r > a$

Boundary Condition

at $r = a$ for all time, $\left. \begin{aligned} u &= u_a \\ h &= h_a \end{aligned} \right\}$ (18)

where u_a and h_a are connected by the constancy of flow condition

$\dot{Q} = 2\pi a\, u_a\, h_a$ (19)

The set of equations 13 through 19 forms a coupled set of nonlinear partial differential equations. There is no exact solution to the above set.

A simplified solution is given below, based on certain assumptions and simplifications. The method followed is similar to that generally used in fluid mechanics, called the Pohlhaussen's technique. In this method, the equations of continuity, momentum, etc. are satisfied only in their integrated sense and not at every point within the flow field.

170

Simplified Solution for the Radius of the Spread Front

To obtain this simplified solution, we make the following assumptions:

- Only the gravity-inertia regime of spread is considered; i.e., the viscous-frictional term is neglected.

- The film thickness profile can be represented by a similarity

- The spreading front of the liquid moves with a velocity equal to the wave velocity corresponding to the thickness of liquid at the end; i.e.,

$$u(R) = \sqrt{G\ h(R)} \tag{20}$$

The third assumption is based on observed experimental evidence which indicates that the above is true when the radius of spread is large.[5] In the present problem large radius implies an order of magnitude greater than the radius of the impinging jet.

We define the following dimensionless and characteristic variables to simplify the procedure for obtaining the solution.

$$F = \frac{u_a^{\ 2}}{h_a G} = \text{Froude number at the source radius}$$

$$\chi = R/a = \text{Dimensionless radius of spread front}$$

$$v = u/u_a = \text{Dimensionless velocity}$$

$$\delta = h/h_a = \text{Dimensionless liquid film thickness} \tag{21}$$

$$t_{ch} = \frac{a}{u_a} = \text{Characteristic time}$$

$$\tau = \frac{t}{t_{ch}} = \text{Dimensionless time}$$

$$\xi = r/a \quad \text{and} \quad \eta = \frac{\xi-1}{\chi-1}, \quad \psi = \chi - 1$$

Substituting for $\dot{Q}$ in equation 14 from equation 19 and using the dimensionless parameters defined in equation 21, we get

Global Continuity Equation

$$\int_{\xi=1}^{\chi(\tau)} \delta\ \xi\ d\xi = \tau \tag{22}$$

171

Front Condition

From equations 20 and 21, we get

$$v_e = v(\chi) = \sqrt{\frac{\delta(\chi)}{F}} \qquad (23)$$

Let us now assume a similarity solution dependent on the similarity variable η. Note η value varies from 0 (at radius a) to 1 (at radius R).

Let $\dfrac{\delta - 1}{\delta_e - 1} = E_\delta \left(\dfrac{\xi - 1}{\chi - 1}\right) =$ a function of the similarity coordinate η (24)

where E_δ is an unknown factor.

The above equation can be written as

$$\delta = 1 + E(\eta) \; f(\tau) \qquad (25)$$

where $E(\eta)$ is a function of η only, satisfying the conditions

$$\left.\begin{array}{l} E(0) = 0 \\ E(1) = 1 \end{array}\right\} \qquad (26)$$

and $f(\tau)$ is a function of time τ; the function is as yet unknown.

Substituting equation 25 in equation 22 and rewriting ξ in the integral in terms of η and integrating, we get

$$\tau = \psi \; [(1 + E_o f) + \psi \; (1/2 + E_1 f)] \qquad (27)$$

where

$$\left.\begin{array}{l} E_o = \displaystyle\int_0^1 E(\eta) \; d\eta \\[20pt] E_1 = \displaystyle\int_0^1 \eta \; E(\eta) \; d\eta \\[20pt] E_n = \displaystyle\int_0^1 \eta^n \; E(\eta) \; d\eta \end{array}\right\} \qquad (28)$$

substituting 25 in 23.

Also $\frac{d\psi}{d\tau} = v_e = \sqrt{\frac{[1 + f(\tau)]}{F}}$ (29)

For <u>any given values</u> of E_0 and E_1 (which can be obtained if a proper thickness profile function E is chosen) equations 27 and 29 form a coupled set of equations for the unknowns ψ and $f(\tau)$. Because of the square root term in equation 29, the nonlinearity presents an analytical solution. Therefore, we attempt asymptotic solutions.

$\psi \gg 1$: i.e., radius of the front is very large compared to the hydrualic jump radius.

Then equation 27 becomes

$$\tau = \psi^2 [1/2 + E_1 f]$$ (30)

i.e., $\tau = \psi^2 [1/2 - E_1 + E_1 (1 + f)]$

Substituting for $(1 + f)$ from equation 30, we get

$$\frac{d\psi}{d\tau} = \frac{1}{\sqrt{F} E_1} \left[\frac{\tau}{\psi^2} + E_1 - 1/2 \right]^{1/2}$$ (31)

with $\psi = 0$ at $\tau = 0$

The solution to equation 31 is obtained in Appendix F and is for $\psi \gg 1$

$$\psi = \left(\frac{2}{1 - 2E_1} \right)^{1/2} \sqrt{\tau - \frac{FE_1}{(1 - 2E_1)^2}}$$ (32)

provided $E_1 < \frac{1}{2}$ (33)

Equation 32 indicates that:

 • After a long time, the radius is proportional to the square root of time.

Specific Example

The data from experiment # 14 used in Section A will be considered for this example also.

173

The experimental data indicates that a mean straight line through the data (on log paper with radius of the pool spread as ordinate and time as abscissa) for large values of R/a can be correlated by

$$R = 4.25 \, t^{1/2} \quad \text{for } R > 10 \text{ cms}$$

where R = Radius of spread front in cms

t = Time from the instant of spill

which becomes in dimensionless notation (see example in Section A)

$$t_{ch} = \frac{0.54}{3.08} = 0.175 \text{ secs}$$

$$a = 0.54 \text{ cms}$$

$$\chi = 3.3 \, \tau^{1/2} \quad \text{for } \chi > 18$$

Since $\chi \gg 1$, we write the above experimental correlation as ($\psi = \chi - 1$)

$$\psi = 3.3 \, \tau^{1/2}$$

Comparing this equation with that in equation 32, we get

$$\left(\frac{2}{1 - 2E_1} \right)^{1/2} = 3.3$$

i.e., $E_1 = 0.408$ which satisfies the condition in equation 33.

Suggestion for Thickness Profile

Experimental observation indicates that the thickness of the oil slick at radii close to the left core stabilizes fairly quickly, whereas the thickness continues to change in regions near the spreading front. In the analysis presented, we have assumed a similarity profile. Because of this assumption, the thickness at all radii are affected as the spread radius continues to grow. A consequence of this assumption is the prediction that the thicknesses near the core of the jet are continuously increasing (approaching the constant thickness value equal to that present on the downstream side of the hydraulic jump). In order, therefore, to minimize the effect of similarity assumption on the thickness change in regions of jet neighborhood and to better conform to the experimental observations, we suggest the following exponential function. It is noted that the exponential function given below for the thickness has the uniqueness that changes in the value of the radius of spread has minimal effect on the thickness in regions close to the jet.

174

$$E(\eta) = \left[\frac{1 - e^{-3\eta}}{1 - e^{-3}} \right]$$

Substituting this into equation 28, we get

$$E_0 = 0.68$$

and $\quad E_1 = 0.41$

DISCUSSION ON THE THEORETICAL ANALYSIS OF SPREAD WITHOUT MASS LOSS

In this part, an analysis has been carried out to predict the development of the radius of a pool of liquid with time when the liquid is spilled on water at a uniform and continuous rate. The analysis indicates that when the radius of spread is sufficiently large compared to the radius of the jet (by say a factor greater than 5 to 10), the pool radius increases with the square root of time.

This square root dependence agrees with the experimental data discussed in Part 1. The theoretical analysis also indicates that in the very early stage of development of the pool, the pool radius increases almost linearly with time. In other words, the front expands with a constant velocity. However, this constant velocity expansion lasts only for a very brief period.

In the first section of the analysis, the phenomenon of hydraulic jump (that may occur) has been investigated. It is found that for most spill situations, the hydraulic jump occurs (if at all) very close to the region at which the jet enters the water. In fact, it is a common observation in a kitchen sink that the radius of the hydraulic jump becomes smaller and smaller as the sink fills up and finally completely vanishes when depth of water in the sink is only a few tenths of an inch. The same phenomenon would be true in the case of a jet of liquid coming into a water body of large depth. Therefore, we feel that for most spill situations, the location of the hydraulic jump can be assumed to coincide with radius of the jet at the point where the jet enters the water surface. The downstream of hydraulic jump values of velocity, thickness, and Froude number can then be calculated using equations 12, 11, and 10 respectively.

In the analysis of the spread phenomenon, the equation for conservation of mass and the known fact that the front moves with a local wave velocity corresponding to its thickness are used. In addition, the

175

solution postulates that the thickness profiles are similar. Because
of the latter assumption, it is not necessary to solve the momentum
equation at all. In fact, the solutions we have obtained (equations
32 and 36) do not use the momentum equation. However, the correctness
of the solution has been more than adequately justified by experimental
data. To this extent, the crucial assumption in the analysis is the
similarity assumption. Abbot and Hyashi[7] have obtained a solution
which includes the momentum equation but does not satisfy the momentum
equation completely. However, their solution, which indicates a constant
velocity of radial spread, is not corroborated by the experimental data.

Numerical values indicate that the initial constant velocity
spread regime (equation 36) does not last very long (at best 1 to 10
seconds), and most of the spread is in the square root time dependence
regime.

Part 3: Spreading of a Cryogenic Liquid on the Water Surface When Spilled at a Constant Rate

THEORETICAL DEVELOPMENT

When a cryogenic liquid (which boils at a temperature below the
ambient temperature) is spilled on the water surface in a continuous
stream, the liquid spreads radially at the same time as it evaporates.
If the evaporation rate per unit pool area remains a constant (as is
probably the case for spills of such liquids as LNG), then the liquid
pool expands to a maximum radius consistent with the liquid inflow
rate. A similar situation is expected to occur when the spreading
liquid catches fire.

The objectives of the analysis presented below are to estimate
the maximum radius of spread and to calculate the duration of time
taken to reach the maximum radius from the instant the spill is initi-
ated. Most analyses for cryogenic liquid spills have treated the spill
as being instantaneous.[8,9] Although from the point of view of the spread
area the instantaneous spill is the worst situation, it is not at all
clear whether it would represent the worst case when there is a fire
also. The same mass of liquid released over a long time (as a continuous
spill) and sustaining a fire on the pool may cause a severe thermal damage
to nearby structures because of the long exposure time. The analysis
presented below for the spread problem will aid in the evaluation of the
hazards of the above kind.

The analysis presented in this part is in two sections. In Section A, the maximum pool spread radius is calculated for a constant spill rate and constant rate of evaporation per unit pool area. In Section B, the analysis is concerned with the description of the pool spread problem during the transient period between the time the spill is initiated to the time at which the pool spread is a maximum. To obtain the answers needed, the analysis performed is similar to that made in Part 2 (Oil Spread Problem) except that in this case there is the added complication due to the continuous mass loss due to boiling.

Section A: Steady State Pool Size Calculation

For a constant spill rate of a cryogenic liquid which boils on the water surface at a constant rate (of mass loss) per unit of pool area, there exists a maximum pool size to which the liquid will spread. This maximum size is determined by equating the spill rate to the evaporation rate. This calculation is illustrated below.

$$\underbrace{\pi R_{max}^2 \, \dot{y} \, \rho_\ell}_{\substack{\text{Total rate of} \\ \text{evaporation} \\ \text{of mass from the} \\ \text{pool}}} = \underbrace{\dot{Q} \, \rho_\ell}_{\substack{\text{Mass inflow} \\ \text{rate}}} \tag{37}$$

where $\dot{y}$ = liquid regression rate (i.e., the rate of volume loss of liquid per unit pool area). Therefore,

$$R_{max} = \sqrt{\frac{\dot{Q}}{\pi \dot{y}}} \tag{38a}$$

We now define a dimensionless evaporation rate parameter Γ as

$$\Gamma = \frac{a \dot{y}}{2 u_a h_a} \tag{39}$$

Physically, Γ represents the ratio of evaporation rate from the pool of area equal to the cross sectional area corresponding to the outer radius of the hydraulic jump of the jet (πa^2) to the inflow rate (note $2 \pi a u_a h_a = \dot{Q}$). For most spill situations, this parameter Γ example). This observation is important in that it helps to simplify the mathematics of the spread problem (in Section B).

Substituting for $\dot{Q}$ in terms of u_a, a, h_a from equation 19 and utilizing equation 39 and the definitions of dimensionless variables (equation 21) we write equation 38a as

177

$$x_{max} \sqrt{\frac{1}{\Gamma}} \qquad\qquad (38b)$$

Therefore, given the flow conditions and the liquid regression rate, the maximum pool radius can be evaluated using equation 38a or 38b. This is illustrated in the example given later.

Section B: Transient Spreading Analysis

In this section, we obtain a timewise description of the radius of the pool as a function of time. Based on this result, we calculate the time to reach the maximum radius given in equation 38.

The equation of continuity is written in the global form. It is solved using the assumption that the front moves at a velocity equal to the wave velocity corresponding to the thickness of the liquid layer at the spread front. In addition, we use the thickness profile similarity assumption which was used in Part 2. The equation of continuity obtained after the substitution of the other two of the above equations results in a nonlinear integro differential equation for the radius as a function of time. Fortunately, however, the order of magnitude of the evaporation term is small (because $\Gamma \ll 1$). Therefore, we obtain perturbation solutions to the equation of spread. These steps are illustrated below.

Global Continuity Equation

$$\dot{Q} t \;=\; \underbrace{\int_{r=a}^{R(t)} 2\pi r h \, dr}_{} \;+\; \underbrace{\int_{t'=0}^{t} \pi R^2(t') \, \dot{y} \, dt'}_{} \qquad (40a)$$

| Total Volume of Liquid Spilled in Time t | Volume of Liquid in the Spread System at Time t | Volume of Liquid Evaporated in a Duration of Time t |

In writing equation 40a, the following assumptions are made:

- The volumetric spill rate $\dot{Q}$ and the liquid regression rate y are independent of time.

- The time t is counted from the instant when the spread radius is equal to the radius corresponding to a possible hydraulic jump. (Generally, this radius in a liquid-liquid system is the same as the radius of the jet at the entry into water.)

178

- Evaporation area is the total contact area of liquid pool with water (πR^2) although the "spread system" considered is between radii a and R.

Using equations 21 and 39, we write equation 40a in dimensionless form as

$$\tau = \int_{\xi=1}^{\chi(\tau)} \delta\xi \, d\xi + \Gamma \int_{\tau'=0}^{\tau} \chi^2(\tau') \, d\tau' \tag{40b}$$

In addition, from equation 23 we have (with the wave velocity considerations for the spreading front)

$$v_e = \frac{d\chi}{d\tau} = \sqrt{\frac{\delta_e}{F}} \tag{23}$$

where F is the downstream of hydraulic jump Froude number defined in equation 21 and δ_e is the dimensionless thickness at the spreading front.

Now imposing the assumption as to the similarity profiles for thickness of the liquid layer, we have from equation 25a

$$\delta = 1 + E(\eta) \, f(\tau) \tag{25a}$$

where E is a function of the spatial similarity coordinate η and f is an as-yet-unknown function of time τ. (See equations 21 and 24a for definitions.) Also, we have from equation 21

$$\psi = \chi - 1 \tag{21}$$

In equation 40b, substituting equations 21 and 25a and writing ξ in terms of η (using equation 21) and performing the spatial integration ($w \cdot r \cdot t \, \eta$) and noting the definitions of E_0 and E_1 from equation 28 we get

$$\tau = \psi \left[(1 + E_0 f) + \psi(1/2 + E_1 f) \right] + \Gamma \int_0^\tau (1 + \psi)^2 \, d\tau' \tag{41}$$

with $\psi = 0$ at $\tau = 0$

In the above equation 41, we substitute for f from equation 23 in terms of the differential $\frac{d\chi}{d\tau}$. In the resulting equation, E_0, E_1, F and Γ will be constants. The resulting equation is an extremely complicated, highly nonlinear integro differential equation which describes

179

the behavior of ψ (the radial spread) with τ (the time). Because of the very nature of the complications, we make several approximations, none of which is of any serious consequence as far as the solution is concerned, which nevertheless result in enormous simplifcation in the mathematics.

Before attempting an analytical solution to the coupled equations 23 and 41, we recognize the following physical facts:

- In general, the final spread radius of the pool is considerably larger than the jet radius

  i.e. $\chi \gg 1$, i.e. $\psi \gg 1$ (43a)

- The evaporation parameter $\Gamma \ll 1$ (43b)
  (This has already been discussed.)

Substituting 43a in 41, recognizing that in view of 43a, $\psi^2 \gg \psi$, substituting for f from 29, we finally get

$$\tau = \psi^2 \left[(1/2 - E_1) + E_1 F \left(\frac{d\psi}{d\tau} \right)^2 \right] + \Gamma \int_0^\tau \psi^2(\tau') \, d\tau' \qquad (44)$$

$$\text{with conditions} \quad \left. \begin{array}{l} \psi = 0 \\ \\ \dfrac{d\psi}{d\tau} = \dfrac{1}{\sqrt{F}} \end{array} \right\} \text{at } \tau = 0 \qquad (45)$$

Solution

The solution to equation 44 cannot be obtained in closed form. However, because of the smallness of Γ, we can obtain _perturbation solutions_. The detailed mathematics and the procedure for obtaining the solutions (up to 2nd order perturbation) are given in Appendix C. Only the final results are given below.

with

$$\left. \begin{array}{ll} c = \left(\dfrac{2}{1 - 2E_1} \right)^{1/2} & \bar{\tau} = \tau/\kappa \\ \\ \kappa = \dfrac{E_1 F}{(1 - 2E_1)^2} & \epsilon = \kappa \, \Gamma \, c^2 \\ \\ \sigma = \dfrac{\psi^2}{c^2 \kappa} & \sigma_{max} = \dfrac{1}{\epsilon} \end{array} \right\} \qquad (46)$$

180

Zeroth Order Solution

$$\sigma = \bar{\tau} \tag{47}$$

and

$$\bar{\tau}_{max} = \frac{1}{\varepsilon} \tag{48}$$

where $\bar{\tau}_{max}$ is the dimensionless time to reach the maximum radius given in equation 38a.

Second Order Solution

$$\sigma = \frac{\varepsilon^2}{6}\bar{\tau}^3 - \frac{\varepsilon}{2}\bar{\tau}^2 + \bar{\tau} \tag{49}$$

and

$$\bar{\tau}_{max} = \frac{1.6}{\varepsilon} \tag{50}$$

The first order perturbation solution is not physically valid.

Specific Example

In this example, we consider the release of LNG from a ship onto the water surface and its subsequent spreading.

Physical Conditions Assumed

LNG leaks out of a sperhical tank of diameter = 40 m

The leak hole is at the bottom of the spherical tank
and is of diameter = 0.5 m

The mean flow rate through the hole is equal to one half of the
maximum flow rate

Height of the hole above water level = H = 20 m

Axis of hole is horizontal

Coefficient of discharge of the hole = 0.8

Properties of LNG

Density $\qquad \rho_\ell = 425$ kg/m^3

Boiling temperature = 112 K

Boiling rate $\qquad \dot{y} = 4.233 \times 10^{-4}$ m/s (1 inch/min)

Calculations

Initial flow rate out of the leak hole $= 0.8 \times (\frac{\pi}{4} \times 0.5^2) \times \sqrt{2 \times 9.8 \times 40}$

$$= 4.4 \text{ m}^3/\text{sec}$$

181

Average discharge rate $= \dot{Q} = 2.2 \; m^3/s$

If we assume that all of the liquid released from the leak hole eventually hits the water surface (that there is no flash vaporization) then the vertical velocity in the liquid jet when it enters the water is given by

$$U_{vert} = \sqrt{2g \times H} = \sqrt{2 \times 9.8 \times 20} = 19.8 \; m/s$$

$$U_{horz} = \text{the horizontal velocity (mean value)} = \frac{\dot{Q}}{\frac{\pi}{4} D^2} = 11.205 \; m/s$$

Hence, the velocity with which the liquid jet enters the water

$$U = \sqrt{U_{vert}^2 + U_{horz}^2} = 22.75 \; m/s$$

Of course, in making this calculation, the deceleration of the jet due to air resistance and entrainment, jet instability, flash vaporization, etc. have not been taken into account. These do affect the jet entry velocity and its size. However, inclusion of these phenomena complicates the analysis, and since we are interested in obtaining pool development times accurate to within only an order of magnitude, we neglect the consideration of the above mentioned phenomena.

Therefore, the radius of the jet just before it enters the water

$$\text{is} = b = \sqrt{\frac{\dot{Q}}{\pi \; U}} = 0.1754 \; m$$

Since the entry velocity is very high, the hydraulic jump takes place right at the circumference of the liquid jet.

Hence, Radius of the hydraulic jump $= a = 0.1754 \; m$

Effective gravity $= G = 9.8 \; (1 - .425) = 5.635 \; m/s^2$

Thickness of film before the hydraulic jump (equation 7)
$= h_b = 0.0877 \; m$

Froude number before hydraulic jump (equation 8a) $= \dfrac{(22.75)^2}{5.635 \times 0.0877}$

$$= 1047$$

Froude number after the jump (equation 10) $= F_a = F = 0.013$

Thickness of liquid film after the hydraulic jump (equation 11)

$$= h_a = 0.0877 \left(\frac{1047}{0.013}\right)^{1/3} = 3.97 \; m$$

182

Radial velocity downstream of hydraulic jump (equation 12)

$$\Rightarrow u_a = 22.75 \times \frac{0.0877}{3.97} = 0.5026 \text{ m/s}$$

Characteristic values

$$\text{equation 21} \rightarrow t_{ch} = \frac{0.1754}{0.5026} = 0.349 \text{ s}$$

$$\text{equation 39} \rightarrow \Gamma = \frac{0.1754 \times 4.233 \times 10^{-4}}{2 \times 0.5026 \times 3.97} = 1.861 \times 10^{-5}$$

Hence the maximum radius of spread (equation 38b) $= \chi_{max} = \frac{1}{\sqrt{\Gamma}} = 231.8$

Note $\chi_{max} \gg 1$

In dimensional units, this becomes

$$R_{max} = a \chi_{max} = 0.1754 \times 231.8 = 40.06 \text{ m}$$

$$\psi_{max} = \chi_{max} - 1 = 230.8$$

With the value of $E_1 = 0.408$ obtained from experimental measurements with oil (see page 17) we have the following equations for the development of the radial front (see equation 46)

$$\kappa = \frac{FE_1}{(1 - 2E_1)^2} = \frac{0.013 \times 0.408}{(1 - 2 \times 0.408)^2} = 0.16$$

$$c = \left(\frac{2}{1 - 2E_1}\right)^{1/2} = 3.3$$

$$\epsilon = \Gamma c^2 \kappa = 1.861 \times 10^{-5} \times 3.3^2 \times 0.16 = 3.243 \times 10^{-5}$$

$$\sigma_{max} = \frac{1}{\epsilon} = 3.084 \times 10^4$$

$$\bar{\tau}_{max} = \frac{1}{\epsilon} = 3.084 \times 10^4 \quad \text{(zeroth order - solution to equation 48)}$$

Therefore, $t_{max} = \bar{\tau}_{max} t_{ch} \kappa = 3.084 \times 10^4 \times 0.349 \times 0.16 = 1722$ seconds

Second order solution (equation 50) gives $t_{max} = 1.6 \times 1722 = 2755$ seconds.

DISCUSSION ON THE ANALYSIS IN PART 3

Using the global continuity equation and the assumption that the leading front expands at a velocity equal to the small disturbance wave

183

velocity (corresponding to the liquid film thickness at the spread front)
we have obtained a solution to describe the timewise expansion of the
radius of the pool of a cryogenic liquid spill on water. The liquid
is assumed to be spilled at a constant volumetric rate, and the evapora-
tion rate per unit area is assumed to be constant.

The solutions obtained are not exact because of the use of global
equations and the neglect of the momentum equation completely. (Instead
we have used the velocity at the front condition and thickness similarity
assumption). The perturbation solutions obtained are correct because
of the smallness of the evaporation parameter Γ. There are no experi-
mental data to check the predictions of the spread model. Any improve-
ment to the theoretical model, therefore, has to be done only after
some data are obtained.

The zeroth order perturbation solution (equations 47 and 48)
gives a faster rate of expansion of the pool and therefore a smaller
time to reach the maximum radius. However, when evaporation is included
in the spreading process as is done in the second order perturbation
solution, the rate of expansion of the pool is reduced, and therefore
a longer time is needed to reach a given radius. These facts are shown
clearly by the calculated times given in the specific example.

In an actual situation when the pool spreads to its maximum extent,
the velocity of the front is zero (because it cannot spread any more).
The solutions given in equations 47 and 49 do not give the front velocity
to be exactly zero when the pool size is a maximum. However, this velo-
city is extremely small (of the order of the value of $\sqrt{\Gamma}$ in dimensionless
units) and therefore the error in the solution is negligible. Because
of the better result obtained from second order perturbation solution,
we suggest that it be used in CHRIS.

Part 4: Evaluation of the Thermal Hazard from a Fire on an Expanding Pool of Flammable Liquid Released Continu-ously on Water

THEORETICAL DEVELOPMENT

In Parts 2 and 3 of this memo, models were developed to predict the
size (radius) of spread as a function of time for a given liquid release
rate. In this part (Part 4), we analyze the thermal hazard from such an
expanding pool which also sustains a fire.

Basically, the thermal hazard to an observer outside of the flame is
due to flame radiation. For an observer at a fixed location with respect

184

to the center of the spill, the intensity of radiation received from the fire increases with time (as the pool expands) because of the increasing dimensions of the flame. In the case of continuous release of liquid, the pool reaches a maximum radius for constant liquid regression rate. Therefore, when a fire results on an expanding pool from a continuous source, the intensity of radiation at any given observer location increases continuously at first until the pool attains a maximum radius and then remains a constant. Therefore, in calculating the thermal hazard, one should consider two regimes - the initial transient regime and the steady state regime.

In the analysis below, expressions are derived to calculate the thermal dosage to an observer at a given observer location as a function of time. A specific example is given to illustrate the method.

Section A: Thermal Dosage Calculations During the Pool Spread Period

Consider an observer located at the water level at a distance X from the spill point. We assume that X is greater than the maximum radius attained by the pool (see equation 38a).

The flux of radiation received by the observer due to the flame on the pool is given by

$$\dot{q}''(t) = S\ T\ \dot{q}''_F \tag{51}$$

where

$\dot{q}''(t)$ = rate at which thermal energy is received by the observer at X per unit area

S = view factor between the flame and the observer

T = atmospheric transmissivity (which is a function of distance and relative humidity)

$\dot{q}''_F$ = mean emissive power of the flame (at the flame surface)

In the above equation, generally $\dot{q}''_F$ remains a constant once the size of the flame exceeds a certain value (typically 30 feet diameter for LNG flames). The parameter that is sensitive to the size of the flame (for a given X) is the view factor S. Similarly, the value of T (transmissivity) also varies depending on the distance between the flame surface and the observer surface.

The thermal dosage to the observer per unit area in a time duration t is calculated by

$$q''(t) = \int_0^t \dot{q}''(t)dt \qquad (52a)$$

Substituting equation 51 in 52a, we get

$$q''(t) = \dot{q}''_F \int_0^t S(t) \, T(t) \, dt \qquad (52b)$$

In order to obtain the dose q" from equation 52b, the details of the variation of S and T with time have to be known. S can be calculated if the pool size (radius) and the flame height are known. For most flames, a conservative assumption for flame height to pool diameter ratio is 3. The transmissivity also has to be calculated at every instant of time by knowing the flame size and therefore the distance between the observer and flame surface. The pool radius itself is calculated from equation 49. The integration on the RHS of equation 52b has to be performed numerically.

Evaluation of Equation 52b when $X \gg R_{max}$ and When Humidity in the Atmosphere is low $(T \simeq 1)$

When $X \gg R_{max}$, it can be easily shown (if we assume the flame to be of cylindrical shape with base radius R and height L) that*

$$S = \frac{2R^2 \, (L/R)}{\pi \, X^2} \qquad (53)$$

Equation 53 is the same as the famous inverse square law. It is obtained by using the fundamental definition of the view factor.[14] The view factor between a large rectangular plane surface and a unit plane surface parallel to it and located at a far off distance is equal to $(1/\pi)$ times the solid angle subtended by the large surface at the unit surface.

$$T(t) = 1 \qquad (54)$$

It is noted that by assuming equation 54 to be true, the estimated thermal intensity at the position of the observer is very much larger than what it would be if the atmospheric absorption is accounted for. Hence, equation 54 represents a conservative assumption.

Substituting equation 53 and 54 in equation 52b, we get

$$q''(t) = \left(\frac{2}{\pi}\right) \dot{q}''_F \left(\frac{1}{X^2}\right) \int_0^t R^2 \left(\frac{L}{R}\right) dt \qquad (55)$$

186

If we assume

$$\frac{L}{R} \simeq 6 \tag{56}$$

and substitute for R from equation 49 we get

---

*The plane of the viewing element is vertical.

$$q'' \simeq \left(\frac{12}{\pi}\right) \dot{q}_F'' \left(\frac{R_{max}^2}{X^2}\right) \frac{\kappa}{} t_{ch} \left[\frac{y^4}{24} - \frac{y^3}{6} + \frac{y^2}{2}\right] \text{ for } t \leq t_{max} \tag{57}$$

where $y = \varepsilon\bar{\tau} = \Gamma c^2 \left(\frac{t}{t_{ch}}\right)$ 　(58)

Equation 57 applies within the time duration in which the pool radius becomes a maximum (i.e. $\varepsilon\bar{\tau} = 1.6$, see equation 50).

Beyond the time $t = t_{max}$, the dose calculation is simple. It is obtained by multiplying the intensity at t_{max} by the difference in time between t and t_{max} and adding the result to the dose at t_{max}.
i.e., $t > t_{max}$

$$q''(t) = q''(t_{max}) + \dot{q}''(t_{max}) \quad (t - t_{max}) \tag{59}$$

Specific Example

We assume the burning of an LNG pool when LNG is released continuously. The conditions given in the example in Part 3 are assumed to hold for this example. For the purposes of illustration of the thermal dose calculation procedure, we assume that the boiling rate $(\dot{y})$ does not change very much in spite of the existance of fire on the pool. In addition, we assume the following additional data:

$\dot{q}_F''$ = Emissive power of the flame = 10^5 W/m^2 (31700 B/hr ft^2)

T = Transmissivity of the atmosphere = 1.0

X = Distance to the observer from the center of spill = 300 m

Substituting the above values in equation 57, we get (noting that R_{max} = 40 m, κ = 0.16, t_{ch} = 0.349 secs, ε = 3.24 x 10^{-5})

$$q''(t) = \frac{12}{\pi} \times \frac{10^5}{3.74 \times 10^{-5}} \left(\frac{40}{300}\right)^2 \times 0.16 \times 0.349 \left[\frac{y^4}{24} - \frac{y^3}{6} + \frac{y^2}{2}\right]$$

187

where $y = \dfrac{1.861 \times 10^{-5} \times (3.3)^2}{0.349}\ t = 5.807 \times 10^{-4}\ t$

where t is in seconds.

Note that the maximum radius $R_{max} = 40$ m is attained in time $t_{max} = 2755$ seconds, i.e. at $y = 1.6$. Hence,

$$q''(t_{max}) = 1.1703 \times 10^7 \left[\frac{1.6^4}{24} - \frac{1.6^3}{6} + \frac{1.6^2}{2}\right] = 1.019 \times 10^7\ \text{J/m}^2$$

DISCUSSION OF ANALYSIS IN PART 4

It is interesting to note that in general, for long exposure times (greater than 10 minutes), wood catches fire spontaneously when the energy absorbed is about 250 Btu/ft^2 (2.8×10^6 J/m^2) and skin injury takes place when about 2 cal/cm^2 (8.4×10^4 J/m^2) of energy is incident in reasonably short time durations (of the order of a few minutes). As can be seen from the above result in the example calculation, 300 meters from the spill center is safe from both wood ignition as well as skin injury point of view.

CONCLUSIONS

The problem of spread of a lighter than water immiscible liquid has been analyzed in this chapter in four parts. The spread of both non-volatile and volatile liquids has been considered.

It is seen from the data from the experiments using motor oil that the radius of spread increases as the square root of time. The same result is also obtained by the theoretical analysis presented in Part 2.

In Part 2, a model for the spread on water of a continuously released non-evaporating liquid has been worked out. The model uses only the mass conservation equation and the known fact that the front spreads at a characteristic wave velocity corresponding to the thickness of the liquid film at the front. Similarity assumption is made for the thickness profile. The theoretical analysis predicts the same law of spread as has been observed experimentally. The one free constant in the analysis is determined by the use of experimental information.

A model has been derived in Part 3 to predict the rate of spread of a cryogenic liquid on the water surface when it is released continuously. The model incorporates both spreading and simultaneous evaporation due to boiling or vaporization due to fire. The solutions to the spread equations are obtained using the method of perturbations. The time to reach the maximum pool diameter is predicted using the solutions derived.

188

The analysis presented in Part 3 and the example considered in it indicates the time to spread to the maximum radius in the case of a continuously spilled cryogenic liquid is not small. This observation is important because in most analyses of cyrogenic spills, it was always assumed that the pool would develop "almost instantaneously" to the maximum radius.

Finally, in Part 4, an example is considered for calculating the hazard distance from a growing pool of burning liquefied gas. The results from the example considered indicate that the hazard distances are not large compared to the maximum radius of pool spread.

APPENDIX F

Solution to equation 31: Radial Spread Without Mass Loss

$$\frac{d\psi}{d\tau} = \frac{1}{\sqrt{FE_1}} \left[\tau/\psi^2 + E_1 - \frac{1}{2} \right]^{\frac{1}{2}} \tag{F1}$$

with $\qquad \psi = 0 \quad$ at $\qquad \tau = 0$

$$\text{i.e.,} \quad \psi \frac{d\psi}{d\tau} = \frac{1}{\sqrt{FE_1}} \left[\tau + (E_1 - \frac{1}{2}) \psi^2 \right]^{\frac{1}{2}} \tag{F2}$$

Let $\qquad \tau + (E_1 - \frac{1}{2}) \psi^2 = \epsilon^2 \tag{F3}$

Since at $\tau \to \infty$, $\frac{d\psi}{d\tau} \to 0$ we see from equation F2 that $E_1 - \frac{1}{2}$ must be negative;

$$\text{i.e.,} \qquad E_1 < \frac{1}{2} \tag{F4}$$

Substituting F3 in F2 and simplifying, we get

$$\frac{d\epsilon^2}{d\tau} - 1 = \frac{2(E_1 - \frac{1}{2})}{\sqrt{FE_1}} \epsilon$$

$$\text{i.e,} \qquad \int_{\epsilon = 0}^{\epsilon} \frac{2\epsilon\, d\epsilon}{1 - \lambda \epsilon} = \tau$$

where $\qquad \lambda = \frac{(1 - 2E_1)}{\sqrt{FE_1}} \tag{F5}$

i.e.,

$$\left[\frac{1}{\lambda} \ln \frac{1}{(1 - \lambda \epsilon)} - \epsilon \right]_0^{\epsilon} = \frac{\lambda \tau}{2} \tag{F6}$$

190

as $\tau \to \infty$, $\epsilon^2 \to \dfrac{1}{\lambda^2} = $ constant $\hspace{2cm}$ (F7)

Substituting for ϵ and λ in F6, from F3 and F5, we have

$$\tau = \frac{2FE_1}{(1-2E_1)^2} \, \ell n \left[\frac{1}{1 - \dfrac{(1-2E_1)}{\sqrt{FE_1}} \sqrt{\tau - \dfrac{(1-2E_1)}{2} \psi^2}} \right] - \sqrt{\tau - \frac{(1-2E_1)}{2} \psi^2} \hspace{1cm} (F8)$$

and asymptotically

$$\tau - \left(\frac{1-2E_1}{2} \right) \psi^2 \to \frac{FE_1}{(1-2E_1)^2}$$

i.e.,

$$\psi^2 \to \left(\frac{2}{1-2E_1} \right) \left[\tau - \frac{FE_1}{(1-2E_1)^2} \right]$$

i.e., $\displaystyle\lim_{\tau \to \infty} \psi \to \left(\frac{2}{1-2E_1} \right)^{\frac{1}{2}} \sqrt{\tau - \frac{FE_1}{(1-2E_1)}} \hspace{1.5cm} (F9)$

APPENDIX G

Solution to Equation 35a: Small Time Solution to the Radial Spread Without Mass Loss

$$\frac{d\psi}{d\psi} = \frac{1}{\sqrt{E_o F}} \left(\frac{\tau}{\psi} + E_o - 1 \right)^{\frac{1}{2}} \tag{G1}$$

with $\psi = 0$ at $\tau = 0$, E_o and F are constants.

Let

$$\frac{\tau}{\psi} + E_o - 1 = Z \tag{G2}$$

and

$$\beta = \frac{1}{\sqrt{F E_o}} \tag{G3}$$

Hence, equation G1 becomes

$$\beta \frac{d\tau}{d\psi} Z^{\frac{1}{2}} = 1 \tag{G4}$$

From G2, we have after rearranging,

$$\psi (Z + 1 - E_o) = \tau \tag{G5}$$

Differentiating the above w.r.t. ψ we have

$$(Z+1-E_o) + \psi \frac{dZ}{d\psi} = \frac{d\tau}{d\psi} \tag{G6}$$

Substituting for $d\tau/d\psi$ from equation G4 in G6, we get

$$(Z + 1 - E_o) + \psi \frac{dZ}{d\psi} = \frac{1}{\beta Z^{\frac{1}{2}}} \tag{G7}$$

Let

$$S = \ln \psi$$

$$\Gamma = E_o - 1 \tag{G8}$$

Therefore, G7 becomes

$$\beta Z^{\frac{1}{2}} \left[\frac{dZ}{dS} + Z - \Gamma \right] = 1$$

Let
$$\zeta = Z^{\frac{1}{2}} \qquad \qquad \text{(G9)}$$

Hence, we get from 9 and the equation above that

$$\zeta \left(2\zeta \frac{d\zeta}{dS} + \zeta^2 - \Gamma \right) = \frac{1}{\beta}$$

i.e.,
$$2\zeta^2 \frac{d\zeta}{dS} = \frac{1}{\beta} + \Gamma\zeta - \zeta^3$$

Integrating, we get

$$- 2/3 \; \ell n \left(\frac{1}{\beta} + \Gamma\zeta - \zeta^3 \right) + \frac{2}{3} \Gamma \int \frac{d\zeta}{(\frac{1}{\beta} + \Gamma\zeta - \zeta^3)} = S + \text{Constant}$$

If $\alpha_1 \; \alpha_2 \; \alpha_3$ are the roots of the equation

$$\frac{1}{\beta} + \Gamma\zeta - \zeta^3 = 0 \qquad \qquad \text{(G10)}$$

we have

$$\int \frac{d\zeta}{\frac{1}{\beta} + \Gamma\zeta - \zeta^3} = \int \frac{d\zeta}{(\zeta-\alpha_1) \; (\zeta-\alpha_2) \; (\zeta-\alpha_3)}$$

i.e.,
$$= \int \frac{A}{(\zeta-\alpha_1)} + \frac{B}{(\zeta-\alpha_2)} + \frac{C}{(\zeta-\alpha_3)}$$

where

$$A = \frac{1}{(\alpha_1 - \alpha_2)(\alpha_1 - \alpha_3)} \qquad ; \qquad B = \frac{1}{(\alpha_2 - \alpha_1)(\alpha_2 - \alpha_3)} \qquad \text{(G11)}$$

$$\text{and } C = \frac{1}{(\alpha_3 - \alpha_1)(\alpha_3 - \alpha_2)}$$

193

i.e., $\psi^{3/2} = \dfrac{(\zeta-\alpha_1)^{A\Gamma}(\zeta-\alpha_2)^{B\Gamma}(\zeta-\alpha_3)^{C\Gamma}}{(\frac{1}{\beta} + \Gamma\zeta - \zeta^3)}$ (G12)

where $\quad \zeta = (\dfrac{\tau}{\psi} + \Gamma)\quad$ and $\quad \Gamma = E_0 - 1$

where $\alpha_1\ \alpha_2\ \alpha_3$ are the three roots of equation G10

The above equation is an implicit solution for the differential equation G1.

However, we can obtain a simpler solution given by

$$\psi = c\ \tau \tag{G13}$$

where c is a constant.

This satisfies the condition $\psi = 0$ at $\tau = 0$

Substituting G13 in G1 we get

$$c = \beta\left[\Gamma + \frac{1}{c}\right]^{\frac{1}{2}}$$

This cubic equation in c has to be solved for given values of β and Γ.

It can be shown that only one real positive of c is possible for

all values of β and Γ with some restrictions.

i.e., $\quad c^3 = \beta^2\left[1 + \Gamma c\right]$

which can be written as

$$\left[\dfrac{c}{\beta^{\frac{2}{3}}}\right]^3 = 1 + \Gamma\beta^{\frac{2}{3}}\left[\dfrac{c}{\beta^{\frac{2}{3}}}\right]^3$$

The above equation is a cubic equation in $(c/\beta^{2/3})$ and can be solved using

the exact solution given in Reference 13. Hence, the solution is

$$c = \beta^{2/3}\left[\left\{\frac{1}{2} + \left(\frac{1}{4} - \frac{\lambda^3}{27}\right)^{\frac{1}{2}}\right\}^{\frac{1}{3}} + \left\{\frac{1}{2} - \left(\frac{1}{4} - \frac{\lambda^3}{27}\right)^{\frac{1}{2}}\right\}^{\frac{1}{3}}\right] \tag{G14}$$

where it is assumed that $\lambda < 3/4^{1/3}$

with $\quad \lambda = \Gamma\beta^{2/3} = (E_0-1)\left(\dfrac{1}{E_0 F}\right)^{\frac{1}{3}}$ (G15)

194

Therefore,

$$\frac{3}{4^{\frac{1}{3}}} \;>\; (E_o - 1)\,\left(\frac{1}{E_o F}\right)^{\frac{1}{3}}$$

Note that for all positive values of E_o less than unity, the above condition is satisfied.

$$E_o \;<\; 1 \tag{G16}$$

Substituting for c and $\psi = c\tau$, we have

$$\psi = \tau \left(\frac{1}{E_o F}\right)^{\frac{1}{3}} \left[\left\{ \frac{1}{2} + \left(\frac{1}{4} + \frac{(1-E_o)^3}{27 E_o F}\right)^{\frac{1}{2}} \right\}^{\frac{1}{3}} + \left\{ -\frac{1}{2} + \left(\frac{1}{4} + \frac{(1-E_o)^3}{27 E_o F}\right)^{\frac{1}{2}} \right\}^{\frac{1}{3}} \right] \tag{G17}$$

195

APPENDIX H

Perturbation Solutions to Equation 44: Radial Spread with Mass Loss

$$\tau = \psi^2 \left[\frac{1}{2} - E_1 \right) + E_1 F \left(\frac{d\psi}{d\tau} \right)^2 + \Gamma \int_{\tau'=0}^{\tau} \psi^2 (\tau') \, d\tau' \qquad (H1)$$

with $\qquad \psi = 0 \quad$ at $\quad \tau = 0$ $\qquad\qquad\qquad\qquad\qquad$ (H2)

We define the following parameters

$$c = \left(\frac{2}{1-2E_1} \right)^{\frac{1}{2}} \qquad\qquad (H3)$$

$$\kappa = \frac{E_1 F}{(1-2E_1)^2} \qquad\qquad (H4)$$

$$\sigma = \frac{\psi^2}{c^2 \kappa} \qquad\qquad (H5)$$

$$\bar{\tau} = \tau/\kappa \qquad\qquad (H6)$$

$$\epsilon = \kappa \Gamma c^2 \qquad\qquad (H7)$$

From equations 38b, H5 and H7, we get

$$\sigma_{max} = \frac{1}{\epsilon} \qquad\qquad (H8)$$

Substituting equations H3 through H7 in H1, it can be shown that the equation reduces to

$$\bar{\tau} = \sigma + \left(\frac{d\sigma}{d\tau} \right)^2 + \epsilon \int_{\tau'=0}^{\bar{\tau}} \sigma (\tau') \, d\tau' \qquad (H9)$$

with
$$\sigma = 0 \qquad \text{at} \qquad \bar{\tau} = 0$$

196

It is noted from the solution given in equation 32 (Part I) and its application in the example given in Part I, that the value of c is of the order of unity (actually $c = 3.3$) and c^2 is of the order of ten. Also, the value of κ from the same example is of the order of 0.1 (actual value $\kappa = 0.16$). Therefore, we see that ε (equation C7) is still very small compared to unity.

Perturbation Solution to Equation C8

Zeroth Order Solution

i.e., $\varepsilon = 0$

$$\overline{\tau} = \sigma + \left(\frac{d\sigma}{d\overline{\tau}}\right)^2$$

The asymptotic solution for this (for large $\overline{\tau}$ or σ) is

$$\sigma = (\overline{\tau} - 1) \tag{H10a}$$

This is exactly the same equation that was derived in Appendix G and presented in equation 32.

i.e., $$\psi \simeq c\sqrt{\overline{\tau}} \tag{H10b}$$

From equation 38 b, we have

$$X_{max} \simeq \psi_{max} \quad * \quad \sqrt{\frac{1}{\Gamma}}$$

Therefore

$$\sqrt{\frac{1}{\Gamma}} = c\sqrt{\overline{\tau}_{max}}$$

i.e., $$\tau_{max} = \frac{1}{c^2\Gamma} \tag{H11a}$$

which can be written as

$$\overline{\tau}_{max} \ \varepsilon = 1 \tag{H11b}$$

where τ_{max} is the time taken to attain maximum radius

First Order Perturbation

We substitute the result of equation C10a (noting that $\tau \gg 1$) in the differential and the integral of equation C9. Then we get

$$\bar{\tau} = \sigma + 1 + \epsilon \frac{\bar{\tau}^2}{2}$$

i.e.,

$$\sigma = - \frac{\epsilon}{2} \bar{\tau}^2 + \bar{\tau} - 1 \tag{H12}$$

It is noted, however, that C12 is not a physically valid solution.* Hence, one more order of perturbation has to be worked out.

Second Order Perturbation

Substituting C12 in equation C9 in the integrand and the differential, we get

$$\bar{\tau} = \sigma + \left[1 - \epsilon \bar{\tau} \right]^2 + \epsilon \left[-\bar{\tau} + \frac{\bar{\tau}^2}{2} - \frac{\epsilon}{6} \bar{\tau}^3 \right]$$

Nothing that $\sigma \gg 1$ and $\tau \gg 1$ and $\epsilon \ll 1$, we get

$$\sigma = \frac{\epsilon}{6} \bar{\tau}^3 - \frac{\epsilon}{2} \bar{\tau}^2 + \bar{\tau} \tag{H13}$$

To obtain maximum time, we have (using equation D8 and D13)

$$\left(\epsilon \bar{\tau}_{max} \right)^3 - 3 \left(\epsilon \bar{\tau}_{max} \right)^2 + 6 \left(\epsilon \bar{\tau}_{max} \right) - 6 = 0$$

It can be shown that for the above equation, there is only one real root[11] and this is given by

$$\bar{\tau}_{max} \epsilon = 1.6 \tag{H14}$$

It is interesting to compare the results of equation H11b and H14.

---

*This is because if equation H8 is substituted in 12 and τ_{max} is obtained, one obtains a complex number.

NOMENCLATURE

a   = radius of the outside of the hydraulic jump   m

b   = radius of the jet just before it enters the water   m

c   = constant defined in equation 46 = $\left(\dfrac{2}{1 - 2E_1}\right)^{1/2}$

D   = diameter of the jet nozzle   m

d_ℓ = maximum depth to which the liquid sinks underneath the jet   m

$E(\eta)$ = a function defined in equation 25

E_0, E_1 = constants obtained from integrating E function; see equation 28

F   = source Froude number; see equation 21

F_a = Froude number at radius a - also interpreted as the Froude number downstream of a hydraulic jump

F_b = Froude number at radius b = $\dfrac{u_b{}^2}{Gh_b}$

$f(\tau)$ = a time dependent function defined in equation 25

G   = effective gravity = $g\left(1 - \dfrac{\rho_\ell}{\rho_w}\right)$; see equation 9 m/s^2

g   = acceleration due to gravity m/s^2

H   = height of the exit section of the jet nozzle above the water surface   m

h   = thickness of the liquid film at any radial position   m

κ = constant defined in equation 46 = $\dfrac{E_1 F}{(1 - 2E_1)^2}$

P   = thermodynamic pressure   N

P_{atm} = atmospheric pressure   N

$\dot{Q}$ = volumetric flow rate m^3/s

$\dot{q}_F''$ = emissive power of flame (W/m^2) W/m^2

$q''(t)$ = radiative heat flux received by an observer at ground level (W/m^2)

$q''(t)$ = total radiative heat dosage in a time duration t (J/m^2)

R   = radius of the spread front at any time   (m)

R_{max} = maximum radius to which a cryogenic liquid spill would spread   m

r = radius   m

S = view factor between the flame and the observer (see equation 51)

T = atmospheric transmissivity to thermal radiation from flame

t = time   s

t_{ch} = characteristic time = a/u_a; see equation 21   s

U = mean velocity in the jet just before it hits the water level   m/s

u = radial velocity at any radial position   m/s

V = mean velocity of liquid at the exit section of the nozzle   m/s

v = dimensionless velocity; see equation 21

X = distance from spill center to an observer receiving radiant heat   m

$\dot{y}$ = liquid regression rate (in length/time) (m/s)   m/s

Γ = dimensionless evaporation rate = $\dfrac{a\dot{y}}{2u_a h_a}$ (see equation 39)

δ = dimensionless thickness of liquid film = h/h_a

η = similarity variable (radial) = $\dfrac{\xi - 1}{\chi - 1}$

ξ = dimensionless radius = r/a

ρ = density of fluids kg/m^3

σ = a radius parameter defined in equation 46.
Also, liquid-water interfacial (viscous) shear stress (equation 15)

τ = dimensionless time = t/t_{ch}

χ = dimensionless radius of spread front = R/a

ψ = $\chi - 1$

ε = dimensionless evaporation rate defined in equation 46

Subscripts

a,b,r   = the conditions at the corresponding radii

ch   = characteristic values

e   = the conditions at the spread front

j   = the condition in the jet at the exit of the nozzle

ℓ = liquid

0_1 = the condition at 0_1

0_2 = the condition at 0_2

w   = water

REFERENCES

1. "Santa Barbara Oil Spill," Oil on the Sea, edited by D. P. Hoult, Plenum Press, New York, 1969.

2. Spill from Cheveron Oil Well in the Gulf of Mexico, March, 1970, "Oceanographic Observations and Theoretical Analysis of Oil Slicks During the Cheveron Spill, March 1970," Coastal Stud. Inst. LA State University, Tech. Report 87, 59p, by Smith, W. G. and Sonu, C. J., 1970.

3. Jay, J. A., "Oil on the Sea," Edited by D. P. Hoult, Plenum Press, NY 1969.

4. Hoult, D. P. and Suchan, W., "The Spread of Oil in a Channel," Report, Fluid Mechanics Laboratory, MIT, 1970.

5. Fannelop, T. K. and Waldman, G. D., "Dynamics of Oil Slicks," AIAA Journal, v. 10, n4, pp. 506-510, April 1972.

6. Murray, S., "Turbulent Diffusion of Oil in the Ocean," Limnology and Oceanography, v. 17, n5, pp. 651-660, September 1972.

7. Abbot, M. B. and Hayashi, T., "Unsteady Radial Flow of Oil Being Discharged from a Source on the Ocean," Proc. 14th Coastal Engineering Conference, Japan Soc. Civ. Engs., v. 14, n1, pp. 226-229, 1967.

8. Raj, Phani P. and Kalelkar, A. S., "Fire-Hazard Presented by a Spreading, Burning Pool of Liquefied Natural Gas on Water," Paper Presented at the Western States Section/The Combustion Institute, Fall, 1973.

9. Muscari, "On the Spread of an Instantaneously Released Cryogenic Liquid on Water," M.S. Thesis, MIT Mechanical Engineering Department, 1974.

10. Watson, E. J., "The Radial Spread of a Liquid Jet Over a Horizontal Plane," J. Fluid Mech., v. 20, part 3, pp. 481-499, 1964.

11. Sabersky, R. H. and Acosta, A. J., "Fluid Flow - A First Course in Fluid Mechanics," The McMillan Company, New York, p. 265, 1964.

12. Birkoff, G., and Zarantonello, E. H., "Jets, Wakes, and Cavities," Academic Press, 1957.

13. Abramowitz, M and Stegun, I., "Handbook of Mathematical Functions," National Bureau of Standards, Applied Mathematics, Phase 55, p. 17, 1967.

14. Hottel, H. C. and Sarofim, A. F., "Radiative Transfer," McGraw Hill Book Co., New York, page 27, equation 2.5c, 1967.

CHAPTER V

HEATING, RUPTURE, AND RELEASE OF A PRESSURIZED CARGO IN A FIRE

OBJECTIVES

The objectives of the analysis presented below are to obtain a timewise history of the pressure in a pressurized propylene tank on a barge exposed to a fire and to identify the important parameters or physical conditions that affect the time and pressure at which the tank ruptures.

INTRODUCTION

A common method of transporting large quantities of bulk propylene is by river or ocean-going barge. These barges tend to have shallow draft hulls with either two or three long cylindrical tanks mounted on them across the beam. A typically configured pressurized propylene barge used by Union Carbide Corporation and built by Bethlehem Steel Corporation (see Figure 1) has three cylindrical tanks aboard. Each tank measures 14.75 feet in diameter by 193.5 feet in length. The tank has an uninsulated steel wall 1.5 inches thick and contains no internal baffles. The propylene contents are in a liquid state with an 8% ullage volume during shipment. Safety devices on each tank consist of four relief valves (set at 260 psig), two each of the 4" x 6" and 6" x 8" variety.

From a structural standpoint, the barge itself is a relatively flimsy device, having a thin (0.5 inch or so) hull and being quite rectangular in cross-section. The tanks are supported on internal bulkheads and saddles (typically seven) which serve to transfer much of the bending and torsional loads on the hull to the tanks so that the tanks themselves are the principal structural elements of the vessel. Atop the hull is a rain shield which seals the hold from the elements. This shield consists of horizontal plates between tanks and between the outside tanks and the top edge of the hull side. It is located so that a 150° arc of the upper half of each tank is exposed.

Due to the heavy traffic on crowded river and inland waterways, there is always the possibility of a collision with another vessel. If we recognize the fact that the propylene cargo is flammable as are the cargoes of any number of barges with which it could collide, then

there exists the real potential of a fire's occurring subsequent to a mishap involving the propylene barge. It would be helpful, then, to make a prior evaluation of the hazard which a collision would pose, i.e., to describe scenarios which might naturally occur as the result of a collision, to evaluate the adequacy of safety devices on the tanks in terms of these likely events, and from these to make an estimation of the failure mode and resultant damage.

We will assume here that the most disastrous event which would prevail in the event of a collision involving a propylene barge would be that of a fire and the rapid pressure rise which would accompany it. There are myriad other post-collision events which are likely, e.g., the barge merely sinks due to a ruptured hull, or the tanks rupture and all the propylene evaporates, but they are understandably benign when compared with the damage potential posed by a rupturing or fragmenting tank. So, we will concern ourselves here with the fire hazard alone and attempt to quantify its effect on the tank's integrity subsequent to a collision. Implicit in our treatment is the assumption that the fire is sustained by fuel sources other than the propylene contents of the barge itself. Only vapor which has vented in a normal fashion can participate in the exterior heat addition; the analysis stops with any rupture which would permit the external fire to ignite part of the contents.

THEORETICAL DEVELOPMENT

A. Formulation of the Physical Models

1. The Fire

Virtually any flammable material which is transported in barges along the same waterways in which propylene barges ply could supply the fire we are concerned with here. The flame characteristics of different materials vary widely in their spatial heat flux characteristics. Some flames are transparent to the radiation and consequently transfer heat to objects outside the flame periphery; others are opaque near the flame edge and unable to transfer much heat to objects outside the periphery, e.g., gasoline fire). However, in both of these cases, an object engulfed by the flame would be subjected to an intense heat dosage, both radiative and convective. It is this latter situation where the flame is in close proximity to our propylene barge that we must examine. This will provide us with the "worst case" heating condition for the vessel which we can presume is the severest hazard that can occur.

204

Studies of objects engulfed in aviation fuel fires[1,2] indicate
that the heat transfer to the exterior of the vessel may be considered
in two regimes; namely, one dominated by radiation transfer and one by
convective transfer. The temperature of the exterior surface of the
object being heated is used to establish limits on the dominance of each
of these mechanisms. As might be expected, radiation provides the bulk
of the heat transfer in the initial stages of burning and continues to
do so until the outside wall begins to re-emit a significant portion of
the incoming radiation. The point at which this occurs is, of course,
arbitrary but has been chosen by some[2] to be a 10% re-emitted flux.
This corresponds to a ratio of absolute wall temperature to flame tempera-
ture of 0.56. At this point, a heat transfer coefficient, h_{wall}, is deduced
such that (assuming both flame and vessel surfaces to be black bodies)[1]

$$h_{wall}(T_{flame} - T_{wall}) = \sigma(T_{flame}^4 - T_{wall}^4)$$

Throughout the remainder of our analysis of heat transfer to the tanks
when engulfed by flames, the heat addition is considered to be linearly
proportional to the temperature difference between flame and wall.

Another uncertainty in quantifying the thermal characteristics of
a fire is that of the flame temperature itself. There is large variation
in the background radiation temperature which is associated with any
flame. There is a spatial variation within the flame itself and a
decrease in the mean temperature level as distance between the object
being heated and the flame periphery increases. One resolution of this
dilemma is to choose an effective flame temperature such that the radiation
from a black body at this temperature will provide a measured flux at
the surface of an object engulfed in flames. This measured flux is
typically[1] deduced from the thermal behavior of a solid sphere or
cylinder engulfed in the fire because the response of such geometries
is well known.

For our analysis, we will use a flame temperature of 900°C for
the fire which this propylene barge is exposed to. This agrees closely
with a standard LNG flame temperature of 1610°F (877°C). When the flame
at 900°C is radiating to the tank wall, it will radiate a flux in the
neighborhood of 30,000 Btu/hr ft^2 (9.46 w/cm^2) for tank wall temperatures
below about 800°F (435°C). This flux of 30,000 Btu/hr ft^2 is also a
standard figure which is used for the net flux transferred to an object
engulfed in flames. For that area of the barge which we designate as

205

being exposed to fire, then, the background radiation source will yield a uniform (over the area) incident flux of 9.46 w/cm^2. Throughout the fire exposure time, the sole transport mechanism will be thermal radiation.

2. Heat Transfer to Contents of Tank

There are several conceivable means of transferring heat from an external fire to propylene in the tank, and each is governed, for the most part, by the location of the flame relative to the tank. For instance, the rate of heat transfer which we would expect from a flame located above the barge is quite different, at least phenomenologically, from that due to a fire in the hold. The fundamental differences in heat transfer rates, though, are governed by the local geometry and may be described by two conditions: (1) the physical state of the propylene adjacent to the wall; and (2) the orientation of the wall with respect to the gravity vector. With this in mind, we proceed to a description of some feasible situations.

Thermal stratification will occur if the heat input to the propylene proceeds in the direction of the gravity gradient, i.e., from a flame above to a tank wall below to a vapor at the top of the contents bulk. Assuming that the tank wall and contents are initially at a uniform temperature of 60°F (15.6°C) and a fire suddenly erupts above the tank, we would witness the following (see Figure V-1). Initially, there would be a rapid increase in the temperature of the outside surface of the wall adjacent to the vapor as it attempted to come to thermal equilibrium with the flame. Similarly, a radial thermal gradient would quickly establish in the wall at a rate governed by the thermal diffusivity of the steel. Once this spatial gradient is established, continuing heat transfer to the wall would prompt a rise in the wall's temperature level as the heat capacity of the steel absorbed some of the energy radiated by the flame. The rising inside wall temperature would start a heat addition to the propylene vapor adjacent to it by conduction and a radiative transmission through the vapor to the liquid mass below. Any nonuniformities in heat flux at the wall-vapor interface would provoke motion in the vapor and enhance the conductive heat transfer mechanism with a bulk fluid motion, i.e., convection.

Once this process of heat addition to the contents has been established, the tank wall, vapor, and surface layer of the liquid would continue to rise in temperature level with the bulk liquid's temperature remaining relatively

206

Fire Outside The Barge

Radiant Heat From Tank Wall To Liquid Surface

Vapors Liberated at The Bottom
Due To Boiling Rising To The
Ullage Volume

Liquid Propylene

Water Line

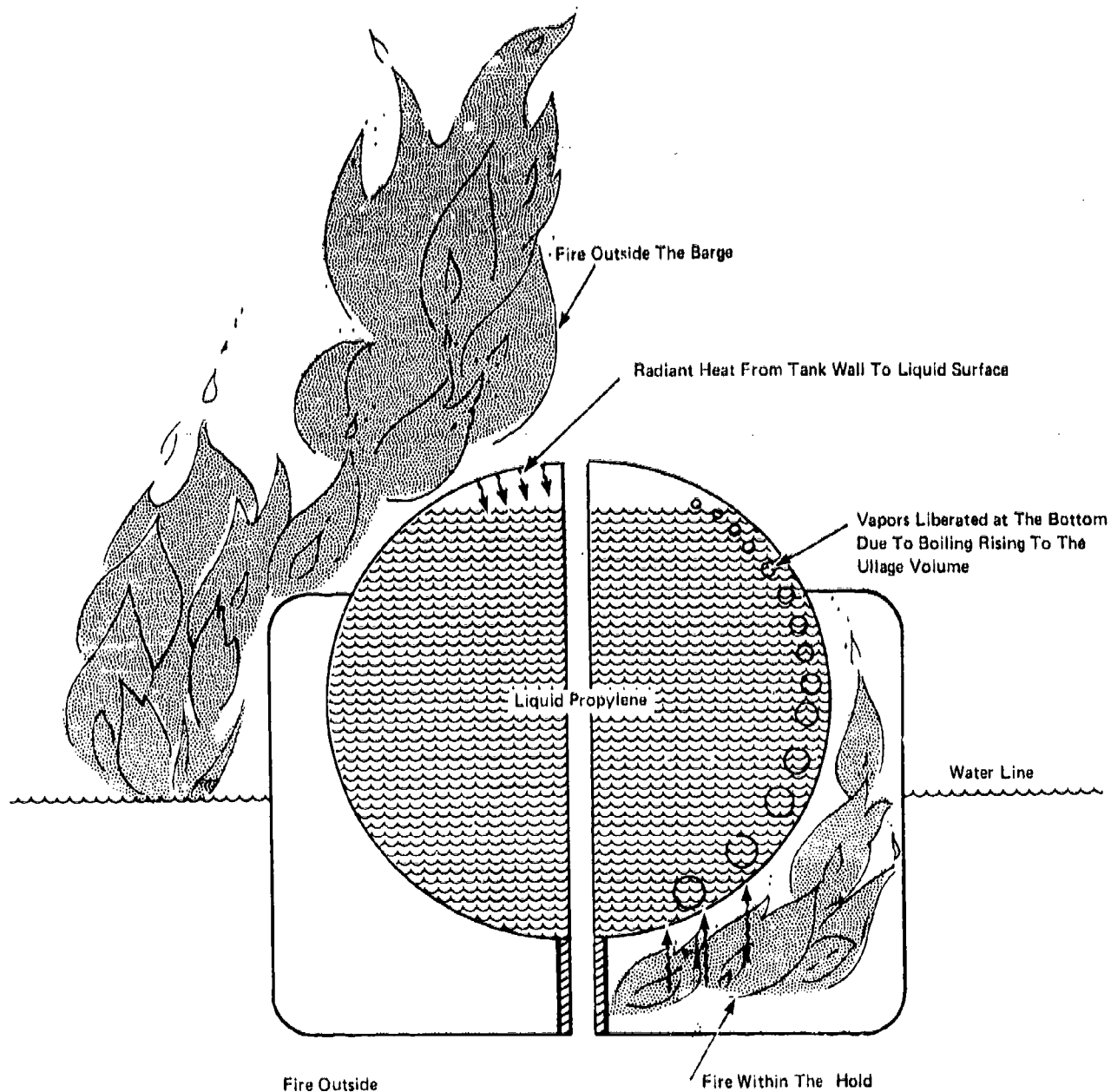Fire Outside

Fire Within The Hold

FIGURE V-1   SCHEMATIC REPRESENTATION OF THE TWO FIRE
SITUATIONS CONSIDERED IN THE ANALYSIS

fixed. Because of the high metal thermal conductivity relative to that of the vapor, the wall temperature at the top of the tank would progressively approach that of the flame, while there would be a gradient through the vapor to a temperature at the liquid surface equal to the saturation temperature at the tank pressure. Throughout all of this heat addition, the large liquid mass in the tank would be almost totally unaffected by the increase in temperature (and pressure, since the ullage volume would remain nearly constant) of the vapor. Only a thin stratum atop the liquid mass would be warmed enough to generate vapor. The circumferential conduction through the tank wall to the deeper reaches of the liquid bulk would not constitute a significant thermal path.

Eventually, the tank pressure would rise to the relief valve setting and vapor would begin to flow out of the tank through the four relief valves. Flow through each valve would reach choke flow conditions if the evaporation rate were high enough. The tank pressure would then adjust, upward if necessary, to maintain flow through the relief valves equal to the contents' evaporation rate.

Natural convection will provide the principal means of heat transfer in a case where there is liquid in contact with the wall. This would apply to any heat addition on the sides or bottom of the tank as shown in the right half of Figure V-1. Because of buoyancy effects, any heat transfer to the liquid will cause fluid motion along the inside surface of the wall and an increased heat transfer coefficient over that which could be expected for conduction alone.

The temperature history of the tank wall when exposed to a fire along the sides or bottom proceeds much like it does when exposed to a fire on top. Again, the temperature which the wall will assume as it approaches the steady state is wholly determined by the heat transfer coefficient on the inside of the wall. This film coefficient will initially be that due to conduction alone. Once the buoyancy effects are felt and motion is induced in the fluid, the film coefficient will increase with increasing wall temperature until the onset of pool boiling (bubble generation) at the inside surface of the wall. This boiling regime may be inadequate to support the flux coming through the wall from the fire outside and will be supplanted by film boiling in which a vapor layer is formed adjacent to the inside surface of the wall.

208

The boiling curve for propylene is shown in Figure V-2. Both curves for pool boiling and film boiling are derived from correlations found in the literature[3,4,5,6] and applicable to organic liquids. Superimposed upon the boiling curve is one relating the heat transfer from the external fire to the outside of the wall. The "wall" temperature shown on the abscissa is that of the inside surface of the wall. For an external flux of 30,000 Btu/hr ft^2 or so, the gradient across the wall is only 149°F (83°C). An error of this magnitude in the outside wall temperature is minuscule in evaluating the radiative flux. The intersections of this external flux curve with the two boiling curves constitute steady-state conditions in which the rate of heat addition to the wall from the fire is equal to the removal rate due to boiling for the inside surface.

Because of the manner in which the wall heat flux develops, the nucleate boiling regime will be appropriate for the propylene tank. Since the flux at the inside surface of the wall develops gradually from zero to about 30,000 Btu/hr-ft^2, the wall superheat ($T_{wall} - T_{sat}$) will also increase from zero to a value which can sustain removal of the external flux supplied by the fire. Film boiling will prevail only if the wall superheat is reduced from a very high initial value or if the "burnout" condition is reached in nucleate boiling. As indicated on Figure 3, burnout in nucleate boiling in propylene doesn't occur until a flux of about 186,000 Btu/hr ft^2.

3. Pressure Rise

The rate of pressure rise in the tank may be determined from an energy analysis of the tank contents. Prior to opening of the relief valve, the contents may be modeled as a closed, single system. No work transfers or mass would cross the system boundary and the heat transfer could be evaluated from the discussion above. Similarly, once the relief valves open, the analysis would proceed with the added consideration of a mass flow across the system boundary. Since we can only keep track of total energy from a thermodynamic analysis of the tank, we need to make some assumptions about the actual processes which occur as a result of the heat addition. In the case of heating from above the tank, we can reasonably assign the heat conducted across the wall-vapor interface to the sensible heat of the vapor and expect some vapor generation at the liquid interface due to a radiative
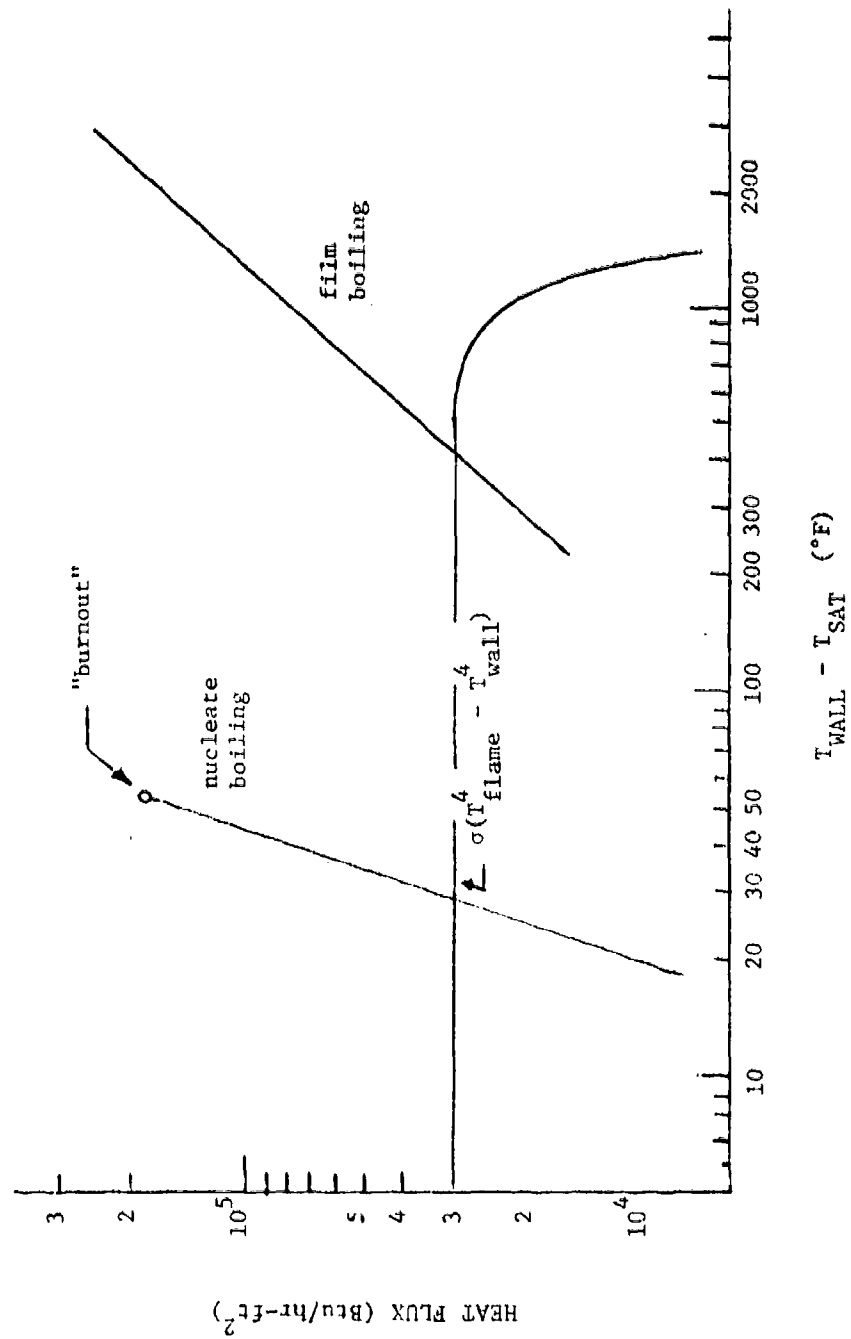
FIGURE V-2   Boiling curve for propylene showing equilibrium
between tank wall and 900°C flame.

210

component of the total heat flux into the tank. This process would continue until the tank was empty, provided the tank structure is able to withstand pressure and high temperature.

For those situations in which we could expect a fire along the sides or bottom of the tank, the distribution of energy within the contents could be nicely bounded, even though quantifying the actual process would be extremely difficult. One extreme of this limit analysis would be to assume that the liquid mass has a wholly passive role in the pressure rise save as a source of vapor. We would allocate all of the heat flux across the wall-vapor interface to generating vapor (latent heat) and raising the vapor temperature of the film adjacent to the wall. Virtually none of the total heat flux from the wall would manifest itself in an increase in the bulk liquid temperature. Accordingly, from the rate of vapor generation within the tank, we could deduce a rate of pressure rise. This process would continue until the tank was empty with appropriate modifications being made in the heat transfer rates to account for the relative tank areas which were in contact with vapor and with liquid as the tank emptied.

At the other extreme of the limit analysis, we would require the bulk liquid to have an active participation in the heat addition to the tank. We would simply require that the contents remain in the saturated state as the heat is added with the result that there would be a single uniform temperature throughout the tank contents. The pressure rise would be considerably slower because the heat addition could only manifest its presence in the sensible heat of the liquid.

4. Structural Analysis

The structural integrity of the tank which experiences a rapid pressure rise due to exposure to a fire can be mitigated in two ways: (1) the pressure rise is so severe and the relief valves are so inadequate that the tank wall stress exceeds the tensile strength of the material and a rupture with associated fragmentation, etc., occurs; and (2) because of the heat transfer limitations at the inside surface of the wall, the wall temperature tends to approach the flame temperature and undergoes a reduction in tensile strength as a result of this. For large increases in wall temperature, the tensile strength would plummet severely, to nearly zero in fact, if the melting temperature of the metal were reached. More modest increases would induce creep in the wall material and make rupture a complicated function of time, temperature, and strain rate.

211

An accurate estimate of the tank's rupture potential would be a for-
midable task. Among the requirements for the analysis are: (1) time-
pressure history of contents, (2) detailed transient temperature distri-
bution in the tank wall, (3) a consideration of local geometry and any
penetrations, and (4) procedures to simulate the elastic-plastic behavior
of the tank.

For our purposes here we have chosen to consider only the gross tank
geometry and will consider it to be a thick-walled cylinder closed at each
end. Using standard equations for the state of stress at a point in the
wall, we can calculate the various stress components which arise from in-
ternal pressure. From these stress components and a fracture criterion,
such as from the maximum shear stress theory, we can calculate the stress
condition which will cause local fracture in the tank wall. When the ten-
sile strength of the steel wall has fallen to this stress value because of
its temperature increase, we can conclude that a fracture will occur.

B. Approach to Analysis

The principal parameters of interest in the analysis are the time wise
variations of the tank pressure and the tank wall temperature. In order
to calculate these values for given radiant heat flux and exposure area and
location of fire, governing equations are written down. These equations
together with the details of derivations are given in Appendix A. The equa-
tions essentially represent the relationships between energy input, mass
loss by venting through the vents, and the volume changes in liquid pro-
pylene and gaseous fraction, steel wall and propylene thermal properties.

The equations for the case of heat input into the ullage volume are
quite different from the case in which heat soaks into the liquid due to
a fire in the hold. Both these situations are analyzed. In the case of
the latter two extremes, conditions of heat soaking into the liquid-vapor
system are considered. These include a direct vapor path to the ullage
volume from the boiling sites at the tank bottom and the second case in
which the bubbles of gas agitate the liquid and keep the system in satura-
ted condition corresponding to the pressure existing at that instant.

The derivations of the governing equations are tedious and involved.
Hence, they are given in a separate Appendix I. The thermodynamic
properties of propylene are given in Appendix J, and Appendix K
contains the structural analysis of the shell wall. Only results
are discussed below.

DISCUSSION

A. Heating from Above

The analysis we proffered in the THEORETICAL DEVELOPMENT resulted in a system of simultaneous differential equations in a single independent variable, time. The system parameters of interest in this formulation were the tank pressure, vapor volume fraction, mean vapor temperature, and the temperatures at the inside and outside of the wall. Initial conditions chosen are as follows:

P 8.94 atm (saturation pressure of propylene at 60°F)

β 8%

T 288.8°K (60°F)

T_{wi} 288.8°K

T_{wo} 288.8°K

Implicit in this choice of initial conditions is our assumption that the tank contents are saturated at 288.8°K (60°F) with an 8% ullage volume. We further assume that at time zero there is a step increase in the heat flux over the 150° arc between rain shields on the top of the tank.

The results of the numerical integration are shown by the solid lines in Figure V-3 for the period up to 30 minutes after ignition of the fuel source around the tank top. Note that there is a rapid rise in tank pressure up to the 18.7 (260 psig) relief valve setting.

The rapid rise (just over a minute) is to be expected in light of the large surface area which is exposed to fire. The vapor (on the inner side of the tank wall) heats up very quickly and as a result is accompanied by an equally rapid pressure rise. Note that the slopes of the curves for the temperatures of the inside and outside surfaces of the wall are similar for an elapsed time of a minute or less. Very quickly, though, the temperature at the inside of the wall levels off at around 335°K. This temperature corresponds to a 16°K (29°F) temperature differential between the wall and the saturation temperature at the tank pressure of 18.7 atm (260 psig). At this ΔT, a heat flux of 9.46 W/cm^2 (30,000 Btu/hr-ft^2) can be sustained by
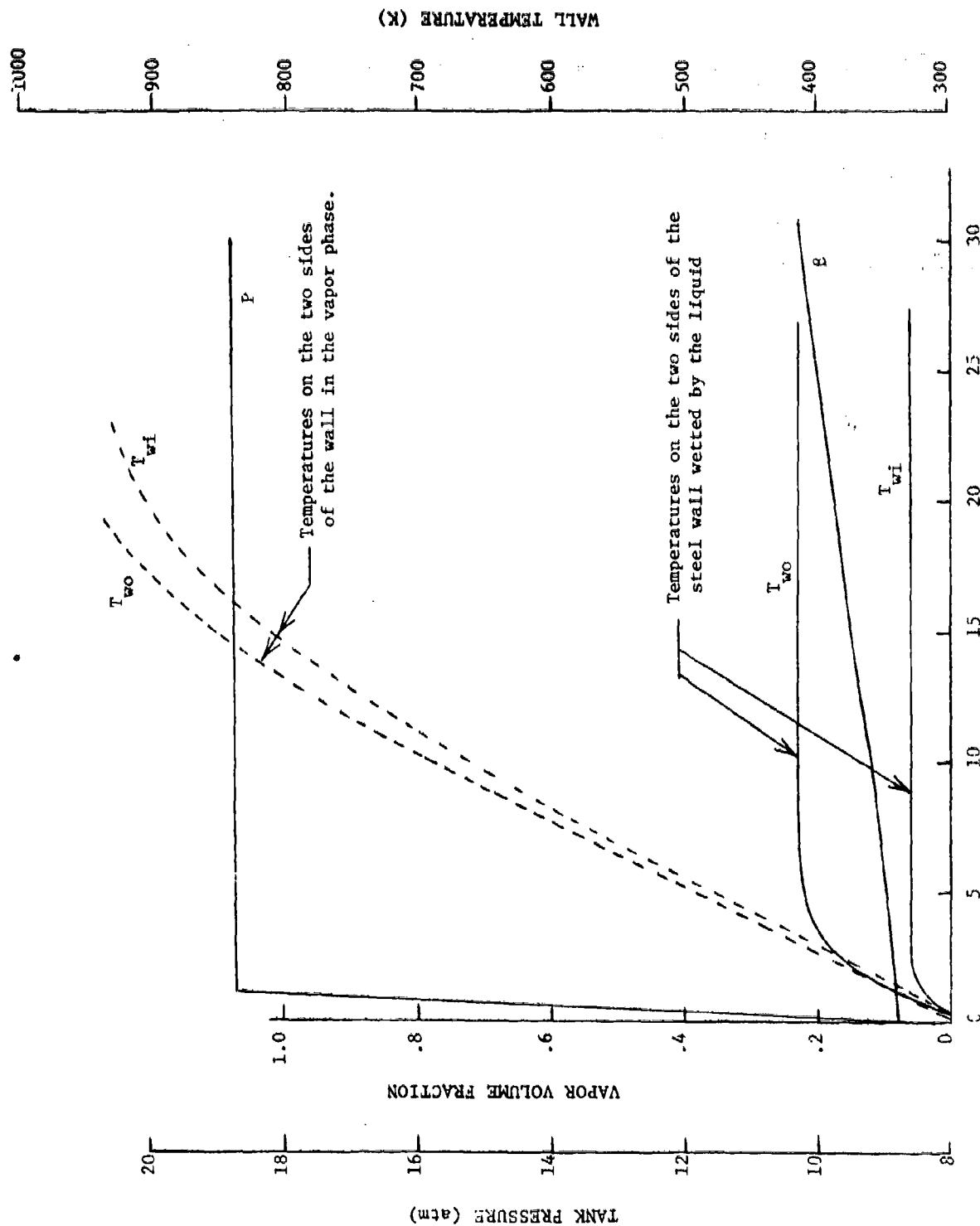
213

FIGURE V-3   Transients in propylene tank when exposed to fire on tank top.

214

nucleate boiling. Even though the temperature at the inside surface
stabilizes very quickly, that of the outside surface continues to rise un-
til an 83 K temperature differential exists across the wall. Given a wall
thermal conductance of 0.113 W/cm^2-K, this ΔT will sustain the 9.46 w/cm^2
flux from the fire. At this point, perhaps six minutes after ignition, the
tank pressure and the temperature differential through the wall have reached
steady state conditions. The rate of boiloff of the liquid propylene is
easily handled by the four relief valves on the tank. There is sufficient
flow area provided in the valves that the tank pressure need not rise much
(about 0.1 atm) above the relief valve setting of 18.7 atm in order to sus-
tain the boiloff in a choke flow condition.

With a steady state condition established in the tank wall and in the
pressure and temperature of the propylene contents, there results a grad-
ual increase in the vapor volume fraction as the liquid evaporates. The
rate at which this volume fraction increases, though, is decreasing with
increasing time. Tank geometry is responsible for this, since the princi-
pal component of heat transfer to the tank is due to boiling at the wall-
liquid interface above the rain shield (see Figure 1). As the liquid
level falls due to evaporation, and the vapor volume fraction increases,
the surface area which is wetted by this liquid will decrease until ulti-
mately the edge of the meniscus falls below the rain shield.

It would appear from a first glance at Figure V-3 that the tank wall
temperature will never rise above 335° K on the inside so long as there is
liquid in contact with it. This is a plausible result for that part of the
wall which is actually wetted by the liquid because a large heat flux may
be sustained by small temperature differences in nucleate boiling. But
for that section of the wall which has vapor adjacent to it on the inside,
this is inconceivable. Even if there were a high velocity flow of vapor
over the underside of the tank top, a ΔT much larger than 16° K or so would
be required to sustain a heat flux of 30,000 Btu/hr ft^2. We conclude from
these results of the numerical integration that our model is inadequate.

The error in our modelling of this heat addition from above the tank
is contained in the assumption that there are no circumferential gradients
in the tank wall. This enabled us to use a single node for the tank wall
and resulted in the dominance of the boiling heat transfer in determination

of the wall temperature. A closer examination of the relative magnitudes of the thermal conductance along the steel wall and that from the wall across the boiling interface reveals that there is an extremely small coupling through the steel wall. Because of this, the wetted section of the wall and the section adjacent to vapor will respond independently of each other.

A revision of the analysis to include a two node model of the tank wall above the rain shield resulted in far more plausible results for the temperature excursion of the tank wall. For that portion which is in contact with liquid, the solid lines on Figure V-3 were in essence repeated in this new solution. However, for the wall adjacent to the vapor, the broken lines on Figure V-3 were the resulting temperature excursions. Because of the extremely weak thermal coupling along the steel wall, the (unwetted) top of the tank responds independently of the behavior of the wetted portion of the wall. As a result, the wall adjacent to the propylene vapor rises in temperature so as to come to radiative equilibrium with the fire and the saturation temperature of the liquid surface. Steady state radiative equilibrium will occur for a wall temperature in the vicinity of 1138 °K (1588°F). As can be seen from Figure V-3, the wall is well on the way to this temperature having risen to 900 °K in 20 minutes after start of the fire. Note that the profiles of the inside and outside surface temperatures have begun to diverge in the 15 - 20 minute region. The profiles will ultimately level off at a difference of 83 °K just as the profiles for the wetted wall do. The radial thermal conductance of the wall will pass 9.46 w/cm^2 across a ΔT of 83°K. All this while, the tank pressure remains constant at roughly 18.7 atm, the relief valve setting. What happens after the 20 minute point is immaterial as far as the exact wall temperatures are concerned because at these elevated temperatures there is a sufficient reduction in the mechanical strength of the wall that yielding and even fracture will likely occur. This is discussed in greater detail in a later section.

B. Heating from Below

1. General

As we indicated in our discussion of the physical models which we chose for this analysis, the reaction of the tank contents to a fire in the hold

216

of the barge is difficult to quantify. Rather, it is far easier to bound the extremes which can occur and infer from them that the actual physical processes which occur will chart a course somewhere between these extremes.

Since we have assumed that the entire lower half of the tank is exposed to the fire, then we can anticipate nucleate boiling to occur along whatever portion is wetted by the liquid propylene. This wetted area that is also exposed to the fire of course decreases for vapor volume fractions greater than 0.5 as the meniscus falls below the horizontal centerline of the tank. Vapor which is generated as a result of the boiling will partially condense in the liquid and partially rise along the wall to the vapor space above the liquid. That vapor generated near the tank bottom will most likely be condensed, while that which emerges farther up toward the horizontal centerline will rise, due to buoyancy effects, into the vapor space above the liquid. The relative fractions which are recondensed or not will of course have a dependence on the exact liquid level in the tank, too.

Rather than attempt to model this process, we have chosen to observe the extremes. One of these would be the case where none of the vapor condensed and all of it rose to the vapor space above. In this situation, the liquid bulk would be wholly passive, save as a source of liquid to evaporate, and its thermodynamic properties would remain constant in time. The other case considers total recondensation of vapor with the result that the liquid gradually warms up. In this process, the liquid would remain saturated and in equilibrium with the vapor above throughout the heating from below. Consequently, the properties of the liquid would have a time dependence as long as the tank pressure was changing. The actual rate of pressure rise which will occur when a propylene tank is exposed to a fire from below will lie somewhere between those predicted by these two models.

2. Contents Stratified

When we formulated a model for the pressure rise, etc. in the tank, the vapor and liquid were considered to be separate systems with only a mass exchange connecting them at each instant in time, the vapor generated at the wall was added to the vapor space and the liquid from whence it came in turn deducted from the liquid mass. The transient which

results from this analysis is shown in Figure V-4 subject to the same initial
conditions we described in the previous discussion, i.e.,

P   8.94 atm (saturation pressure at 60°F)

β 8%

T   288.8 °K (60°F)

T_{wi} 288.8 °K

T_{wo} 288.8 °K

From Figure V-4, we can see that the pressure rise in the tank is extremely
rapid, as might be expected, since whatever vapor is generated along the
underside of the tank rises directly to the vapor space above the liquid.
The tank pressure rises to relief valve setting of 18.7 atm in slightly over
one minute and subsequently proceeds to hover about the relief valve setting.
Again, this is due to the adequacy of flow area in the four relief valves
and our assumption that choke flow conditions prevail for any fractional
opening up to and including the full open condition.

The temperature of the inside of the wall rises to 330 K in about one
minute at which point the steady state is established. In this steady state
condition, a 16 °K temperature differential between the 314 °K saturation
temperature and the wall temperature will sustain a nucleate boiling flux
of 9.46 W/cm^2. Note that the inside and outside wall surfaces have vir-
tually identical temperature rises for the first minute after the fire is
ignited. This is due to the high boiling heat transfer coefficient on the
inside surface. With this low heat transfer impedance present on the in-
side wall, the wall is free to absorb much of the incoming flux in its
sensible heat. Once the ΔT between the liquid and the inside of the wall
is established, the inside wall temperature becomes fixed and the rise in
sensible heat of the wall manifests solely as an increase in the temperature
of the outside surface of the wall. This rise continues for about 10 min-
utes after ignition until a ΔT across the wall of 83 °K is established. At
this temperature differential, the wall can conduct the 9.46 W/cm^2 from the
fire to the boiling interface in a steady state condition.

Once the steady state is established in the tank wall, all parameters
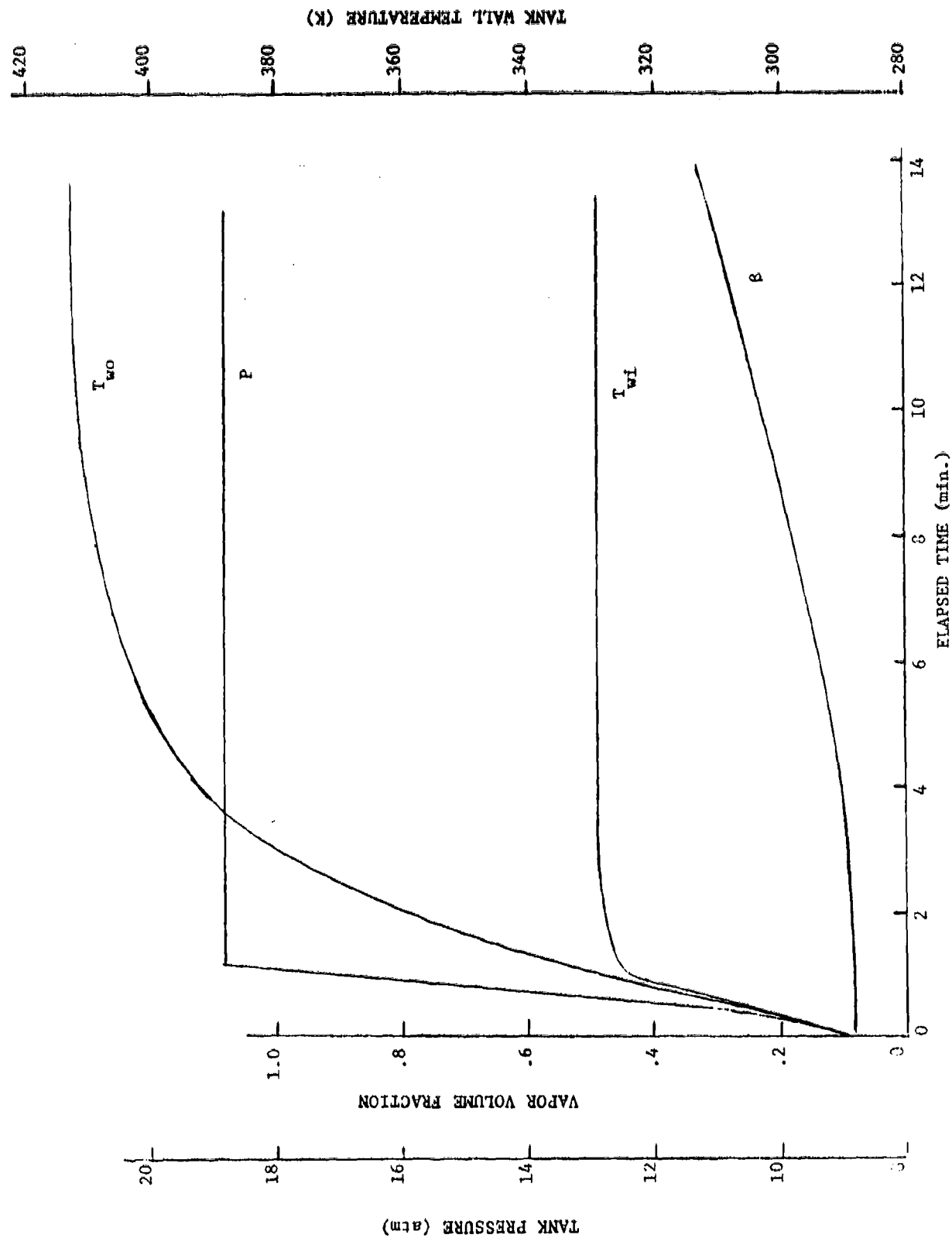of the system, save the vapor volume fraction, remain fixed in time. Only

FIGURE V-4   Transients in propylene tank when exposed to fire on bottom; contents stratified

219

the vapor fraction changes as the tank gradually empties. When the meniscus falls below the horizontal centerline of the tank, the rate of increase of the vapor fraction will slow down due to the reduction in wetted area on the bottom of the tank. As long as the wetted interface provides a thermal sink for the incoming flux from the fire, the tank wall temperature will retain the same temperature level and gradient as the tank empties. The tank is empty 101 minutes after the fire begins.

3. Contents Saturated

At the other extreme of the possible contents interactions during heating from below is that situation where the contents are always in a saturated state. This would occur in the event that all of the vapor generated at the boiling interface condensed in the liquid mass thereby warming up the liquid. Above the liquid, the vapor would be kept in equilibrium by evaporation at the vapor-liquid interface. It would be expected that the pressure rise be much slower than if the contents were stratified simply because the heat addition to the tank manifests itself in a temperature rise of the large liquid mass rather than in the small vapor mass atop the liquid. Figure V-5 shows the time behavior of the parameters of interest subsequent to start of a fire underneath the tank. There is a rapid initial rise only in the temperature at the outside surface of the tank wall. The inside surface temperature hardly moves, as does the tank pressure. This may be explained by the fact that we have assumed the heat transfer resistance between the inside surface of the wall and the liquid to be negligible. Furthermore, since the liquid mass is considered homogeneous in the analysis, the temperature at the interface with the wall is identical to that at the center of the tank. Since the liquid mass is so large, any heat addition through the wall will result in an almost imperceptible temperature rise in the liquid. The liquid temperature is coupled to its vapor pressure at saturation; hence, the slow pressure rise.

A rapid rise in the temperature at the outside surface of the wall is necessitated by the inside surface's temperature being pegged at 16°K above the saturation temperature of the contents. The incoming flux is then partially absorbed in the sensible heat of the wall as the outside wall
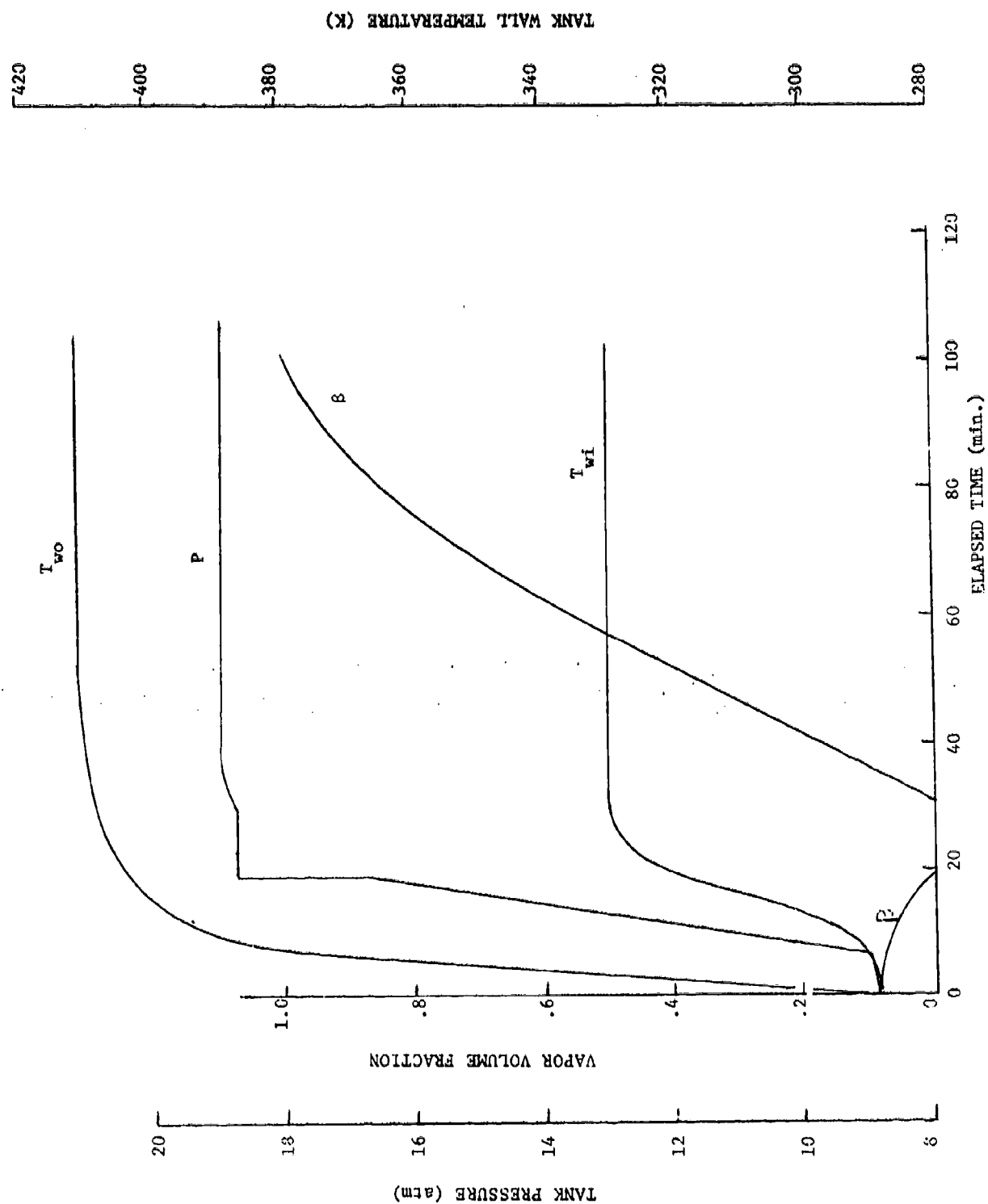
220

FIGURE V-5   Transients in propylene tank when exposed to fire on bottom; contents saturated.

221

temperature rises and establishes a radial thermal gradient in the wall.
Once this gradient is sufficient to conduct the incoming flux from the
fire to the liquid in the steady state, the relative changes in the two
temperatures ceases at a differential of 83°K. Given the wall conductance
of 0.113 W/cm²-K, this ΔT is sufficient to conduct the 9.46 W/cm² (30,000
Btu/hr ft²) from the fire to the contents. Only the temperature level
changes after this point.

Changes in the wall's temperature level is manifested by the rapid
pressure rise which begins about 6 minutes after start of the fire. At
this point, the radial thermal gradient in the wall has reached its steady
state value. Consequently, the entire flux from the fire must now be
absorbed by the liquid with a concomitant rise in the tank pressure.
From Figure V-5, it can be seen that the temperature level in the wall
and the tank pressure rise rapidly during the period between 6 and 19
minutes after start of the fire. All this while, the liquid density
is gradually decreasing as its saturation temperature rises. At the 19
minute point, the liquid density has decreased by 8% so that the ullage
volume has been absorbed and the tank goes liquid full. Once the tank
is liquid full, of course, the limited compressibility of the liquid
effects an almost instantaneous pressure rise to the relief valve setting.

At the relief valve setting, subcooled liquid flows through the
relief valves with a negligible pressure drop as the liquid density
continues to decrease in deference to the heat addition along the
tank's bottom. This liquid relief takes place during the 19-30 minute
period following start of the fire. After 30 minutes, the liquid
density has decreased to that of the saturated liquid at 18.7 atm.
and vapor relief begins to offset the increased pressure drop through
the relief valves.

Vapor continues to flow through the relief valves at a constant
rate during the period between 30 and 57 minutes after ignition as
the vapor volume fraction increases from zero to 0.5. The constant
evaporation rate is due to the constant heat addition rate along the
bottom of the tank. When the volume fraction reaches 0.5, the meniscus
coincides with the horizontal centerline of the tank. Beyond this
point, a falling liquid level results in a reduced wetted area on the
bottom of the tank. Since the heat transfer to the vapor is negligible

222

compared to that transferred via boiling, the rate of increase of the
vapor volume fraction falls off gradually until the tank empties, 101
minutes after the start of the fire. Just as in the case where the
contents were considered to be stratified during heating from below,
the maximum tank pressure hovers very near the relief valve setting
of 18.7 atm. Similarly, the maximum surface temperatures in the wall
are 330°K (134°F) and 413°K (283°F) at the inside and outside, respec-
tively.

4. Rupture of the Tank Wall

As noted in our discussion of the physical models chosen for this
analysis, we intend to predict a rupture of the tank wall from either
the maximum shear stress failure criterion or from the maximum distor-
tion energy criterion. Tank pressure is used to calculate the stresses
in the wall as a function of time and the temperature of the wall
is used to evaluate the tensile strength. Since the analysis allows
for a radial temperature gradient in the wall, the stress and tensile
strength must both be evaluated at a particular point in the wall.

Our results show that the maximum tank pressure hovers near the
relief valve setting (260 psig) because of the adequacy of the relief
valves; the appropriate internal pressure is 260 psig. Using the
standard formulae for stresses in a thick-walled cylinder, we calculate
the following stresses.

	Inside Radius	Outside Radius
σ_r	−260 psi (compressive)	0 psi
σ_θ	15471 psi	15211 psi
σ_z	7606 psi	7606 psi

If these stresses are translated into the two failure criteria which we
discussed, we get the following failure stresses.

	Maximum Distortion Energy Theory	Maximum Shear Stress Theory
Inside Radius	13623 psi	15731 psi
Outside Radius	13173 psi	15211 psi

The implication of the values of a failure stress is simply that local
fracture will commence once the tensile strength of the wall has fallen

223

to the failure stress. Note that there is a slight discrepancy in the failure stress at the inside and outside radii due to the radial stress gradient in the wall. The discrepancy is small because the tank has a small wall thickness-to-radius ratio.

Examination of the failure stresses predicted by our two chosen theories shows the maximum shear stress criterion to predict failure at a 15% higher stress than the maximum distortion energy theory. The literature (see Reference 15) has alluded to this variance in the two theories and further contends that the maximum distortion energy theory is more accurate in predicting the onset of yielding in a material. The implications for prediction of ductile fracture are less clear, but we choose here to invoke the maximum distortion energy criterion in our prediction of a rupture in the tank wall.

From the time-temperature histories of the inside and outside surfaces of the wall and the variation of the tensile strength with temperature (see Reference 16), we can construct a time-tensile strength curve for the tank wall. When the tensile strength falls to the predicted failure stress, we can conclude that a rupture in the tank wall will occur.

The maximum state of stress in the wall exists during that time when the tank pressure is 260 psig. As we can see from Figures V-4 and V-5, the pressure transients in the tanks are quite rapid and rise to relief valve setting in a maximum time of less than 20 minutes. During this pressure transient, the thermal transient in the wall proceeds at a far slower rate. The discrepancy in the rise times of these two para- meters is due to the liquid in contact with the wall. Since the boiling heat transfer is capable of transferring the flux from the fire to the liquid at the relatively small temperature difference of 16°K (29°F), the inside surface of the wall never rises to more than 16°K above the saturation temperature at the tank pressure. For a maximum tank pressure of about 260 psig, this corresponds to an inside wall tempera- ture of 335°K (144°F). At this temperature, there is virtually no degradation in the tensile strength of the steel wall. Then so long as the inside surface of the wall is wetted, the high heat fluxes into the liquid mass (which result from nucleate boiling) remove incoming heat from the fire and maintain the wall temperature at an acceptably

low level. So long as the liquid surface is above the horizontal center-
line of the tank and only that part below this centerline is exposed to
fire, the integrity of the tank wall is assured. Should the liquid
level fall to the extent that some of the wall exposed to flame suddenly
has only vapor on the inside surface, then the heat removal mechanism
on the inside will be much mitigated and the wall temperature will begin
to rise.

For the case where the propylene tank is heated from above, the
varied behavior of wetted and unwetted walls is quite pronounced.
It can be seen in Figure V-3 that the temperature of the inside surface
of the wall which is wetted rises to the 355°K, which is characteristic
of a wall in contact with boiling propylene. This is due to the presence
of liquid in the tank above the level of the rain shield as is shown
in Figure V-1. However, for that portion of the tank wall which
has vapor adjacent to it, the temperature at the inside surface rises
to over 900°K in about 20 minutes as shown by the broken line in Figure
V-3. Note that the temperature at the outside surface follows a simi-
lar excursion in time at a slightly higher temperature. At elevated
temperature such as this, the tensile strength of the steel wall does
undergo a drastic reduction. Since the inside surface of the wall is
in radiative equilibrium with the fire and the saturated liquid when
the wall temperature is 1138°K (1588°F), it is appropriate to examine
the tensile strength at this temperature. An examination of the tensile
strength of mild steel at 1138°K shows it to be virtually zero (see
Reference 16). We can conclude that the wall will undergo ductile frac-
ture at some time during its temperature excursion.

From the temperature history of the wall as shown in Figure V-3 and
the temperature dependence of the tensile strength of mild steel,
we can construct a tensile strength history for the inside of the wall
as shown in Figure V-6. The anomalous behavior of the curve in the 0-5
minute area is due to an anomaly in temperature dependence of the tensile
strength. As can be seen from Figure V-3, there is a smooth and continuous
increase in the wall temperature during this period.

There are two curves for the tensile strength of the wall shown
on Figure V-6. They apply to the inside and outside surfaces and are
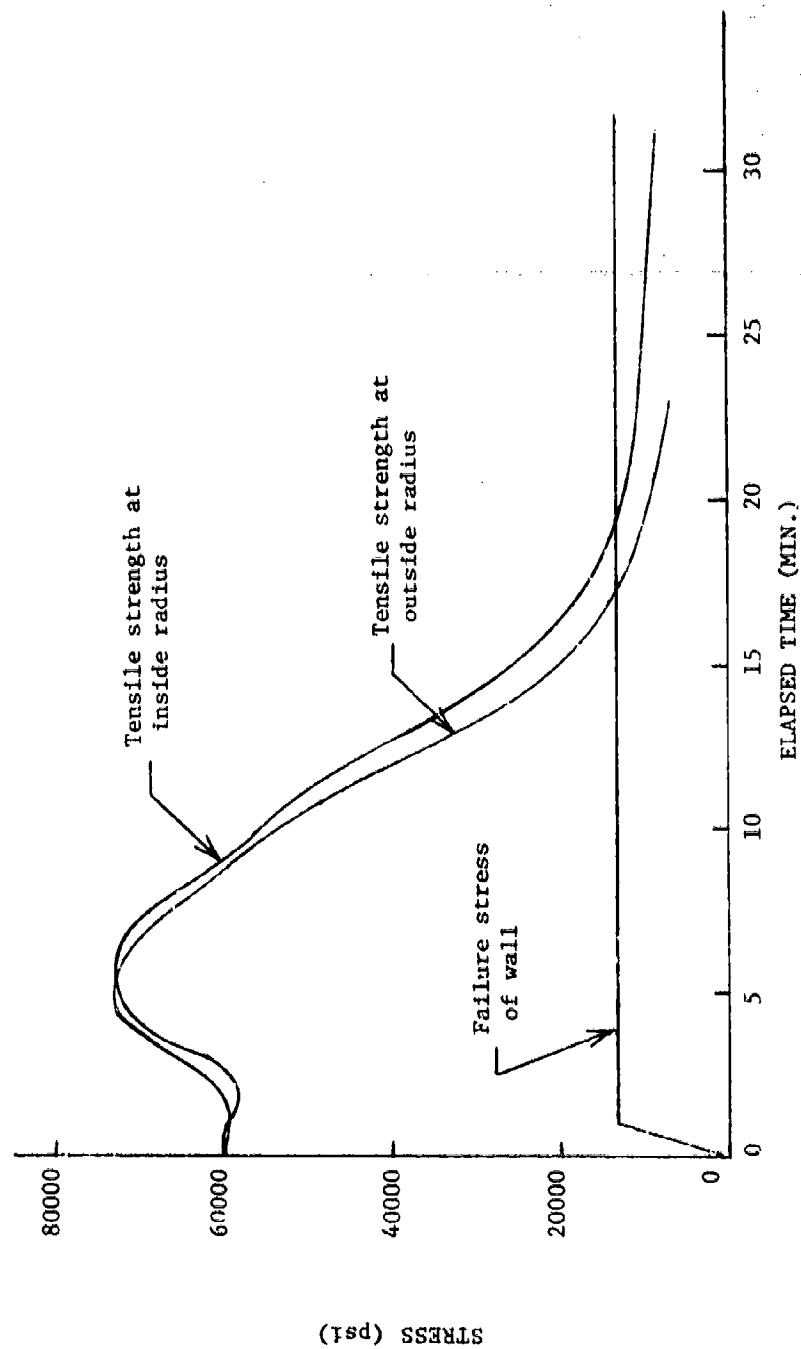shifted in time because the temperature at the outside surface is always

5

Figure V-5 Reduction in tensile strength of steel wall due to
fire exposure on top of tank.

226

slightly higher (see Figure V-3) than at the inside. Because the failure stresses at the inside and outside radii of the wall differ by only 3%, a single curve is shown on Figure V-6. When the tensile strength of the wall at its outside surface falls to 13173 psi at approximately 17 minutes after start of the fire, the tank wall ruptures.

CONCLUSIONS

In this study, an effort has been made to quantify the hazard represented by the flame engulfment of a propylene transport barge. Of interest in this regard are the nature of potential hazards and the time elements involved in avoiding or counteracting them.

The cargo barge studied is modeled after a typical barge built by Bethlehem Steel and used by Union Carbide Corporation. It is designed for the transport of a pressurized, uninsulated cargo. The barge carries three identical cylindrical propylene tanks, each with dimensions of 14.75 feet in diameter by 193.5 feet in length with a 1.5 inch thick steel wall. Each tank is provided with four safety relief valves set at 260 psig and having a total flow area (for the four) of 0.567 ft^2. The tanks are mounted on saddles in the hull, and the hold is closed to the elements by a rain shield between tanks at approximately the level of their horizontal centerlines.

Two scenarios of fire exposure have been analyzed. The first includes exposure of the top of the tank above the rain shield along its entire length; the second considers flame exposure on the underside of the tank below its horizontal centerline over the whole length of the tank. Irradiation by the fire is characterized as a uniform constant heat flux to the exposed area of 30,000 Btu/hr ft^2.

Physical modeling of the propylene contents' reaction to the fire exposure is as follows. In the case where the top of the tank is exposed to fire, the contents of the tank are assumed to remain thermally stratified. Most of the heat input to the tank is manifested by a rise in the tank wall temperature and in the vapor temperature in the ullage space. When the bottom of the tank is exposed to a fire, the contents' reaction is considered to lie between two limiting cases of (1) saturated contents at all times during the heat addition so that the vapor and liquid are in

thermal equilibrium, and (2) thermal stratification in which the vapor generated by boiling at the tank wall rises directly to the vapor space with no recondensation in the liquid bulk.

In the two examples of fire exposure which are considered, the relief valves on the tank are adequate to limit the pressure excursion of the contents. The tank pressure rises only 3 or 4 psi above the relief valve setting as the boiloff is vented to the atmosphere. Maximum temperatures which the tank wall will reach are almost wholly determined by the physical state of propylene on the inside of the wall section which is exposed to a flame. If the propylene is liquid, the temperature excursion of the wall is moderate because nucleate boiling of propylene at the inside wall surface can sustain very large heat fluxes with a relatively small degree of wall superheat. It is typical for a flux of 30,000 Btu/hr ft^2 to be sustained by less than a 30°F elevation of the wall temperature above the propylene saturation temperature at tank pressure. On the other hand, if propylene vapor is adjacent to the wall on the inside, the tank wall temperature will rise until the wall is in radiative equilibrium with the fire and a thermal sink represented by the liquid surface inside the tank.

When there is a fire above the tank, the tank wall will rise to 1160°F within 20 minutes of the start of the fire. At this point, the tensile strength of the wall is sufficiently mitigated by the temperature rise that the tank wall ruptures. In the case of fire exposure of the bottom of the tank, the tank wall does not exceed 290°F as long as the inside of the wall is wetted by propylene. This benign situation will exist until the liquid level in the tank falls (due to contents evaporation) sufficiently to permit vapor to contact a portion of the wall which is exposed to fire on the outside. Once this happens, the tank wall will behave as it did in the case where the fire exposure was from above the tank; namely, the wall temperature will rise rapidly and rupture will ensue. It would take a minimum of 50 minutes for the liquid level in the tank considered here to fall to the half-filled level. This 50 minute estimate of course assumes that the entire underside of the tank below the horizontal centerline and along its entire length is exposed to the flame.

The study discussed here is useful as a qualitative index of the hazard represented by the exposure of a propylene barge to fire. In order to obtain some quantitative information, however, it was necessary to make many assumptions about the physical processes occurring during the fire exposure. Naturally, we chose the severest of conditions which could be imposed within the limits of our modeling and as a result feel that our results are more drastic than would likely occur in a fire. This should not imply, though, that more detailed modeling would not reveal even more dangerous circumstances during the fire exposure of the barge. Unfortunately, the complexities of more rigorous modeling are usually manifested in increasingly costly and complicated solution techniques. We feel that for the expense and effort involved, it would be far simpler to conduct a test program with a scale model of a propylene barge. If properly done, such a program could yield some extremely useful information about the behavior of a propylene tank in a fire. The test data would be particularly revealing as to pressure rise times and failure modes in the event of a rupture. Given the availability of such data, current models could be validated and improved, if necessary.

APPENDIX I

DERIVATION OF GOVERNING EQUATIONS

1. Heating from Above

We consider here the situation in which the fire is located above the propylene tank and consequently heats the tank wall above the vapor space. In modeling this condition, we will assume that there is a uniform flux over the exposed top surface of the tank for the 150° arc between rain shields (see Figure 1). Since these tanks are typically filled to an 8% ullage volume, part of the exposed section of the tank will be in contact with vapor and part with liquid. Once evaporation of the liquid has taken place to the point that the liquid level falls below the rain shield, the vapor alone will be in contact with the tank surface which is exposed to the fire.

Our assumption of a uniform flux into the tank wall will dictate that the vapor between liquid and tank top will tend to stratify. Any nonuniform heat addition to the tank top will result in density gradients on the inside and an induced fluid motion. Similarly, the curvature of the tank surface itself will give rise to buoyancy effects when the vapor near the meniscus is heated, thereby tending to rise along the inside of the wall. We have chosen to ignore any augmentation of heat transfer to the vapor as a result of these effects. The reason for this is that in the absence of this fluid motion, the thermal resistance on the inside of the wall will be higher and the wall will come to equilibrium at a temperature closer to that of the flame. This higher wall temperature will result in a greater reduction in the tensile strength of the wall, with a correspondingly conservative estimate of the hazard posed by heating in this manner.

The vapor and liquid are considered as separate thermodynamic systems with components of the total heat transfer to the system allocated to each. To the liquid, heat is transferred via radiation from the inside surface of the wall to the surface of the liquid which has a temperature equal to the saturation temperature of heat to the liquid which wets the tank wall above the rain shield. The vapor which is assumed transparent to the thermal radiation emitted by the inside surface of the wall is heated solely by conduction from the wall.

230

To quantify the heat transfer to the liquid, we first define an angle ϕ (see Figure 1) to be the arc between the vertical centerline of the tank and the edge of the meniscus. If L_t is the tank length and T_{wi} the inside wall temperature, then heat transfer to the liquid due to radiation from the inside of the tank wall may be expressed as

$$\dot{Q}_{rad} = 2 r_t L_t \sin\phi \, \sigma \left(T_{wi}^4 - T_{sat}^4 \right) \tag{1}$$

where we have assumed the emissivity-view factor product to be unity. The saturation temperature at the tank pressure, T_{sat}, is used as the low temperature sink because of the two-phase equilibrium condition which exists at the surface.

There is an additional contribution to heat transfer to the liquid while the liquid level is above the rain shield. For ϕ angles less then 75° (1.309 radian), nucleate boiling will take place where the liquid contacts the wall. Heat transfer to the liquid may be expressed as

$$\dot{Q}_b = 2 r_t L_t \left(1.309 - \phi \right) q \tag{2}$$

where q is the heat flux (W/cm^2) which may be calculated from a boiling heat transfer correlation. This is expressed as[5,6]

$$q = \frac{\lambda \mu_\ell}{B} \left(3.25 \times 10^5 \right) \left[\frac{c_{p_\ell} \Delta T}{\lambda} \left(\frac{T_r}{P r_\ell} \right)^{1.18} \right]^{2.89} \tag{3}$$

These two contributions then make up the total heat transfer to the liquid, i.e.,

$$\dot{Q}_\ell = \dot{Q}_{rad} + \dot{Q}_b \tag{4}$$

From the conductance of the wall, K_w, and the temperature difference across the wall, $T_{wo} - T_{wi}$, we can calculate the total heat coming through the wall from the fire. Since we have already formulated the heat transfer to the liquid contents, that to the vapor is simply the difference, i.e.,

$$\dot{Q}_v = K_w A_w \left(T_{wo} - T_{wi} \right) - \dot{Q}_\ell \tag{5}$$

231

where A_w is the tank area which is exposed to the fire. In this case, the $150°$ arc between rain shields is considered to be exposed to a uniform flux of $9.46 \, W/cm^2$ (30,000 Btu/hr ft^2). The exact mechanism by which this heat is transferred to the vapor is difficult to evaluate. The heat will obviously be conducted into the vapor in contact with the wall. Distribution of this heat in the vapor will likely be enhanced by some bulk fluid motion in the vapor, but the analysis of that motion is difficult to do. It will suffice here merely to let the vapor absorb that fraction of the incoming heat which we cannot allocate directly to the liquid.

When considering the energy equations for the tank contents, we write separate equations for the liquid and vapor with the associated heat transfer of each. The interaction between the two systems is taken care of by mass crossing from one to the other as the liquid evaporates. The energy equation for the vapor may be written as[*]

$$\frac{\partial}{\partial t} \left(m_v u_v \right) = \dot{Q}_v + \left(\dot{m} h \right)_{in} - \left(\dot{m} h \right)_{out} \tag{6}$$

which is the equation for an open system with no work transfers crossing the system boundary. The mass leaving the system is that through the relief valves, and the enthalpy is simply the average vapor enthalpy, i.e.,

$$\left(\dot{m} h \right)_{out} = \dot{m}_{out} \, h_v \tag{7}$$

For the mass flux into the system, we note the evaporation taking place at the surface of the liquid where

$$\left(\dot{m} h \right)_{in} = \dot{m}_{in} \, h_g \tag{8}$$

The enthalpy of the mass entering the system is that of saturated vapor at the system pressure, h_g. We can now expand (6) in terms of the intensive thermodynamic properties of the system to yield

$$\left(\dot{m}_{in} - \dot{m}_{out} \right)\left(h_v - P v_v \right) + m_v \left[\left(\frac{\partial h_v}{\partial T} \right)_P \dot{T} + \left(\frac{\partial h_v}{\partial P} \right)_T \dot{P} - v_v \dot{P} \right.$$
$$\left. - P \left(\frac{\partial v_v}{\partial T} \right)_P \dot{T} - P \left(\frac{\partial v_v}{\partial P} \right)_T \dot{P} \right] = \dot{Q}_v + \dot{m}_{in} \, h_g - \dot{m}_{out} \, h_v \tag{9}$$

[*]Refer to "Thermodynamics," J. H. Keenan, p. 33, MIT Press, 1970.

232

where the overdotted symbols designate time derivatives of temperature and pressure, $\dot{T}$ and $\dot{P}$ respectively. For the enthalpy derivatives, note that

$$\left(\frac{\partial h_v}{\partial T}\right)_P \equiv c_P$$

and for the superheated vapor,

$$\left(\frac{\partial h}{\partial P}\right)_T \approx 0$$

If substitutions are made in (9) and terms are rearranged we will arrive at the following expression.

$$\left[\dot{m}_{in}\left(h_v - Pv_v - h_g\right) + \dot{m}_{out} Pv_v\right] + m_v\left[c_P - P\left(\frac{\partial v_v}{\partial T}\right)_P\right]\dot{T} \qquad (9a)$$

$$- m_v\left[v_v + P\left(\frac{\partial v_v}{\partial P}\right)_T\right]\dot{P} = \dot{Q}_v$$

The energy equation for the liquid yields

$$\frac{\partial}{\partial t}\left(m_\ell u_\ell\right) = \dot{Q}_b + \dot{Q}_{rad} - \dot{m}_{in} h_g \qquad (10)$$

in which the last term on the right is the same as that expressed in (9). Because the dominant heat transfer to the liquid occurs only at its surface and because this heat addition will result largely in evaporation and not in conduction into the liquid mass, we will hold the bulk liquid temperature constant in time. This would correspond to a specific energy corresponding to that of saturated liquid at 60°F. Hence, when we expand the energy equation for the liquid, we get

$$\dot{m}_\ell u_\ell = \dot{Q}_{rad} + \dot{Q}_b - \dot{m}_{in} h_g$$

which may be solved directly for the evaporation rate of the liquid.

$$\dot{m}_{in} = -\dot{m}_\ell = \frac{\dot{Q}_{rad} + \dot{Q}_b}{h_g - u_\ell} \qquad (11)$$

233

Flow through the relief valve may be approximated by that of one dimensional isentropic flow of a perfect gas. The frictional effects which give rise to irreversibilities in nozzles are small for short lengths with the result that the nozzle efficiencies are 98% to 99% of ideal. We will assume that choke-flow conditions will obtain in the relief valve for whatever fraction of full-flow area is dictated by system pressure. The relief valves on a typical propylene tank are set at 18.7 atm. (260 psig) and achieve full flow area at 10% over set pressure (20.5 atm. or 286 psig). Assuming that the valve opens with a first order lag, the flow area of the four valves is given by

$$A_f = A_o \left[1 - \exp\left(\frac{-\Delta P}{0.44}\right) \right]$$ (12)

where ΔP is pressure difference across the valve in atmospheres, A_o is the total flow area of the four valves in their full open position, 527 cm^2 (0.567 ft^2), and the term 0.44 in the argument of the exponential is one quarter of the ΔP required to open the valve fully. When the pressure has risen to 10% over set pressure ($\Delta P = 1.77$ atm), the exponential will decay to 2%. At this point, 98% of the full flow area will be operable.

To relate the flow which may be achieved at choke conditions at each flow area, we can invoke the choke flow condition (see Reference 8), i.e.,

$$\frac{\dot{m}_{out}}{A_f} = \left[\frac{\gamma}{R} \left(\frac{2}{\gamma+1} \right)^{\frac{\gamma+1}{\gamma-1}} \right]^{\frac{1}{2}} \frac{P}{\sqrt{T}}$$ (13)

where $\dot{m}_{out}$, P, and T are the same as in (9), γ is the ratio of specific heats of the vapor, and R is the gas constant for propylene.

All that remains now is that we write the energy equation for the tank wall. Because of the low circumferential thermal conductance in the wall relative to the radial path, we will consider the tank wall above the rain shield to be thermally isolated from its continuation

234

below the rain shield. Accordingly, for the 150° arc of wall, we can write

$$\frac{C_w}{2}\left(\dot{T}_{wi} + \dot{T}_{wo}\right) = \sigma\left(T_{flame}^4 - T_{wo}^4\right) - K_w\left(T_{wo} - T_{wi}\right) \tag{14}$$

where $\dot{T}_{wo}$ and $\dot{T}_{wi}$ are the time rates of change of the surface temperatures at the outside and inside of the wall, respectively. The terms C_w and K_w are in order the heat capacitance and thermal conductance W/cm^2-K) for a unit area of the 150° segment of the wall. Note that we view the wall above the rain shield as having no circumferential thermal gradients, merely a radial gradient between the two surfaces. (This assertion is amended in the DISCUSSION.) Furthermore, this radial thermal gradient is assumed to be linear as is evidenced by the expressions in (14) for the rate of change of internal energy of the wall and for the heat conducted through it.

We now have succeeded in obtaining equations which quantify the thermal behavior of the tank during heating from above the rain shield. The unknowns are the time derivatives of vapor temperature and pressure, mass of vapor in the ullage space, and the time derivatives of the inside and outside surface temperatures of the wall -- five unknowns. To solve for them, we have two equations: (9a) and (14).

One additional equation is available if we assume that the mean vapor temperature T is the average of the saturation temperature at the liquid surface and the surface temperature of the inside of the wall. Stating this more explicitly, we get

$$\dot{T} = \frac{1}{2}\dot{T}_{wi} + \frac{1}{2}\dot{T}_{sat}$$

or

$$\dot{T} = \frac{1}{2}\dot{T}_{wi} + \frac{1}{2}\left(\frac{dT}{dP}\right)_{sat}\dot{P} \tag{15}$$

Another equation is available to us and is related to volume conservation within the tank. If the tank volume is constant in time, then

$$V_t = m_v v_v + m_\ell v_\ell = constant \tag{16}$$

which simply states that the sum of volumes occupied by both the liquid and vapor is constrained to a fixed total. Recalling that we are assuming the bulk liquid properties to be constant in time, we may differentiate (16) to obtain

$$m_v\left[\left(\frac{\partial v_v}{\partial T}\right)_P \dot{T} + \left(\frac{\partial v_v}{\partial P}\right)_T \dot{P}\right] + \dot{m}_v v_v + \dot{m}_\ell v_\ell = 0 \tag{16a}$$

Now define a vapor volume fraction, β, such that

$$m_v = \frac{\beta V_t}{v_v} \tag{17}$$

If we recognize that $\dot{m}_v = \dot{m}_{in} - \dot{m}_{out}$, and substitute (17) into (16a), we get

$$\dot{m}_{in}(v_v - v_\ell) - \dot{m}_{out} v_v + \frac{\beta V_t}{v_v}\left(\frac{\partial v_v}{\partial T}\right)_P \dot{T} + \frac{\beta V_t}{v_v}\left(\frac{\partial v_v}{\partial P}\right)_T \dot{P} = 0 \tag{16b}$$

We have now substituted the vapor volume fraction, β, for the vapor mass, m_v. We need an expression for the time derivative of β and can obtain it by differentiating (17) to get

$$\dot{m}_v = \frac{V_t}{v_v^2}\left\{v_v \dot{\beta} - \beta\left[\left(\frac{\partial v_v}{\partial T}\right)_P \dot{T} + \left(\frac{\partial v_v}{\partial P}\right)_T \dot{P}\right]\right\} \tag{17a}$$

Recalling again that $\dot{m}_v = \dot{m}_{in} - \dot{m}_{out}$, we may substitute in (17a) and rearrange to get

$$\left(\dot{m}_{in} - \dot{m}_{out} \right)\frac{V_v}{V_t} = \dot{\beta} - \frac{1}{V_t}\left[\frac{\beta V_t}{V_v}\left(\frac{\partial v_v}{\partial T} \right)_P \dot{T} + \frac{\beta V_t}{V_v}\left(\frac{\partial v_v}{\partial P} \right)_T \dot{P} \right] \quad (18)$$

Our system of governing equations, viz., (9a), (14), (15), (16b) and (18) may now be expressed as

$$\begin{aligned}
F_6 + F_7 \dot{T} - F_8 \dot{P} &= \dot{Q}_v \\
\dot{T}_{wi} + \dot{T}_{wo} &= F_1 \\
\dot{T} &= 1/2\ \dot{T}_{wi} + F_2 \dot{P} \\
F_3 + F_4 \dot{T} + F_5 \dot{P} &= 0 \\
F_9 &= \dot{\beta} - \frac{1}{V_t}\ [F_4 \dot{T} + F_5 \dot{P}]
\end{aligned} \qquad (19)$$

Where the terms F_1 through F_9 are defined in Table 1. Note that the term F_1 indicates our choice of a constant radiative heat flux to the exterior of the tank of 9.46 W/cm^2 (30,000 $Btu/hr\text{-}ft^2$).

The result of this effort to here is that we now have five equations which are linear in the time derivatives of our five unknowns. These may be solved algebraically to yield a system of simultaneous differential equations. By rearranging the equations in (19), we obtain the equations in (20),

$$\begin{aligned}
\dot{P} &= \frac{F_4\ (F_6 - \dot{Q}_v) - F_3 F_7}{F_4 F_8 + F_5 F_7} \\
\dot{T} &= \frac{\dot{Q}_v + F_8 \dot{P} - F_6}{F_7} \\
\dot{\beta} &= F_9 + \frac{1}{V_t}\ (F_4 \dot{T} + F_5 \dot{P}) \\
\dot{T}_{wi} &= 2(\dot{T} - F_2 \dot{P}) \\
\dot{T}_{wo} &= F_1 - \dot{T}_{wi}
\end{aligned} \qquad (20)$$

TABLE 1

Definition of terms in the equations on Page App. I-8a

$$F_1 = \frac{2}{C_w}\left[9.46 \, {}^W\!/_{cm^2} - K_w (T_{wo} - T_{wi})\right] \qquad K/sec$$

$$F_2 = \frac{1}{2}\left(\frac{dT}{dP}\right)_{sat} \qquad K/atm$$

$$F_3 = \dot{m}_{in}(v_v - v_\ell) - \dot{m}_{out}\, v_v \qquad cm^3/sec$$

$$F_4 = \frac{\beta V_t}{v_v}\left(\frac{\partial v_v}{\partial T}\right)_P \qquad cm^3/K$$

$$F_5 = \frac{\beta V_t}{v_v}\left(\frac{\partial v_v}{\partial P}\right)_T \qquad cm^3/atm$$

$$F_6 = \dot{m}_{in}(h_v - Pv_v - h_g) + \dot{m}_{out}\, Pv_v \qquad J/sec$$

$$F_7 = \frac{\beta V_t}{v_v}\left[C_P - P\left(\frac{\partial v_v}{\partial T}\right)_P\right] \qquad J/K$$

$$F_8 = \frac{\beta V_t}{v_v}\left[v_v + P\left(\frac{\partial v_v}{\partial P}\right)_T\right] \qquad cm^3$$

$$F_9 = \left(\dot{m}_{in} - \dot{m}_{out}\right)\frac{v_v}{V_t} \qquad sec^{-1}$$

This system of simultaneous differential equations in the single independent variable, time, may be numerically integrated via any one of the standard programs which handle "state equation" formulations for systems.

2. Heating from Below

A possible occurrence in the collision of a propylene barge with another vessel would be that a fire might develop in the hold of the barge itself. In such a situation, the propylene cargo tank would be heated from below so that at least initially the wall being heated would be in contact with liquid on the inside. An evaluation of the hazard posed by the response of the propylene to this heat addition proceeds very much as it did when it was assumed that the top of the tank was exposed to fire. Equations need to be developed which will relate the pressure rise to the relief valve capacity and to the structural integrity of the tank wall. To bound the problem, we will consider two extremes in the behavior of the propylene contents during external heating of the tank:

1. All of the vapor generated at the wall-liquid interface is transported directly to the vapor space above the liquid with none of it being recondensed in the liquid. The liquid has a passive role, save as a source of liquid which the incoming heat will vaporize.

2. The vapor generated at the wall is all condensed in the liquid so that the contents remain saturated throughout the heat addition.

239

Stratified Contents

We have defined our problem here such that the incoming heat from the fire generates vapor at the interface between wall and liquid and the vapor then collects atop the liquid and contributes to a pressure rise in the tank.

The heat transfer regime which exists at the wall may be deduced from an examination of the boiling curve for propylene (see Figure 3). As was previously assumed, the fire is characterized by an external black body radiation source at 900°C. If we assume that there is a step change in the temperature of this source at time zero, then the thermal diffusivity of the wall will mitigate this so that at the inside surface there is a gradually increasing heat flux to the liquid. This corresponds to following the boiling curve to the right, from lower wall superheat to higher, into the pool boiling regime, and to increasingly greater wall superheat until a steady state wall flux of about 30,000 Btu/hr ft^2 is achieved. From the curve, it can be seen that this corresponds roughly to a wall superheat of 30°F. This ΔT at the wall will be maintained throughout the heat addition until the tank empties (through the relief valves) or ruptures.

The pool boiling of propylene may be quantified by a relationship of the following form (see References 5,6):

$$Re = (3.25 \times 10^5) \left[\frac{c_{p_\ell} \Delta T}{\lambda} \left(\frac{T_c}{Pr_\ell} \right)^{1.18} \right]^{2.89} \tag{21}$$

where Re is a bubble Reynolds number defined to be

$$Re = \frac{q B}{\lambda \mu_\ell} \tag{22}$$

The terms in (22) are as follows:

q = heat flux to liquid(W/cm^2)

$B = \left[\dfrac{\sigma_\ell}{g(\rho_\ell - \rho_v)} \right]^{\frac{1}{2}}$ = Laplace reference length(cm)

λ = latent heat(J/g)

μ_ℓ = liquid viscosity(g/cm-sec)

240

In the expression for the Laplace reference length, g is the gravitational acceleration, σ_ℓ the surface tension of the liquid, ρ_ℓ and ρ_v the saturated liquid and saturated vapor densities respectively.

In the analysis here it will be assumed that the lower half of the tank wall, along its entire length, will be exposed to the fire. The product of the area wetted by the liquid in the tank and the heat flux from the boiling correlation above will be the net heat transfer to the tank's contents.

To relate the state of the propylene contents to the heat addition, we first write the energy equation for the contents, i.e.,

$$\frac{\partial}{\partial t}\left(m_\ell u_\ell + m_v u_v\right) = \dot{Q}_b - \dot{m}_{out}\, h_v \tag{23}$$

where the enthalpy of the superheated vapor above the liquid mass is associated with mass flow out of the tank. The left side of (23) may be expanded to yield

$$\dot{m}_\ell u_\ell + \dot{m}_v u_v + m_v \frac{\partial u_v}{\partial t} = \dot{Q}_b - \dot{m}_{out}\, h_v \tag{24}$$

where the absence of a time derivative of the liquid specific energy indicates that we are holding it constant throughout the heat addition.

Conservation of mass within the control volume requires that

$$\frac{\partial}{\partial t}\left(m_\ell + m_v\right) = -\dot{m}_{out} \tag{25}$$

or

$$\dot{m}_\ell = -\dot{m}_{out} - \dot{m}_v \tag{26}$$

If (26) is substituted into (24) and terms are collected, the result is:

$$\dot{m}_v\left(u_v - u_\ell\right) + m_v \frac{\partial u_v}{\partial t} = \dot{Q}_b + \dot{m}_{out}\left(u_\ell - h_v\right) \tag{27}$$

Noting that $h_v = u_v + Pv_v$, we may expand (27) to yeild

$$\dot{m}_v\left(h_v - Pv_v - u_\ell\right) + m_v\left(\frac{\partial h_v}{\partial t} - P\frac{\partial v_v}{\partial t} - v_v\frac{\partial P}{\partial t}\right) = \dot{Q}_b + \dot{m}_{out}\left(u_\ell - h_v\right) \tag{28}$$

241

From the chain rule we may write

$$\frac{\partial h_v}{\partial t} = \left(\frac{\partial h_v}{\partial T}\right)_P \dot{T} + \left(\frac{\partial h_v}{\partial P}\right)_T \dot{P} \tag{29}$$

where

$$\left(\frac{\partial h_v}{\partial T}\right)_P = c_p \tag{30}$$

and for the superheated vapor,

$$\left(\frac{\partial h_v}{\partial P}\right)_T \approx 0 \tag{31}$$

Substituting these expressions into (28) and collecting terms will give us

$$\dot{m}_v \left(h_v - P v_v - u_\ell\right) + \dot{T}\left[m_v c_p - m_v P \left(\frac{\partial v_v}{\partial T}\right)_P\right] - \dot{P}\left[m_v P \left(\frac{\partial v_v}{\partial P}\right)_T + m_v v_v\right]$$

$$= \dot{Q}_b + \dot{m}_{out}\left(u_\ell - h_v\right) \tag{32}$$

We have an additional equation available from a requirement that the volume of the tank be constant throughout the heat addition.

$$V_t = m_v v_v + m_\ell v_\ell = constant \tag{33}$$

Holding the specific energy of the liquid constant and differentiating (33) with respect to time, we get

$$\dot{m}_v = \left(\frac{-m_v}{v_v - v_\ell}\right)\left[\left(\frac{\partial v_v}{\partial T}\right)_P \dot{T} + \left(\frac{\partial v_v}{\partial P}\right)_T \dot{P}\right] + \dot{m}_{out}\left(\frac{v_\ell}{v_v - v_\ell}\right) \tag{34}$$

For flow through the relief valves, we will assume that choke flow conditions exist, irrespective of the flow available. The valves begin to open when the set pressure is reached and allow full flow at 10% over set pressure. If we model the dynamics of the valve as a first order lag with a "time constant" of one quarter of the 10% over pressure, then the area response of the valve is given by

$$A_f = A_o \left[1 - exp \frac{-(P - P_{set})}{0.44}\right] \tag{35}$$

242

In equation (35), A_o is the full flow area of the four relief valves, and A_f is the flow area at pressure P. For P less than P_{set}, the flow area is zero.

Combining the area-pressure relationship with the expression for maximum flow at choke conditions, we get

$$\dot{m}_{out} = A_o \left[1 - \exp \frac{-(P-P_{set})}{0.44} \right] \left[\frac{\gamma}{R} \left(\frac{2}{\gamma+1} \right)^{\frac{\gamma+1}{\gamma-1}} \right]^{\frac{1}{2}} \frac{P}{\sqrt{T}}$$ (36)

where P is the tank pressure in atmospheres and T is the mean vapor temperature, i.e., $T = 0.5 (T_{wi} + T_{sat})$. T_{wi} is the temperature of the inside surface of the wall and T_{sat} is the saturation temperature at the tank pressure.

To evaluate the energy interactions of the wall, we will consider a unit area. If the thermal gradient in the wall is linear, the energy equation for the wall yields

$$\frac{d}{dt} \left[C_w \frac{T_{wi} + T_{wo}}{2} \right] = q - K_w (T_{wo} - T_{wi})$$ (37)

where C_w and K_w are respectively the thermal mass (J/K-cm^2) and thermal conductance (W/cm^2-K) of the steel wall, both assumed constant.

If we now state explicitly what we have been assuming all along, we define the mean vapor temperature to be the average of the inside surface temperature of the wall and the saturation temperature at tank pressure; namely,

or when differentiated with respect to time,

$$\dot{T} = \frac{1}{2} \dot{T}_{wi} + \frac{1}{2} \left(\frac{dT}{dP} \right)_{sat} \dot{P}$$ (38)

A look at equations 32, 34, 37, and 38 will reveal four equations which are linear in the time derivatives of T, P, T_{wi}, T_{wo}, and $\dot{m}_v$. Equation (36) may be used to define $\dot{m}_{out}$. We need an additional equation in order to have a complete system of equations for the five unknowns. This additional relationship may be derived from equations (21) and (22) which may be combined to yield

243

$$q = \frac{\lambda \mu_\ell}{B}(3.25 \times 10^5)\left[\frac{c_{p_\ell} \Delta T}{\lambda}\left(\frac{T_r}{P_\ell}\right)^{1.18}\right]^{2.89} \tag{39}$$

If we arbitrarily select a wall superheat of 1.0°K and plot the boiling flux as a function of saturation temperature, T_{sat}, we will obtain the curve in Figure I-1 for propylene. A curve for a superheat of 16°K (28.8°F) is also shown. In essence, then, we may express the boiling flux as

$$q = \xi(T_{sat})\, \Delta T^{2.89} \tag{40}$$

where $\xi(T_{sat})$ is the curve for a superheat of 1.0°K. Assuming that we can obtain an expression for $\xi(T_{sat})$, we can equate the heat flux leaving the wall on the inside to that passing through the wall via the linear thermal gradient, i.e.,

$$K_w(T_{wo} - T_{wi}) = q$$

or

$$K_w(T_{wo} - T_{wi}) = \xi(T_{sat})(T_{wi} - T_{sat})^{2.89} \tag{41}$$

We may now differentiate (41) with respect to time and get (after some manipulation)

$$K_w(T_{wo} - T_{wi}) = (T_{wi} - T_{sat})^{1.89}\left(\frac{dT}{dP}\right)_{sat}\dot{P}\left[(T_{wi} - T_{sat})\frac{d\xi}{dT_{sat}} - 2.89\,\xi(T_{sat})\right]$$
$$+ 2.89\,\xi(T_{sat})(T_{wi} - T_{sat})^{1.89}\dot{T}_{wi} \tag{42}$$

Collecting terms in equations 32, 34, 37, 38, and 42, and using the expression in (36) for the mass flow out through the relief valves will yield the following system of equations

$$\dot{m}_v H_1 + \dot{T} H_2 + \dot{P} H_3 = H_4 \tag{32a}$$

$$\dot{m}_v = H_5 \dot{T} + H_6 \dot{P} + H_7 \tag{34a}$$

$$\dot{T}_{wi} + \dot{T}_{wo} = H_8 \tag{37a}$$

$$\dot{T} = \tfrac{1}{2}\dot{T}_{wi} + H_9 \dot{P} \tag{38a}$$

$$\dot{T}_{wo} - \dot{T}_{wi} = H_{10}\dot{P} + H_{11}\dot{T}_{wi} \tag{42a}$$
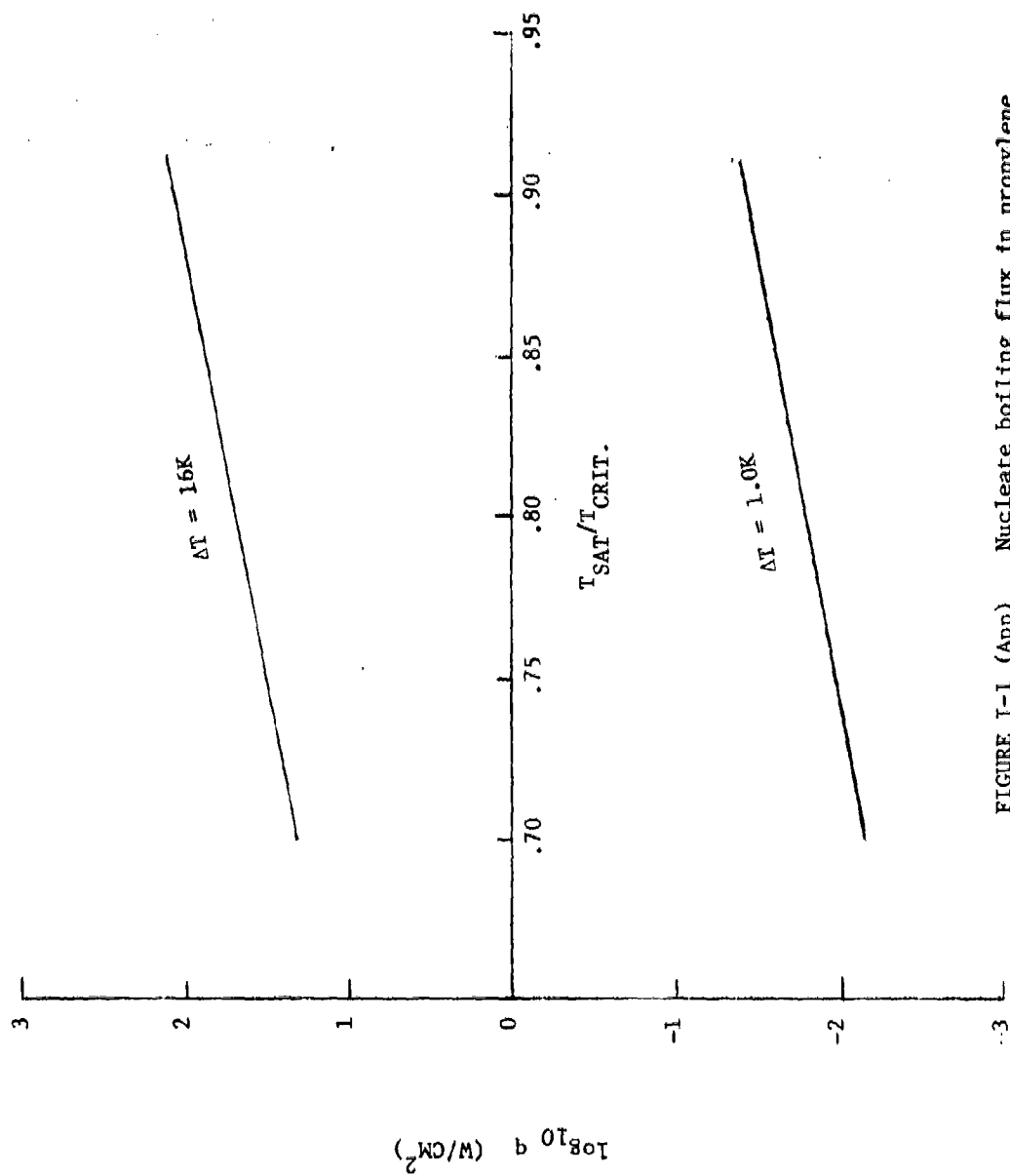
244

FIGURE I-1 (App)   Nucleate boiling flux in propylene
as a function of saturation temperature

245

The groups of collected terms H_1 through H_{10} are defined in Table 2. Some algebraic manipulation of these five equations will result in explicit expressions for the time derivative of each of the five variables in terms of the variables themselves and not of their derivatives. For example,

$$\dot{P} = \frac{H_4 - H_1 H_7 \cdot \dfrac{H_8(H_1 H_5 + H_2)}{2(H_{11} + 2)}}{H_1(H_6 + H_5 H_9) + H_2 H_9 + H_3 - \dfrac{H_{10}(H_1 H_5 + H_2)}{2(H_{11} + 2)}} \tag{43}$$

$$\dot{T} = \frac{H_8}{2(H_{11}+2)} + \left[H_9 - \frac{H_{10}}{2(H_{11}+2)} \right] \dot{P}$$

$$\dot{m}_v = \left[H_6 - \frac{H_5 H_{10}}{2(H_{11}+2)} + H_5 H_9 \right] \dot{P} + \frac{H_5 H_8}{2(H_{11}+2)} + H_7$$

$$\dot{T}_{wi} = \frac{H_8 - H_{10} \dot{P}}{H_{11} + 2}$$

$$\dot{T}_{wo} = H_8 - \dot{T}_{wi}$$

246

TABLE 2

DEFINITION OF TERMS IN EQUATION (43)

$$H_1 = h_v - Pv_v - u_\ell \qquad\qquad J/g$$

$$H_2 = m_v \left[c_P - P\left(\frac{\partial v_v}{\partial T}\right)_P \right] \qquad\qquad J/K$$

$$H_3 = -m_v \left[P\left(\frac{\partial v_v}{\partial P}\right)_T + v_v \right] \qquad\qquad cm^3$$

$$H_4 = \dot{Q}_b + \dot{m}_{out}(u_\ell - h_v) \qquad\qquad J/sec$$

$$H_5 = -\left(\frac{m_v}{v_v - v_\ell}\right)\left(\frac{\partial v_v}{\partial T}\right)_P \qquad\qquad g/K$$

$$H_6 = -\left(\frac{m_v}{v_v - v_\ell}\right)\left(\frac{\partial v_v}{\partial P}\right)_T \qquad\qquad g/atm$$

$$H_7 = \dot{m}_{out}\left(\frac{v_\ell}{v_v - v_\ell}\right) \qquad\qquad g/sec$$

$$H_8 = \frac{2}{C_w}\left[9.46 \, W/cm^2 - K_w(T_{wo} - T_{wi}) \right] \qquad\qquad K/sec$$

$$H_9 = \frac{1}{2}\left(\frac{dT}{dP}\right)_{sat} \qquad\qquad K/atm$$

$$H_{10} = \left(T_{wi} - T_{sat}\right)^{1.89}\left(\frac{dT}{dP}\right)_{sat}\left[\left(T_{wi} - T_{sat}\right)\frac{d\xi}{dT_{sat}} - 2.89 \, \xi\right]\left(\frac{1}{K_w}\right) \qquad K/atm$$

$$H_{11} = 2.89 \, \xi \left(T_{wi} - T_{sat}\right)^{1.89}\left(\frac{1}{K_w}\right) \qquad\qquad dimensionless$$

In such a form, the five equations for each of the time derivatives may be integrated in time via one of the standard computer programs for solution of a state variable formulation of dynamic systems.

One additional change might be added. If we want to nondimensionalize the problem formulation so that the solution would not involve extensive parameters of the tank and contents, it would be helpful to define a vapor volume fraction, β, such that

$$\beta = \frac{m_v v_v}{V_t} \tag{44}$$

Taking the time derivative of each side will yield

$$\dot{\beta} = \frac{1}{V_t} \left\{ \dot{m}_v v_v + \frac{\beta V_t}{v_v} \left[\left(\frac{\partial v_v}{\partial T} \right)_P \dot{T} + \left(\frac{\partial v_v}{\partial P} \right)_T \dot{P} \right] \right\} \tag{45}$$

which may be included in the governing equations of the system.

Contents Saturated During Heat Addition

As we alluded to previously, the other limiting case for pressure rise in the tank when exposed to a fire on the bottom is that of saturated contents during the heat addition. This restriction will result in a slower pressure rise (than if the liquid and vapor are stratified) because the large liquid mass may be used as sink for much of the heat coming in through the wall. Hence, the heat addition will manifest itself largely as an increase in the liquid enthalpy (and temperature) rather than as the driving force for vaporization alone.

The rate of heat addition may be expressed by the boiling correlation as was done in the previous section. Similar relationships will prevail among the inside and outside wall surface temperatures and the flux to the tank contents. Only the energy allocation will be different in this case where we require that the contents be saturated.

248

We may express the energy equation for the propylene contents of the tank as

$$\frac{\partial}{\partial t}\left(m_f u_f + m_g u_g\right) = \dot{Q}_b - \dot{m}_{out} h_g \tag{46}$$

where the subscripts f and g refer to the saturated liquid and vapor respectively. This expression may be expanded to yield

$$\dot{m}_f\left(h_f - Pv_f\right) + m_f\left(\dot{h}_f - P\dot{v}_f - v_f\dot{P}\right) + m_g\left(\dot{h}_g - P\dot{v}_g - v_g\dot{P}\right)$$

$$+ \dot{m}_g\left(h_g - Pv_g\right) = \dot{Q}_b - \dot{m}_{out} h_g \tag{47}$$

Note that the intensitive properties of the liquid now have nonzero time derivative (time derivatives are indicated by an overdot), indicating that we are no longer holding liquid properties constant during the heat addition.

Because we are requiring the propylene contents remain in a saturated state, the intensive properties are now functions of pressure alone since the saturation temperature may not be varied independently of the pressure. So, expanding (47) will give us

$$\dot{m}_f\left(h_f - Pv_f\right) + m_f\left(\frac{dh_f}{dP}\dot{P} - P\frac{dv_f}{dP}\dot{P} - v_f\dot{P}\right) + \dot{m}_g\left(h_g - Pv_g\right)$$

$$+ m_g\left(\frac{dh_g}{dP}\dot{P} - P\frac{dv_g}{dP}\dot{P} - v_g\dot{P}\right) = \dot{Q}_b - \dot{m}_{out} h_g \tag{48}$$

249

Conservation of mass within the control volume may be expressed as

$$\frac{\partial}{\partial t}\left(m_f + m_g\right) = -\dot{m}_{out}$$

or

$$\dot{m}_f = -\dot{m}_{out} - \dot{m}_g \qquad (49)$$

Substituting (49) into (48) and collecting terms will give us

$$\dot{m}_g\left[h_g - h_f - P(v_g - v_f)\right] + \dot{P}\left[m_f\left(\frac{dh_f}{dP} - P\frac{dv_f}{dP} - v_f\right) + m_g\left(\frac{dh_g}{dP} - P\frac{dv_g}{dP} - v_g\right)\right]$$

$$= \dot{Q}_b - \dot{m}_{out}\left(h_g - h_f + Pv_f\right) \qquad (50)$$

Since the tank volume is constant during heat addition, we have

$$V_t = m_f v_f + m_g v_g$$

which when differentiated with respect to time yields

$$\dot{m}_g\left(v_g - v_f\right) + \dot{P}\left(m_f\frac{dv_f}{dP} + m_g\frac{dv_g}{dP}\right) = \dot{m}_{out}\, v_f \qquad (51)$$

Again define a vapor volume fraction, β, such that

$$m_g = \frac{\beta V_t}{v_g} \qquad (52)$$

250

The corresponding liquid fraction is given by

$$m_f = \frac{(1-\beta)V_t}{v_f} \tag{53}$$

Differentiating (52) with respect to time will give us

$$\dot{m}_g = \frac{\dot{\beta}V_t - \frac{\beta V_t}{v_g}\frac{dv_g}{dP}\dot{P}}{v_g} \tag{54}$$

Substituting the expressions in (52), (53), and (54) into (50) results in

$$\dot{\beta}\frac{V_t}{v_g}\left[h_g - h_f - P(v_g - v_f)\right] - \dot{P}\frac{\beta V_t}{v_g^2}\frac{dv_g}{dP}\left[h_g - h_f - P(v_g - v_f)\right] \tag{55}$$
$$+ \dot{P}\left[\frac{V_t(1-\beta)}{v_f}\left(\frac{dh_f}{dP} - P\frac{dv_f}{dP} - v_f\right) + \frac{\beta V_t}{v_g}\left(\frac{dh_g}{dP} - P\frac{dv_g}{dP} - v_g\right)\right]$$
$$= \dot{Q}_b - \dot{m}_{out}\left(h_g - h_f + Pv_f\right)$$

Now substitute the expression in (54) into (51) and collect terms.

$$\dot{\beta}\frac{V_t}{v_g}(v_g - v_t) + \dot{P}\left[\frac{V_t(1-\beta)}{v_f}\frac{dv_f}{dP} + \frac{\beta V_t}{v_g}\left(\frac{dv_g}{dP}\right) - \frac{\beta V_t}{v_g^2}\frac{dv_g}{dP}(v_g - v_f)\right]$$

$$\tag{56}$$

$$= \dot{m}_{out}v_f$$

Equations (55) and (56) together with formulation of heat transfer at the wall, previously expressed in ( ) and ( ), and the mass flow through the relief valve, equation ( ) will yield the following system of equations:

$$\dot{\beta} G_1 + \dot{P} G_2 = G_3 \tag{55a}$$

$$\dot{\beta} G_4 + \dot{P} G_5 = G_6 \tag{56a}$$

$$\dot{T}_{wo} + \dot{T}_{wi} = H_8 \tag{37a}$$

$$\dot{T}_{wo} - \dot{T}_{wi} = H_{10} \dot{P} + H_{11} \dot{T}_{wi} \tag{42a}$$

The expressions for G_1 through G_6 may be found in Table 3; those for H_8, H_{10} and H_{11} were previously defined in Table 2. Solving for the time derivative of each variable explicitly, we get

$$\dot{P} = \frac{G_6 - \dfrac{G_4 G_3}{G_1}}{G_5 - \dfrac{G_4 G_2}{G_1}}$$

$$\dot{\beta} = \frac{G_3 - G_2 \dot{P}}{G_1} \tag{57}$$

$$\dot{T}_{wi} = \frac{H_8 - H_{10} \dot{P}}{H_{11} + 2}$$

$$\dot{T}_{wo} = H_{10} \dot{P} + (H_{11} + 1) \dot{T}_{wi}$$

This set of equations may be integrated in time by numerical procedure simply by solving them in order: $\dot{P}$, $\dot{\beta}$, $\dot{T}_{wi}$, $\dot{T}_{wo}$.

TABLE 3

DEFINITION OF TERMS FOUND IN EQUATIONS (55a) AND (56a)

$$G_1 = \frac{V_t}{v_g} \left[h_g - h_f - P(v_g - v_f) \right] \qquad\qquad J$$

$$G_2 = \frac{V_t(1-\beta)}{v_f} \left(\frac{dh_f}{dP} - P\frac{dv_f}{dP} - v_f \right) + \frac{\beta V_t}{v_g} \left(\frac{dh_g}{dP} - P\frac{dv_g}{dP} - v_g \right)$$

$$- \frac{\beta V_t}{v_g^2} \frac{dv_g}{dP} \left[h_g - h_f - P(v_g - v_f) \right] \qquad\qquad J/atm$$

$$G_3 = \dot{Q}_b - \dot{m}_{out} \left(h_g - h_f + Pv_f \right) \qquad\qquad J/sec$$

$$G_4 = \frac{V_t}{v_g} \left(v_g - v_f \right) \qquad\qquad cm^3$$

$$G_5 = \frac{V_t(1-\beta)}{v_f} \left(\frac{dv_f}{dP} \right) + \frac{\beta V_t}{v_g} \left(\frac{dv_g}{dP} \right) - \frac{\beta V_t}{v_g^2} \frac{dv_g}{dP} \left(v_g - v_f \right) \qquad\qquad cm^3/atm$$

$$G_6 = \dot{m}_{out} \, v_f \qquad\qquad cm^3/sec$$

APPENDIX J

THERMODYNAMIC AND TRANSPORT PROPERTIES OF PROPYLENE

The problem formulation for the pressure rise in a propylene barge exposed to fire has been done in a format which will allow numerical solution. This format is simply the "state equation" formulation where the pertinent system variables and their dynamic behavior are expressed as a series of simultaneous first order differential equations. Time is the independent variable. So, given a set of initial conditions, the differential equations may be integrated in time, using any one of the standard computer programs available.

In performing the numerical integrations, it is time-consuming if the program is configured so that it must search tabular data for the desired property values of propylene. It is far easier to use analytical correlations so that the physical property may always be evaluated from a single equation. This latter route was chosen here and required a search of the literature for the properties and for whatever correlations (equations of state, etc.) were available.

Thermodynamic properties of propylene are available in several sources (References 9, 10, 11, and 12). To facilitate use in the computer program we selected the specific heat relationship from Reference 10. An equation of state for the superheated vapor was obtained by truncating the $P - v - T$ relationship of Reference 10 to a van der Waals equation which can be inverted to yield the specific volume as a function of temperature and pressure.

In this manner the volume may be calculated directly rather than from an iteration which would be necessary with the longer equation in Reference 1. This latter equation is more accurate, of course, but the truncated version is quite satisfactory here.

Enthalpies of the superheated vapor are calculated from an integration along the appropriate isobar from the saturation temperature

254

to the superheated temperature. More specifically, the integration yields

$$h_v(T,P) = h_g(T_{sat},P) + \int_{T_{sat}}^{T} c_p(x)\,dx \tag{58}$$

where x is a dummy variable. Using this method, and the specific heat equation from Reference 10, we can calculate enthalpies of the super-heated vapor to within 6% of the tabular values in Reference 9.

Specific volumes and enthalpies along the saturation curve are correlated by Chebyshev polynomial curve fits of the data in Reference 10. Equations for the viscosity and thermal conductivity of the vapor are presented in References 13 and 14, respectively. Properties of the liquid are taken from Reference 12 and include the surface tension viscosity, thermal conductivity, and specific heat. The graphical data for these liquid properties are correlated by parabolic functions of temperature over the range 0°C to 80°C which is adequate for purposes here.

APPENDIX K

STRUCTURAL ANALYSIS OF TANK WALL

The previous discussions have alluded to two different conditions which would exist as far as heat transfer through the tank wall is concerned. In one case the side of the wall opposite that exposed to the fire is in contact with propylene vapor; the second case has the wall wetted by liquid propylene. Heat is transferred away from the wall strictly by conduction (since we have eliminated the presence of any fluid movement in the analysis) in the former case and by nucleate boiling heat transfer in the latter. Since the flux impinging on the outside of the wall due to the fire is the same in both cases, 9.46 W/cm^2 (30,000 $Btu/hr-ft^2$) the wall temperature is wholly determined by the heat transfer potential on the inside surface. For a low potential, as in the case where there is vapor adjacent to the wall, the wall will assume a temperature nearly equal to that of the flame (900°C). On the other hand, since boiling is a very efficient means of transferring heat over small temperature differences, the wall temperature will be much akin to the saturation temperature of the propylene at the tank pressure.

Structural integrity of the tank wall will depend directly on two parameters: the mechanical stress in the wall and the tensile strength of the wall material. These in turn may be directly related to the tank pressure and wall temperature respectively. Unfortunately, establishing this relationship for a particular tank and fire condition is a formidable analytical problem. It would require a detailed temperature distribution in the wall, together with an elastic-plastic structural analysis of the vessel, taking into account all the vagaries of geometry, local penetrations, etc. That is quite beyond the intentions of this study and, therefore, a far simpler approach is taken.

If we consider only the gross geometric characteristics of the tank, then it can be modeled as a thick-walled elastic cylinder subjected to internal pressure. The mechanical stresses which result

256

from this have three orthogonal components, radial, tangential, and axial. Using the standard formulae for stresses in a thick-walled cylinder (Reference 15) we can calculate the magnitude of each component as a function of the internal pressure in the tank. For an inside radius r_i and an outside radius r_o, the stresses at a radius r are given by

$$\sigma_r = \frac{(P - P_{atm}) r_i^2}{r_o^2 - r_i^2} \left(1 - \frac{r_o^2}{r^2}\right)$$

$$\sigma_\theta = \frac{(P - P_{atm}) r_i^2}{r_o^2 - r_i^2} \left(1 + \frac{r_o^2}{r^2}\right) \qquad (59)$$

$$\sigma_z = \frac{(P - P_{atm}) r_i^2}{r_o^2 - r_i^2}$$

where $P - P_{atm}$ is the differential pressure acting on the tank wall (260 psi). Since there are no shear stresses associated with these three components, they are identically the principal stresses at a point.

To relate these principal stresses to a rupture of the tank wall, we will need to consider a failure criterion. Many theories have been developed for the failure of ductile materials under static loading. Usually, the failure mode of greatest concern is that of yielding, where the plastic deformation of the material reaches some arbitrary limit. Another failure, that of greatest interest to us, is that of fracture, where there is separation of the material. In the case of yielding, the "maximum distortion energy theory"[15] has been found to predict ductile yielding under combined loading with greater accuracy than any other recognized theory. For a given state of triaxial stress, this theory predicts that yielding will occur when the following equation is satisfied:

$$S_y = \frac{\sqrt{2}}{2} \left[(\sigma_r - \sigma_\theta)^2 + (\sigma_\theta - \sigma_z)^2 + (\sigma_z - \sigma_r)^2 \right]^{\frac{1}{2}} \qquad (60)$$

The term S_y here is the yield strength of the material as determined from the uniaxial tension test.

Another classic failure criterion is the "maximum shear stress"

257

theory which, applied to the thick-walled cylinder, states that yield
will occur when the maximum shear stress in the material is equal to
that determined from the uniaxial tension test. In the case of the
thick-walled cylinder, this translates to the following,

$$\frac{S_y}{2} = \frac{\sigma_\theta - \sigma_r}{2} \tag{61}$$

where S_y is again the yield strength of the material as determined
from the uniaxial tension test. This criterion tends to be less ac-
curate than the maximum distortion energy theory with the error being
on the conservative side.

The prediction of fracture with these two theories may be done
simply by substituting the tensile strength of the material in place
of the yield strength above. Unfortunately this fracture criterion
is not as accurate as the yield criterion since both theories are
based on elastic behavior of the material. There is an arbitrarily
small (typically 2%) plastic strain associated with the definition
of ductile yield in a material, so the deviation from elastic behavior
is minimal. However, ductile fracture occurs after a considerable
amount of plastic strain has occurred, so the validity of elastic
theories is understandably mitigated in predicting this. Barring a
detailed elastic-plastic analysis of the tank wall, though, these
simple fracture criteria are the best methods available to us in pre-
dicting a rupture of the tank wall.

NOMENCLATURE

A_f	Flow area in relief valves (partially open), cm^2
A_o	maximum flow area through relief valves, cm^2
A_w	tank wall area exposed to fire, cm^2
B	Laplace reference length (defined in equation 23), cm
c_p	specific heat of vapor, J/g-K
c_{p_ℓ}	specific heat of liquid, J/g-K
C_w	thermal mass of tank wall, $J/K-cm^2$
g	gravitational acceleration, 980.665 cm/sec^2
h	specific enthalpy, J/g
K_w	radial thermal conductance of tank wall, W/cm^2-K
L_t	tank length, cm
m	mass (propylene), g
P	tank contents pressure, atm (absolute)
P_{set}	relief valve setting, atm
P_{atm}	atmospheric pressure (1.0 atm)
$\dot{q}$	heat flux from fire, 9.46 W/cm^2 (30,000 Btu/hr-ft^2)
$\dot{Q}_b$	boiling heat transfer, Watts
$\dot{Q}_\ell$	total heat transfer to liquid, Watts
$\dot{Q}_{rad}$	radiative heat transfer to liquid, Watts
$\dot{Q}_v$	total heat transfer to vapor, Watts
r_t	tank inside radius, cm
R	gas constant for propylene, 0.1977 J/g-K
R_e	bubble Reynolds number (defined in equation 23), dimensionless
S_u	tensile strength of tank wall, psi
S_y	yield strength of tank wall, psi
T	mean vapor temperature, K
T_{crit}	critical temperature of propylene, 364.92K
T_r	reduced temperature (T_{sat}/T_{crit}), dimensionless
T_{sat}	saturation temperature of propylene, K
T_{wi}	temperature of inside surface of wall, K
T_{wo}	temperature of outside surface of wall, K
ΔT	($T_{wi} - T_{sat}$) in equation 4, 22, 40
u	specific internal energy, J/g
V_t	tank volume, cm^3

259

Subscripts

f   saturated liquid

g   saturated vapor

ℓ subcooled liquid

v   superheated vapor

Greek Letters

β fraction of tank volume occupied by vapor, dimensionless

γ ratio of specific heats of propylene, dimensionless

λ latent heat of propylene, J/g

μ absolute viscosity, g/cm-sec

ξ function defined in equation 40

σ Stefan - Boltzmann constant, 5.669×10^{-12} W/cm^2-K^4

σ_ℓ surface tension of propylene, dynes/cm

σ_r radial stress in tank wall, psi

σ_Θ tangential stress in tank wall, psi

σ_z axial stress in tank wall, psi

ϕ angle between vertical centerline and edge of meniscus (see Figure 1), radians

REFERENCES

1. Gierre, Alb... C., "An Analysis of the Temperature-Time Data Obtained From a Steel Cylinder Engulfed by an Aircraft Fuel Fire", NAVWEPS Rpt. 8292 (29 Feb. 64), Defense Documentation Center, Alexandria, Va.

2. Gordon, Wm. and McMillan, R.D., "A Study of the Temperature Distribution Within Aircraft-Fuel Fires", NAVWEPS Report 8277 (1 Aug. 63), Defense Documentation Center, Alexandria, Va.

3. Wright, R. D., Clements, L. D. and Colver, C. P., "Nucleate and Film Pool Boiling of Ethane-Ethylene Mixtures", AIChE J. 17, 3, 626 (1971).

4. Sciance, C. T., Colver, C. D. and Sliepcevich, C. M., "Film Boiling Measurements and Correlation for Liquefied Hydrocarbon Gases", Chem. Eng. Prog. Sym. Ser., Vol. 63, No. 77, P. 115 (1967).

5. Sciance, C. T., Colver, C. P. and Sliepcevich, C. M., "Pool Boiling of Methane Between Atmospheric Pressure and the Critical Pressure", Adv. Cryogenic Eng., Vol. 12, p. 395.

6. Rohsenow, W. M., "A Method of Correlating Heat-Transfer Data for Surface Boiling of Liquids", Trans. ASME 74, 969 (1952).

7. Rohsenow, W. M. and Griffith, P., "Correlation of Maximum heat-flux Data for Boiling of Saturated Liquids", Chem. Eng. Prog. Sym. Ser., Vol. 52, No. 18, p. 47 (1956).

8. Shapiro, A. H., The Dynamics and Thermodynamics of Compressible Fluid Flow, Ronald Press, New York (1953), P. 85.

9. Canjar, L. N. and Manning, F. S., Thermodynamic Properties and Reduced Correlations for Gases, Chapter 10: Thermodynamic Properties of Propylene, Gulf Publishing Co., Houston (1967).

10. Das, T. R. and Kuloor, N. R., "Thermodynamic Properties of Hydrocarbons: Part VII-Propylene", Ind. J. Tech 5, 81 (1967).

11. Kobe, K. A. and Long, E. G., "Thermochemistry for the Petrochemical Industry, Part III - Monoolefinic Hydrocarbons, C_2, C_4", Petro, Refiner 28, 3, 125 (1949).

12. Gallant, R. W., "Physical Properties of Hydrocarbons", Vol. 44, No. 8, p. 127 (August 1965), Vol. 45, No. 12, p. 113 (Dec. 1966).

13. Flynn, L. W. and Thodos, G., "The Viscosity of Hydrocarbon Gases at Normal Pressures", J. Chem. Eng. Data 6, 3, 457 (1961).

14. Misic, D. and Thodos, G., "The Thermal Conductivity of Hydrocarbon Gases at Normal Pressures", AIChE J. 7, 2, 264 (1961).

15. Juvinall, R. C., Stress, Strain and Strength, McGraw-Hill (1967), p. 118.

16. ASME Handbook, Metals Engineering Design, 2nd Edition, McGraw-Hill (1965), p. 21

CHAPTER VI

ON THE COOLING BY WATER DELUGING OF A
PROPYLENE BARGE TANK EXPOSED TO FIRE

OBJECTIVE

The objective of the analysis presented here is to calculate the
rate at which water has to be applied to a propylene tank (on a barge)
exposed to a fire to cool the tank wall and thereby minimize the proba-
bility of explosion of the tank.

INTRODUCTION

When a barge carrying liquid propylene gets involved in an accident
with another ship or barge carrying a flammable cargo, there is a likeli-
hood of fire. The propylene tank, in such a case, may be exposed to the
fire. The consequences of such an exposure are the increase in the pres-
sure within the propylene tank and a loss of strength of the steel shell
due to excessive heating. The combination of these two may eventually
lead to tank rupture and explosion. The problem of heating of the tank
exposed to fire has been analyzed previously, and an analytical means
exists now to predict, with some degree of confidence, the time at which
the rupture of the tank is likely to occur.

Because of the potential hazards to life involved in the explosion
of a steel tank, the United States Coast Guard is interested in preventing
the possibility of such barge tank ruptures caused by exposure to external
fires. In the case of a propylene barge tank, the analysis indicates that
the primary cause of tank rupture is due to the loss of strength of steel
at high temperatures that result from fire exposure. Therefore, the
simplest way of reducing explosion possibility is to reduce the metal
tank wall temperature to a reasonably low level (say 300°F). This can
be achieved by deluging the tank wall surface with water so that the
wall temperature is never greater than the boiling temperature of water
or slightly above it. The analysis presented in this memorandum
indicates a method to calculate both the temperature history of the
wall when cooled by water and the minimum amount of water needed to
cool the tank wall to a low temperature level.

262

Before considering the method of calculation shown below, it is important to delineate its limitations. The method of calculation shown has assumed that the entire tank surface is deluged with water. Considering the physical situation of a fire around the barge and water jet being squirted on the tanks from fire boats stationed anywhere from 300 to 1000 feet from the barge, it is hard to imagine that the entire tank surface will be covered by a water film. Some of the water droplets in the water jet may never reach the tank surface at all but may be carried up and away by the fire convection plume. Also, when a jet of water strikes a curved surface (such as that of the cylindrical propylene tanks), a large part of water may not spread uniformly on the wall surface but may be deflected. Finally, if the fire is hidden under thick black smoke (as in gasoline fires), it may not even be possible to locate the tank on the barge properly to apply the water.

Of course, a proper water deluge system can be installed on the tanks themselves (to cover the exposed tank surface with water film). This will involve the provision of additional equipment such as pumps, power supply, and activation circuitry, etc. Many barges do not have any active machinery on board. In addition, in an accident, it is very likely that (due to the very exposed nature of the plumbing), the deluge system will be affected and may become ineffective, defeating the very purpose of their installation. Therefore, there seems to be no guaranteed method by which the entire exposed surface of the tank can be protected by water against overheating by fire.

Finally, there are some questions about making proper decisions at the time of the accident. For example, if the tank has been exposed to the fire for 10 minutes, when the predicted rupture time is 20 minutes, should a fire boat venture close to the disabled barge to squirt water onto the tank surface to keep it cool? There is no precise and definitive answer simply because we do not know the area of the tank that can be cooled, whether there are any weak spots (structurally) on the tank or whether quenching of hot steel by a cold jet of water may not induce some structural stresses and even fractures that may propagate, leading to tank failure. If, indeed, the water squirting results in sudden quenching and consequent failure, the decision to squirt water may accelerate the failure time. In fact, this may even jeopardize the safety of the crew of the fire boat(s).

263

It is therefore emphasized that the method indicated below is based on certain idealistic assumptions simply with a view to obtaining an order of magnitude estimate for the rate at which water has to be applied to the tank to keep it from further heating. This number will be useful in comparing with the capacity available on conventional fire boats so that one can have on hand an information base before making a decision to commit a fire boat to combat the tank heating problem. The method indicated should, therefore, be viewed as an aid toward decision making. The procedure indicated does not provide a means of estimating what might happen if, in fact, a fire boat is committed to fighting the fire and cooling the tank.

In Section 1, a simple method is developed to calculate the rate of application of water so that the mass loss of water by evaporation is made up by the incoming water. Boiling heat transfer data for water is utilized. In Section 2, the cooling transient of the wall metal is calculated to obtain the time within which the metal surface cools to a given temperature level.

Tank and Other Data Used in the Calculations

Tank diameter (outer)	= 15 feet
Length of cylindrical portion of tank	= 193.5 feet
Shell wall thickness	= 1.5 inches
Angular arc of the shell above the rain shield	= 150°
K = Thermal conductivity of steel	= 9.4 Btu/hr ft °R
C_p = Specific heat of steel	= 0.12 Btu/lbm °R
ρ = Density of steel	= 8.03 gm/cm^3
$\dot{q}''_{fire}$ = Heat flux from fire	= 30,000 B/hr ft^2
λ = Heat of vaporization of water = 1000 B/lbm	= 8340 B/gallon
T_{water} = Water temperature in the jet	= 60°F

THEORETICAL DEVELOPMENT

Section 1: Calculation of the Rate of Water Application Needed for Tank Wall Cooling

Consider the situation $\underline{10 \text{ minutes}}^{*}$ after the exposure to a fire. a fire. It is seen from Figure V-3 (on the analysis of heating, release, and rupture of a pressurized propylene tank in a fire) that after 10 minutes of heating from above (which is the more serious situation), the tank wall temperatures are

Outer surface temperature (vapor phase wall) = 700°K

Inner surface temperature = 660°K

Hence, the initial temperature difference between the wall surface temperature and the water boiling temperature (T_{sat}) is

$$\Delta T = (T_{wall} - T_{sat}) = 700 - 373 = 327°K$$

Referring to the boiling heat flux vs. ΔT curve for water (see Ref. 1, page 370), it is seen that at this temperature difference film boiling results.

The heat flux at this temperature difference is

$$\dot{q}''_{\text{at } \Delta T=327°K} = 0.27 \, \dot{q}''_{max} = 1.03 \times 10^5 \text{ B/hr ft}^2$$

where $\dot{q}''_{max}$ = Peak heat flux (Ref. 2) $\simeq 3.8 \times 10^5$ Btu/hr ft^2

Assuming that the evaporation rate of water from this boiling heat flux has to be supplied, we have

$\dot{v}''$ = Volume of water evaporated per unit area per unit time

$$\dot{v}'' = \frac{\dot{q}''}{\lambda} = \frac{1.03 \times 10^5}{8340} = 12.30 \text{ gallons/hr ft}^2 = 0.21 \text{ gallons/min ft}^2$$

Total surface area of the tank above the rain shield = $\pi \times 15 \times 193.5$
$$x \left(\frac{150}{360}\right) \simeq 3800 \text{ ft}^2$$

Hence minimum rate of water application is = $3800 \times 0.21 = 780$ gpm

It is, however, seen that due to the cooling of the wall surface, the temperature difference ΔT decreases, and in the transitional boiling

---

*Ten minutes is chosen only to illustrate the methodology. Any other time could also have been chosen. However, the final conclusion seems to be independent of this time chosen.

region, the heat flux to water and therefore the evaporation rate, increases. Hence, in order to obtain a conservative estimate of the water requirement, we make the following assumptions:

- Water applied should be able to absorb the peak heat flux without leaving dry spots on the wall.

- Water should also absorb the heat flux from the fire.

Hence, $\dot{q}''_{design} = \dot{q}''_{peak} + \dot{q}''_{fire}$

$$= (3.8 \times 10^5 + 0.3 \times 10^5) \text{ Btu/hr ft}^2$$

$$= 4.1 \times 10^5 \text{ B/hr ft}^2$$

Where the value for the peak heat flux is taken from Reference 2. Hence the design water application rate:

$$\dot{V}''_{design} = 4.1 \times 10^5/(8340 \times 60) = 0.82 \text{ gal/ft}^2 \text{ min.}$$

Hence, $\dot{V}$ = Total design application rate of water = 3800 x 0.82

$$= 3115 \text{ gal/min}$$

It is indicated that in the above number, some conservativeness is already built in. This is because we have estimated the heat flux levels based on peak heat flux. During the continuous cooling of the tank wall, the heat flux level first increases, reaches the peak value, and then decreases. The average flux level is probably about 30% of the peak value.

It is seen, therefore, that even the smallest of the fire boats in service (with a capacity of 4000 gpm) should be sufficient to cool the tank walls provided an even distribution of water is achieved. Hence, the problem of explosion prevention by water deluging using fire boats is not limited by the fire boat capacity but rather by the uncertainty in the even distribution of water on the tank.

Section 2: Calculation of Temperature of the Tank Shell During the Cooling Process

Figure VI-1 shows the boiling curve for water. It is seen that when water at ambient temperature is applied on the tank wall surface at 700°K ($\Delta T = 327°K$) boiling takes place in the film boiling regime. Because of the rapid heat extraction, the metal surface cools down resulting in a decrease in ΔT. In the film boiling regime, a decrease in ΔT results in a decrease in the heat flux until minimum heat flux in film boiling regime results. Any decrease in temperature results in an increase of heat flux leading to an unstable condition (transition regime) until peak heat flux is attained.
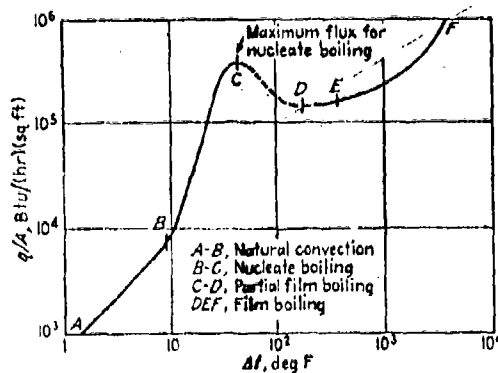
FIGURE VI -1

Heat Flux Vs. Temperature Difference for Water Boiling
(at 212 °F) Over an Electrically Heated Wire

Using the above physical picture of the cooling, a thermal model has been worked out to obtain the temperature history of the metal wall. It is shown in Appendix N that the heat content of the vapor in the vapor phase, when compared to the heat content of the shell wall (in contact with the vapor), is negligible. In other words, the steel wall contains most of the heat that has to be extracted, and therefore the cooling rate is primarily determined by steel thermal properties. With this in mind, we impose an adiabatic boundary condition for the inner face of the shell wall.

267

Model:

Figure VI-2 shows schematically the basic features of the model.

Initially, the temperature across the thickness is assumed to be uniform* at T_1. As soon as the water is applied to the outside surface, film boiling ensues with the surface temperature dropping, and a temperature distribution establishes itself.

We denote the thermal penetration depth by S_1. In order to calculate the cooling process, we assume a temperature distribution within the steel and equate the rate of change in the heat content of the system to the heat flux out. Using this relationship, we solve for the surface temperature and internal temperature changes. It is, however, to be kept in mind that in film boiling region, the heat flux from the wall depends on the temperature difference between the wall and the water saturation temperature. These are illustrated in the following steps. Appendix B indicates the relation-ship between the heat flux and temperature difference.

Model:

We assume the following temperature profile within the steel:

$$\frac{T - T_s}{T_1 - T_s} = \left[\frac{x}{s_1} - \frac{x^2}{4s_1^2} \right] \quad \text{for } x \leq s_2 \tag{1a}$$
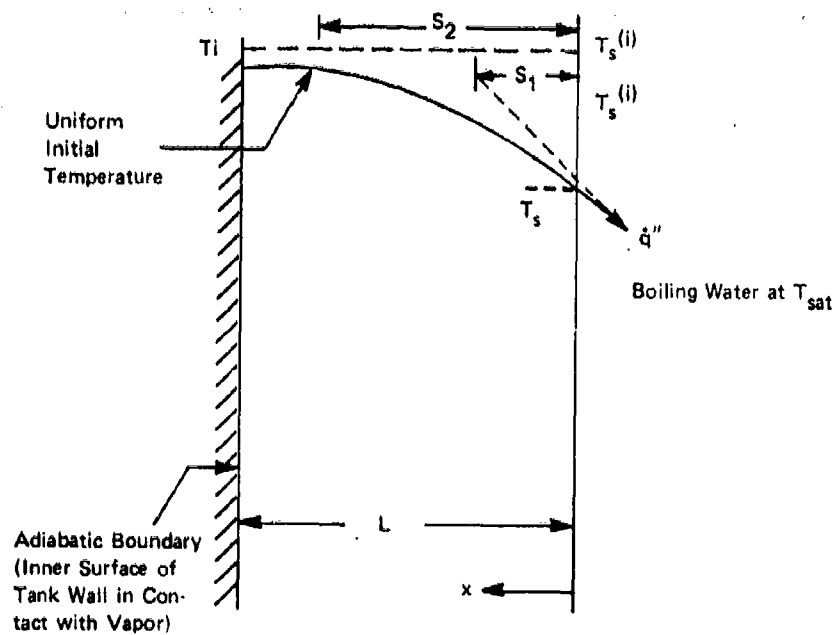
Arthur D. Little Inc.

FIGURE VI-2   SCHEMATIC DIAGRAM ILLUSTRATING THE COOLING
OF TANK WALL DUE TO BOILING OF WATER ON THE SURFACE

269

where T_i = the initial uniform temperature

$T_s \equiv T_s(t)$ = the time dependent surface temperature

x = thickness direction distance measured from the surface

s_1 = thermal penetration depth (see Figure 2) which is a function of time

$$T = T_i \text{ for } x \geq s_2 \tag{1b}$$

where s_2 = distance at which the the temperature is T_i and also the slope of the temperature profile is zero.

It can be shown easily (from slope and temperature conditions) that for the profile chosen in equation 1a,

$$s_2 = 2s_1 \tag{2}$$

The heat content of the steel above the boiling temperature of water is given by

$$Q''(t) = \rho c \int_{x=0}^{L} (T - T_{sat}) \, dx \tag{3}$$

Also, we have from the heat flux condition at the surface

$$\dot{q}''(t) = k \left(\frac{\partial T}{\partial x} \right)_{x=0} \tag{4}$$

Energy Balance

$$-\frac{dQ''}{dt} = \dot{q}'' \tag{5}$$

$\dot{q}''(t)$ is related to $(T_s - T_{sat})$ by the boiling heat transfer correlations given in Appendix Q. Using equations 1 through 6, together with the correlations in Appendix B, we can obtain a timewise description of the surface and internal temperature. The calculation procedure is shown in Appendix O, and the results are given in Table O-1.

---

*Actually, there will be a 40°K temperature drop from outside to inside. However, from the point of view of conservative calculations, we assume uniform initial temperature distribution with the temperature equal to the initial outside temperature.

DISCUSSION

The calculation results indicate that the surface of the steel plate cools down fairly rapidly -- in about 2 seconds from an initial 700°K to 473°K -- and probably reaches the peak heat flux temperature (T_{peak} = 393°K) very shortly thereafter. At the end of the film boiling period, the thermal penetration depth is still less than half the thickness of the plate (i.e., $s_1 < \frac{1}{2}L$) indicating that the back-face temperature has not been affected by the surface cooling. Because of this, there is close to 300°K temperature difference between the outer and inner surfaces of the steel shell. This considerable difference over a relatively small thickness (1.5") may result in thermal stresses. It is not at all clear what these stresses would do in addition to the hoop and axial stresses existing in the shell wall (due to the pressure loading). Clearly, the structure will be loaded more than when it is uncooled. Because of the additional stresses resulting due to thermal effects, it is quite likely that squirting water on a heated tank may accelerate the failure time. At the present time, there is no data to indicate whether water stream has a bene-ficial effect or a detrimental effect on a heated pressurized tank.

The calculations in Appendix O also indicate that for a complete cool down to peak heat flux temperature (20°C above boiling point of water), the time duration is relatively short (of the order of a minute), but this duration is long compared to the cool down time in the film boiling regime. In effect, most of the cool down duration will be in the nucleate boiling regime.

CONCLUSIONS

A simple method has been worked out to calculate the water require-ment for cooling down a typical propylene barge tank exposed to an external fire over the top of the tank. It is observed that the water requirement can be adequately met by conventional medium sized fire boats. However, it is pointed out that most of the difficulty lies in ensuring a uniform distribution of water on the tank surface.

The analysis is extended to determine the rate of cooling of the tank wall and the temperature gradients set up. It is seen that the surface temperature rapidly achieves the peak heat flux temperature

271

for nucleate boiling. The time for further cooling of the entire metal is relatively long (about one minute) compared to the surface cool down time. Because of the considerable temperature gradient that results due to the high heat transfer rate (due to the boiling process) thermal stresses may result in the shell wall. These stresses, together with the pressure load stresses, may, in fact, accelerate tank failure. Therefore, it is felt that only experiments can give a clear indication of the effectiveness of water deluging a hot pressurized tank, from the standpoint of safety.

APPENDIX L

COMPARISON OF THE HEAT CONTENT OF STEEL
AND THE HEAT CONTENT OF PROPYLENE VAPOR

Heat content of steel per unit area above 60°F when the mean temperature is 700°K (800°F)

$$= L \rho C_p (T - T_{standard}) = \left(\frac{1.5}{12}\right) \times (8.3 \times 62.4) \times 0.12 \times (800 - 60)$$

$$= 5748 \text{ Btu/ft}^2$$

Mass of vapor in the ullage volume after 10 minutes of exposure to fire on the top is calculated below.

Ullage volume fraction	$= \beta = 0.13$
Pressure	$= p = 275.0$ psia
Saturation temperature of propylene at 275 psia	$= T_{sat} = 115°F$
Mean vapor temperature	$= \dfrac{115 + 800}{2} \approx 460°F$
Mean heat capacity (C_n) of propylene vapor over the temperature range 0 to 600°F	$= 0.45$ Btu/lbm F
Density of vapor at 275 psia and 460°F	$= (1.4 \times .0764)\left(\dfrac{275}{14.7}\right)\left(\dfrac{520}{920}\right) = 1.13 \text{ lbm/ft}^3$
Volume of tank over unit axial length (inner volume)	$= \pi/4 \times (14.75)^2 = 170.87 \text{ ft}^3/\text{ft}$
Volume of vapor per unit axial length	$= 170.87 \times 0.13 = 22.21 \text{ ft}^3/\text{ft}$

Hence, heat content of vapor per unit axial length = volume of gas per unit length x density x C_p x temperature excess over standard temperature = $22.21 \times 1.13 \times 0.45 \times (460 - 60) = 4518.14$ Btu/ft

If this heat is distributed over the surface of the fire exposed steel surface per unit axial length, then the heat content of vapor per unit steel area is given by

$$\text{heat of vapor/ft}^2 \text{ of steel} = \frac{4518.14}{\pi \times 15 \left(\dfrac{150}{360}\right)} = 230 \text{ Btu/ft}^2$$

When this is compared to the heat content of steel per unit surface area, we have

273

$$\frac{\text{Vapor heat per unit steel area}}{\text{Steel heat per unit steel area}} = \frac{230}{5748} = 0.04 = 4\%$$

The above calculation indicates that the heat content of vapor can be neglected compared to the heat content of steel; that is, in "cooling of wall" calculations, the boundary condition for the inner wall surface can be considered to be adiabatic without too much error.

APPENDIX M

BOILING HEAT TRANSFER CORRELATIONS FOR POOL BOILING OF WATER

The correlations given below are derived from the data published in the Handbook of Heat Transfer[3] (pages 13-28, figure 24a) and from ref. 2.

Peak heat flux $\dot{q}''_{peak} = 3.8 \times 10^5$ Btu/hr ft^2

$$= 1.2 \times 10^6 \text{ W/m}^2$$

Let $\Delta T = T_{wall} - T_{sat}$

$$(\Delta T)_{peak} = (T_{wall} - T_{sat}) = 20°K \text{ for water}$$
at peak
heat flux

Let $\theta = \dfrac{\Delta T}{(\Delta T)_{peak}}$ (M-1a)

and $q = \dfrac{\dot{q}''}{\dot{q}''_{peak}}$ (M-1b)

Nucleate Boiling Region

$5°K < \Delta T < 20°K$

i.e. $0.25 < \theta < 1$

$$\dot{q}'' = \dot{q}''_{peak} \left(\frac{\Delta T}{(\Delta T)_{peak}}\right)^3 \qquad (M-2)$$

i.e. $q = \theta^3$ (M-3)

Transition Region

$20°K < \Delta T < 100°K$

i.e. $1 < \theta < 5$

$$\dot{q}'' = \dot{q}''_{peak} \left(\frac{T}{20}\right)^{-1} \qquad (M-4)$$

i.e. $q = \dfrac{1}{\theta}$ (M-5)

Film Boiling Region

$100°K < \Delta T < 500°K$

i.e. $5 < \theta < 25$

$$\dot{q}'' = \dot{q}''_{transition} \left(\frac{\Delta T}{100}\right)^{0.25} = 0.2 \; q''_{peak} \left(\frac{\Delta T}{100}\right)^{0.25} \qquad \text{(M-6)}$$

i.e. $q = 0.134 \; \theta^{0.25}$ \qquad (M-7)

Before solving equations 1 through 6, we nondimensionalize the equations. We define the following dimensionless parameters:

$$\alpha \quad = \text{thermal diffusivity of steel} = \frac{k}{\rho c}$$

$$\theta \quad = (T - T_{sat})/(\Delta T)_{peak}$$

$$\dot{q} \quad = \frac{q''}{q''_{peak}} = \text{dimensionless heat flux}$$

$$\xi \quad = x/L = \text{dimensionless coordinate distance}$$

$$\delta \quad = s_1/L = \text{dimensionless thermal penetration depth.}$$

$$B \quad = \text{Biot number corresponding to peak heat flux} = \frac{L}{k} \frac{q''_{peak}}{(\Delta T)_{peak}}$$

$$t_{ch} \quad = \text{characteristic time} = \frac{L^2}{\alpha}$$

$$\tau \quad = t/t_{ch} = \text{dimensionless time}$$

$$\phi \quad = \frac{\theta - \theta_s}{\theta_i - \theta_s}$$

$$\overline{Q} \quad = \frac{Q''}{t_{ch} \, q''_{peak}} = \text{dimensionless heat content in the steel}$$

(O-1)

Hence, equation 1-a becomes

$$\phi = \frac{\theta - \theta_s}{\theta_i - \theta_s} = \left(\frac{\xi}{\delta} - \frac{\xi^2}{4\delta^2} \right) \qquad (O\text{-}2a)$$

for $\xi < 2\delta$

$$\phi = 1 \text{ for } \xi \geq 2\delta \qquad (\dot{O}\text{-}2b)$$

Equation 3 becomes

$$\frac{Q''}{\rho c L (\Delta T)_{peak}} = \int_{\xi=0}^{1} \theta \, d\xi = \theta_i (1 - 2\delta) + \int_{\xi=0}^{2\delta} \theta d\xi \qquad (O\text{-}3a)$$

Substituting equation O-1, we have

$$\frac{Q''}{\rho c L (\Delta T)_{peak}} = \theta_i (1 - 2\delta) + (\theta_i - \theta_s) \int_{\xi=0}^{2\delta} \left(\frac{\xi}{\delta} - \frac{\xi^2}{4\delta^2} \right) d\xi + \theta_s \, 2\delta \qquad (O\text{-}3b)$$

277

$$= \theta_i (1 - 2\delta) + (\theta_i - \theta_s) \delta \frac{4}{3} + \theta_s 2\delta$$

$$\frac{Q''}{\rho c L (\Delta T)_{peak}} = \theta_i - 2/3 \, \delta \, (\theta_i - \theta_s)$$

$$\bar{Q} = \frac{Q''}{q''_{peak} \, t_{ch}} = \frac{1}{B} \left[\theta_i - 2/3 \, \delta \, (\theta_i - \theta_s) \right] \qquad (0\text{-}3c)$$

Equation 4 becomes

$$q = \frac{k \, (\Delta T)_p}{L \, q''_{peak}} \left(\frac{\partial \theta}{\partial \xi} \right)_{\xi=0}$$

Substituting for θ from equation 0-1, we have

$$q = \frac{(\theta_i - \theta_s)}{B} \, \frac{1}{\delta} \qquad (0\text{-}4)$$

Equation 5 becomes

$$\frac{d\bar{Q}}{d\tau} = -q \qquad (0\text{-}5)$$

From boiling correlations for film boiling from Appendix M, we have

$$q = 0.134 \, \theta_s^{0.25} \qquad (0\text{-}6)$$

Solutions for θ_s, $\bar{Q}$, δ, etc. as functions of time are not possible to evaluate completely analytically. What follows is a graphical method of calculation. The steps are illustrated.

1. Choose a value of θ_s slightly lower than θ_i.

2. From equation 0-6, obtain q.

3. From the q that is calculated and with known values of B, θ_i, and θ_s, δ is calculated from equation 0-4.

4. From known values of θ_i, θ_s, δ and B, $\bar{Q}$ is calculated from equation 0-3c.

5. The calculation is repeated for several values of θ_s until δ becomes 0.5 (i.e. the temperature profile is fully developed).

6. A plot of q vs. $\bar{Q}$ is made from the table of values generated for each θ_s.

7. The time for reaching a certain θ_s is then calculated using equation 0-5 as

$$\int_{\bar{Q}}^{\bar{Q}_{initial}} \frac{d\bar{Q}}{q} = \tau$$

Table 0-1 gives the values obtained from the above calculations, using

$$B = \frac{\dot{q}''_{peak} L}{(\Delta T)_{peak} k} = \frac{3.8 \times 10^5 \times (1.5/12)}{36 \times 9.4} = 140.37$$

$$t_{ch} = \frac{L^2}{(k/\rho c)} = \frac{(1.5/12)^2}{9.4} \times (8.3 \times 62.4 \times 0.12) \times 3600 = 372 \text{ secs}$$

$$\dot{q}''_{peak} = 3.8 \times 10^5 \text{ B/hr ft}^2$$

$$\Delta T_{peak} = 20°C = 36°F$$

Initial Steel Temperature $T_i = 700°K$

$$\theta_i = \frac{T_i - T_{sat}}{(\Delta T)_{peak}} = \frac{700 - 373}{20} = 16.35$$

The variation of the total heat content $\bar{Q}$ with heat flux q is shown in Figure VI-3 for the values given in Table 0-1.

The calculations of temperature profile within the steel when the surface boiling goes through transition boiling regime and the subsequent cooling in the nucleate boiling regime is exceedingly difficult. However, it can be said that because of the instability of temperature (with the heat flux) in the transition regime, the surface temperature very rapidly reaches the temperature corresponding to peak heat flux in nucleate boiling regime.

Even under the conservative assumption that the peak heat flux is maintained at the surface, the time taken to cool the entire metal down to T_{peak} is somewhat longer than the cool down duration in the film boiling period.

For example, $\bar{Q}$ (when the entire steel is at $T = T_{peak}$, i.e., $\theta = 1$)

$$= \frac{1}{B} = \frac{1}{140.37} = 7.13 \times 10^{-3} \qquad \text{(See equation 0-3a)}$$

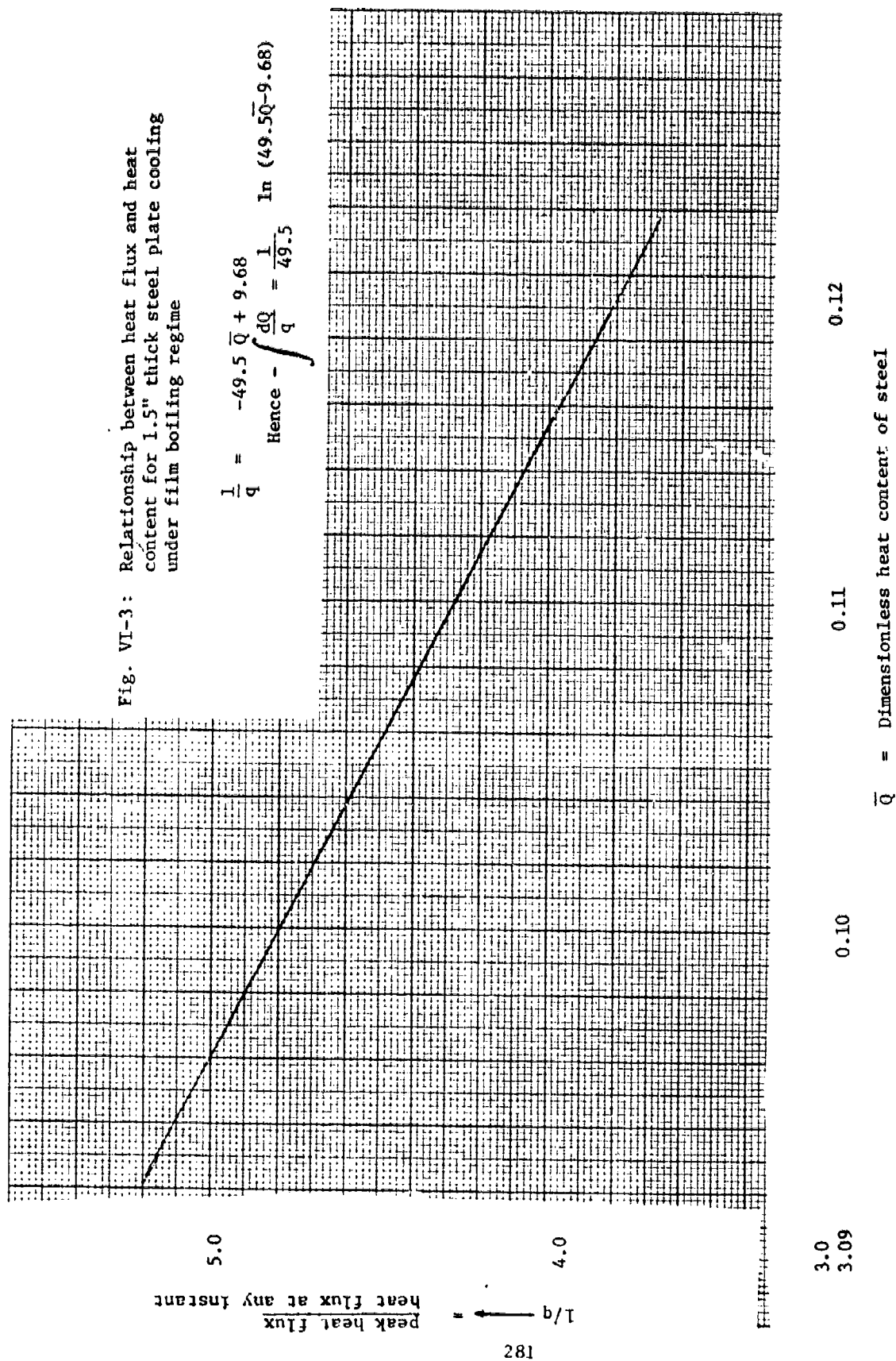Heat flux $= q = 1$ (because $\dot{q}'' = \dot{q}''_{peak}$)

279

TABLE O-1

T_s °K	$\theta_s = \dfrac{T_s - T_{sat}}{(\Delta T)_{peak}}$	$\theta_i - \theta_s$	$q = q(\theta_s)$	δ from O-4	$\bar{Q}$ from O-3	τ Using Fig. O-1 Results	t Seconds	Remarks
700	16.35 = θ_i	0	0.269	0	0.1165	0	0	
650	13.85	2.5	0.2585	0.0689	0.1157	0.0002	0.0757	
600	11.35	5.0	0.2460	0.1448	0.1130	0.0009	0.3256	
550	8.85	7.5	0.2311	0.2312	0.1082	0.002	0.7503	
500	6.35	10.0	0.2127	0.3349	0.1006	0.0037	1.3772	
473	5.00	11.35	0.2004	0.4035	0.0947	0.0049	1.8302	Transition Boiling Regime Starts

Fig. VI-3: Relationship between heat flux and heat content for 1.5" thick steel plate cooling under film boiling regime

$$\frac{1}{q} = -49.5\,\overline{Q} + 9.68$$

$$\text{Hence } -\int \frac{dQ}{q} = \frac{1}{49.5} \quad \ln\,(49.5\overline{Q}-9.68)$$

$\dfrac{1}{q} \longleftarrow = \dfrac{\text{peak heat flux}}{\text{heat flux at any instant}}$

5.0

4.0

3.0
3.09

0.10   0.11   0.12

$\overline{Q}$ = Dimensionless heat content of steel

281

Then time taken to cool down from

$$\bar{Q}_{initial} = 0.0947 \text{ (end of film boiling regime)}$$

to $\bar{Q}_{final} = 7.124 \times 10^{-3}$ for given time

$$\Delta \tau = \frac{(0.0947 - 7.124 \times 10^{-3})}{1} \cdot \underline{\hspace{0.5cm}} = 8.758 \times 10^{-2}$$

i.e., $\Delta t = 8.758 \times 10^{-2} \times 372 = 32.58$ secs

In general, the cooling time to T_{peak} temperature is greater than the 32.6 seconds indicated above.

Nomenclature

B = Biot number = $\dfrac{\dot{q}''_{peak}}{(\Delta T)_{peak}} \dfrac{L}{k}$ (See equation C-1)

c = specific heat at constant pressure for steel

k = thermal conductivity of steel

L = thickness of propylene tank shell

p = pressure

Q'' = heat content (above water saturation temperature) of the steel per unit surface area

q = dimensionless heat flux = $\dfrac{q''}{q''_{peak}}$ (See equation C-1)

$\dot{q}''$ = heat flux per unit of outer surface area of tank shell (used with subscripts, fire, peak). When used without subscript, it represents boiling heat flux to water.

S_1 = thermal penetration depth confunction of time

$\Delta T = T - T_{sat}$

T = temperature (used with subscripts)

t = time

t_{ch} = characteristic time = $\dfrac{L^2}{\alpha}$

x = thickness direction coordinate

$\dot{v}$ = volume rate at which water is squirted

Greek Letters

α = thermal diffusivity of steel = $\dfrac{k}{\rho c}$

β = ullage volume fraction of tank

δ = dimensionless thermal penetration depth = s_1/L (See equation C-1)

θ = dimensionless temperature difference $(T - T_{sat})/(\Delta T)_{peak}$ (See equation C-1)

λ = heat of vaporization of water

ξ = dimensionless distance = x/L

ρ = density of steel

τ = dimensionless time = t/t_{ch}

ϕ = temperature ratio = $\dfrac{\theta - \theta_s}{\theta_1 - \theta_s}$

283

Subscripts

peak = refers to peak heat flux condition

sat = saturated condition of water

s = outer wall surface

i = initial condition (before water application)

fire = fire condition

REFERENCES

1. "Heat Transmission," William H. McAdams, McGraw-Hill Book Company, Inc., New York, 1954.

2. "Analysis of Heat and Mass Transfer," E.R.G. Eckert and R.M. Drake, 1974, p. 556, Figure 13-9.

3. "Handbook of Heat Transfer," W.M. Rohsenow and J.P. Hartnett, McGraw-Hill Inc., 1973, New York.

CHAPTER VII

REACTIVE CHEMICAL MODELS

OBJECTIVES

The objectives of the analyses presented in this chapter are to consider three chemicals having considerably different types of reactions with water and to develop methods to obtain reaction rates or dissolution rates; also to identify the products of reaction and their quantity of release.

INTRODUCTION

Some chemicals shipped in bulk and included in the CHRIS list of chemicals are classed as reactive. This generic term has a broad meaning. For example, derivatives of acrylic acid are considered as reactive, but polymerization rates are normally so low that other branches of the hazard assessment tree are more appropriate for spills in ambient water (or on land). Polymerization is important only in selected temperature and pressure ranges, and normally, a catalyst is also necessary.

In contrast, other chemicals decompose rapidly when in contact with humid air or water. At one extreme, chlorosulfonic acid ($ClSO_2OH$) decomposes to form sulfuric acid and HCl in a rather violent manner when spilled in water. Clearly it is not appropriate to consider $ClSO_2OH$ as a single chemical when in contact with water. Then there are several important chemicals which react with water at slow to moderate rates to form secondary products. Phosgene ($COCl_2$) forms CO_2 and HCl in contact with water, but the hydrolysis rates are such that one must consider the simultaneous dispersion and reaction of $COCl_2$, CO_2, and HCl should this material be spilled into water. For this last class of chemicals, each material must be treated as a special case since chemical reaction rates vary significantly, and few general rules may be formulated.

In this report, we have chosen three reactive chemicals and discuss in some detail how one may predict their dispersal and hazards. One is chlorosulfonic acid which, as noted above, reacts very rapidly. The other two, phosgene and nitrogen tetroxide, are illustrative of cases where reaction rates are moderate and the dispersal hazards due both to the original chemical and to the reaction products must be taken into consideration. All three chemicals selected are important intermediates in the chemical process industry and are shipped in substantial quantities.

We first discuss the physical and thermodynamic properties of each, including the rates of solution and thermal effect and, in a later section, indicate how these basic data may be employed to determine the dispersion and hazards which may result from a spill.

THEORETICAL DEVELOPMENT

● Chemicals Selected

1. Chlorosulfonic Acid

This acid may be considered as the acid chloride of sulfuric acid, i.e., one chlorine has replaced a hydroxyl group. It is an important chemical in the production of synthetic detergents, drugs, and dyes. As shipped it is a clear, colorless mobile liquid. When in contact with moist air, it fumes strongly and, with liquid water, it reacts quite violently and rapidly in the following manner:

$$ClSO_2OH + 2\ H_2O = H_2SO_4 + 2\ HCl$$
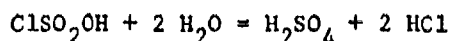
Presumably the fume noted above consists of fine droplets of sulfuric acid suspended in air; as such, these fumes are very damaging to nasal passages and lungs.

The liquid freezes about $-80°C$ and boils (with some decomposition) at $150-155°C$. At $20°C$, the vapor pressure is quite low (circa 1 mm Hg) The liquid is more dense than water ($1.75\ g/cm^3$ at $20°C$) so for large spills the chlorosulfonic acid would simultaneously sink and react.

Should the spilled acid contact combustible materials, ignition may result since it is a powerful oxidizing agent.

287

The heat of solution in water to form aqueous H_2SO_4 and HCl is 40.3 kcal/g mol or 623 Btu/lb of acid. Reaction is extremely rapid. The H_2SO_4 formed is essentially nonvolatile (though if small mist droplets are formed, they are persistent), but the HCl product is volatile though quite soluble in water.

Spills under a large head of water would probably result in little vapor formation; any HCl and steam generated would be absorbed or recondensed before reaching the surface. Spills into water or spills under water in a shallow basin would quite definitely result in a significant fume of steam, sulfuric acid, and hydrochloric acid which would move downwind and only slowly be dissipated. Large spills in a local area could, in fact, generate so much steam and hydrochloric acid vapor to resemble a flameless explosion and contaminate large areas with this very acid and oxidizing material.

The hazards are, therefore, of several types:

1. Sulfuric acid product will remain largely in the water though if there is significant concomitant HCl vapor production, some sulfuric acid will be entrained as a mist.

2. Hydrochloric acid will be formed as a vapor but will dissolve in the water as it rises toward the surface. Vapors of this acid are more dense than air and will disperse with difficulty; the problem is exacerbated if there is any H_2SO_4 fume present as this will lead to an even denser vapor plume.

A very large amount of water must be available to dissolve the reaction products without large temperature rises or steam evolution. As an approximate rule, at least 10 lbs of water/lb acid are necessary to keep the increase in water temperature below 65-80°F. For a 1000-gallon spill, some 15000 lbs of acid are involved and, with the rough rule given above, 150,000 lbs of water should be immediately available. (18,000 gal = 2400 ft^3)

288

2. Phosgene

Phosgene, $COCl_2$, is a colorless liquid, when pure, but is usually described as being pale yellow to green as it is invariably slightly contaminated. In very dilute concentrations, the odor is not unpleasant and is often described as similar to new-mown hay. In more concentrated vapors, the effects are serious, unusual, and insidious. The odor is perceptible to most humans when there is only 4 μg/liter; irritation occurs at 40 μg/liter; and lethal concentrations are about 100 μg/liter (30 min). Even in the more dilute ranges, subjects often feel little distress while exposed and the phosgene enters the deep lungs. Several hours after exposure, labored breathing becomes evident and, in severe cases, death may occur from palmonary edema. It is important to realize these delayed symptoms and enforce rest with the attention of a physician after any exposure to phosgene vapors. Exertion must be avoided even though the subject feels normal after removal from areas where there are phosgene vapors.

Very delayed symptoms may occur if the subject is exposed to the odor of cut grass or green corn.

These interesting effects have been utilized in the use of phosgene as a war gas; today phosgene is an important chemical intermediate in the manufacture of many chemicals.

It is a relatively low boiling liquid (8°C at atmospheric pressure), and it freezes at -128°C. It is more dense than water (1.39 g/cm^3) at 20°C. There is an interesting possibility that a phosgene spill into water at 20°C could result in a non-boiling pool if the water head exceeds about 20 ft since the pressure of the water at this depth essentially equals the vapor pressure of phosgene at 20°C (23.4 psia). Spills in lesser depths would result in rapid boiling; the heat of vaporization is about 106 Btu/lb.

In addition to this phase-transition effect, phosgene reacts with water:

$$COCl_2 \ (\ell) + H_2O \ (\ell) = CO_2 \ (g) + 2 \ HCl \ (g)$$
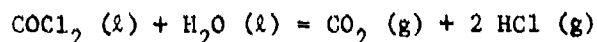
For this reaction (at ~ 18°C), the standard heats of formation are:

$$\Delta H^\circ{}_f \ (18°C)$$

kcal/g mole	Compound
-58.0	$COCl_2$ (ℓ)
-68.4	H_2O (ℓ)
-94.4	CO_2 (g)
-22.0	HCl (g)

Thus, the heat of reaction is

$$\Delta H = -94.4 + 2(-22.0) - (-58) - (-68.4)$$
$$= -12 \text{ kcal/g-mol } COCl_2$$
$$= -218 \text{ Btu/lb } COCl_2$$

In addition, if the HCl dissolves in the water, there is a further heat effect which can be estimated as

$$-17,500 \text{ cal/g-mole HCl absorbed.}$$

For the reaction as shown, two moles of HCl result per mole of phosgene, so the maximum energy liberated from the HCl solution is

$$-17,500 \times 2 = -35,000 \text{ cal/g-mole } COCl_2$$
$$= -637 \text{ Btu/lb } COCl_2$$

Thus, the heat of solution of product HCl could, in fact, exceed the heat of reaction -- though some HCl would, in all probabilities, escape to the air. Also, the heat of solution would be absorbed over a larger volume of water as the gas bubbles rise towards the surface.

The rate of hydrolysis of phosgene is relatively rapid when water is in excess and there is vigorous agitation. Strong acids reduce the hydrolysis rate and bases accelerate it. Lime slurry addition is an effective way to neutralize the product HCl. Upon occasion, it has been reported that there is an "induction" period after $COCl_2$ and water have come into contact before significant reaction. (This may have been the result of a stagnant layer of strong HCl at the interface which prevented reaction.)

The rates of hydrolysis have not received extensive study. Manogue and Pigford[1] studied the kinetics of absorption of phosgene vapor into water at temperatures between 16 and 45°C. The reaction rate was found to be approximately first order, and the rates a strong function of temperature. Thus, the rate of disappearance of phosgene (C) may be expressed as

$$dC/dt = k\ C \tag{1}$$

(If solution occurs in an alkaline medium, this first order expression may not be valid unless a large excess of hydroxyl ions are present.)

At the lower temperatures (16-25°C), the rate of reaction was slow and the mechanisms of dissolution could be well approximated by two independent steps, i.e., physical dissolution of $COCl_2$ into the water, followed by slow decomposition within the water phase. Thus, there is little enhancement of the dissolution rate due to reaction. This is not true at 35-45°C where the reaction influences (and increases) the rate of dissolution.

The solubility of phosgene as well as the diffusivities and reaction rate constants are shown in Table VII-1 as a function of temperature. From the solubility data, the heat of solution (without reaction) was estimated to be about -6800 cal/g-mol (-124 Btu/lb $COCl_2$). This is a rather large heat of solution, and some reaction may have occurred to yield this value.

The use of these data to estimate reaction rates and dispersion is discussed later.

3. Nitrogen Tetroxide

Nitrogen tetroxide (N_2O_4) is a volatile liquid that boils at 21.1°C (1 atm) and freezes at -11.2°C. The liquid range at one atmosphere is, therefore, quite small. It is difficult to obtain in a very pure state but, with little NO dissolved, the color is described as reddish-brown, while with NO present there is a characteristic green tint. The heat of vaporization is 9110 cal/g-mole N_2O_4 (178 Btu/lb), and the density of the liquid (at 21.1°C) is 1.45 g/cm^3.
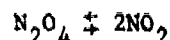
291

TABLE VII-1

Phosgene Solution in Water

T, °C	Solubility g-mol/liter-atm	Diffusion Coef. cm^2/s	k s^{-1}
15	0.109	9.6×10^{-6}	3*
25	0.069	12.7×10^{-6}	6*
35	0.046	16.1×10^{-6}	22
45.5	0.027	20.4×10^{-6}	75

*Estimated from higher temperature data

Vapors from the liquid decompose very rapidly to form an equilibrium mixture of NO_2 and N_2O_4, i.e.

$$N_2O_4 \leftrightarrows 2NO_2$$

At 21.1°C, the equilibrium mixture contains about 15% NO_2 and, at 100°C, about 90%. The time constant for this reaction is less than 1 us.

Liquid N_2O_4 is a powerful oxidizing agent, and either liquid or vapor is toxic to life. Contact of the liquid with combustible material may lead to ignition and, if spilled on the skin, severe burns result. The symptoms of N_2O_4 (NO_2) inhalation are similar in some ways to phosgene as discussed above. Pulmonary edema may develop some time after exposure, and with breathing difficult, serious cyanosis symptons may be noted.

The liquid contains essentially 100% N_2O_4 (very little NO_2). It is more dense than water and will sink if spilled into water. It reacts with water in a complex manner. The current theory indicates that reaction occurs in a two-step process. First, the N_2O_4 forms nitrous and nitric acids,

$$N_2O_4 + H_2O \rightarrow HNO_2 + H^+ + NO_3^- \tag{1}$$

and the unstable nitrous acid decomposes more slowly to form nitric acid and nitric oxide,

$$3HNO_2 \rightarrow H_2O + H^+ + NO_3^- + 2NO \tag{2}$$

The net reaction is then

$$3N_2O_4 + 2H_2O \rightarrow 2NO + 4H^+ + 4NO_3^- \tag{3}$$
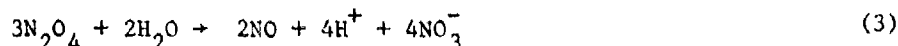
These reactions occur in absorption columns for the production of nitric acid.

Few data exist on the reaction of liquid N_2O_4 with water. The manufacturer warns [2] that water in large quantities will "promote the rapid release of nitrogen oxides." Gray and Yoffe [3] indicate that under quiescent conditions, liquid N_2O_4 and water form two liquid

phases; at 20°C, the less dense contains water and about 52% N_2O_4 (largely as nitric acid) while the more dense contains 98% N_2O_4. In the formation of the aqueous phase, NO is liberated.
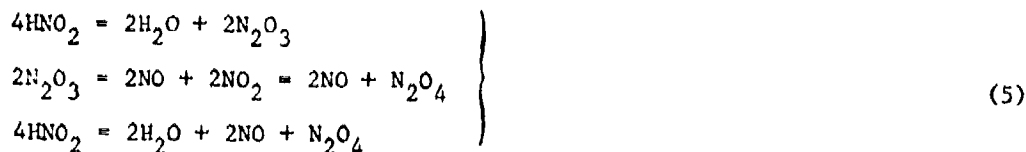
Lowry and Lemon[4] state that N_2O_4 and H_2O do not "dissolve" in each other but interact at the surface to form two layers. The more dense is almost entirely N_2O_4 while the less dense contains aqueous HNO_3, HNO_2, and some dissolved NO. This latter phase was found to contain 17.7 mole percent (52.3 weight percent) N_2O_4, while the dense phase had 98.1 weight percent N_2O_4.

Dulong[5] as far back as 1816 described an experiment wherein liquid N_2O_4 was dropped into water. It fell to the bottom of the vessel and became deep green; some NO gas was found simultaneously.

The reaction apparently occurs at the interface both for the case of liquid N_2O_4 reacting with water or gaseous N_2O_4 - NO_2 absorbing in water. The actual kinetics are in doubt. Gray and Yoffe[3] and others[6,7] suggest the rate controlling step is reversible and may be written as shown in reaction (A). Simple kinetics then indicate that

$$- \frac{d}{dt} [N_2O_4] = \frac{3}{4} \left\{ k_f [N_2O_4][H_2O] - k_r [H^+][NO_3^-][HNO_2] \right\} \qquad (4)$$

The factor (3/4) is obtained by assuming that the decomposition of nitrous acid in reaction (1) is rapid, i.e.,

$$
\left.
\begin{aligned}
4HNO_2 &= 2H_2O + 2N_2O_3 \\
2N_2O_3 &= 2NO + 2NO_2 = 2NO + N_2O_4 \\
4HNO_2 &= 2H_2O + 2NO + N_2O_4
\end{aligned}
\right\} \qquad (5)
$$

Thus, for every mole of HNO_3 formed, one-fourth of a mole of N_2O_4 is reformed.

If we further assume that equilibrium exists for the HNO_2 decomposition,

$$[HNO_2] = (constant)[N_2O_4]^{1/4} [NO]^{1/2} [H_2O] \qquad (6)$$

Substituting in (4),

$$-\frac{d}{dt}[N_2O_4] = \frac{3}{4}\left\{k_f[N_2O_4][H_2O] - k_r'\ [H^+][NO_3^-][N_2O_4]^{1/4}[NO]^{1/2}[H_2O]^{1/2}\right\}$$

$$-\frac{d}{dt}[N_2O_4] = k_a\left([N_2O_4] - C\ [N_2O_4]^{1/4}[NO]^{1/2}\right) \tag{7}$$

In the early stages of an absorption, the [NO] concentration is low, and it is a good assumption to simplify Eq. (7) to

$$-\frac{d}{dt}[N_2O_4] = k[N_2O_4] \tag{8}$$

In words, one may interpret Eq. (8) as stating that for a pure layer of N_2O_4 on the bottom of a stream, the dissolution into water flowing over it is a constant and proportional to the area of the pool. This assumes, of course, that the concentration of N_2O_4 and its reaction products are low in the aqueous phase.

- Modelling of a N_2O_4 Spill on Water

The properties and chemistry pertinent for nitrogen tetroxide (N_2O_4) were discussed earlier. The dissolution and dispersion of a spill in water are now considered. To our knowledge, no experimental data exist with which to compare predictions.

As evident from the high density of liquid N_2O_4, spills of this chemical will allow pools to be formed on shallow bottoms. Dissolution and reaction are relatively rapid, with the production of nitric acid and nitric oxide (NO) as end products. The nitric acid remains predominantly in the water phase and disperses downstream in a manner similar to other soluble chemicals; the nitric oxide will, to a certain extent, dissolve, but most will leave the aqueous phase and disperse downwind.

Data indicate that dissolution rates are strongly dependent upon the area of contact between the N_2O_4 bottom layer and the water.

The first important problem is to estimate the rate of dissolution for a pool of finite size and depth.

With no experimental data to provide a guide, we take two rather extreme case models that represent limiting cases.

1. Infinite Rate of Dissolution

In this case, we allow no resistance to exist to the transfer of N_2O_4 into the water phase, i.e., the water side interface is in equilibrium with the denser N_2O_4 layer. From data discussed earlier, it is believed that equilibrium is attained when the water contains about 50% (by weight) nitric acid. The rate controlling step is then the molecular and eddy transport of this acid away from the interface into the bulk water, i.e., the rate process is controlled solely by the mass transfer resistance in the aqueous side.

A 50% nitric acid solution has a density of about 1.3 g/cm^3 and a concentration of 10.3 kg-mol/m^3. If the free stream is assumed to have a low acid level, the rate of transfer of HNO_3 away from the water surface is

$$N = k(10.3 - 0) \text{ kg-mol/m}^2 \text{s} \tag{9}$$

where k is the mass transfer coefficient in m/s. To obtain k, we make use of "j" factor analogies for flow over a flat plate.

$$j = N_{sh}/N_{Re} \ N_{sc}^{1/3} = 0.037 \ N_{Re}^{-0.2} \tag{10}$$

where

N_{sh} = Sherwood number = k L/D $\qquad\qquad$ (11)

L $\quad$ = Length of pool, m

D $\quad$ = Diffusion coefficient of nitric acid in water

N_{Re} = Length Reynolds number = $u\rho L/\mu$

u $\quad$ = Free stream velocity, m/s

ρ $\quad$ = Free stream density, kg/m^3

μ $\quad$ = Free stream viscosity, kg/m s

N_{sc} = Schmidt number = $\mu/\rho D$

An estimate of the diffusivity of nitric acid in water yielded a value between 3.5 and 4.0 x 10^{-5} cm^2/s depending upon the concentration.

Choosing $D \sim 3.7 \times 10^{-5}$ cm^2/s $= 3.7 \times 10^{-9}$ m^2/s, then, with the solution viscosity about 1.3×10^{-3} kg/m s and the density 1300 kg/m^3

$$N_{sc} = \mu/\rho D = \frac{1.3 \times 10^{-3}}{1300 \times 3.7 \times 10^{-9}} = 270$$

Let the stream velocity be 3 ft/s $\sim$ 1 m/s and L = 10 m

Then,

$$N_{Re} = \frac{(1)(1300)(10)}{(1.3)(10^{-3})} = 10^7$$

From Equation (2),

$$N_{sh} = (0.037)(10^7)^{0.8} (270)^{1/3}$$

$$= 9.5 \times 10^4$$

$$= kL/D = k \ (10)/(3.7 \times 10^{-9})$$

$$k = 3.5 \times 10^{-5} \text{ m/s}$$

Then, $N = (10.3)(3.5)(10^{-5}) = 3.6 \times 10^{-4}$ kg moles/m^{2}s

If L were only 5 m, $N = (3.6 \times 10^{-4})(2)^{0.2} = 4.2 \times 10^{-4}$ moles/m^{2}s

This approximate calculation indicates the transfer rate when based on a mass transfer limitation.

2. Kinetic Model

In this case, we assume no rate limiting mechanism on the water side, and all resistance is centered in the dissolution-reaction step at the interface. The theory has only been developed for gas phase dissolution and reaction in which case an approximate solution is

$$N = P_{N_2O_4} \ H\sqrt{k_1 D} \tag{12}$$

where

$P_{N_2O_4}$ = Partial pressure (fugacity) of N_2O_4 at the interface, atm

H = Solubility constant for N_2O_4 into water or dilute acids, kg mole/m^3 atm

k_1 = Reaction rate constant, s^{-1}

The diffusivity D is given above and $H\sqrt{k_1}$ can be obtained from experimental data of Kramers et al, [7] as 22.0 kg mole/m³ atm s$^{1/2}$ at about 20°C. At 20°C, the vapor pressure of the nitrogen oxide vapor is about 1 atm, but it consists of an equilibrium mixture of NO_2 and N_2O_4, i.e.,

$$2NO_2 \leftrightharpoons N_2O_4$$
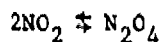
$$\log K = \log(p_{N_2O_4}/p_{NO_2}^2) = \frac{3198}{T} - 9.8696$$

at 20°C, K = 11.1

Since $p_{N_2O_4} + p_{NO_2} = 1$ atm, $p_{N_2O_4} \sim 0.74$ atm

Then, with Eq. (3)

$$N = (0.74)(22.0)(3.7 \times 10^{-9})^{1/2}$$

$$= 9.9 \times 10^{-4} \text{ kg moles } N_2O_4 /m^2s$$

3. Discussion

Since 3 moles of N_2O_4 form 4 moles of nitric acid and 2 moles of NO, then the rate from case II must be multiplied by 4/3 to obtain an equivalent transfer rate of HNO_3. The true rate will, of course, be less than either from cases I or II, and a reciprocal mean is a good way to combine these results,

$$N^{-1} \sim (4/3 \ N_{II})^{-1} + N_I^{-1}$$

$$N = 2.8 \times 10^{-4} \text{ kg moles } HNO_3 \text{ formed}/m^2s$$

$$= 2.1 \times 10^{-4} \text{ kg moles } N_2O_4 \text{ dissolved}/m^2s$$

$$= 1.4 \times 10^{-4} \text{ kg moles NO formed}/m^2s$$

4. Example

Suppose 5000 lb N_2O_4 is spilled into water. This is equivalent to 2270 kg or 24.7 kg-moles N_2O_4. The density is 1450 kg/m³ or 15.8 kg-moles/m³. The volume spilled is, therefore, 1.56 m³. If the pool dimensions at the bottom were 5 x 5m, the depth is 6.2 cm.

By the estimates above,

N_2O_4

$N = 5.3 \times 10^{-4} \times 25 = 5.3 \times 10^{-3}$ kg-moles/s

$= 5.3$ moles/s

$= 1.2$ lb/sec

HNO_3

$N = 2.8 \times 10^{-4} \times 25 = 7 \times 10^{-3}$ kg moles/s

$= 7$ g moles/s

$= 1.0$ lb/sec

NO

$N = 3.5$ moles/s $= 0.23$ lb/s

Pool duration $= 24.7/(5.0 \times 10^{-3}) = 4112$ x $= 68.5$ mins.

Although the pool dimensions may shrink during dissolution, a conservative prediction would assume that the rates given above for HNO_3 and NO were maintained over the course of the dissolution.

● Modeling of a Phosgene Spill in Water

As noted for the nitrogen tetroxide case, no experimental rate data are available to determine dissolution rates for liquid phosgene dissolution-reaction with water. We will, therefore, consider again two limiting cases. There is one other case, applicable to spills in shallow water, and this is discussed last.

1. Infinite Rate of Dissolution

In this case, no chemical reaction occurs. Phosgene is transported across the interface as a molecular entity, and the water side is saturated. The rate limiting step is the mass transfer of phosgene into the bulk water -- where it will slowly react to form aqueous hydrochloric acid and carbon dioxide gas.

From the data given previously, assume that the head of water is sufficiently great that the pressure on the pool of liquid phosgene

299

exceeds the vapor pressure. With the temperature $\sim 20°C$, the vapor pressure is about 23.4 psia = 1.6 atm. From Table 3.1, the equilibrium solubility is then about equal to $(1.6)(0.09) = 0.14$ kg mole/m^3. The rate of dissolution is, therefore,

$$N = k(0.14 - 0) \text{ kg moles/m}^2\text{s} \tag{13}$$

with k in m/s.

The aqueous phase is quite dilute, so the properties of pure water are used, i.e.,

$$\rho = 1000 \text{ kg/m}^3$$

$$\mu = 1 \times 10^{-3} \text{ kg/m s}$$

The diffusivity of phosgene, given on Table 3.1, is about 1.1×10^{-5} cm^2/s = 1.1×10^{-9} m^2/s. Then, with Eq. (2)

$$N_{sc} = \mu/\rho D = \frac{1 \times 10^{-3}}{(1000)(1.1 \times 10^{-9})} = 909$$

Using the same pool size as for the N_2O_4 case shown earlier (L = 10 m) and with the water velocity again 1 m/s,

$$N_{Re} = \frac{u\rho L}{\mu} = \frac{(1)(1000)(10)}{1 \times 10^{-3}} = 10^7$$

Then

$$N_{sh} = (0.037)(10^7)^{0.8}(909)^{1/3}$$

$$= 14.3 \times 10^4$$

$$= kL/D = k(10)/(1.1 \times 10^{-9})$$

$$k = 1.6 \times 10^{-5} \text{ m/s}$$

Thus, from Eq. (13)

$$N_I = 1.6 \times 10^{-5} \times 0.14 = 2.2 \times 10^{-6} \frac{\text{kg-moles}}{\text{m}^2 \text{ s}}$$

2. Kinetic Model

In this case, we assume that all resistance to transfer is in the reaction-dissolution step. Eq. (3) is then applicable with

$$P_{COCl_2} = 1.6 \text{ atm}$$

$$H = 0.09 \text{ kg-moles/m}^3 \text{ atm}$$

$$k_1 = 4.2 \text{ s}^{-1} \text{ (Table 3.1)}$$

$$D = 1.1 \times 10^{-9} \text{ m}^2/\text{s} \text{ (Table 3.1)}$$

$$N_{II} = P_{COCl_2} H (k_1 D)^{1/2} \qquad \text{(See equation 12)}$$

$$= (1.6)(0.09)[(4.2)(1.1 \times 10^{-9})]^{1/2}$$

$$= 9.8 \times 10^{-6} \text{ kg moles/m}^2\text{s}$$

3. Discussion

From examination of both models, it is clear that neither resistance in the dissolution step nor in the aqueous mass transfer step is controlling. With reciprocal combination,

$$N^{-1} = N_I^{-1} + N_{II}^{-1}$$

$$N = 1.8 \times 10^{-6} \text{ kg-moles } COCl_2/\text{m}^2\text{s}$$

4. Example

Using the same case as for N_2O_4, let 5000 lbs of phosgene spill into a stream where the temperature is about 20°C and the depth exceeds 20 ft. 5000 lbs is equivalent to 2270 kg or 22.9 kg moles. With a phosgene density of 1390 kg/m³, this is equivalent to 1.63 m³. Let the spill be 5 x 5 m in size. The depth is then 6.5 cm. The rate of phosgene dissolution is then estimated as

$$N = 6 \times 10^{-6} \times 25 = 0.45 \times 10^{-4} \text{ kg-moles/s}$$

$$= 0.045 \text{ g moles/s}$$

$$= 9.13 \times 10^{-3} \text{ lbs/s}$$

The duration of the pool, assuming no area shrinkage, is $22.9/(0.45 \times 10^{-4}) = 5.1 \times 10^5$ s = 141.4 hrs.

As opposed to the rapid rate of solution for N_2O_4, it is predicted that phosgene only slowly reacts and dissolves -- providing that the liquid head precludes boiling (see below).

301

- Boiling of Phosgene

As noted earlier, phosgene boils at about 8°C. If spills occur in a shallow body of water, boiling will occur. The liquid water will be quite agitated and the heat of reaction is more than sufficient to supply the latent heat of vaporization. In this case, gas bubbles of phosgene will rise through the water. Some will react to form HCl and CO_2, but the low solubility coupled with the expected high film temperatures around each bubble will lessen the dissolution. In this case, therefore, rapid evolution of phosgene gas is expected in the near vicinity of the spill. It is not possible to estimate rate of evolution since this depends quite strongly on the degree of agitation, the bubble size, water temperature, and the head of liquid.

Should one assume no reaction to occur, then drops of liquid phosgene would fall through water and boil. Estimates of the rate of fall yield values of the terminal velocity of about 0.5 ft/sec.[8] The low value of ΔT between the water and phosgene would indicate that boiling would occur primarily in the natural convection regime. For drops of liquid phosgene with effective diameters over 1 inch, the quantity vaporized during the descent to 20 ft (the depth where boiling is suppressed) would amount to only 10 - 20% of the drop. Thus, for the "no-reaction" case, vaporization is not important. However, if the liquid drops were smaller and if reaction is allowed, significant vaporization of the phosgene is possible during the fall to 20^+ ft. No experimental data are available to estimate this effect in a real case.

Phosgene spills present an interesting example of a dangerous chemical which may react in different ways depending on the type of spill. Even for spills into deep water, some phosgene will be liberated from flashing and from boiling in the shallow depths. The analysis, however, predicts that if the pool is deep, dissolution becomes quite slow and the hazard small. Water is acidified with HCl, and CO_2 passes harm- lessly into the atmosphere. For spills into shallow water, a completely

different picture emerges. Boiling is violent and continuous, the vapor is essentially pure phosgene, and the hazard to persons in the near vicinity real and severe.

DISCUSSIONS

In this chapter the reaction of three chemicals with water have been considered. The chemicals chosen represent those that have slow, moderate and violent reactions respectively.

Chlorosulfonic acid reacts violently with water producing H_2SO_4 and HCl, both of which may disperse as fine droplets in a cloud. Because of the rapidity with which the reaction takes place and because of the lack of knowledge of the fractions of H_2SO_4 and HCl that may be projected into the vapor phase, we suggest that for hazard estimation, the total quantities of HCl and H_2SO_4 produced be used as the quantities in the vapor phase.

Nitrogen tetroxide (N_2O_4) which has a moderate reaction rate with water produces HNO_3 and NO as end products. N_2O_4 being heavier than water sinks to the bottom of the water body and then reacts with it. This has been modeled with two dissolution controlling steps being considered. One of them is based on mass transfer limited step and the other is based on the resistance centered in the dissolution reaction step at the interface between the water N_2O_4 interface. It is suggested that the actual rate of dissolution of N_2O_4 is probably equal to the harmonic mean between the rates obtained when each of the individual steps is taken separately.

In the case of phosgene spills, the reaction rate is dependent on the depth of release. In the case of release at depths shallower than about 20 feet, phosgene boils producing phosgene gas which may escape without appreciable dissolution in water. On the other hand, for phosgene release at depths greater than 20 feet, phosgene dissolves slowly reacting with water, producing CO_2 and HCl. The latter phenome- non has been modeled also as a two-step reaction; one being controlled by the mass transfer limits and the other by the kinetics of the reaction. In the case of phosgene boiling, the rapid evolution of phosgene gas is

303

expected in the vicinity of the spill. Since it is not possible at
present to estimate the amount of dissolution of this vapor in water,
we recommend that vapor hazard calculating the total quantity of spill
used as the amount present in the vapor cloud. It is, however, noted
that because of the extremely hazardous nature of phosgene gas, the
use of the above conservative approximation may lead to a grossly over-
estimated hazard. Only experimental investigation of the phosgene
boiling and vapor generation phenomenon can give definitive results.
Until such time as such data become available (on the dissolution of
vapor in water) it is better to err on the over conservative side.

CONCLUSIONS

The reaction of chlorosulfonic acid, nitrogen tetroxide and
phosgene with water have been c. ..dered. The first represents a
chemical that reacts violently with water, the second has a moderate
reaction rate, and the third has certain peculiar reactions with water
depending on environmental conditions. The reaction products from each
of these reactions are soluble in water. Because of the lack of ex-
perimental data the extent of disolution of the products are unknown
and have been calculated, where possible, using the well established
mass transfer and kinetic model theories. Suggestions have been made
regarding the way these reactions can be incorporated in the hazard
calculations.

NOMENCLATURE

C   = Concentration of the Specie (kg moles/m^3)

D   = Diffusivity of a specie in water (m^2/s)

H   = Solubility constant   kg mole/m^3 atm

j   = Dimensionless mass transfer coefficient (See equation 10)

k   = Reaction rate constant (s^{-1}) Also used for mass transfer coefficient (m/s)

L   - Length of the chemical   m

N   = Dissolution rate (kg moles/m^2 s)

N_{Re} = Reynolds number = $u\rho L/\mu$

N_{Sc} = Schmidt number = ν/D

N_{Sh} = Sherwood number (equation 11) = $\dfrac{kL}{D}$

p   = Partial pressure (fugacity) of the specie at the interface (atm)

ρ = Density (kg/m^3)

μ = Viscosity of the solvent (N S/m^2)

ν = Kinematic viscosity of the free stream liquid (m^2/s)

REFERENCES

1. Manogue, W. H. and R. L. Pigford, AIChE Journ. 6, 494 (1960).

2. Hercules, Inc. Wilmington, Deleware, Bulletin S1-111.

3. Gray, Peter and A. D. Yoffe, Chem. Rev. 55, 1069, (1955).

4. Lowry, T. M. and J. T. Lemon, J. Chem. Soc. (1936), 6.

5. Dulong, A., Ann. Chem. Phys., 2, 317 (1816).

6. Andrew, S. P. S. and D. Hanson, Chem. Eng. Sci. 14, 105 (1961).

7. Dramers, H., M. P. P. Blind, and E. Snoeck, Chem. Eng. Sci., 14, 115 (1961).

8. Klee, A. J. and R. E. Treybal, Rate of Rise or Fall of Liquid Drops, AIChE Journal 2, 444 (1956).